IEK-3 Report 2013

Durable Electrochemical Process Engineering

Member of the Helmholtz Association

JÜLICH
FORSCHUNGSZENTRUM

Schriften des Forschungszentrums Jülich
Reihe Energie & Umwelt / Energy & Environment Band / Volume 184

Forschungszentrum Jülich GmbH
Institute of Energy and Climate Research (IEK)
Electrochemical Process Engineering (IEK-3)

IEK-3 Report 2013

Durable Electrochemical Process Engineering

Schriften des Forschungszentrums Jülich
Reihe Energie & Umwelt / Energy & Environment Band / Volume 184

ISSN 1866-1793 ISBN 978-3-89336-893-8

Bibliografische Information der Deutschen Nationalbibliothek.
Die Deutsche Nationalbibliothek verzeichnet diese Publikation in der
Deutschen Nationalbibliografie; detaillierte Bibliografische Daten
sind im Internet über <http://dnb.d-nb.de> abrufbar.

Herausgeber und Vertrieb:	Forschungszentrum Jülich GmbH Zentralbibliothek, Verlag D-52425 Jülich Telefon (02461) 61-5368 · Telefax (02461) 61-6103 E-Mail: zb-publikation@fz-juelich.de Internet: http://www.fz-juelich.de/zb
Umschlaggestaltung:	Grafische Medien, Forschungszentrum Jülich GmbH
Druck:	Druckerei Mainz GmbH, Aachen

Schriften des Forschungszentrums Jülich
Reihe Energie & Umwelt / Energy & Environment Band / Volume 184

ISSN 1866-1793
ISBN 978-3-89336-893-8

Vollständig frei verfügbar im Internet auf dem Jülicher Open Access Server (JUWEL)
unter http://www.fz-juelich.de/zb/juwel

Preface

Successful proof of low degradation rates and lifetimes meeting market introduction requirements were the major achievements of our long-standing fuel cell research within the last two years. In the context of the transformation of the German energy sector, water electrolysis for energy storage was reintroduced into the research portfolio. A strong group of 15 staff is established with the perspective of expansion to over 20 staff in the next two years. The focus is set on polymer membrane electrolysis and modeling of alkaline electrolyzers. Battery research was included in the portfolio through systems analysis as a first step and is now being extended to in operando visualization and analytics of passive layers on lithium ion battery materials. The systems analysis group was geared toward hydrogen infrastructure investigations in view of increasing demand for energy storage of renewable energy. On the other hand, the carbon capture activities which were planned for further expansion were reduced in the wake of the political decision not to pass the envisaged law for carbon dioxide storage and the following sobering appreciation by industry. Nonetheless, a very successful international conference, the 3rd CEPE, was held on the subject with substantial involvement and support from the IEK-3. Besides the conference proceedings a comprehensive book was edited in summer 2011, just before the aforementioned lack of clarity for carbon dioxide storage gave rise to let the activity taper off to the level of observation. Membrane separation and carbon capture for carbon dioxide reuse are still vital research objects.

These major changes in the portfolio caused a name change from Institute for Fuel Cells to Institute for Electrochemical Process Engineering. It covers the interdisciplinary work from fundamental electrochemistry and modeling, via electrode, membrane-electrode-assembly and stack design, analytics and manufacture up to process engineering of subsystems and systems, including systems analysis for the focus areas of the institute.

Select notable results are the life time proof of an SOFC stack over 53,000 hours with a degradation of about 0.8%/1000 hours in realistic operating conditions. A further stack has already achieved 23,000 hours of operation exhibiting a degradation of only 0.2%/1000 hours, thanks to a new coating of the metal interconnects. In addition a 20 kW system based on four stacks was successfully tested. The autothermal reforming of kerosene was proven with a stable conversion rate of 99.997 % over 5000 hours. An integrated system comprising two HT-PEFC stacks and a fuel processing unit scored an electrical power of 5.6 kW in a test with gas-to-liquid kerosene. Moreover, a 2 kW direct methanol fuel cell system powering a forklift was dynamically operated in a test bed for 20,000 hours under a real driving profile gathered from the same type of battery forklift operated in a typical warehouse. The test was terminated after the system reached 20,000 hours, which is the nominal lifetime of the forklift itself. For these results the ‘f-cell Award Innovation Price Fuel Cell’ was granted.

I would like to express my gratitude to all of my colleagues at IEK-3 for their involvement, dedication and their good ideas. I would also like to thank the BMBF for the continuous and profound funding and the cooperation partners in industry and other research organizations for the confidence in our institute.

Jülich, September 2013

1

ICEPE

Contributions to the International Conference on Energy Process Engineering (ICEPE)

- Preparation, organization and result of the 2nd ICEPE 2011
- Scientific coordination of the 3rd ICEPE 2013
- Outlook for the 4th ICEPE 2015

1.1 Preparation, organization and result of the 2nd ICEPE 2011

ProcessNet – an initiative of DECHEMA e.V. and VDI-GVC – works on behalf of professional bodies in the areas of process engineering, chemical engineering and industrial chemistry. This includes organizing a range of events on current topics in the three fields. The Energy Process Engineering subject division headed by Prof. Stolten organized the 2nd International Conference on Energy Process Engineering (ICEPE) in 2011 on efficient carbon capture for coal power plants. The international conference targeted not only scientists but also interested individuals from the private and political sectors. It aimed to provide a detailed overview of the current state of the art of science and technology in the area of industrial CO_2 capture. The organizing committee was chaired by Prof. Detlef Stolten and Prof. Viktor Scherer was co-chairman. Around 240 participants from 14 countries attended the 2nd ICEPE 2011, which took place from 20 – 22 June 2011 in Frankfurt am Main.

1.1.1 Scientific coordination

The conference topic was introduced in plenary sessions on the first day with six presentations on the potentials, industry perspectives and technological options for efficient CO_2 capture for coal power plants. The second day began with a plenary session on the physics of membrane separation. The conference was concluded with two plenary sessions on downstream gas separation processes. These presentations dealt with the compression and pipeline transport of carbon dioxide. The conference comprised a total of 72 scientific and technical presentations on the main topics of materials, processes, plants and framework conditions. Each of the main topics comprised up to eight detailed topics, which involved 16 review presentations by experts, each lasting approx. 25 – 30 mins. An overview of the detailed topics is shown in Tab. 1.

Emphasis	Session Topic	Code	Session Chair
Materials	Chemical Absorbtion Materials	M1	K. Thomsen, Denmark
	Physical Absorbtion Materials	M2	M. Grünewald, Germany
	Inorganic Membranes	M3	W.A. Meulenberg, Germany
	Polymer Membranen for Seperation of CO_2	M4	V. Abetz, Germany
	Chemical Looping Materials	M5	A. Lyngfelt, Sweden
Process Engineering	Oxyfuels with Cryogenic Air Separation	P1	A. Kather, Germany
	Post-Combustion with Chemical Absorption	P2	H. Fahlenkamp, Germany
	Pre-Combustion with Physical Absorption	P3	van den Brink, Netherlands
	Pre-Combustion with Membranes	P4	T. Melin, Germany
	Oxyfuel Combustion with O_2 Transport Membranes	P5	M. Modigell, Germany
	Pre-Combustion Capture with Membranes	P6	V. Scherer, Germany
	Chemical Looping in Power Plants	P7	B. Epple, Germany
	Terrestrial Storage	P8	K. Lackner, USA
Plants	CCS for Gas Power Plants	GAS	C. Bauer, Switzerland
	Plant Engineering		F. Wohnstand, Germany
Frame Conditions	Economics, Politics and Life Cycle Assessment	EPL	P. Viebahn, Germany

Tab. 1: Overview of detailed topics

Depending on the topic, between three and eight 25-minute presentations were given, each focusing on specific aspects of the topic at hand. This part of program was organized in three parallel sessions, which took up the first afternoon, the whole of the second day and most of

the morning on the last day of the conference. Poster sessions with a total of 27 scientific and technical posters were held during the social event at the end of the first day and the two-hour lunch break on the second day of the conference. The conference dinner and reception on the second day of the conference provided an ideal backdrop for presenting awards to the best three posters.

1.1.2 IEK-3 conference contributions

IEK-3 scientists working on research and development in the area of gas separation within power plant engineering were involved on all levels of ICEPE 2011. IEK-3 was represented by four presentations and three posters. Tab. 2 provides an overview of the different conference contributions.

Presentation Typ	Session Topic	Presentation Topic	Speaker
Overview	Plenum	Carbon Capture Options for Coal Power Plants	Detlef Stolten
	M2	Physical Absorption Materials for CO_2 Capture	Sebastian Schiebahn
Parallel	P4	Cascaded Membrane Processes for Post-Combustion CO_2 Capture	Li Zhao
	P5	Oxygen Supply for Oxyfuel Power Plants by Oxy-Vac-Jül Process	Michael Weber
Poster	P6	Integration of Water-Gas Shift Membrane Reactor in IGCC for Pre-Combustion Capture	Sebastian Schiebahn
	P7	CO_2 Separation from a Thermodynamic Viewpoint: 100% - Pure - Reversible	Ernst Riensche
	P7	CO_2 Absorbtion by MEA Scrubbing: Impact of Process Design Parameters on the Thermal Energy Consumption	Alexander Otto

Tab. 2: Presentations and posters by IEK-3 scientists

Prof. Stolten provided an introduction to the technological options for carbon capture in his plenary presentation. Another highlight was Mr. Schiebahn's review presentation on physical absorption materials. Process engineering aspects were covered by presentations by Dr. Zhao and Dr. Weber. Three posters rounded off the contributions made by IEK-3 to ICEPE 2011.

1.1.3 Books and series of publications

VCH and edited by the conference chairmen Prof. Stolten and Prof. Scherer (see Fig. 1, left), was distributed to all participants together with the conference documentation. The 619-page book contained the full texts of most of the plenary sessions and review presentations at the 2nd ICEPE 2011. It is intended as a comprehensive reference work providing experienced experts with access to data and publications and inexperienced individuals interested in the field with an introduction to the topic. It contains a total of 21 articles with an average length of 30 pages, which have been broken down into the following sections:

- Introduction and Overview
- CO_2 Scrubbing
- CO_2 Removal with Cryogenic Air Separation
- Separation with Membranes
- Chemical Looping for CO_2 Separation
- Transportation and Storage of CO_2

IEK-3 scientists wrote two review articles, thus making a significant contribution to the book.

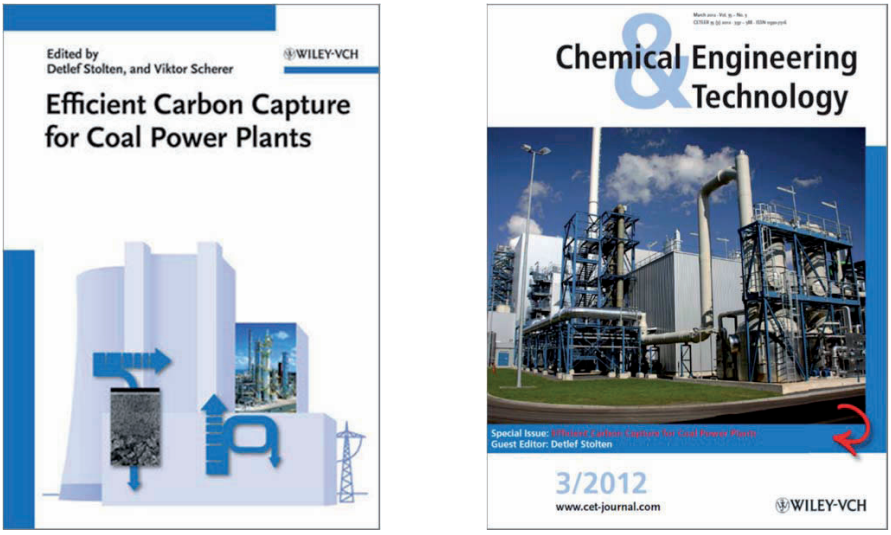

Fig. 1: Book comprising plenary and review articles (left) and journal containing selected conference papers (right)

About a year after the 2nd ICEPE 2011, a selection of 21 conference papers were published by WILEY-VCH in the journal “Chemical Engineering & Technology” (see Fig. 1, right). On 180 pages, the most important aspects of efficient CO_2 capture for coal power plants were outlined and explained, and experiments and operating results were documented. IEK-3 scientists contributed two articles dealing with different methods of integrating gas separation membranes into power plant processes. They detailed aspects associated with design and discussed their performance.

1.2 Scientific coordination of the 3rd ICEPE 2013

The third International Conference on Energy Process Engineering (3rd ICEPE 2013) focuses on concepts and large-scale technology applications that will facilitate the transition from the existing fossil-based energy supply system to a renewable energy system in the foreseeable future. Selected presentations will outline how the future energy market can react to the dwindling and evermore expensive fossil energy reserves, the shutting down of nuclear power plants, and the relationship between CO_2 emissions, global warming and environmental catastrophes. Technological progress over the last decade has shown that renewable energies have the potential to cover a substantial proportion of the energy supply on both a regional and national level. The preliminary program for the 3rd ICEPE is shown in Fig. 2. It has been divided into three main parts.

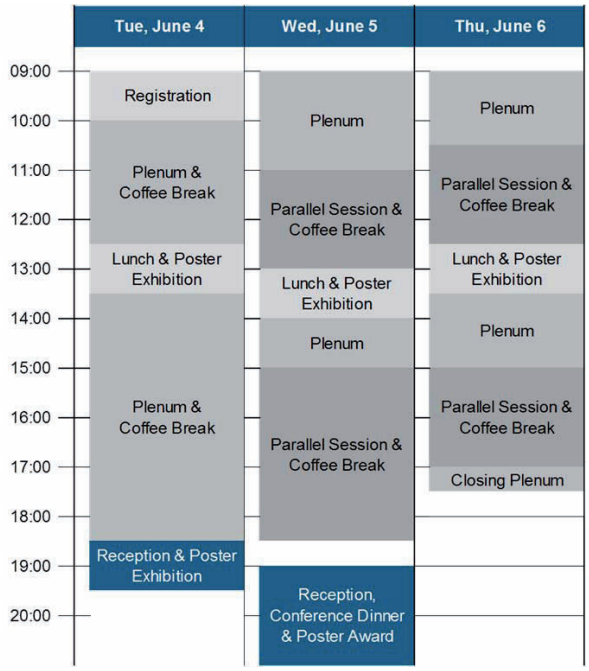

Fig. 2: Overview of topics

The presentations in the plenary session on the first day of the conference will outline comprehensive energy supply strategies from energy provision to consumption. During the days that follow, the presentations will focus on the economic and ecological prospects of a transition to renewables, as well as on the more general technical aspects of energy transport and energy storage in relation to renewables. A total of 26 speakers from nine countries have been invited to give presentations in the plenary sessions.

Topic Field	Power Generation	Gas Production	Biomass & Biofuels	Energy Storage	Energy Distribution	End-user Technologies	Other
Topic	Onshore Wind Power Offshore Wind Power Photovoltaic Power Solarthermal Power Maritime Power Hydro Power Geothermal Power Futur Role of Fossil Power Plants	Chemical Gas Production Electrochemical Gas Production Photoelectrical Gas Production	Globale Aspects & Resources Biomass for Power Production Biofuels	Pumped Storage Hydropower Geological Gas Storage Near Surface Gas Storage Advanced Batteries	Smart Grid Power-to-Gas Technology	Sustainable Buildings - Europe Sustainable Buildings E-Mobility	Emerging & Developing Countries

Tab. 3: Overview of topics

The four parallel sessions on the second and third days will deal with 24 different topics related to renewable energy systems. Each topic will be introduced by a review presentation outlining the basic principles, technological implementation, present state of the art in science and technology and recommend references. These will be followed by three more detailed presentations dealing with specific aspects of the topic with reference to the latest scientific and technological knowledge. Tab. 3 provides an overview of the selected topics.

Each day of the conference will also feature poster presentations. The posters will be showcased throughout the conference and the poster presenters will be available to discuss their results in detail with interested conference delegates during the breaks.

1.3 Outlook for the 4th ICEPE 2015

The decision on the strategic orientation and thematic focus of the next conference in the series of ICEPE conferences held every two years will be made by the Energy Process Engineering Expert Committee of VDI-GVC and ProcessNet of DECHEMA. Prof. Stolten plays a key role here as head of the committee. The first suggestions for topics made by committee members focus on the generation, processing, distribution and use of next-generation fuels for all transportation sectors. The 4th ICEPE 2015 would thus discuss the energy process steps of relevant process chains from a scientific and technical point of view and relate them to their economic, ecological and energy policy impacts. This would allow the next ICEPE to make an important contribution to estimating the future potential of biofuels and to provide the sectors of science, industry and politics with a platform for exchanging knowledge.

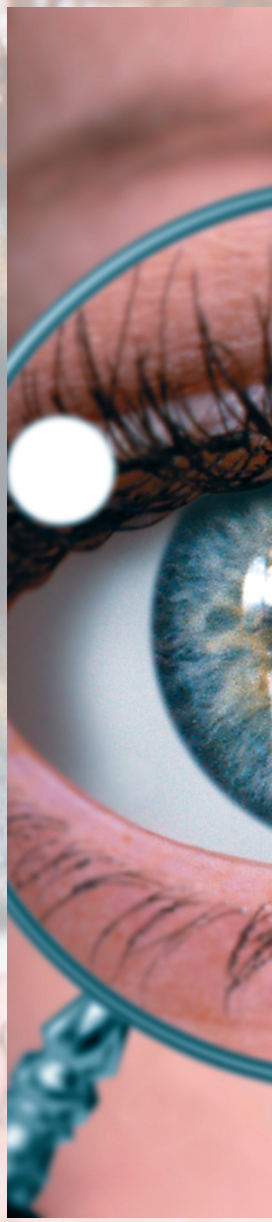

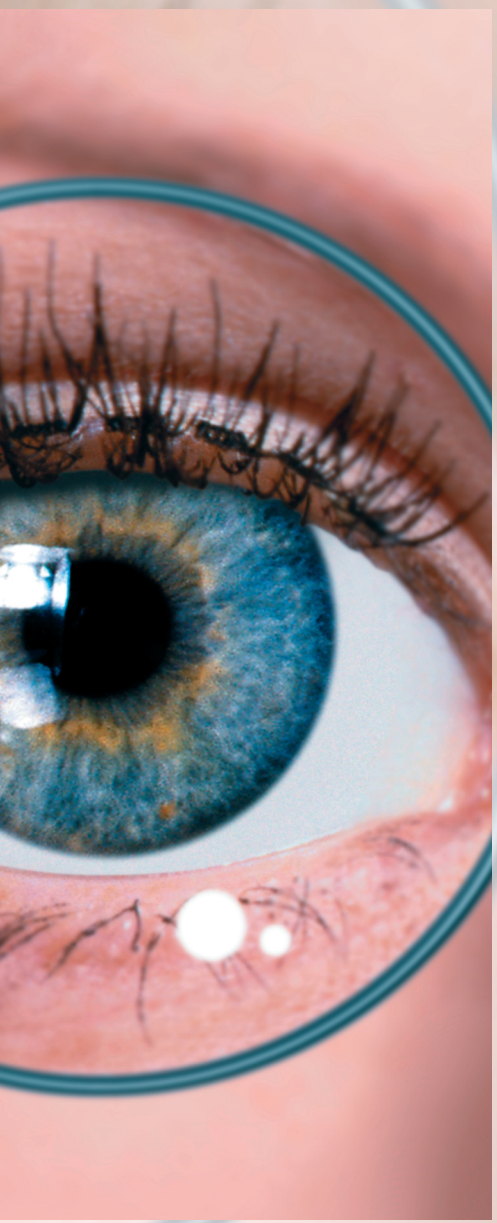

2

Education

Education and Training

- University education
- Contributions to information provision, further education and training

In keeping with the guiding principles of IEK-3, several research scientists at the institute are committed not only to producing knowledge in the fields of advanced energy conversion technologies but also to specialized education and further training. This is reflected in contributions to the education of undergraduates (see Fig. 3), postgraduates and PhD students as young scientists, as well as contributions to the training of qualified personnel for laboratories, and specialized scholarships for mathematical and technical software developers. IEK-3 employees also contribute to a range of information and further education events for different target groups.

2.1 University education

RWTH RHEINISCH-WESTFÄLISCHE TECHNISCHE HOCHSCHULE AACHEN	http:///www.rwth-aachen.de/
ulm university universität uulm	http://www.uni-ulm.de/
JUSTUS-LIEBIG-UNIVERSITÄT GIESSEN	http://www.uni-giessen.de/
FH AACHEN UNIVERSITY OF APPLIED SCIENCES	http://www.fh-aachen.de/

Fig. 3: Universities where IEK-3 staff lecture

The spectrum of topics taught ranges from the fundamentals of science and theoretical modeling and simulation methods to detailed technical knowledge and the characterization of technical applications. In total, seven lectures and three tutorials are offered each semester in the form of 1.5-hour blocks. An additional half-day practical course is offered every summer semester. Up to eighty students participate in the individual courses each semester. The scientists at IEK-3 also play an important role in supervising term papers, undergraduate dissertations and PhD theses. In 2011, seven diploma/master's dissertations were successfully submitted as was one PhD thesis. In 2012, eight undergraduate/master's dissertations and five PhD theses were completed.

2.1.1 Courses taught by professors

Tab. 4 provides an overview of the courses taught at universities by the professors at IEK-3.

Name	Subject area	Type/extent semester		University
Prof. L. Blum	Brennstoffzellen – Die Zukunft der dezentralen Energieversorgung!?	V/2	WS	Aachen Univ. of Applied Sciences, Campus Jülich
	Fuel Cells – The Future for Dispersed Power Supply!?	V/2	WS	
Prof. Dr. W. Lehnert	Modellierung in der Elektrochemischen Verfahrenstechnik (*Modeling in Electrochemical Process Engineering*)	V/2 Ü/2	WS	RWTH Aachen Univ. since WS12/13
Prof. Dr. R. Peters	Basics and Applications of Chemical Reaction Theory – Simulation of Dynamic Processes in Energy Systems with Matlab/Simulink	V/2 Ü/2	WS	Aachen Univ. of Applied Sciences, Campus Jülich
Prof. Dr. D. Stolten	Grundlagen und Technik der Brennstoffzellen (*Principles and Technology of Fuel Cells*)	V/2 Ü/2	WS	RWTH Aachen University

Tab. 4: Courses taught by professors

2.1.1.1 Brennstoffzellen – Die Zukunft der dezentralen Energieversorgung!? (Fuel Cells – The Future of Decentralized Energy Supply!?)

Prof. Ludger Blum teaches fuel cell technology at Aachen University of Applied Sciences, Campus Jülich. The optional subject “Fuel Cells for Stationary Applications” in the bachelor’s course on energy and environmental technology and the Master of Science in Energy Systems covers the function, construction, behavior, advantages and disadvantages of different types of fuel cells. It also lays the groundwork for the process engineering design of fuel cell systems. The topics include: basic principles of fuel cells; fuel supply; efficiency, function and construction of different types of fuel cells; fuel cell system requirements; process engineering of various fuel cell systems for different applications; energy balance of a fuel cell system; and modern plant engineering. An average of 20 – 30 students in the master’s program take these courses, and an average of 10 in the bachelor’s program.

2.1.1.2 Modellierung in der Elektrochemischen Verfahrenstechnik (Modeling in Electrochemical Process Engineering)

Prof. Werner Lehnert teaches modeling in electrochemical process engineering at RWTH Aachen University. His lecture course focuses on the mathematical description of electrochemical converter systems. In addition to the basic approach for modeling, different modeling techniques are also outlined. Low- and high-temperature fuel cells are used as examples to develop 1D, 2D and 3D models with varying degrees of complexity and their validity is then discussed. The application examples are used as a basis to mathematically describe the interactions of mass and heat transport with the electrochemical processes. One priority is the description of processes in the porous components in fuel cells. The lecture was offered for the first time in winter semester 2012/2013 and was attended by six students.

2.1.1.3 Basics and applications of chemical reaction theory – simulation of dynamic processes in energy systems with MATLAB/Simulink

Prof. Dr.-Ing. Ralf Peters is responsible for teaching energy process engineering at Aachen University of Applied Sciences, Campus Jülich. The course “Basics and applications of chemical reaction theory – Simulation of dynamic processes in energy systems with Matlab/Simulink” links the basic principles of chemical process engineering with dynamic simulations of reactors. The lectures and tutorials use the following as examples: fuel processing and fuel cell system technology for methanol fuel cell drive systems and for diesel-based on-board power supply. The course is compulsory for the 30 – 40 students enrolled in the Master of Science in Energy Systems.

2.1.1.4 Grundlagen und Technik der Brennstoffzellen (Principles and Technology of Fuel Cells)

Prof. Dr.-Ing. Detlef Stolten holds the Chair for Fuel Cells at RWTH Aachen University. The courses offered deal with the conversion of renewable and fossil energy carriers for use in fuel cells for portable, stationary and mobile applications. The process engineering and systems technology aspects cover high-temperature and low-temperature fuel cells, as well as the processing of specific fuels for fuel cells. These elements are accompanied by an examination of the basic physical and chemical principles involved. Systems analysis studies on energy process engineering, including cost estimates, provide a holistic coverage of the subject with a view to future market launch. During the 2012/2013 winter semester, more than 80 students attended the lectures and seminars. As part of the existing cooperation with Forschungszentrum Jülich, the chair offers students the chance to work on term papers and undergraduate dissertations and also provides them with an opportunity to work on projects as research assistants.

2.1.2 Courses taught by university lecturers

Tab. 5 provides an overview of the courses taught at universities by the professors at IEK-3.

Name	Subject area	Type/extent	semester	University
T. Grube	Basics and Applications of Chemical Reaction Theory – Simulation of Dynamic Processes in Energy Systems with Matlab/Simulink	Ü/2	WS	Aachen Univ. of Applied Sciences, Campus Jülich
PD Dr. C. Korte	Physikalisch-Chemische Methoden zur Präparation und Charakterisierung von dünnen Schichten (*Physical and Chemical Methods for the Preparation and Characterization of Thin Films*)	S/2 (block)	SS	Justus Liebig University Gießen
Dr. W. Lehnert	Simulation and Modeling	V/2	WS	University of Ulm until WS11/12
	Fundamentals of Chemical and Electrochemical Process Engineering	V/2	WS	
Dr. Martin Müller	Grundlagen und Technik der Brennstoffzellen (*Principles and Technology of Fuel Cells*)	Ü/2	WS	RWTH Aachen University

Tab. 5: Courses taught by university lecturers

2.1.2.1 Physikalisch-Chemische Methoden zur Präparation und Charakterisierung von dünnen Schichten (Physical and Chemical Methods for the Preparation and Characterization of Thin Films)

Dr. Carsten Korte teaches a seminar course in the Faculty of Biology and Chemistry at Justus Liebig University Gießen. The seminar provides a comprehensive introduction to the preparation and analysis of thin oxide-ceramic films and their use in technical applications. It is aimed at all interested students taking master's courses in chemistry, physics and materials science, as well as at PhD students in the same fields. The course looks at the most important vacuum evaporation processes, including thermal evaporation, sputtering methods, chemical vapor deposition (CVD), molecular beam epitaxy (MBE) and pulsed laser deposition (PLD). Particular emphasis is placed on pulsed laser deposition (PLD). Another topic from the field of preparation is the growth modi for large and small layer thicknesses, which determine the layer morphology, and their dependence on surface energy and surface diffusion. The analytical methods presented are X-ray diffraction (XRD, pole figures, reflectometry), electron microscopy (SEM, TEM) and the associated electron diffraction techniques (EBSD, SAED). A follow-up seminar looks at examples from the literature and discusses them. An average of five students per summer semester took the block seminar.

2.1.2.2 Simulation and Modeling

Dr. Werner Lehnert teaches a lecture series on simulation and modeling during winter semester that is compulsory for students taking the Energy Science and Technology master's course at the University of Ulm. The students are taught the principles of process engineering modeling and simulation. The mathematical description of electrochemical processes and mass and heat transfer phenomena are an important focus of the lectures. How the different processes are coupled is demonstrated using fuel cells. In addition to models describing the operating behavior on a cell level, stack models are also presented that are capable of describing complex behavior in relation to flow, heat balance and electrochemical reactions. An average of 15 students attended the lectures.

2.1.2.3 Fundamentals of Chemical and Electrochemical Process Engineering

Dr. Werner Lehnert lectures at the University of Ulm. The lecture course "Fundamentals of Chemical and Electrochemical Process Engineering" is part of the Energy Science and Technology master's course and takes place during winter semester. The main issues addressed are mass and heat transport processes in electrochemical process engineering and the energy balance of reactors. Different types of electrochemical reactors and their applications in an industrial setting are also dealt with. An average of 12 students attended the lectures.

2.1.2.4 Grundlagen und Technik der Brennstoffzellen (Principles and Technology of Fuel Cells)

Dr. Müller assists Prof. Stolten in his lecturing responsibilities, teaching seminars and conducting examinations at RWTH Aachen University.

2.2 Contributions to information provision, further education and training

The range of events organized to provide information and further education is just as diverse as the needs of the groups themselves. In order to adequately meet the demands made on a research institute to provide training and information, a variety of different events are organized by IEK-3. IEK-3 is also involved in external events on various levels and it works with other institutions preparing, coordinating and offering support.

2.2.1 Contributions to information provision, further education and training

The range of events organized to provide information and further education is just as diverse as the needs of the groups themselves. In order to adequately meet the demands made on a research institute to provide training and information, a variety of different events are organized by IEK-3. IEK-3 is also involved in external events on various levels and it works with other institutions preparing, coordinating and offering support.

The topics dealt with at the events depend on the requirements and requests of each target group. In other words, the events range from information events and training courses for secondary-school students, university students, teachers, tradesmen, technicians, engineers and scientists to practical courses on career choice and work experience for secondary-school students, as well as vocational training and study-related placements for undergraduates and postgraduates. The length of each of the events ranges from a half-day to several weeks depending on the situation. The tasks assigned to secondary-school students and university students during a placement include shadowing technical and scientific staff at the institute as well as supervised independent work on selected practical projects.

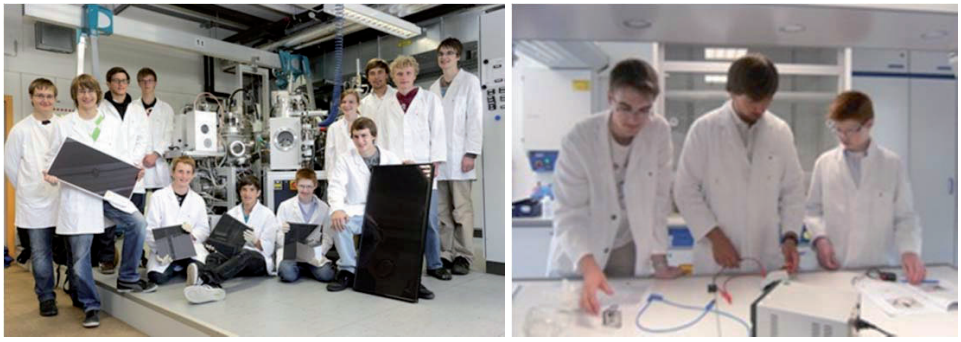

Fig. 4: Participants in the research week (left) and conducting experiments (right)

- Information events and visits to the institute for individuals interested in Jülich's contribution to research and development on fuel cell technology. Every year, an average of 60 guided tours are organized at IEK-3 with approximately 20 people per tour, each of which is headed by two PhD students.
- Vocational training and work experience for secondary-school students from local schools on the topic of "Specialist careers in fuel cell technology" (2011: 3 school students and 2012: no students on placement). The range of activities offered cover a

broad interdisciplinary range of topics. Placements for secondary-school students are generally for one or two weeks depending on requirements.

- Seminar on “Energy from fuel cells” for students involved in the ProMINat academy as part of the research placements offered at Jülich in July 2011 and in June 2012.
- Experiments and tours of the research field of fuel cells as part of the JuLab research week “Energy – Researching for the Future” for 12 secondary-school students from local schools at the end of August/beginning of September 2011 (see Fig. 4).

2.2.2 Involvement in external events

Several scientists from IEK-3 gave review presentations and more in-depth specialized presentations on fuel cells and hydrogen at a number of external events as invited experts.

- With review and in-depth presentations as well as scientific posters, scientists at IEK-3 played an important role in the success of the 2nd ICEPE 2011 in Frankfurt am Main (vgl. 1.1.2).
- Workshops and courses for developers and users of fuel cells in the “Polymer Electrolyte Fuel Cell Introduction Course (PEFC)” as part of the WBZU events in Ulm. The course is offered every year in March. One IEK-3 scientist gave two presentations on each of the specialized topics of “Lifetime Aspects of PEFC” and “Porous Media”.
- International summer schools for “Advanced Studies of Polymer Electrolyte Fuel Cells” in 2011 and 2012 featured lectures on “Modeling of Fuel Cells”. IEK-3 was also involved in the first European summer school on “Fuel Cell and Hydrogen Technology” in 2011, with two lectures on “Proton Exchange Fuel Cells & Direct Methanol Fuel Cells: Materials, Experiences, Challenges” and “Macroscopic Modelling of Fuel Cell Degradation”. The second European summer school on “Fuel Cell and Hydrogen Technology” was held in 2012, and IEK-3 scientists gave presentations on six specialized topics: “Modeling Basics”, “Macroscopic Modeling of Fuel Cells Degradation”, “Thermo-mechanical Modeling”, “Multi Physics Modeling”, “PEM Electrolysers – Materials, Properties and Challenges” and “Electrolysis – Technological Status and Future”.

2.2.3 Collaboration with other organizations

More and more attention is being devoted to designing, launching and implementing training and further education measures and qualification programs focusing on fuel cell technology both in the manufacturing industry and in the relevant educational establishments. In order to cater for this demand, special initiatives have been launched. The combination of specialist technical knowledge and existing opportunities provide an excellent basis for collaboration.

- Involvement in the Fuel Cells Qualification Initiative (IQ-BZ), working to implement information and training measures for fuel cell and hydrogen technologies.
- Promotion and sale of a “Fuel Cells” CD-ROM through the Federal Technology Centre for Electrical Engineering and Information Technology, Oldenburg, and Vogel Industrie Medien GmbH, Würzburg, which is designed to provide information, increase the acceptance of fuel cells, and promote further training and education.

- Adaptation of existing teaching modules to meet consumer demands.
- Support and incorporation of training centers and centers of excellence (WBZU and RAG Bildung) in the planning and realization of joint training events held at the respective center.
- Involvement in the school student competition “Fuel Cell Box”, organized annually by the EnergyAgency.NRW: assessment of the theoretical and practical results of 20 teams of students in the final round of the competition. In Fig. 5, the winning teams in 2011 and 2012 are pictured holding their certificates together with the organizers.

Fig. 5: **The winning teams of secondary-school students receive their certificates from Minister Remmel in 2011 (left) and from State Secretary Paschedag in 2012 (right)**

The Jülich Schools Laboratory has set itself the task of introducing students to the research and development activities of Forschungszentrum Jülich and showing them what careers are out there by encouraging them to conduct their own experiments. IEK-3 represented the area of energy and climate research and developed and created experiments and operating procedures from the world of hydrogen and fuel cells. Five experiments aimed to motivate school students to solve the following theoretical and practical tasks:

Fig. 6: **Secondary-school students conduct their own experiments in the IEK-3 laboratories during the 2012 careers week**

- Experiments with fuel cells
- Creating an LED lighting system for the fuel cell model car
- Constructing a bumper for the fuel cell model car
- Setting up (Fig. 6, left) and measuring (Fig. 6, right) a membrane electrode assembly in a fuel cell

School students were also given an overview of energy technology with fuel cells, a tour of the IEK-3 laboratories, and a chance to speak to employees working in different areas of the scientific institutes. The supervised experiments and operating procedures in the Schools Laboratory, in the training centers and in IEK-3 gave students an opportunity to put what they have learnt in chemistry and physics class into practice and fostered their craftsmanship skills. A total of nine (2011) and ten (2012) school students aged between 15 and 18 (grades 9 to 13) participated in the five-day programs.

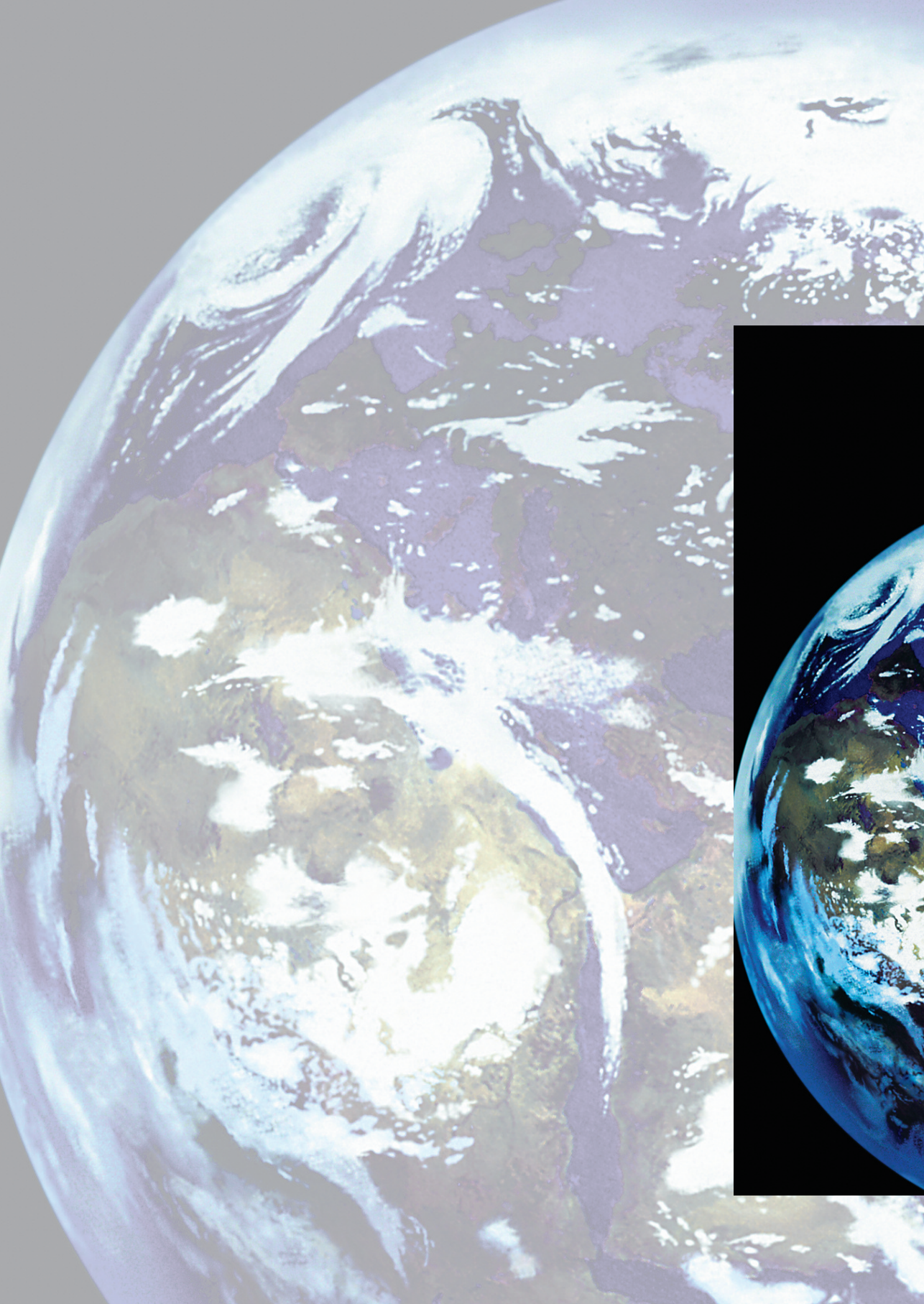

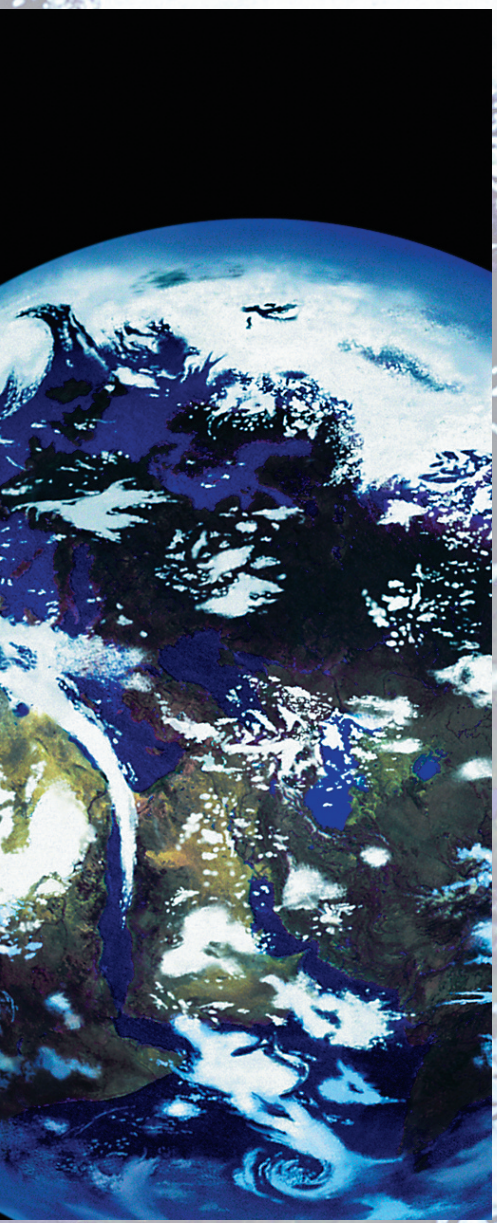

3

Reports

Scientific and Technical Reports

- Solid oxide fuel cells
- Fuel processing systems
- High-temperature polymer electrolyte fuel cells
- Direct methanol fuel cells
- Polymer electrolyte membrane electrolysis
- Process and systems analysis
- Analysis
- Quality assurance

3.1 Solid oxide fuel cells

3.1.1 Objectives and fields of activity

Cells, components, stacks and systems are being developed within the fuel cells program topic for high-temperature fuel cells with solid electrolytes (SOFCs). This topic is strategically directed at the highly efficient provision of electric energy for mobile and stationary applications, both in a decentralized and centralized context, on a scale ranging from a few kilowatts up to several hundred kilowatts. Research focuses on increased power density, long lifetimes, the identification of degradation mechanisms in the stack and how to prevent them, advanced design, and highly integrated system engineering. Development work led to improved materials for cells, as well as improved joining techniques for stacks and highly integrated system components, and the first 20 kW system. Important supporting activities include the modeling of mechanical and thermal component loads as well as the development and characterization of components for fuel cell systems and their evaluation by means of process engineering analyses.

3.1.2 Important results

3.1.2.1 Tests with cassette stacks

As one of the newer research lines, cassette or lightweight stacks are being developed for use as auxiliary power units (APUs) in vehicles. This application is particularly demanding in terms of the thermal cyclability of the stack.

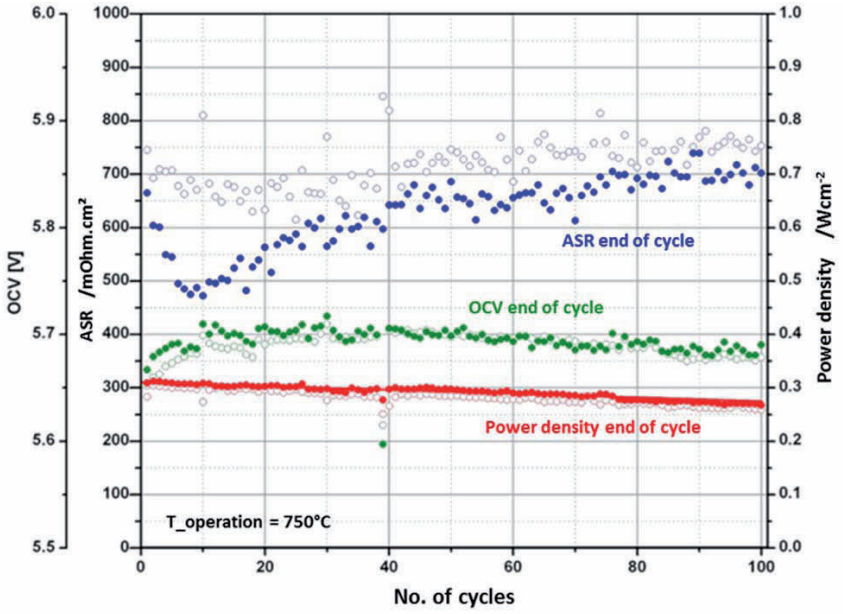

Fig. 7: CSII05-04: OCV, resistance and power density as a function of number of cycles

Thermal cycling tests (750 °C → 50 °C → 750 °C) were performed on the lightweight stack CSII05-04 with a heating rate of 10 K/min. The aim of the tests was to achieve 100 deep thermal cycles. The stack lost 15 % of its initial power (the cell resistance rose correspondingly from approx. 650 to 750 m Ωm²). The change in open circuit voltage (OCV) was extremely small and in relation to the maximal value after approx. 10 cycles was only 6 mV per cell (see Fig. 7). However, the leak test performed after it had been removed from the test stand showed clear internal and external leakages. This design therefore still requires considerable development work, particularly in terms of thermomechanical load capacity. An application was made to the EU in cooperation with national and international partners for support in implementing existing findings. The project “MMLCR” was approved on 1 January 2012 and work began on redesigning and optimizing joining techniques.

3.1.2.2 Stack technology of the kW class with improved performance

Stack joining

Stack development work focused on the proof of a stack design, suitable for use in a real-world environment, operated with different fuels with high efficiency. Stacks comprising larger cells with outer dimensions of 20 x 20 cm² with an effective electrode area of 360 cm² have been used in tests since 2000. After the demonstration of a first 1 kW stack at the end of 2000, followed by stacks with 9.2 kW in 2002 and 13.3 kW in 2004, the main focus was on improving the stack thermomechanical robustness. A key issue here is the transfer of the sealed and reduced stack from the furnace to the system, which leads to different and more pronounced requirements on the thermomechanical stability of the stack. A large number of investigations and improvements – design, operating conditions, materials, quality assurance – were necessary to reach a stage where a stack can be transferred to a system [1].

A generally accepted requirement is a leakage rate of less than 1 % of the fuel fed into the stack. Recent results with larger stacks after the first thermal cycle are about two orders of magnitude below this threshold. Numerous dummy-stack tests and tests with specially designed electrically heated dummies for fast thermal cycling tests were performed to investigate different designs and materials. Finally, improvement was mainly achieved by adapting the sealing process, and by optimizing the interconnect geometry with respect to reduced thermomechanical stress caused by temperature gradients during operation. An essential contribution to this work was provided by finite element modeling (FEM) based on CFD stack modeling coupled with validation results from stack post-test analysis (see Fig. 8) [2].

Problems were repeatedly observed as the stack subsided during the joining process despite the fact that the joining of the planes was considerably improved by structural modifications. In order to eliminate the remaining risk of components jamming, it was proposed that the guide be done away with. This should be possible, as the planes have a relatively large surface expansion and come into mechanical contact with each other during subsidence,

---

[1] Blum, I:, Groß, S.M.; Malzbender, J.; Pabst, U.; Peksen, M.; Peters, R.;. Vinke, I.C.: Investigation of solid oxide fuel cell sealing behavior under stack relevant conditions at Forschungszentrum Jülich. Journal of Power Sources 196 (2011), 7175-7181

[2] Peksen M.: A coupled 3D thermofluid–thermomechanical analysis of a planar type production scale SOFC stack. International Journal of Hydrogen Energy, 36 (2011), 11914-11928

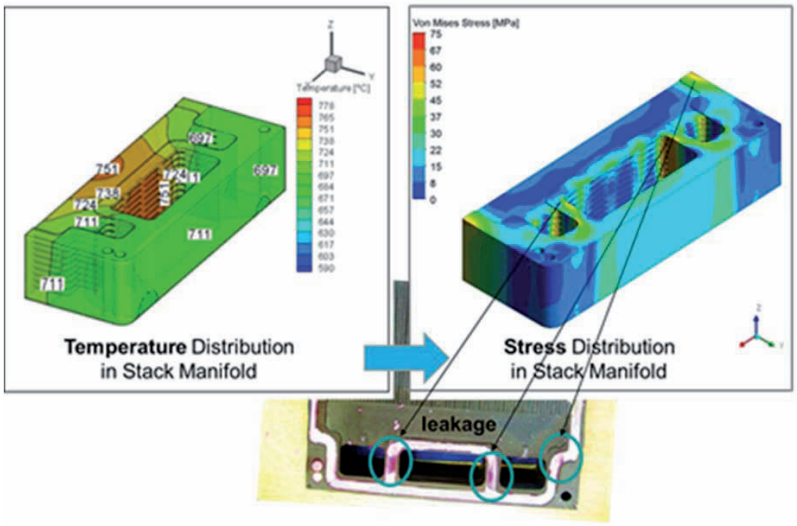

Fig. 8: **Temperature and stress distribution in the manifold of a kW stack together with the corresponding post-test analysis result**

before the glass sealant reaches a very low viscosity and the plates move against each other slightly. In order to verify this, a dummy with 72 joining planes was set up (F'2072-Dummy 34), which is equivalent to a 5 kW stack, and joined without an outer guide. The dummy and furnace were aligned to each other exactly using a LASER measuring device. The results were very positive:

- The stack exhibited internal and external tightness (better than 10^{-4} mbar.l/s)
- It showed good subsidence behavior
- The seam gaps had a uniform height:

Based on these results, all subsequent stacks with cells measuring 20 x 20 cm² were constructed without a guide and no problems were encountered.

As an alternative to the design using glass 87 (with a joining temperature of 580 °C), we tested whether it was possible to join the stack at 950 °C with glass 48, which exhibits a more suitable expansion coefficient and greater strength at operating temperature. However, this glass has the disadvantage that it is highly viscous and there is therefore a risk that the required low gap height in the cell joining region will not be achieved as the cell subsides during the joining process. A stack with five levels (F'''2005-09) was constructed and joined with the maximum possible pressing force. Due to its low power (poor contacting because of too great a joint gap) and a short circuit on level 1, the stack was cooled down again after one week. A subsequent tightness measurement revealed internal and external leakages. This ruled out glass 48 as a potential sealant for soldering technology and joining devices currently available. Work will continue on another application technique that will allow thinner solder layers.

Work on improved glass sealing material and sealing application techniques, such as green foil and screen printing, is ongoing. Here, an essential issue is the characterization of the mechanical properties of the sealing material at operating temperature.

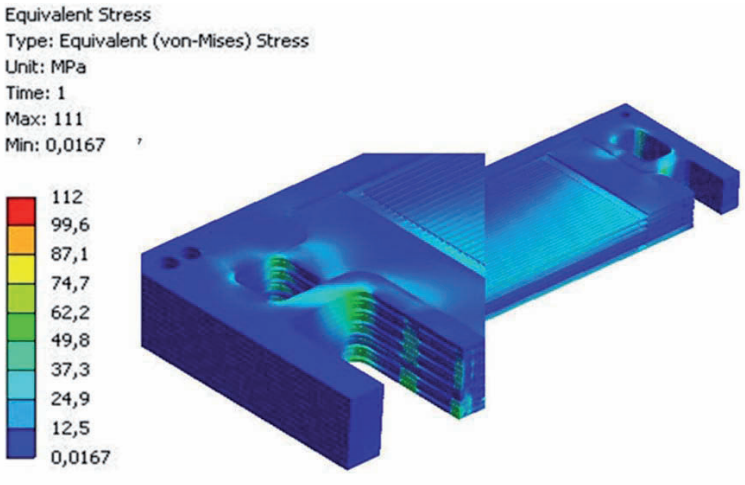

Fig. 9: **Stress distribution in the interconnect of a stack with six levels at the end of heating**

Stack design and stack modeling

An unsteady calculation was performed for heating up, operating and cooling down of a stack comprising six levels (isolated operation) with cells measuring 20 x 20 cm². The stack was heated from below by means of a heating plate (similar to the 20 kW system currently being tested). The results show that the greatest stresses in the component occurred during heating. Fig. 9 shows the distribution of the main stresses in the metallic interconnect. The highest stresses occurred in the manifold around the ribs between the gas and air channels and were max. approx. 40 MPa in the glass sealant (due to the low Young's modulus), aside from individual points in the corners of the channels. During steady-state operation, the max. stresses were identified on the long side of the stack around the maximal temperature because of the heat produced by the cell and in the area around the manifold radii. They were around 36 MPa in the glass sealant. During cooling, the max. stresses occurred near the corners of the gas/air channels and were around 16 MPa in the glass sealant for the times calculated.

Based on temperature measurement data for the stack F'''2010-13, a comparative study was performed on the thermomechanical stresses during steady-state operation of a stack comprising ten levels with cells measuring 20 x 20 cm². Operation of the stack in a furnace was compared to operation in ideal isolation. The air and fuel gas inlet sides were each analyzed. H_2 with a fuel utilization of 24 % (case 1) and CH_4 with respective fuel utilizations of 77 % (case 2) and 38 % (case 3) were taken as the operating cases. The temperature profiles measured in the stack are shown in Fig. 10. The results of the FEM analysis for metallic interconnects show that operation in the furnace led to lower maximal stress values, while the mean stress in the furnace was of a higher value than that of the stack operated in isolation. Fig. 11 shows the results of the stress calculations for the air inlet side. It can be clearly seen that the lowest stresses occur when the stack is operated in isolation with

methane and higher fuel utilization (case 2). These conditions are also closest to real operation.

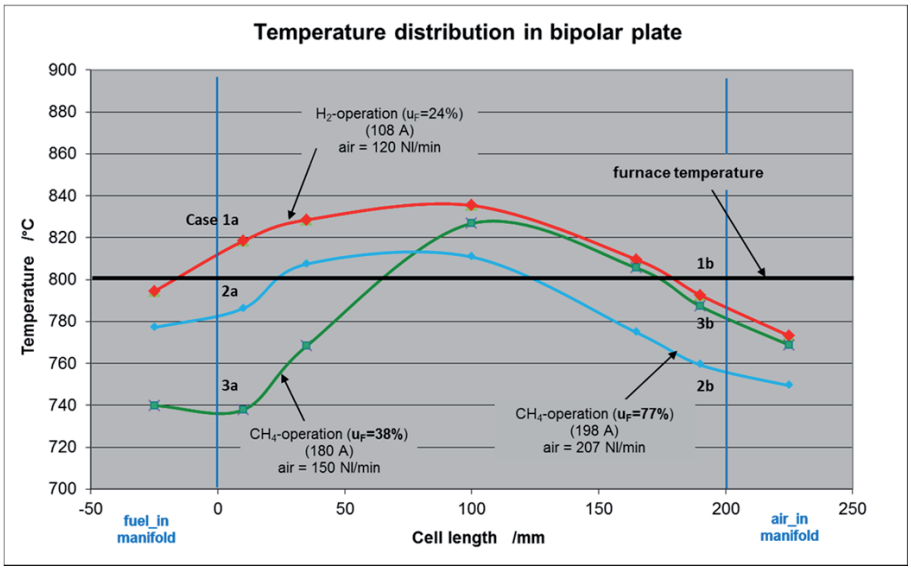

Fig. 10: **Temperature distribution in the interconnect of a stack with ten levels (F'''2010-13) during steady-state operation using different fuel gases**

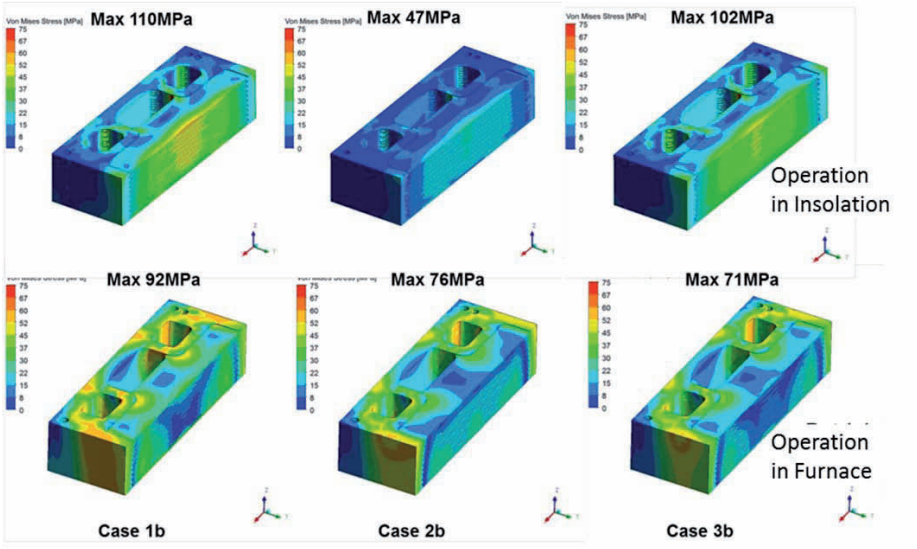

Fig. 11: **Distribution of stresses in the interconnect on the air inlet side of a stack with ten levels during steady-state operation using different fuel gases – Comparison of operation in isolation with operation in a furnace (i.e. external heating)**

In general, it can be concluded that the highest stresses occur relatively locally at the inner radii of the fuel gas and air holes. High stresses over a slightly larger area occur particularly around the ribs between the drilled holes and at the edge in the internal manifold.

Long-term stack tets

Based on the results of stack design and the long-term operation of short stacks, a 2 kW stack was built, comprising 18 layers and cells with outer dimensions of 20 x 20 cm². The aim was to demonstrate stable operation with different fuel gases at a fuel utilization of at least 60 % for 5000 hours of operation under load. On the cathode side, an MCF layer was applied by APS on the interconnect plates made of Crofer22APU. The cathodes were made of LSCF with a CGO interlayer, which was applied by screen printing. The contact layer was a perovskite (LCC10) applied by wet powder spraying. Except for layer 1 (on the bottom plate), all cells perform very well: 0.8 $A.cm^{-2}$ at 800 to 840 mV at 750 °C furnace temperature (see Fig. 12). The temperature depicted in Fig. 12 is measured in the interconnect plate in the middle of the stack half way between the fuel inlet and outlet. The stack was operated at a furnace temperature of 700 °C and a current of 180 (corresponding to 500 $mA{\cdot}cm^{-2}$) with hydrogen (approx. 500 hours) and methane (approx. 4500 hours) with an amount of internal reforming of about 90 % at a fuel utilization of 70 % (for shorter times also 60 %, 77 % and 80 %). The required 5000 hours of operation under load were achieved in July 2012. At the beginning the top layer (cell no.18) showed some contact problems, which resulted in big changes in cell voltage.

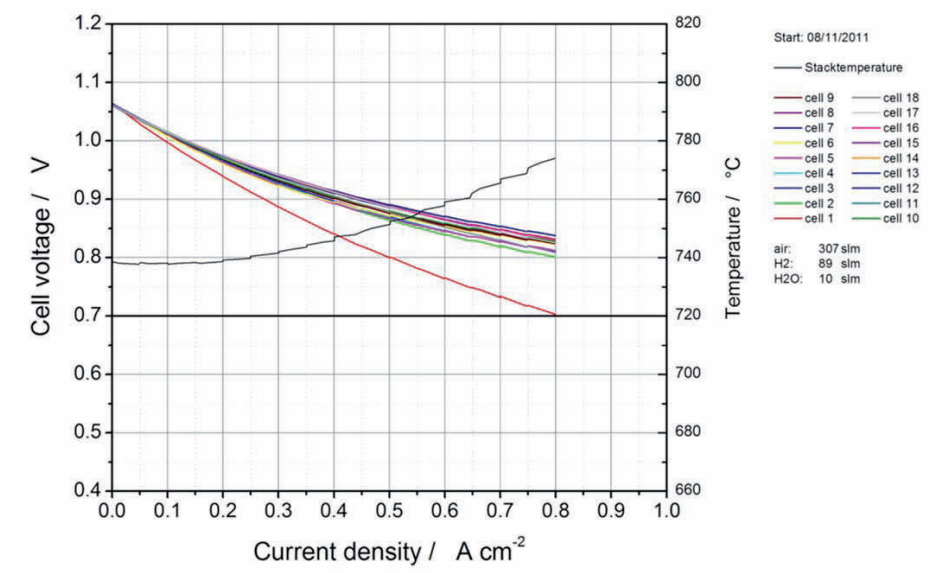

Fig. 12: Current-voltage characteristic of stack F'''2018-07

After a thermal cycle, caused by a problem with the gas supply to the building, this contact problem vanished (see Fig. 13). After 5000 hours, the stack still delivered 2.6 kW DC power. The power loss during this time (including two thermal cycles) was 1.5 %, which corresponds to a degradation of 0.3%/1000 h. This test has therefore proven that bigger stacks operated

under real conditions show low degradation that is comparable to that of the smaller short stacks, as described in section 4.3. In the next step, further design optimizations based on CFD/FEM analyses will be realized and tested in bigger stacks, aiming at concepts for even larger stacks of more than 10 kW.

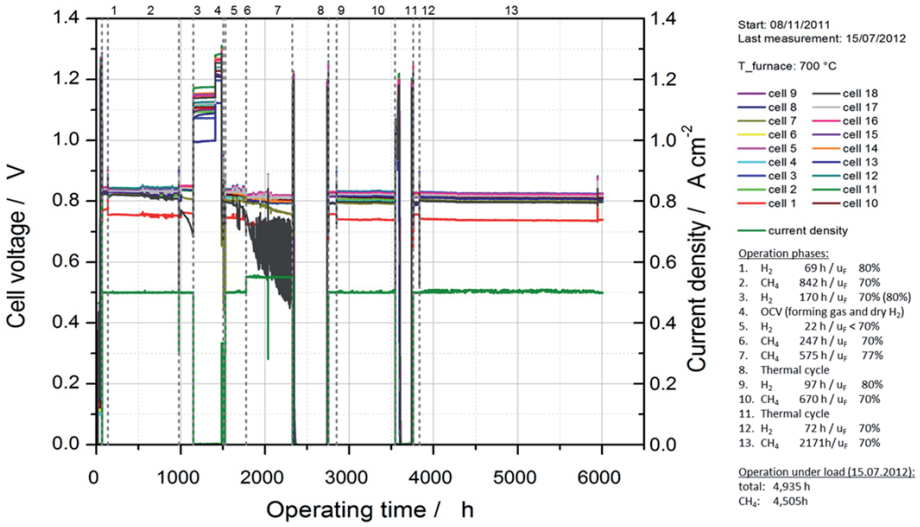

Fig. 13: Cell voltages as a function of time for the 2.6 kW stack during 5000 hours of operation under load

3.1.2.3 Integrated module and systems engineering

Component modeling for the 20 kW system

In order to investigate system behavior of the combination of air preheater, reformer, afterburner and stack, all individual system components were first modeled with CFD and FE. The modeling results were validated using measurement results from the tests on the individual components [3].

Based on this, a model was made of the integrated module and a transient 3D simulation based on coupled computational fluid dynamics (CFD) and computational structural mechanics (CSM) was created, which was validated with measurement results. All components were simulated in their real geometries. This 3D model of the integrated module with all high-temperature system components represents a breakthrough in SOFC modeling and provides us with detailed time-dependent information on the process and critical areas of the design, which are subjected to exceptional thermomechanical loading (see Fig. 14).

[3] Peksen, M.; Peters, R.; Blum, L.; Stolten, D.: Hierarchical 3D Multiphysics Modelling in the Design and Optimisation of SOFC System Components. International Journal of Hydrogen Energy 36 (2011), 4400-4408

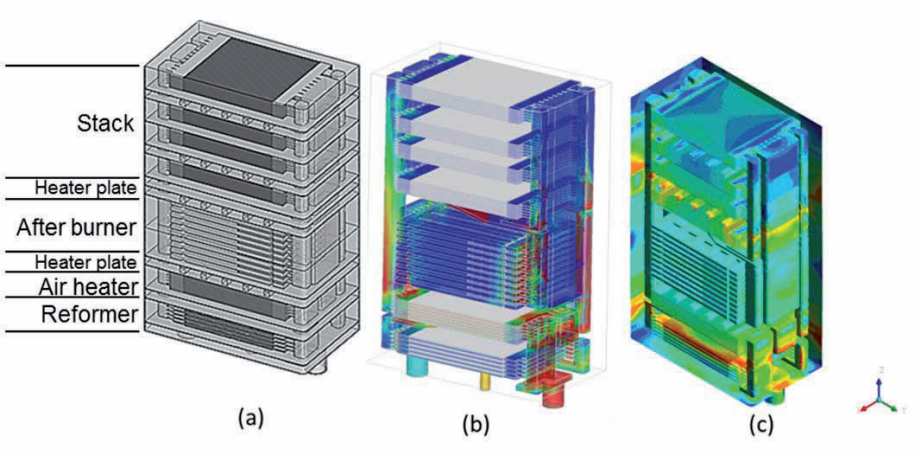

Fig. 14: Voltage and power characteristics of the four stacks for the 20 kW system 3-D Modell des Integrierten Moduls(a) mit Strömungsverteilung (b)

20 kW System

The commissioning of the 20 kW system was delayed due to the work detailed above on improving the stack joining techniques. Based on the good results of work optimizing the stack tightness, four 5 kW stacks were set up and successfully operated. Each of the stacks comprises 36 levels with cells measuring 20 x 20 cm². According to acceptance measurements in the test stand, all stacks had a power of 7.3 – 7.5 kW for mean cell voltages of 802 – 831 mV (measured with hydrogen at 0.7 A cm^{-2} and 35 % fuel utilization;

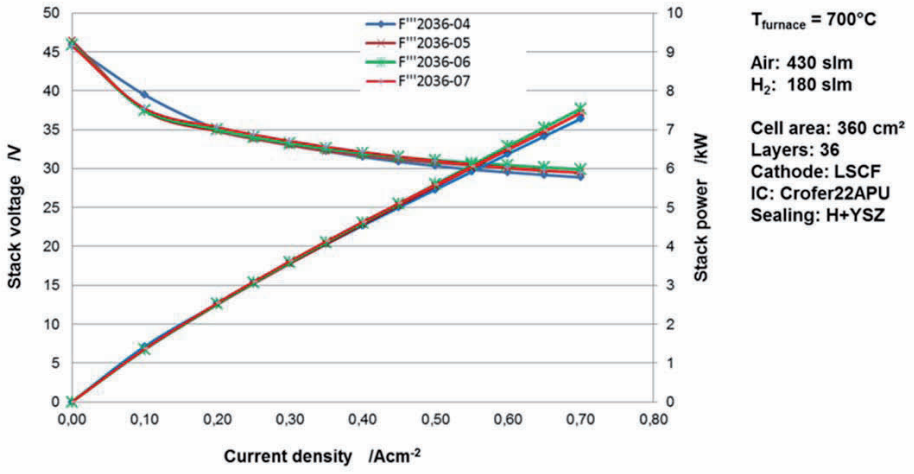

Fig. 15: Voltage and power characteristics of the four stacks for the 20 kW system

(see Fig. 15) and showed very high open circuit voltages, which indicates very good internal tightness. This was confirmed in tightness measurements performed after removal from the test stand. All stacks had leak rates that were at least one order of magnitude below the required leak rate. Due to these good results, all four stacks were installed in the 20 kW system (see Fig. 16).

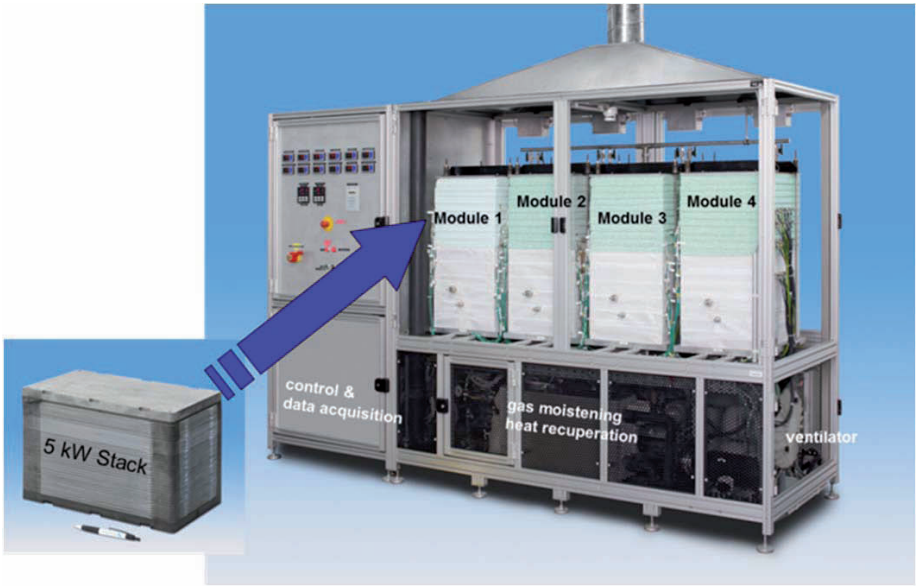

Fig. 16: Set-up of the 20 kW system with the positioning of the 5 kW stacks

In August 2012, the system was successfully put into operation. After a running-in phase, 21.3 kW power was generated with the stacks (28.7 V = 0.79 V mean cell voltage at 743 A = 0.515 A/cm²), of which 20.0 kW was registered at the load device. The difference

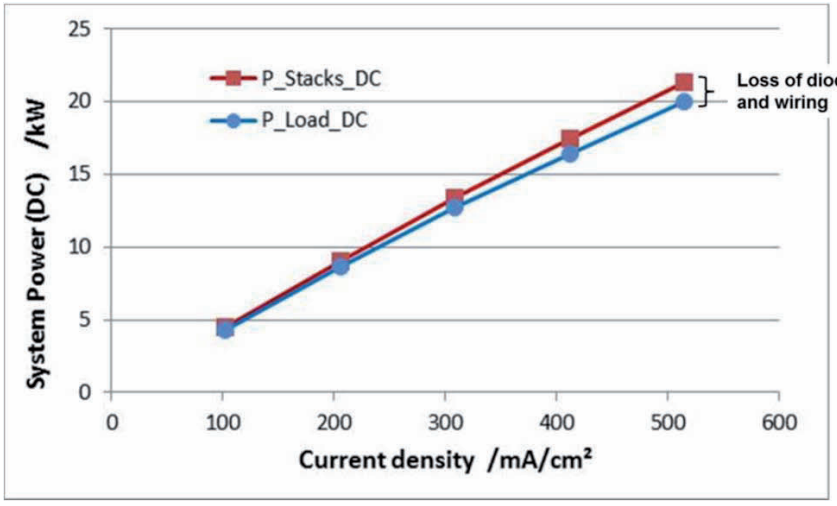

Fig. 17: Power characteristics of the 20 kW system

was consumed by the high-voltage wiring (mainly in the hot area of the stack) and by the protective diodes. The latter prevent equalizing currents between the stacks during open-circuit operation. The test will now concentrate on whether safe operation is possible without the use of diodes. The powers measured as the current density was increased are shown in Fig. 17.

The net electrical load of the system was determined based on these results, the power consumption of the air compressor (conditions at 20 kW: 2.3 kW at 200 mbar pressure increase and 167 kg/h air mass flow rate), an assumed additional system consumption of 0.2 kW for measurement and control technology and an inverter efficiency of 95 %. As shown in Fig. 18, the net efficiency was approx. 43 % at nominal load and 46 – 47 % at 40 % partial load (depending on whether diodes were included or not).

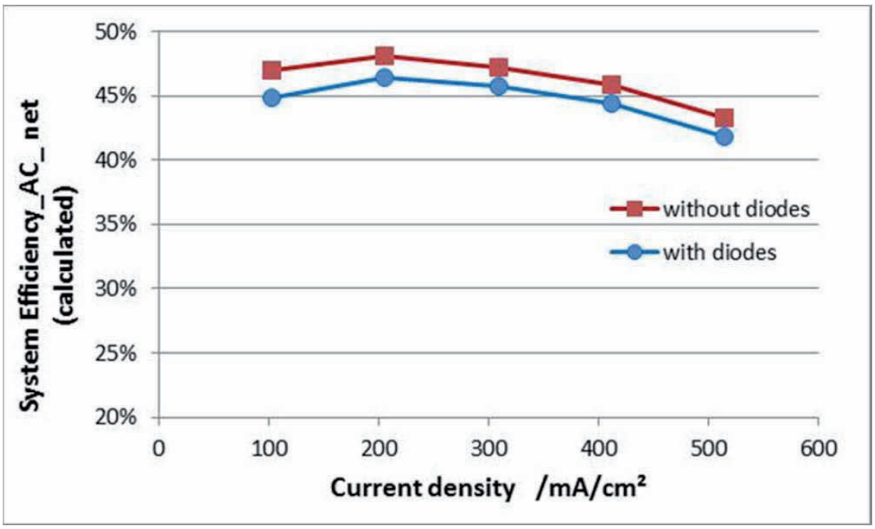

Fig. 18: Net electrical efficiency of the 20 kW system as a function of current density

The system was operated at 15 kW for approx. 500 hours. It then had to be turned off because a leak was detected in module 3. The module was taken apart and the cause was identified: thermomechanical stresses that were too high caused an electric heating plate between the afterburner and the air pre-heater to warp, thus releasing the load on the flat seal between the heating plate and the afterburner, which in turn led to external leakage of the fuel gas and hot cathode air.

A subsequent stack tightness measurement showed an unacceptably high internal leakage at stack 3, which was likely caused by the thermal cycle because no abnormalities were detected in this module during operation. As no replacement stack was available at short notice, the system was put back into operation with two modules in order to learn more about system operation.

As shown by the long-term performance curves in Fig. 19, there were already indications of a very high degradation in the first phase of operation. This continued after a short stable phase of some 300 hours after it was put back into operation. The first analyses indicate that small amounts of H_2S (< 1 ppm), which had not been removed from the desulfurization pellets, were the cause of this. Investigations are still being pursued.

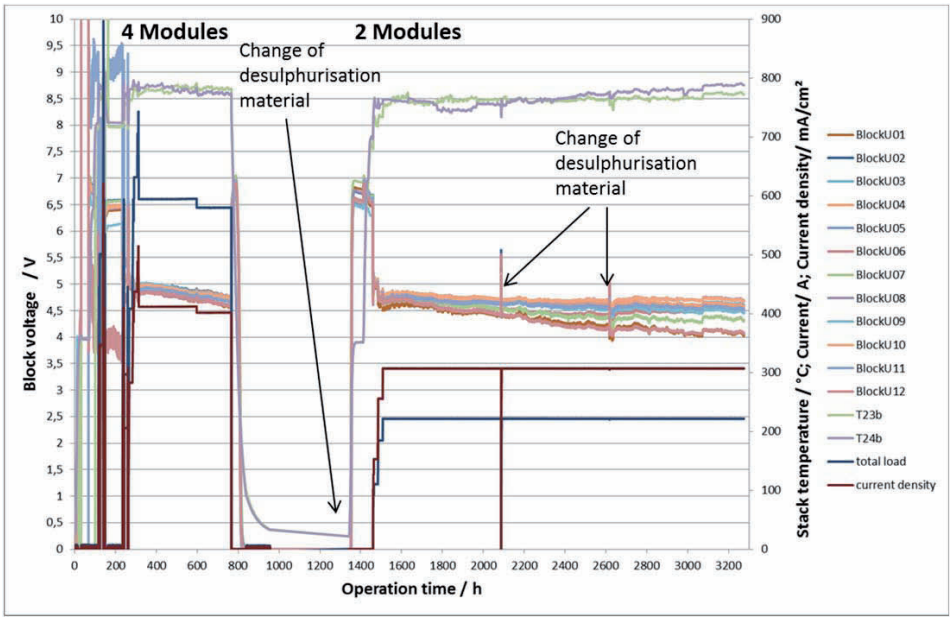

Fig. 19: Operating data of the 20 kW system as a function of operating time

3.1.2.4 Analysis of different system configurations

Fuel cell systems are generally expected to have a higher electrical efficiency. The results achieved with test systems up to now, however, differ considerably, particularly for different types of fuel cells operated with natural gas. The reasons for this behavior were investigated and described, and the realistic potential of different fuel cell systems was determined. To this end, various system concepts were designed and analyzed for PEFCs, PAFCs and SOFCs.

The energy balance calculations performed for eight different system concepts (three for PEFCs, two for PAFCs and three for SOFCs) revealed that the external reforming of natural gas and the heating it requires limited the fuel utilizations of PEFC and PAFC systems to 67 % and 70 %, respectively. Due to internal reforming and the recycling of waste heat from the electrochemical reaction in the cell for this process, high-temperature fuel cells (MCFCs and SOFCs) can achieve a fuel utilization of at least 80 %. With the SOFC, up to 90 % can be achieved when the anode off-gas is recycled.

In combination with a cell voltage for the PEFC, PAFC and tubular SOFC that is approx. 100 mV lower than for the MCFC and planar SOFC (700 mV instead of 800 mV), the PEFC only achieves a net electrical efficiency of 38 %, the PAFC 42 % and the tubular SOFC 54 %. The latter is comparable to the MCFC, which is operated at higher cell voltages but only achieves a lower fuel utilization, as it is difficult to implement recycling of the anode off-gas. The highest net electrical efficiency of 63 % can be achieved with the planar SOFC – this

type of fuel cell allows a high fuel utilization at a simultaneously high cell voltage. The results have been published in [4].

3.1.3 Staff members and fields of activity

Name	Tel. (+49 2461-61-) E-mail address	Field of activity
Prof. L. Blum	6709 l.blum@fz-juelich.de	Head of Fuel Cells Process Engineering
A. Al-Masri	3774 a.al-masri@fz-juelich.de	Simulation of SOFC stacks, CFD and FEM
R. Deja	5291 r.deja@fz-juelich.de	System simulation, development and testing of SOFC system components
Dr. Q. Fang	1573 q.fang@fz-juelich.de	Electrochemistry, testing of SOFC stacks and analysis of test results
I. Hoven	4053 i.hoven@fz-juelich.de	Electrical engineering, measurement data acquisition and systems control
Ms. A. Kind	3850 a.kind@fz-juelich.de	Software development, modeling
Dr. V.N. Nguyen	8393 v.n.nguyen@fz-juelich.de	Chemical process engineering, development and testing of SOFC system components
Ms. U. Packbier	5170 u.packbier@fz-juelich.de	Testing of SOFC stacks and data evaluation
Dr. M. Peksen	8732 m.peksen@fz-juelich.de	Simulation of SOFC stacks and high-temperature system components, CFD and FEM
Ro. Peters	4664 ro.peters@fz-juelich.de	Head of SOFC Systems Technology, component development, plant design, construction and testing

3.1.4 Important publications and patents

Important publications

Blum L.; Groß, S.M.; Malzbender, J.; Pabst, U.; Peksen, M.; Peters, R.; Vinke I.C.
Investigation of solid oxide fuel cell sealing behavior under stack relevant conditions at Forschungszentrum Jülich
Journal of Power Sources 196 (2011) 7175-7181

Peksen, M.
A coupled 3D thermofluid–thermomechanical analysis of a planar type production scale SOFC stack
International Journal of Hydrogen Energy, Volume 36, Issue 18 (2011) 11914-11928

---

[4] Blum, L.; Deja, R.; Peters, Ro.; Stolten, D.: Comparison of efficiencies of low, mean and high temperature fuel cell systems. International Journal of Hydrogen Energy 36 (2011), 11056 - 11067

Peksen, M.; Peters, R.; Blum, L.; Stolten, D.

Hierarchical 3D Multiphysics Modelling in the Design and Optimisation of SOFC System Components

International Journal of International Journal of Hydrogen Energy 36 (7) (2011) 4400-4408

Peksen, M.; Peters, Ro.; Blum, L.; Stolten, D.

3D Coupled CFD/FEM Modelling and Experimental Validation of a Planar Type Pre-heater used in SOFC Technologies

Hydrogen Energy 36 (2011) 11, 6851 – 6861

Blum, L.; Deja, R.; Peters, Ro.; Stolten, D.

Comparison of efficiencies of low, mean and high temperature fuel cell systems

International Journal of Hydrogen Energy 36 (2011) 17, 11056 – 11067

Groß, B.; Blum, L.; Haart, de L.G.J.; Dengel, A.

Development of a Solid Oxide Fuel Cell for the utilization of coal mine gas

Journal of Power Sources 196 (2011) 12, 5309 – 5316

Peters, R.; Deja, R.; Blum, L.; Pennanen, J.; Kiviaho, J.; Hakala T.

System Analysis of Anode Recycling Concepts

Proceedings of the 10th European SOFC Forum 2012, 26 – 29 June 2012, Lucerne, Switzerland, Paper A1308

Important patents

Patent applications:

Principal Inventor	PT	Description
Ro. Peters	1.2503	Solid oxide fuel cell system and method for operating the same
Dr. M. Peksen	1.2474	Fuel cell module

3.2 Fuel processing and systems

3.2.1 Objectives and fields of activity

The availability of hydrogen is a prerequisite for the use of fuel cells in mobile and stationary applications. At present, however, an infrastructure for hydrogen as a future energy carrier does not yet exist. Hydrogen must therefore be produced from readily available energy carriers. For stationary applications, natural gas and heating oil are suitable sources, while for mobile applications, gasoline, kerosene and diesel are options. Currently, the energy carriers listed above are mainly produced from the fossil primary energy carrier crude oil. In the long term, biomass will be used to produce some of the liquid energy carriers needed today.

At IEK-3, research in the field of fuel processing concentrates on the reforming of middle distillates, the desulfurization of kerosene, and system development for on-board power supply in combination with HT-PEFCs. In order to generate electricity or auxiliary power for portable or mobile applications (APU: auxiliary power unit), the same fuel must be used in the fuel cell APU system as is used to power the vehicle. For aircraft applications, kerosene and jet fuel for light aircraft are the only fuels available. However, they are allowed to contain a high level of sulfur-containing components. In the field of fuel processing, theoretical and experimental studies are therefore being conducted on the desulfurization of liquid fuels and their vaporization.

3.2.2 Important results

3.2.2.1 Desulfurization

At IEK-3, work began on the desulfurization of liquid fuels in 2005. The focus is on the desulfurization of kerosene and extra light heating oil (EL) containing a maximum of between 3000 ppm and 2000 ppm sulfur-containing hydrocarbons. The types of kerosene used in European and US infrastructure contain mass percentages of sulfur of less than 500 ppmw. Following a theoretical analysis and the selection of processes that are generally suitable for local desulfurization in fuel cell systems, the individual processes were then examined on a laboratory scale. Using results from experiments, two processes were found to be particularly effective. Hydrodesulfurization with presaturated hydrogen in the liquid phase is the only process that has the potential to be technically implemented in the short term. In the medium to long term, a combination of membranes and adsorbents could also play an important role in desulfurization. However, more research is required in this area.

With respect to the desulfurization efficiency, pervaporation (Perv), adsorption (Ads) and hydrodesulfurization (HDS) with presaturation were investigated as processes using a special methodology.

- Hydrodesulfurization with a presaturator makes it possible to remove 99 % of the sulfur in the kerosene fuel Jet A-1 from 813 ppmw to 8.1 ppmw at an operating temperature of 390 °C. A nitrogen flow of 100 l/h is used as part of this process to remove the dissolved hydrogen sulfide contained in the liquid fuel.
- Using a polymer membrane, up to 72 % sulfur was removed from the kerosene fuel Jet A-1 with 712 ppmw S. The feed stream was separated at a temperature of 90 °C

into a sulfur-enriched retentate fraction and a low-sulfur permeate flow with a transmembrane flow of 3.88 kg/(m² • h).

- An Al_20_3-based adsorbent is suitable for the desulfurization of the kerosene fuel Jet A-1 and its light fractions. An optimal desulfurization capacity of 2.56 mg S/g-Ads was achieved at an adsorption temperature of 100 °C for a light fraction of Jet A-1 with 409 ppmw, where the adsorbent was regenerated in air flow at a temperature of 500 °C for up to 3 h.

Based on the experimental results, a process analysis was performed and a desulfurization process was designed for a fuel cell APU with an electric power of 5 kW. The technical feasibility of the process and its potential for application were evaluated in relation to reductions in the APU efficiency, size and lifetime (see Tab. 6).

			1-stage Perv + Ads	2-stage Perv + Ads	HDS with presaturation
Feed	Flow	kg/h	5.1	10.1	1.35
	S content	ppmw	3000	3.000	3.000
Product	Flow	kg/h	1.35	1.35	1.35
	S content	ppmw	10	10	19
Reduction in efficiency		% points	1.23	0.68	0.98
Size		l	26	18	8.7
Lifetime		h	555	93	2000

Tab. 6: Evaluation of the desulfurization processes investigated with regard to targets. The reduction in efficiency refers to the system efficiency of the APU as a whole

The process analysis showed that hydrodesulfurization with presaturation was most efficient for the targeted application. The advantages of this process are the long service life of 2000 h and the minimal size of 8.7 l, although desulfurization with this process reduces the APU efficiency by 0.96 percentage points. In order to technically implement the process in the short to medium term, the following work is necessary:

- In order to further reduce the size of the HDS process to a level of 6 l, new developments are essential in presaturation techniques as are improvements in the design of the stripper for H_2S separation. Furthermore, the long-term stability of the HDS process must be demonstrated by a long-term test lasting 2000 h using the kerosene fuel Jet A-1 and a pilot facility.
- The HDS process must be further optimized in terms of reactor design and the use of alternative catalysts is essential. Above all, the desulfurization of kerosene fuels with the maximal permissible sulfur concentration of 3000 ppmw must be further investigated and improved so that the sulfur content in the product can be reduced from the current value of up to 19 ppmw to the target value of 10 ppmw.
- In addition, further investigations are necessary to determine the influence of different dyes and additives in heating oils on the service life of the catalyst used.

Combining two-stage pervaporation with adsorption enables desulfurization with very low efficiency losses at a low operating pressure. Assuming that the heat can be supplied by the fuel cell system, the overall system efficiency of the APU drops by only 0.68 percentage points when two-stage pervaporation is performed in combination with adsorption. The combined process should therefore be investigated as an alternative in the long term.

As pervaporation and adsorption are used industrially in different types of application and their process design can be easily adapted for desulfurization, the process will become competitive when more suitable membranes and adsorbents are used. A minimal adsorption capacity of 5.14 mg S/g-Ads is required to reduce the size of the combined process from 18.2 l to 9.1 l. However, a long-term stability of the membrane material in excess of 1000 h is also required, for which an average permeate flow of 0.5 kg/(m² • h) must be achieved.

3.2.2.2 Component development

Over the last few years at IEK-3, reformers have been developed for middle distillates and for synthetic fuels made from biomass. These reformers are shown in Fig. 20. The reformers pictured are also capable of using standard diesel fuels to produce sufficient quantities of hydrogen for fuel cells with a power between 3 kW_{el} and 50 kW_{el}. The preferred process for this is known as autothermal reforming. All reformers have a cold-starting device, internal steam generation, and a device for extracting the process heat that arises during reforming. In addition to hydrogen, autothermal reformers also produce higher levels of carbon monoxide, namely 7 – 10 % (vol.).

Fig. 20: Autothermal reformers constructed or tested at IEK-3 in 2011 and 2012. From left to right: type 13, EU project FCGEN, 13 kW_{th}; type 8B, 13 kW_{th}; type AH1, NRW project ADELHEID, – same design as type 9.1, 18 kW_{th}, type 9.2, 28 kW_{th} and type 10, 140 kW_{th}, the last two from the LuFo IV project BRINKS funded by BmWi

In order to gain a better understanding of the flow and temperature conditions inside the mixing chamber of the reformer, and to be able to predict them more easily, computational fluid dynamics (CFD) modeling is carried out at Jülich. CFD modeling aims to provide precise data on the temperatures reached in the mixing chamber and on the local zones in which the fuel is vaporized under given reaction conditions, such as temperatures, flow rates of air, steam and diesel fuel, and the spray pattern of the nozzle. In 2010 and 2011, existing models were expanded considerably in order to analyze the internal heat exchange. Chemical reactions were modeled as heat sources in a simplified form. The expected pressure losses in the apparatus as a whole can also be estimated. Water evaporation and superheating are performed separately in the catalytic burner and reformer. This has already been taken into account in the modeling of autothermal reformers type 11 and 12. Fig. 21 shows the three-

dimensional simulated temperature profile and droplet distribution in ATR 12 with a wire mesh in the wet steam annular gap at 120 % load. The CFD-based approach used to design the reactor was also implemented for catalytic combustion and the shift reaction.

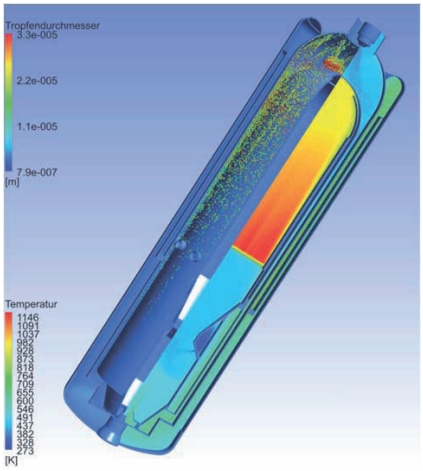

Fig. 21: Three-dimensional simulated temperature profile and droplet distribution in ATR 12 with a wire mesh in the wet steam annular gap at 120 % load

In a water-gas shift reactor (WGS), carbon monoxide is converted with water into carbon dioxide and hydrogen. The concentration of carbon monoxide was reduced to 1 % (vol.). The hydrogen content rose by approx. 6 – 9 % (vol.). Fig. 22 shows the shift reactors in the 5 – 50 kW_{el} class that have been developed and tested over the last few years.

Fig. 22: Shift reactors constructed or tested at IEK-3 in 2011 and 2012. From left to right: WGS type 3, 13 kW_{th}; WGS type 4, 28 kW_{th}; WGS type 5, 140 kW_{th}, the last two from the *LuFo IV project BRINKS funded by BmWi*

The fuel cell uses the hydrogen in the product gas after fuel processing – usually referred to as reformate – at a rate of 80 – 85 %. Residual hydrogen, carbon monoxide and methane, formed in small quantities during reforming, are combusted in a catalytic burner with low emissions. The resulting reaction heat is used together with the heat released during the cooling of the reformate to 400 °C (inlet temperature shift reactor) to generate steam in the

reformer. Fig. 23 shows the shift reactors in the 5 – 10 kW_{el} class developed and tested over the last few years.

Fig. 23: Catalytic burners constructed or tested at IEK-3 in 2011 and 2012. From left to right: CAB type 4, 4-5 kW_{el}; CAB type 2, 5 kW_{el}; CAB type 3, 10 kW_{el}, LuFo IV project BRINKS funded by BmWi

All reactor types were scaled up in 2010 to a reformer thermal capacity of 28 kW_{th} – which is equivalent to a fuel cell capacity of approx. 10 kW_{el}. Reactor types ATR 9.2, WGS 4 and CAB 3 can thus be used to create 10 kW_{el} fuel processing systems as a package.

3.2.2.3 System development

Activities in the area of system development include systems for fuel processing as well as complete fuel cell systems with reforming. Within system development, the priority is currently hydrogen provision for HT-PEFC fuel cells. Ongoing developments will be presented in the following sections.

Fuel processing systems using diesel and kerosene

The core components of fuel processing systems operated with diesel or kerosene are ATR, WGS and CAB. Additional components include two electric heating cartridges and two heat exchangers. These components are connected together at IEK-3 in the form of compact packages. Fig. 24 shows the design model for package 1 with a power of 14 kW_{th} and the system constructed with the core components ATR 9.1, WGS 3 and CAB 2.3.

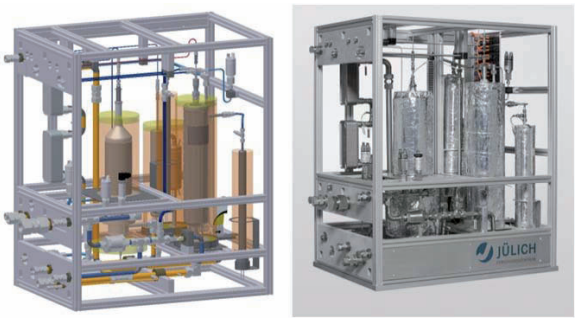

Fig. 24: Design model and set-up of package 1

The package design can be illustrated using a simplified flow chart (Fig. 25). The autothermal reformer (ATR) is operated with the educts kerosene or diesel, air and steam. Part of the air is fed into the reformer cold. The rest is mixed with water and functions as a carrier during

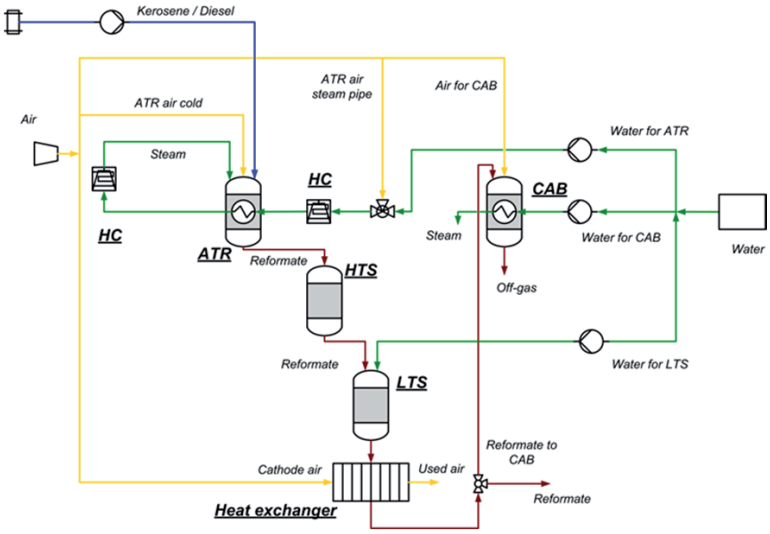

Fig. 25: Simplified flow chart of a fuel processing system in package operation

evaporation in the electric heating cartridges. Water for reforming is evaporated and slightly superheated in the first electric heating cartridge (HC). In the integrated heat exchanger of the reformer, the steam is then superheated further. The second heating cartridge is used only for start-up. Following autothermal reforming, the reformate is cooled down in the integrated heat exchanger of the reformer. The reformate is then fed into the high-temperature shift stage (HTS) of the water-gas shift reactor (WGS). After the exothermic shift reaction in the HTS, water is added to the reformate. This cools the reformate down to a suitable inlet temperature for the low-temperature shift stage (LTS). After the exothermic shift reaction in the LTS, the reformate is cooled down further. In package 1, two heat exchangers connected as a cascade, perform this task. In order to investigate systems technology aspects, cathode air is used as the coolant. The connections in the system as a whole are thus simulated. After cooling, the reformate is split into two streams. The smaller partial flow

is combusted in the catalytic burner. The larger partial flow leaves the package and is fed into the exhaust gas post-treatment module (GPM).

Another difference compared to full system operation is that this water must be completely evaporated as it would not otherwise be possible to control the electric heating cartridge. In real system operation, in contrast, water vapor is present at the inlet to the heat exchanger of the reformer in the form of wet steam. The way that the package is currently connected prevents the electric heating cartridges being shut down completely during normal operation. This is due to the fact that the heat recovery in the catalytic burner can only be integrated into the system to a limited extent. At the design point of package 1, 17.5 % reformate with an air ratio of 2.35 should be combusted in the catalytic burner. As part of this process, 50 % of the water required for the reformer should be evaporated and slightly superheated in the integrated heat exchanger of the catalytic burner. The mass flows for the design point (1350 g/h GTL kerosene) are:

- Water supply LTS: 800 g/h,
- Amount of reformate after WGS: 11,550 g/h,
- Amount of reformate to CAB: 2021 g/h,
- Amount of water CAB: 1624 g/h,
- Air CAB: 5360 g/h,
- Air stack: 18,080 l/h.

Experimental testing of the package allowed the reformate flow after the WGS reactor to be determined and to be split into two flows using a valve control system. The volume of the smaller partial flow was also determined. This partial flow was fed into the catalytic burner. The package design with direct connection of the ATR and WGS reactors and combustion of a partial reformate flow in the catalytic burner was successfully tested. In addition, the evaporation function of the heat exchanger of the catalytic burner was also validated in package operation.

Fig. 26 shows the temperatures measured for steam and exhaust gas at the outlet of the catalytic burner for tests IV–X. Only in test IV was the injected amount of water not fully evaporated. The steam temperature was approx. 100 °C. In all other tests, the total amount

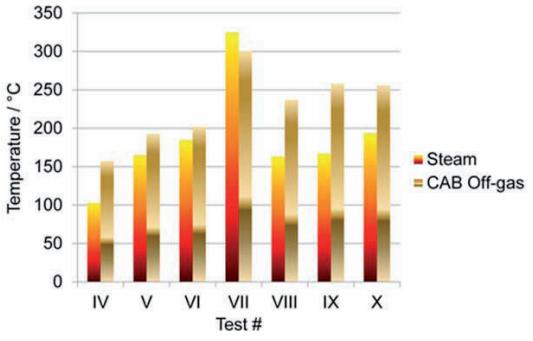

Fig. 26: Temperatures at the outlet of the integrated heat exchanger in the catalytic burner in tests with package 1

of injected steam was fully evaporated and slightly superheated. In tests V and VI with similar parameters, the temperature difference between exhaust gas and steam was 17 – 28 K. In test VII with an increased reformate fraction in CAB, higher temperatures were measured in the steam than in the exhaust gas. This is due to the reactor design, which meant that the exhaust gas was cooled further after the evaporator section. The heat was absorbed by the cold media in the inlet area of the reactor. For this reason, the effectiveness of the evaporator cannot be precisely evaluated. With a constant amount of water compared to test VI, the resulting temperatures increased for both media at the outlet of the heat exchanger in test VII. In further tests (VIII to X), the evaporation function of the heat exchanger of the catalytic burner was tested with increased amounts of water. In all three tests, the total amount of water of 1700 g/h, which is equivalent to more than 50 % of the water required in ATR (3248 g/h), was evaporated and slightly superheated. These results show that the evaporation function of the heat exchanger in the catalytic burner in package operation fulfills the requirements of the integrated system concept.

HT-PEFC systems with reforming

An HT-PEFC system with reforming is a complete fuel cell system comprising, a fuel processing system as shown in Fig. 25 and an HT-PEFC stack. At IEK-3, a complete system, integrated system S1, was also set up and operated as a package.

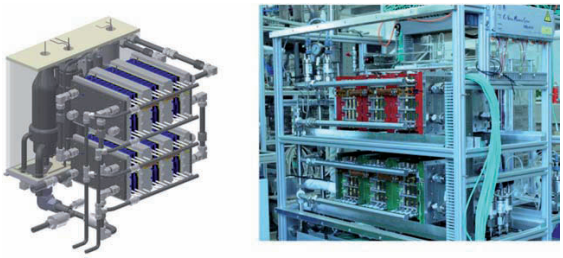

Fig. 27: Design model and set-up of the integrated system S1

Fig. 27 shows system S1. A design model is shown on the left. The fuel processing system comprising the reactors ATR 9.2, WGS 4, CAB 3 and two electric heating cartridges as well as a heat exchanger has a capacity of 28 kW_{th}. This system was coupled to two HT-PEFC stacks (stack type IV) from the HPB group at IEK-3, which provide an electric power of 5 kW in reformate operation. The system as it was set up is shown on the right-hand side of Fig. 27.

Fig. 28 shows a flow chart detailing how the system is connected. The connection concept of fuel processing was developed analogous to that of package 1. However, the integrated system S1 allows the functionality of the system as a whole to be tested. In order to exactly control the temperature of the educt upstream of the stack, two additional heat exchangers were integrated downstream of the cathode air/reformate heat exchanger. Thermal oil flowed through these, which, aided by a temperature controller in the test stand, cooled the stack in normal operation. For start-up, the temperature controller heated the stack. The fuel processing system was heated in a similar manner to package 1 with the aid of two electric heating cartridges. The system also had a bypass flow. By controlling the valves at the anode inlet, it was possible to feed the reformate directly into the catalytic burner. In stationary system operation, part of the water was evaporated and slightly superheated for

reforming in the catalytic burner. This amount of water was then mixed with the rest of the cold water for reforming. The mixture was then completely evaporated and superheated in the integrated heat exchanger of the reformer. The electric heating cartridges were not used in stationary operation.

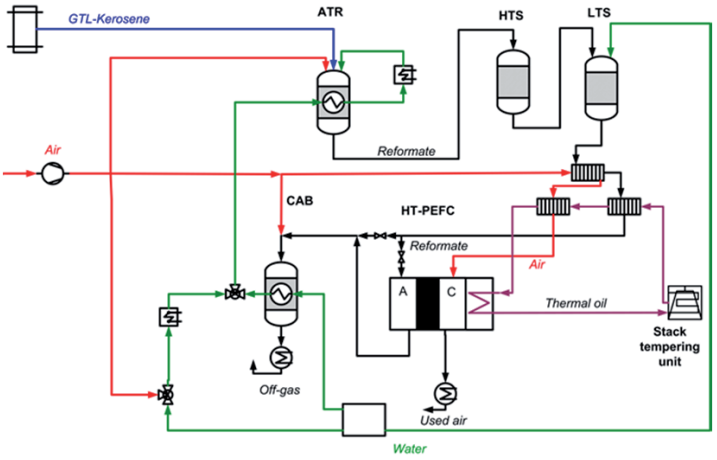

Fig. 28: Simplified flow chart of the integrated HT-PEFC system with reforming

The integrated system S1 was successfully operated and tested. In the first test with GTL kerosene as fuel, the system was operated with all functions. The design point for all reactors and the target power of 5 kW_{el} were achieved. Fig. 29 shows exemplary results from system

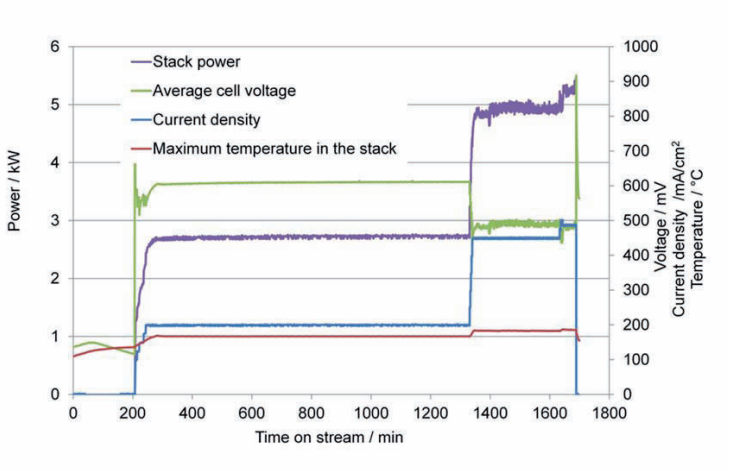

Fig. 29: Results of the system test with the integrated system S1: performance data of the HT-PEFC stack operated with GTL kerosene

operation. In the test shown here, the system generated electricity for a period of more than 24 h from GTL kerosene. The reformer was put into operation with 1674 g/h kerosene and the stacks were operated at a current density of 200 mA/cm^2 overnight. Under these

conditions, the system provided approx. 2.7 kW_e with a mean cell voltage of 610 mV. The air was supplied to the cathode at 21,000 Nl/h. The reformer ATR 9.2 was operated at an O_2/C molar ratio of 0.47 and an H_2O/C molar ratio of 1.9. Between the shift stages, 1000 g/h water was added. Thermal oil flowed through the stacks at an inlet temperature of 160 °C. After approx. 1315 min (test duration), the current density was increased in stages to 450 mA/cm^2.

After approx. 1400 min, air was added to the catalytic burner. After catalytic combustion began in CAB, the reactor was cooled with cold water. In the test sequence, for example, it took between 1450 min and 1530 min to evaporate 62 % of the reforming water in the catalytic burner and to add the remaining 38 % of the water cold to the reformer. The air ratio in the catalytic burner was 1.2 at this steady-state operating point. The stacks were operated with an air ratio of 2.1 and a H_2 utilization of 78 %. The HT-PEFC stacks produced an electric power of 4.95 kW at a mean cell voltage of 492 mV and a current density of 450 mA/cm^2. Further parameter combinations were tested in subsequent experiments. It was shown that up to 75 % of the water required by the reformer could be evaporated and slightly superheated in the catalytic burner. The maximal stack power achieved was 5.56 kW_{el} at a mean cell voltage of 485 mV and a current density of 487.5 mA/cm^2. At a current density of 500 mA/cm^2, a stack power of 4.96 kW was measured with a H_2 utilization of 81.5 % and an air ratio of 2. The mean cell voltage at this test point was 445 mV.

3.2.1 Staff members and fields of activity

Name	Tel. (+49 2461-61-) E-mail address	Field of activity
Prof. Dr. R. Peters	4260 ra.peters@fz-juelich.de	Head of Fuel Processing Systems
Dr. J. Pasel	5140 j.pasel@fz-juelich.de	Head of Chemistry for Fuel Processing
Dr. R. C. Samsun	4616 r.c.samsun@fz-juelich.de	Head of Systems Engineering for On-Board Power Supply
A. Tschauder	4547 a.tschauder@fz-juelich.de	Reactor development, reforming, system design

3.2.2 Important publications, PhD theses and patents

Important publications

Göll, S.; Samsun, R.C.; Peters, R.
Analysis and optimization of solid oxide fuel cell-based auxiliary power units using a generic zero-dimensional fuel cell model
Journal of Power Sources, 196 (2011) 9500-9509

Wang, Y., Geder, J., Schubert, J.M., Dahl, R. Pasel, J., Peters, R.
Optimization of adsorptive desulfurization process of jet fuels for application in fuel cell systems
Fuel Processing Technology, 95 (2012), 144-153

Pasel, J., Wang, Y., Hürter, S., Dahl, R., Peters, R., Schedler, U., Matuschewski, H.

Desulfurization of jet fuel by pervaporation

Journal of Membrane Science, 390-391 (2012), 12-22

Göll, S., Samsun, R. C., Peters, R.

Enhancing the Efficiency of SOFC-Based Auxiliary Power Units by Intermediate Methanation

Fuel Cells, 12, 3 (2012), 474-496

Samsun, R. C., Wiethege, C., Pasel, J., Janßen, H., Lehnert, W., Peters, R.

HT-PEFC systems operating with diesel and kerosene for APU application

Energy Procedia, 29 (2012), 541-551

Pasel, J.; Peters, R.

Desulfurization for Fuel-Cell Systems

Fuel Cell Science and Engineering: Materials Systems, Processes and Technologies, Eds. Stolten, D.; Emonts, B., Wiley-VCH, Weinheim, 2012, Vol. 2, ISBN: 978-3-527-33012-6, pp. 1011-1044

Peters, R.; Scharf, F.

Computational Fluid Dynamic Simulation Using Supercomputer Calculation Capacity

Fuel Cell Science and Engineering: Materials Systems, Processes and Technologies, Eds. Stolten, D.; Emonts, B., Wiley-VCH, Weinheim, 2012, Vol. 2, ISBN: 978-3-527-33012-6, pp. 703 - 732

Samsun, R.C.; Peters, R.

Methodologies for Fuel-Cell Process Engineering

Fuel Cell Science and Engineering: Materials Systems, Processes and Technologies, Eds. Stolten, D.; Emonts, B., Wiley-VCH, Weinheim, 2012, Vol. 1, ISBN: 978-3-527-33012-6, pp. 597 - 644

PhD theses

Scharf, F.

Strömungsmechanische Modeliierung eines Brenngaserzeugungssystems (Fluid dynamics simulations of a fuel processing system)

Schriften des Forschungszentrums Jülich, Reihe Energie & Umwelt, Band 155, ISBN 978-3-89336-784-9, RWTH Aachen 2012

Wang, Y.

Tiefentschwefelung von Flugturbinenkraftstoffen für die Anwendung in mobilen Brennstoffzellensystemen

(Deep desulfurization of jet fuel for applications in mobile fuel cell systems)

Schriften des Forschungszentrums Jülich, Reihe Energie & Umwelt, Band 155, ISBN 978-3-89336-827-3, RWTH Aachen 2012

3.3 High-temperature polymer electrolyte fuel cells

3.3.1 Objectives and fields of activity

Commercial vehicles, construction machines, ships and airplanes will continue to be run on diesel and kerosene in the long term. Substantial energy savings can be made by increasing electrification as this leads to more efficient on-board power generation. From a practical point of view and in the interests of the end user, these devices known as auxiliary power units (APUs) must be run on the fuel that is already available on board, which makes reforming of these “middle distillates” necessary. The combination of a high-temperature polymer electrolyte fuel cell (HT-PEFC) and an appropriate reforming technology on board makes it possible to efficiently generate electricity, even when the engine is not running.

IEK-3 has been pursuing research and development activities on the HT-PEFC since 2005. Work covers basic electrochemical fields, electrode development and stack development. In the area of stack development, it was shown that the method of operation has a significant impact on the lifetime of the stack. Stacks with a power of 5 kW, operated with synthetic reformate, were also demonstrated. The most important findings on the structure-activity relationship within electrodes and MEAs as a whole will help to optimize these structures. A central challenge in the area of HT-PEFC research is the understanding of the oxygen reduction reaction and the adsorption of phosphoric acid species at the platinum catalysts. Parallel to this, modeling and simulation work was performed. Analytical modeling of HT-PEFCs provides the basis for models that are implemented in CFD tools as user-defined functions. These analytical models also provide a detailed analysis of physical effects on the operating behavior of single cells. In order to understand mass transport phenomena in porous gas diffusion layers, more lattice Boltzmann simulations were used. In addition to using freely available open source codes, in-house simulation codes were also developed, verified and applied.

3.3.2 Important results

3.3.2.1 HT-PEFC stack development

At the moment, stack design is aimed at APU applications in the kW range. Typical applications are in airplanes, trains, ships and heavy-duty vehicles. The most important characteristics are an active cell area of 320 cm², a modular stack design and the integration of enclosed oil-saturated temperature control cells. A stack module comprises 12 single cells and 5 temperature control cells where the external temperature control cells are integrated in the module end plates. Simulations and preliminary tests have shown that reformate operation up to a current density of 0.5 A/cm^2 allows the maximal locally allowed temperatures of 180 °C to be observed. Two full stacks with a total of 70 cells were assembled according to the described design. Fig. 30 shows the results for an oil inlet temperature of 160 °C. In hydrogen/air operation, the target electrical output of 5 kW was exceeded at a mean current density of only 0.4 A/cm²; the mean cell voltage was 580 mV. When operated with synthetic reformate at 0.5 A/cm², an electric power of 5.2 kW was measured. The mean cell voltage was 460 mV. The development target was therefore achieved.

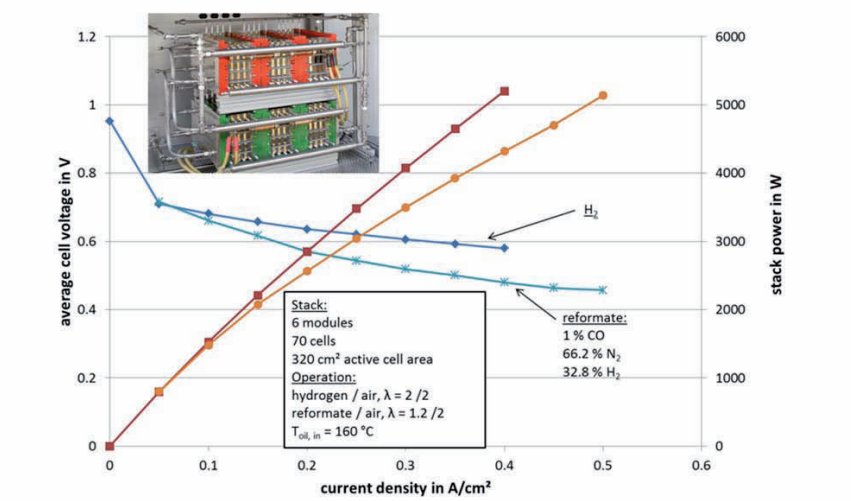

Fig. 30: Current-voltage and current-power curves for two coupled HT-PEFC stacks operated with hydrogen and reformate

In order to determine long-term stability, a long-term test was started with a stack module. Oil tightness, which had posed a significant technical problem in previous stack generations, was demonstrated. The degradation of single cells up to a shut-off limit of 0.2 V led to the end of the test. The test duration was 3400 h.

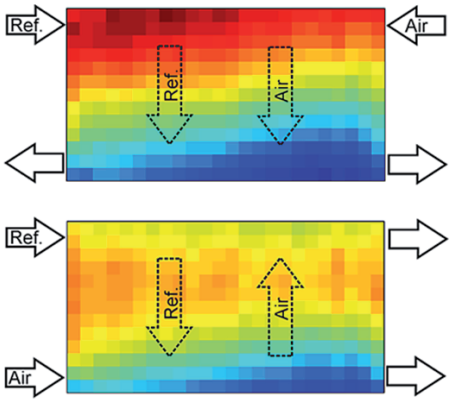

Fig. 31: Current density distribution, measured on a five-cell short stack (synthetic reformate / air, j = 0.4 A cm^{-2}, $\lambda_{an/ca}$ = 2 / 2, $T_{oil,in}$ = 160 °C, f_{oil} = 1.5 L min^{-1})

As part of the analysis of the operating behavior of HT-PEFC stacks, the current density distribution over the cell area between cells number 3 and 4 in a five-cell short stack was measured as a function of different operating states [5]. The influence of the flow direction of

[5] Lüke, L.; Janßen, H.; Kvesić, M.; Lehnert, W.; Stolten. D.: Performance Analysis of HT-PEFC Stacks. International Journal of Hydrogen Energy 37 (2012), 9171–9181

the reactants was shown to be particularly important on the operating behavior when the cell stack was supplied with hydrogen-rich gas from a fuel processing module. Fig. 31 shows the measured current density distribution in counter flow and in parallel flow. In parallel flow, the current density decreases with the main flow direction from top to bottom. In counter flow, the current density initially increases and then decreases. The difference between minimal and maximal current density is 33 % smaller in counter flow operation than in parallel flow operation, and the current density distribution is thus more homogeneous.

The reason for this operating behavior is that the concentration and thus the partial pressure of the reactants in the flow field channels decrease over the course of the flow over the cell area. A decrease in local partial pressure leads to a decrease in local current density, as the local cell performance depends on the partial pressure of the reactants. If the two gases are in parallel flow, the performance decreases on both sides accumulate resulting in a steep gradient of current density distribution. If the gases are added in counter flow, the influences of the decreasing gas concentrations on the current density distribution partially counteract each other. This results in a more homogeneous current density distribution. The interesting point for applications is that the comparison of current-voltage characteristics in the respective operating range up to 0.4 A cm^{-2} reveals that the current density distribution can be homogenized by switching from parallel to counter flow operation without any negative impact on cell performance. The working hypothesis that a more homogeneous current density distribution also leads to a lower degradation rate was verified using comparative stack tests in which two identical HT-PEFC short stacks were set up and operated under identical operating conditions aside from the fact that one was operated in parallel flow and the other in counter flow. In order to minimize the degradation rate of an HT-PEFC stack operated with reformate, the current density distribution over the cell area should therefore be homogenized using a counter flow configuration of reformate and air.

The operating temperature range of an HT-PEFC is 120 °C to 180 °C. In order to heat the stack to at least 120 °C and to avoid exceeding the upper temperature of 180 °C, an active temperature control system is essential. In the envisaged power class of more 1 kW_e, both air-cooled and liquid-cooled stacks can be used. For stacks with a power above 5 kW_e, liquid temperature control is more advantageous than air temperature control. It was shown that thermal oil is very well suited for controlling the temperature in HT-PEFC stacks as no phase change occurs over the entire operating temperature range. Based on this, three temperature control concepts were developed (see Fig. 32): internal temperature control in each cell by means of thermal oil channels integrated in the bipolar plates (concept 1), internal temperature control in every third cell with enclosed cooling cells (concept 2), and external temperature control using a heat pipe (concept 3).

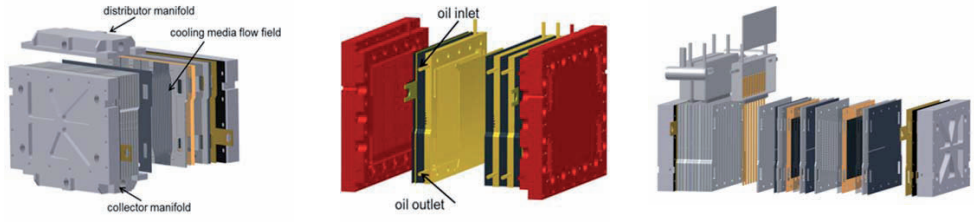

Fig. 32: CAD-graphics of the three stack concepts (1: left, 2: center, 3: right) with oil temperature control

The temperature distribution was tested experimentally from cell to cell and vertically on the MEA level for each stack design. It was demonstrated that each temperature control concept is theoretically suitable for controlling the temperature in HT-PEFC stacks operated using reformate. However, each method has advantages and disadvantages. Concept 1 can be operated with very low temperature gradients (<8 K) for current densities of up to 800 mA/cm². However, possible oil leakage problems mean that a very complex sealing concept is required. Concept 2 in contrast has no sealing problems because the encapsulated cooling cells are sealed during fabrication. Its disadvantages are a limited operating range of up to around 450 mA/cm² and the relatively high temperature gradient from cell to cell (17 K at 750 mA/cm²) [6].Concept 3 has the advantage that sealing problems affect uncritical areas. In addition, external temperature control enables operation with very large temperature gradients between the stack and thermal oil temperatures (>100 K possible), which gives rise to a very effective cooling. The disadvantage of concept 3 is that it also has a limited operating range (<450 mA/cm²). By controlling the oil inlet conditions, however, a larger operating range can be achieved (500 mA/cm²).

3.3.2.2 Investigation of the crack structure of electrodes in dynamically operated HT-PEFCs

One of the main objectives of HT-PEFC development is to improve fuel cell performance under different operating conditions. The influence of these changing operating conditions on the structures within the membrane electrode assembly (MEA), however, is very difficult to determine. In situ synchrotron radiography is a non-invasive measuring technique that allows crack structures within the anode and cathode to be imaged during fuel cell operation under different operating conditions. Synchrotron radiographs taken in the through-plane viewing direction can be used to distinguish between crack structures in the catalyst layers below the ribs and channels of the flow field in a dynamically operated HT-PEFC single cell. Such a radiograph is pictured in the top part of Fig. 33a). The areas outlined in red represent the catalyst layers below the rib and the areas outlined in blue are the catalyst layers below the channel. To evaluate the crack structures within the electrode layers during different operating states, the HPB group at IEK-3 developed a program which can be used to help determine crack width and crack length, as well as the form, size and location of the catalyst damage. In order to determine the crack width in the catalyst layers for different operating states, the synchrotron radiographs must first be converted to black-and-white images and separated into channel and rib areas (Fig. 33a bottom). After the black-and-white conversion, the crack analysis program was used to determine the crack width at different places on the catalyst layer and the crack width distribution was identified for the channel and rib areas as a function of operating state. Fig. 33b shows the determined crack widths in the channel area (blue) and rib area (red) as a function of operational state (OCV and three different current densities).

---

[6] Supra, J.; Janßen , H.; Lehnert, W.; Stolten, D.: Temperature distribution in a liquid-cooled HT-PEFC stack, J. Hydrogen Energy 38 (2013), 1943 - 1951

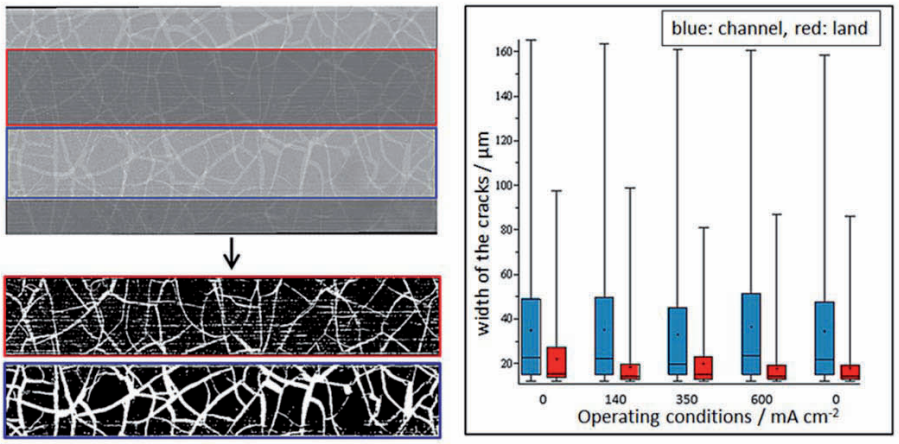

Fig. 33: **a) Synchrotron radiograph and black-and-white images of an HT-PEFC in through-plane direction. b) Crack width distribution under the channels (blue) and under the ribs (red) as a function of the operating conditions**

The crack width analysis revealed that the cracks underneath the channels were almost twice as wide as those below the ribs regardless of the operating state. Work is ongoing on assigning the crack widths to anode and cathode catalyst layers.

3.3.2.3 In situ Raman measurements on HT-PEM fuel cells

In HT-PEM fuel cells, poly(2,5-benzimidazole) doped with phosphoric acid (ABPBI) is being increasingly used as the electrolyte due to its high protonic conductivity. However, there have been very few studies to date on the states of chemical equilibrium of all species in the membrane as a function of the composition of the ternary system PBI - H_3PO_4 - H_2O under operating conditions. In an effort to investigate this in more detail, the first in situ Raman measurements on HT-PEM fuel cells were performed in cooperation with the working group for liquid phase laser spectroscopy at Heinrich Heine University Düsseldorf.

A special fuel cell was developed that allows in situ Raman measurements to be performed on electrolytes simultaneously with time-dependent impedance measurements while the cell is in operation. When the cell was switched from open cell voltage (OCV) to different current densities (140 mA/cm², 350 mA/cm² and 600 mA/cm²), changes were observed in the Raman spectrum of the electrolyte. In particular, the intensity of some Raman peaks altered when the load was changed. The altered peaks originate from vibration modes of different phosphoric acid species, the concentrations of which are influenced by load changes and the associated dehydration/hydration of the phosphoric acid. Comparing Raman spectra of pure phosphoric acids with those of polymer membranes doped with phosphoric acid allows the Raman peaks to be assigned to the phosphoric acid species. For example, a small increase in the peak with increasing load is observed for a wavenumber of 911 cm^{-1}, which can be explained by the vibrations of the 85 % phosphoric acid. However, it has not yet been possible to assign all peaks to a phosphoric acid species.

Further *in situ* Raman measurements are planned in order to investigate a wider wavelength range than in the past. At the same time, an improved set-up will also increase the resolution of the spectra. These measurements will be used to evaluate the equilibrium state of the electrolyte and thus to increase the lifetime of HT-PEM fuel cells.

3.3.2.4 Infrared spectroscopic investigations on the adsorption of phosphoric acid and phosphate species on platinum

Phosphoric acid and phosphate species can adsorb on platinum surfaces, thus blocking the electrochemically active catalyst surfaces and inhibiting oxygen reduction at the cathode. In order to investigate this adsorption in more detail, measurements were conducted using reflection-adsorption infrared spectroscopy (RAIRS) coupled with electrochemical methods. These methods allow potential-dependent adsorbed species to be examined on a highly reflective metal surface. This is made possible by a surface selection rule, which predicts the adsorption of different linearly polarized radiation on a surface. The mean square electric field at the interface is intensified by constructive interference for parallel linearly polarized (*p*-polarized) radiation, whereas it is obliterated by destructive interference in the direction of surface normals for perpendicular linearly polarized (*s*-polarized) radiation. This means that molecules adsorbed on the surface only interact with *p*-polarized radiation, thus enabling differentiation to be made between molecules adsorbed on the surface and those in the surrounding medium, as the latter interact with both *s*- and *p*-polarized radiation.

In each polarization, spectra between 200 mV and 1000 mV were recorded. Changes on the surface were detected for each probe signal compared to a reference signal, which was 50 mV, as the adsorption of phosphate species was not expected here. The potential modulation technique used here was subtractively normalized interfacial Fourier transform infrared spectroscopy (SNIFTIRS).

The spectra reveal the consumption of phosphoric acid from the solution at 990 cm^{-1} in the form of the positive band above 400 mV. The corresponding negative band of the adsorbed phosphoric acid can be seen at 1037 cm^{-1} in the spectrum of the *p*-polarized radiation. At 800 mV, however, this band is no longer visible. Two other bands can be seen at 1064 cm^{-1} and 1137 cm^{-1}, which may indicate adsorbed hydrogen phosphate anions. These could evolve as a result of dissociation on the surface at elevated potential, which is typical of acid species. These measurements were repeated at smaller potential steps in order to investigate these processes in more detail. These investigations were performed at different concentrations, which allowed the dependence of this behavior on concentration to be studied. Future measurements are planned at elevated temperatures.

3.3.2.5 Computational fluid dynamics

An important task of modeling is to support the design and error analysis of fuel cell stacks. A classical tool for this is computational fluid dynamics (CFD). As part of a PhD thesis, a flexible CFD model was developed and validated, which allows the simulation of liquid-cooled fuel cell stacks of the kW class [7, 8, 9]. Fig. 34 shows a set-up in which cooling is

---

[7] Kvesić , M.; Reimer, U.; Froning, D.; Lüke, L.; W. Lehnert, W.; D. Stolten, D.: 3D modeling of a 200 cm^2 HT-PEFC short stack. International Journal of Hydrogen Energy 37 (2012), 2430-2439

implemented after every third fuel cell [6]. This type of cooling means that the internal temperature profile is very heavily dependent on the heat transfer to the cooling plates. Due to their design, however, these cooling plates have additional sealing at the front edge of the stack (material: Viton®; see Fig. 34).

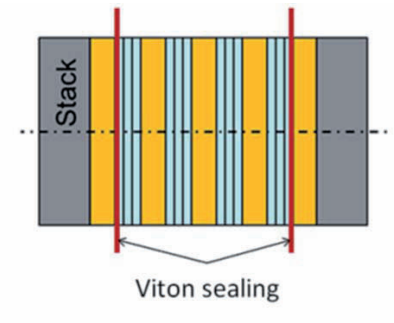

Fig. 34: Schematic of the set-up of a fuel cell stack (blue : fuel cellss; yellow = end plates)

As the Viton® functions as a heat insulator, it reduces the cooling rate of the cooling cells integrated in the end plates. It is difficult to gain precise information on the pressed state of the sealant. By varying the estimated material thickness of the sealant after installation, the experimentally determined temperature distribution could be reproduced well (see Fig. 35). An effective parameter for the insulating effect of the sealant was the result.

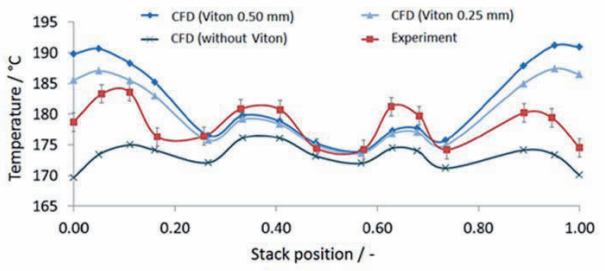

Fig. 35: Temperature profile for three different Viton® thicknesses (i = 0.50 A cm^{-2})

3.3.2.6 Analytical modeling

The individual fuel cells are supplied with reactants via gas channels (known as flow fields). In the simplest case, hydrogen or oxygen flows through the flow field and enters the electrode layers through the gas diffusion layer by means of diffusion or convection. This mass transport costs energy and is recorded as a resistance term when the fuel cell is characterized using impedance spectroscopy. This resistance term can then be interpreted

---

[8] Kvesić , M.; Reimer, U.; Froning, D.; Lüke, L.; Lehnert, W.; Stolten, D.: 3D modeling of an HT-PEFC stack using reformate gas. International Journal of Hydrogen Energy 37 (2012), 12438 – 12450

[9] Kvesić. M.: Modellierung und Simulation von Hochtemperatur-Polymerelektrolyt-Brennstoffzellen. Dissertation, RWTH Aachen, 2012

for oxygen transport at the cathode using an analytical model [10].The model considers both the electrochemical and ohmic processes in the cathodic electrode layer as well as oxygen transport in the gas diffusion layer. Numerical implementation solves the basic equations for local mass and charge conservation along a fictitious straight channel. The mass balance of oxygen transport combines the transport along the channel with the conversion on the electrode surface.

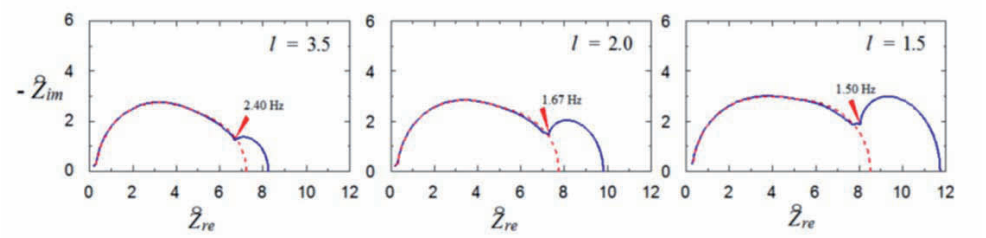

Fig. 36: Impedance spectra of a PEM fuel cell; solid line = limited oxygen diffusion; dotted line = unlimited oxygen diffusion

Fig. 36 shows the simulated impedance spectra for the oxygen stoichiometric factors l = 3.5, l = 2.0 and l = 1.5. The solid line shows the oxygen transport along the channel. The dotted line represents the limit of an infinitely large stoichiometric factor (l = infinitely or unlimitedly fast oxygen diffusion). Fig. 36 clearly shows that the effect of real mass transport along the channel and the associated diffusion boundary give rise to a clear semicircle in the range of lower frequencies. The radius of the semicircle decreases with increasing oxygen stochiometry. The point of intersection of the two semicircles depends weakly on the stoichiometric factor and is in the range of 1.5 Hz to 2.4 Hz. This result agrees well with the literature data and experimental findings.

3.3.3 Staff members and fields of activity

Name	Tel. (+49 2461-61-) e-mail address	Field of activity
Prof. Dr. W. Lehnert	3915 w.lehnert@fz-juelich.de	Head of High-Temperature Polymer Electrolyte Fuel Cells
J. Brinkmann	2177 j.brinkmann@fz-juelich.de	Lattice Boltzmann modeling on a cell-component level
Q. Cao	1923 q.cao@fz-juelich.de	Modeling of fuel cells with OpenFOAM
D. Froning	6676 d.froning@fz-juelich.de	Modeling of fuel cells, computer science, software engineering
Dr. H. Janßen	5082 h.janssen@fz-juelich.de	Head of HT-PEFC Stack Development

[10] Kulikovsky, A.A.: A model for local impedance of the cathode side of PEM fuel cell with segmented electrodes. J. Electrochem. Soc., 159 (2012), 294-300

Prof. Dr. A. Kulikovsky	5396 a.kulikovsky@fz-juelich.de	Development of analytical and numerical models of HT-PEFCs, DMFCs and SOFCs
Ms. F. Liu	9036 f.liu@fz-juelich.de	Electrode development and characterization
Ms. S. Lee	1923 s.lee@fz-juelich.de	Modeling of fuel cells with OpenFOAM
Ms. Dr. W. Maier	9073 w.maier@fz-juelich.de	Electrodes and MEA characterization
Ms. A. Majerus	3018 a.majerus@fz-juelich.de	Membrane and electrolyte characterization
Ms. Dr. M. Nullmeier	9074 m.nullmeier@fz-juelich.de	Principles of electrochemistry HT-PEFC
M. Prawitz	2574 m.prawitz@fz-juelich.de	PEFC, testing and characterization of HT-PEFCs
Dr. U. Reimer	3537 u.reimer@fz-juelich.de	Head of HT-PEFC Modeling and Simulation
Ms. B. Schumacher	5406 b.schumacher@fz-juelich.de	Development of designs for test stands for HT-PEFCs, testing of HT-PEFCs
J. Supra	6029 j.supra@fz-juelich.de	Development of HT-PEFC stacks, benchmarking of stack materials
V. Weißbecker	9576 v.weissbecker@jz-juelich.de	Corrosion investigation on metallic bipor plates

3.3.4 Important publications and patents

Publications:

Kvesić, M.; Reimer, U.; Froning, D.; Lüke, L.; Lehnert, W.; Stolten, D.
3D Modeling of a HT-PEFC Stack Using Reformate Gas
*Int. J. Hydrogen Energy, 2012, **37** (2012) 12438 – 1245*

Maier, W.; Arlt, T.; Wippermann, K.; Wannek, C.; Manke, I.; Lehnert, W.; Stolten. D.
Correlation of Synchrotron X-ray Radiography and Electrochemical Impedance Spectroscopy for the Investigation of HT-PEFCs
*J. Electrochem. Soc **159** (2012) F398-F404*

Lüke, L.; Janßen, H.; Kvesić, M.; Lehnert, W.; Stolten, D.
Performance Analysis of HT-PEFC Stacks
*Int. J. Hydrogen Energy **37** (2012) 9171-9181*

Kulikovsky, A.
A physical model for catalyst layer impedance
J.Electroanal. Chem. 669 (2012) Pages 28-34

Important patents

Patent applications:

Principal Inventor	PT	Description
Prof. W. Lehnert	1.2569	Tensioning means for a fuel cell stack and process for tensioning a fuel cell stack
Dr. H. Janßen	1.2593	Temperature control system for a fuel cell

Patents granted:

Principal Inventor	PT	Description
Ro. Peters	1.2338	High-temperature polymer electrolyte fuel cell system and process for operating the same

3.4 Direct methanol fuel cells

Direct methanol fuel cells (DMFCs) combine the reliability of a fuel cell with the advantages of using a liquid fuel. The high energy density of methanol (~16 MJ/l) makes DMFC systems an interesting alternative to existing energy conversion technologies as they allow operating times that are three to four times longer than batteries of the same size. DMFCs also have simple fuel logistics, making them more advantageous than hydrogen fuel cells (PEMFCs). Fuel cell systems also have fewer emissions (exhaust gases and noise) and lower maintenance costs than conventional converters, such as emergency diesel generators.

3.4.1 Objectives and fields of activity

The development goals involve improving the power density and the efficiency of MEAs and stacks while simultaneously reducing the costs associated with the design and fabrication of such systems. This approach is pursued for MEA development, MEA fabrication techniques and also for stack and system development. In the field of MEA development, new materials are being tested to improve the functionality of the MEA. However, not just new materials but also fabrication processes can impact on the functions of MEAs. MEA fabrication is concerned primarily with transferring the MEA fabrication processes developed in the laboratory to a pilot plant scale. An important intermediate step in MEA production is the fabrication of electrodes. While the active electrode area for laboratory work is only approx. 20 cm², production in a pilot plant concentrates on fabricating rolls of electrodes out of which the required stack electrodes are punched. The closer we come to achieving the aims of producing electrodes with as little catalyst as possible and achieving large electrochemical power density as well as high efficiency, the more important it is that the catalyst weight per unit area is distributed homogeneously over the electrode produced. For stack electrode production, it is extremely important that the electrodes are identical, i.e. the electrode properties must be homogeneous over the entire electrode area. An important electrode property is the catalyst weight per unit area, in other words the mass of catalyst per unit area of the electrode. Therefore, a core objective was and still is quantifying homogeneity in the catalyst weight per unit area of the electrode produced.

Stack and system development is based on the idea of using a direct methanol fuel cell (DMFC) to make it possible to sustainably supply electric energy on a kW scale. DMFCs directly convert methanol as a liquid fuel, in other words with no external fuel processing, into electric energy, heat and exhaust gas. The fuel cell system is characterized by its simple and robust design. Another advantage of the DMFC system is its safe operation, as no explosive fuels are used and the methanol-water mixture in the fuel cell itself is non-combustible.

3.4.2 Important results

In this section, particularly interesting results of DMFC development will be presented.

3.4.2.1 Water-based catalyst inks

In the past, catalyst inks for the fabrication of electrodes were produced using alcoholic solvents. These catalyst inks are easy to process but also require extensive measures for protection against explosion and compliance with the permissible occupational exposure limits. For this reason, catalyst inks were converted to aqueous solvents. Catalyst

dispersions can be fabricated without alcohols or other additives. However, they cannot be coated on gas diffusion substrates or decal substrates due to their hydrophobic surface. A wettability of these substrates was achieved by adding the surfactant triton X-100. In the anode, this surfactant can be used with no loss in performance; however, in the cathode, it causes a strong decrease in cell voltage. The wettability of hydrophobic surfaces can also be achieved by adding small amounts of alcohol to the aqueous ink. Since the percentage of alcohol is less than 10 %, there is no danger of explosion and it is much easier to comply with the occupational exposure limits. As shown in Fig. 37, the performance of MEAs fabricated with aqueous catalyst inks is comparable to that of MEAs fabricated with alcoholic catalyst inks.

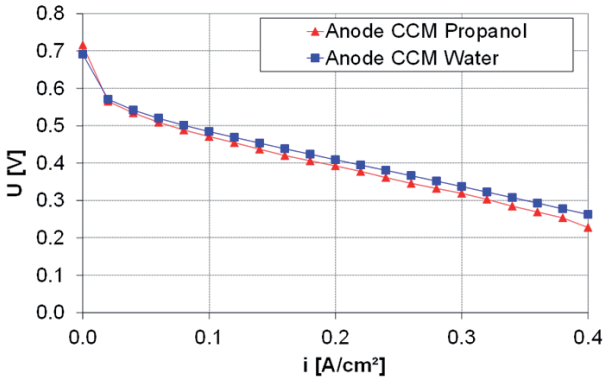

Fig. 37: Characteristics of MEAs whose anodes were fabricated using the decal process with aqueous and propanol-based catalyst inks

3.4.2.2 Variation of Nafion content in the cathode

In the catalyst layer, mass transport must be possible at every reaction site. The resulting protons must be diverted into the membrane and the resulting electrons into the gas diffusion substrate. The electrical conductivity is achieved using carbon, onto which the catalyst is coated. In order to introduce a proton-conducting phase, a solution of the membrane polymer Nafion is used. As the particle-laden catalyst ink dries, the pores required to transport the reactants and products are formed. While the ratio of the proton-conducting phase to the electron-conducting phase can be calculated based on the composition of the catalyst ink, the pores that form during drying can only be analyzed afterwards. Automated standard porosimetry is used to characterize the porosity of the catalyst layers. The catalyst layer is filled with a test liquid. By evaporating the test liquid, the catalyst layer is emptied step by step with the larger pores being emptied first. After each step, the catalyst layer is contacted with a standard of known pore structure and weighed. Contacting with the standard achieves capillary equilibrium, which means that pores of the same size are filled in both the catalyst layer and in the standard. Based on the amount of test liquid still contained in the catalyst layer and the known pore size of the standard, the pore size distribution of the catalyst layer can be calculated. This provides us with information on how many pores of what size are contained in the layer.

In this way, it was shown that for a Nafion-carbon ratio of one, which was assumed to be optimal, there were only a few pores in the nanometer range. For a Nafion-carbon ratio of 0.42, there were considerably more pores (see Fig. 38, left). This difference is particularly important when the cell is heavily loaded and has to produce a lot of electricity. To achieve a current density of > 0.2 A/cm², a lot of oxygen is required. For the Nafion-carbon ratio of around one, the few pores mean that not enough oxygen is supplied, causing the cell voltage to decrease considerably. For a Nafion-carbon ratio of 0.42, the large number of pores ensure that enough oxygen is provided and the cell voltage does not decrease as much with increasing load (see Fig. 38, right).

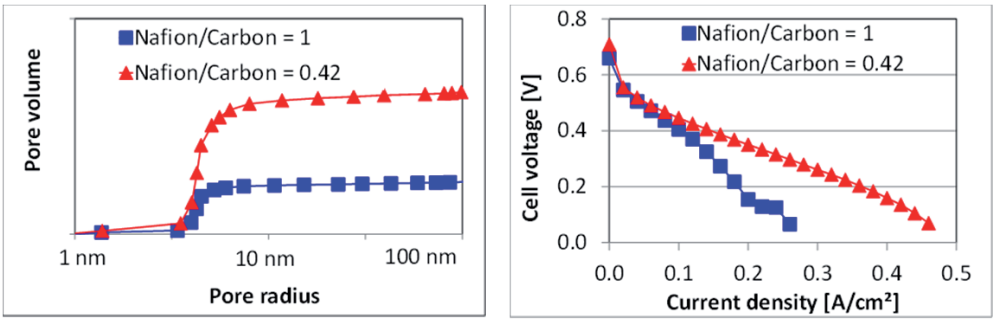

Fig. 38: Total pore volume of pore radii up to the value given on the x-axis (left); MEA characteristics as a function of the Nafion contained in the cathode (right)

3.4.2.3 CCM development

When catalyst layers are fabricated, the substrate (membrane or gas diffusion layer) is altered as the solvent used causes the membrane to swell or the catalyst ink to penetrate the gas diffusion substrate during coating. These influences are minimized when CCMs are fabricated via the decal route. In this way, only pressure and temperature during pressing can still cause changes. For this reason, the decal route was developed in addition to the established GDE route. The new route makes it possible to investigate variations in catalyst inks and to relate the observed effects to the composition of the catalyst inks as different diffusion of the inks in the gas diffusion substrate can be excluded.

3.4.2.4 MEA fabrication

In order to determine the statistical distribution of the electrode properties, samples are taken of the electrodes produced. These samples are the width of the roll (0.4 m) and a meter long. They are cut into smaller sample pieces measuring 4.2 cm x 4.2 cm and are then weighed individually. For each of the small samples, the basis weight bw (mass of the sample divided by its area) is determined as a function of the length and width position of the initial sample. Fig. 39 shows the results of the basis weight analysis of a produced electrode. In addition, Fig. 40 shows the mean values and standard deviations over the electrode width as a function of the electrode length (Fig. 40 A) and over the electron length as a function of the electrode width (Fig. 40 B).

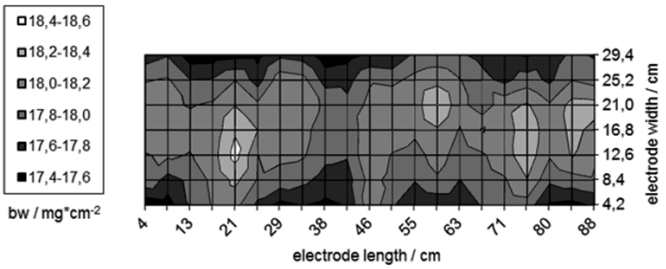

Fig. 39: Electrode weight per unit area as a function of electrode length and width

The analysis of the distribution of the weight per unit area revealed that more catalyst dispersion was deposited in the middle of the electrode path during coating than at the edges. This is shown by the dark edges in Fig. 39 and by the mean values over the electrode length (Fig. 40 B).

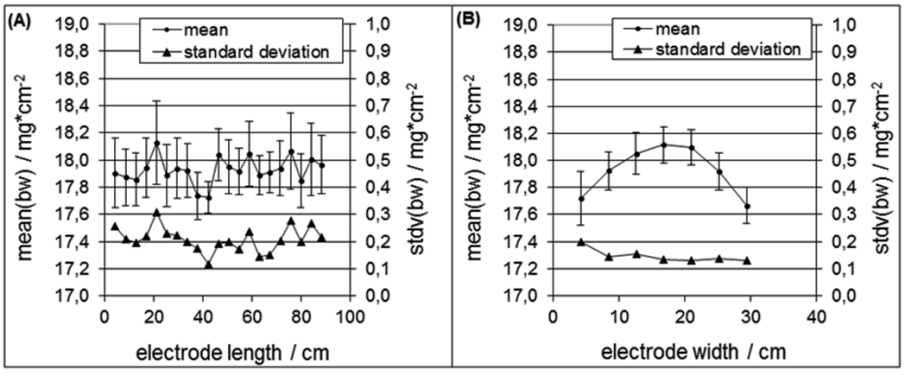

Fig. 40: Mean values and standard deviations over electrode width as a function of electrode length (A) and over electron length as a function of electrode width (B)

The reason for this coating error was discovered to be the doctor blade, which had an imprecisely sharpened knife edge. The doctor blade was resharpened and the coating process was repeated. The analyses of these coatings showed that the clear maximum in Fig. 40 B was corrected (see Fig. 42 B).

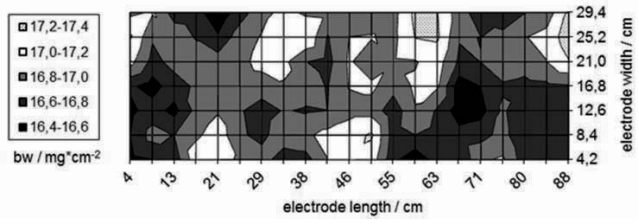

Fig. 41: Electrode weight per unit area as a function of electrode length and width

By reducing the influence of the doctor blade on the electrode weight per unit area, a structure that appeared periodically was also revealed. The bright areas in Fig. 41 represent weight per unit area maxima, which occur at intervals of approx. 25 – 30 cm and which are responsible for a large proportion of the variations in the electrode weight per unit area. Further tests showed that these maxima in the electrode path mean that differences in the catalyst weight per unit area of up to 0.5 mg/cm^2 must be expected within 20 – 30 cm. For present catalyst loading, this value is equal to approx. 16 %, which is much too high for the production of electrodes.

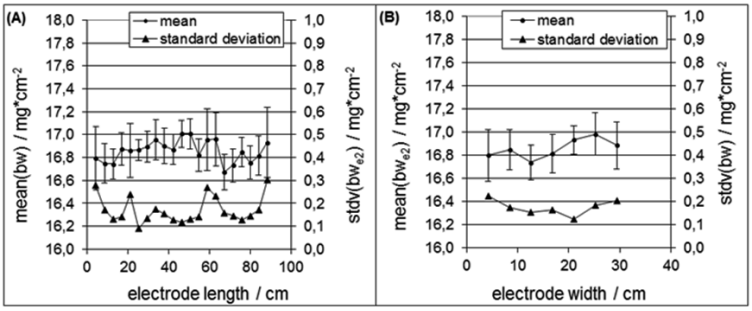

Fig. 42: Mean values and standard deviations over electrode width as a function of electrode length (A) and over electron length as a function of electrode width (B)

One reason for the maxima in the electrode weight per unit area could be variations in the thickness of the substrate used. The results of the substrate analyses presented in section 3.8 show that the structures found in the electrode weight per unit areas agree with those in the substrate weight per unit areas and substrate thicknesses. The substrate thus exhibits periodic variations, which have minima that occur at intervals of 25 – 30 cm. It was shown that these thickness minima could be filled up with catalyst dispersion by means of the blade coating used and that the increased thickness of the catalyst layer transformed the coating minima into maxima.

The results of the distribution of the electrode weight per unit area therefore show that the thickness variations that occur in the substrate used lead to coating inhomogeneities in the catalyst weight per unit area and that the substrate is thus unsuitable for the production of electrodes with small coating fluctuations. Further studies will concentrate on identifying suitable substrates with lower variations in thickness.

3.4.2.5 Development of stacks with metallic bipolar plates

In industrial projects focusing on alternative stack designs, metallic bipolar concepts were developed in cooperation with industrial partners. Activities were pursued in cooperation with the Fraunhofer Institute for Laser Technology in Aachen and Gräbener Maschinentechnik in Netphen-Werthenbach as part of a BMBF-funded project (reference no: 01 RI 0904 B).

At IEK-3, two innovative metallic bipolar plate concepts are currently being developed. Fig. 43 (left) shows the present design status of a single-shell concept. Such bipolar plates are fabricated from a metal sheet shaped in a hydroforming process. This allows the front and back side of a metal sheet to be used as flow distributors for the anode and cathode of a

fuel cell. Compared to conventional graphite bipolar plates, which typically exhibit a thickness of between 3 mm and 4 mm, these single-shell metallic bipolar plates have a thickness of 0.8 mm. This allows the volume of a stack to be reduced by up to 65 %. Due to the low pressure loss of the flow through the open cathodic flow distributor, the single-shell stack design can be operated with an energy-efficient fan instead of a compressor (see Fig. 43, right). This reduces losses caused by the peripheral components and increases the efficiency.

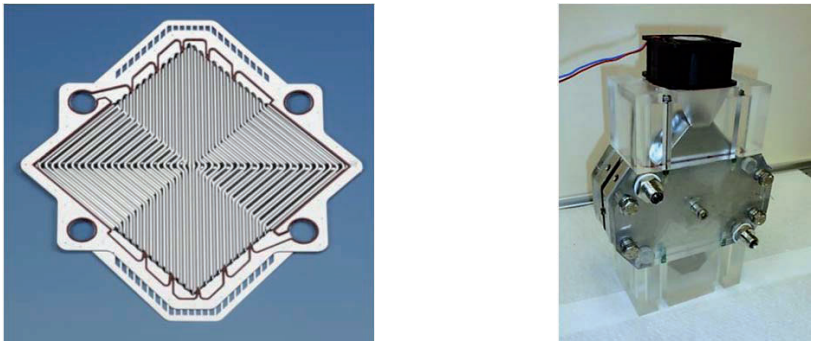

Fig. 43: Single-shell bipolar design (left); single-shell stack design (right)

Parallel to this development, a double-shell bipolar plate was also designed. Double-shell bipolar plates comprise two shaped metal sheets welded together in a laser welding process to form a bipolar unit. This process makes it possible to use different flow distributor geometries on the anode and cathode sides, which have been optimized for the two-phase flow of the corresponding electrode. A flow can be directed through the resulting cavity between the two half-shells for internal cooling or heating. One variant of the double-shell bipolar plate design is shown in Fig. 44 (left). Fig. 44 (right) shows a ten-cell short stack with a double-shell design, which was set up for test purposes at IEK-3. In addition to application in direct methanol fuel cells, the bipolar plate design is also being tested for suitability for use in HT-PEFCs.

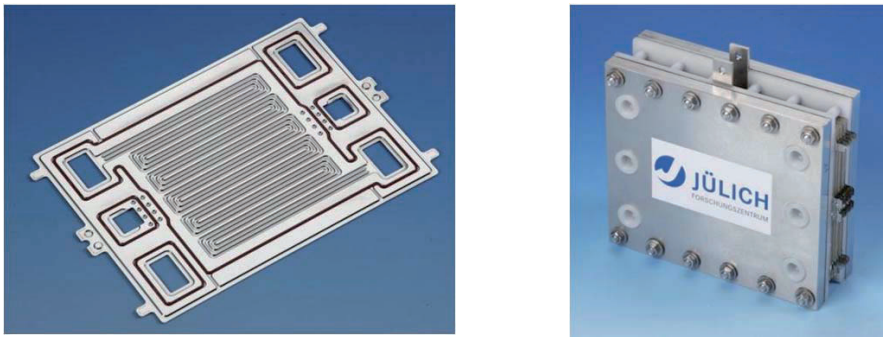

Fig. 44: Double-shell bipolar design (left); double-shell stack design (right)

At the moment, metallic bipolar plates can be operated with a lifetime of up to 2300 hours in a DMFC. Further development is required to increase the corrosion resistance. Different

approaches are being pursued to this end. In addition to the application of surface coatings and the selection of suitable materials, targeted changes in the operating behavior of the DMFC stack are conceivable.

3.4.2.6 Commercialization potential of DMFCs

Discussions with specialists from industry have made it clear that an uninterruptible power supply (UPS) would have a high market potential, particularly for LTE base stations [11] and for protecting security facilities if it could provide backup power for long outages, i.e. at least over a weekend (≥ 72 h).

To compensate for grid failures, systems presently use batteries. However, they are only capable of providing backup power for a few hours. To cover longer power outages, small diesel generators are used as an alternative (disadvantage: high maintenance and emissions) as are hydrogen fuel cells (disadvantage: low volumetric calorific value of hydrogen). DMFCs can provide backup power for several days, whereas the use of PEMFCs is limited because they require eight hydrogen cylinder bundles. Technically more complex fuel cell systems with methanol reforming exhibit a high range similar to DMFCs, but they necessitate higher investment and operating costs.

In order to evaluate the competitiveness of DMFC technology compared to other fuel cell technologies, the consultancy company Management Engineers in Düsseldorf was commissioned to compile a comparison of operating costs (cf. Fig. 45). Ten years with a service life of 5000 operating hours were set as an operating condition. In the technology comparison, the diesel generator and the DMFC were shown to be the most economic technologies. Compared to the diesel generator, the DMFC has the advantage that its operation involves lower exhaust gas emissions and that it prevents vibrations which could cause problems when installed in buildings.

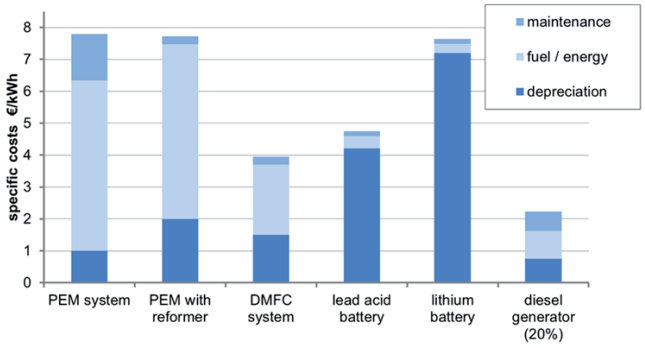

Fig. 45: Competitiveness of DMFC technology

Management Engineers also investigated the target price for a DMFC backup power system. The retail price for a DMFC system with an electric power of 2 kW was taken as € 15,000.

[11] LTE-Netze: Long-Term-Evolution-Netze, Nachfolgetechnik zu UMTS

The number of units produced per year was set initially to 100. This value is considered realistic for the first few years.

In the next step, the technical applicability of DMFC technology will be verified for UPS applications within a project funded by the Helmholtz Validation Fund. This validation project aims to develop and test hybrid energy systems in the 2 kW power class based on DMFCs for application as an uninterruptable power supply (USV). The work required for this concentrates on scaling existing DMFC systems from one to two kilowatts of net electric power and developing an operating mode that prevents the degradation of the DMFC stack during application-related downtimes. At the same time, the aim is to show that the target costs can be achieved by reducing or replacing expensive system and stack components.

3.4.3 Staff members and fields of activity

Name	Tel. (+49 2461-61-) E-mail address	Field of activity
Dr. M. Müller	1859 mar.mueller@fz-juelich.de	Head of Direct Methanol Fuel Cells
Ms. A. Burdzik	2574 a.burdzik@fz-juelich.de	MEA fabrication techniques
Ms. S. Cheriyan	5160 s.cheriyan@fz-juelich.de	MEA development
N. Commerscheidt	5400 n.commerscheidt@fz-juelich.de	MEA development
Ms. I. Friedrich	1984 i.friedrich@fz-juelich.de	MEA fabrication techniques
Dr. A. Glüsen	5171 a.glüsen@fz-juelich.de	MEA development
Ms. D. B. Günther	2378 d.guenther@fz-juelich.de	MEA fabrication techniques, quality management
M. Hehemann	5431 m.hehemann@fz-juelich.de	Stack and system development
T. Heinrichs	6004 t.heinrichs@fz-juelich.de	MEA development
Ms. N. Kimiaie	6484 n.kimiaie@fz-juelich.de	Head of Stack and System Development
Ms. R. Lambertz	5109 r.lambertz@fz-juelich.de	Stack and system development
T. Pütz	1946 th.puetz@fz-juelich.de	MEA fabrication techniques
Ms. S. Renz	9381 s.renz@fz-juelich.de	Stack and system development

A. Schulze Lohoff	1947 a.schulze.lohoff@fz-juelich.de	Stack and system development
Dr. M. Stähler	2775 m.staehler@fz-juelich.de	Head of MEA Fabrication Techniques
R. Wegner	4832 r.wegner@fz-juelich.de	Stack and system development
W. Zwaygardt	2103 w.zwaygardt@fz-juelich.de	Stack and system development

3.4.4 Important publications and patents

Important publications

Kulikovsky, A. A.
A model for carbon and Ru corrosion due to methanol depletion in DMFC
Electrochimica acta 56, 9846 - 9850 (2011)

Kulikovsky, A. A.
A model for mixed potential in the DMFC cathode and a novel cell design
Electrochimica acta 62, 185–191 (2012)

McIntyre, J.; Kulikovsky, A. A.; Müller, M.; Stolten, D.
Large-Scale DMFC Stack Model: Feed Disturbances and their Impact on Stack Performance
Fuel Cells 12(6), 1032 - 1041 (2012)

Kulikovsky, A. A.
A model for carbon and Ru corrosion due to methanol depletion in DMFC
Electrochimica acta 56, 9846 - 9850 (2011)

Dixon, D.; Wippermann, K.; Mergel, J.; Schökel, A.; Zils, S.; Roth, C.
Design Degradation effects at the methanol inlet, outlet and center region of a stack MEA
Journal of power sources, 196, 5538 - 5545 (2011)

Artl, T.; Manke, I.; Wippermann, K.; Tötzke, C.; Markötter, H; Riesemeier, H.; Mergel, J.; Banhart, J.
Investigation of the three-dimensional ruthenium distribution in fresh and aged membrane electrode assemblies with synchrotron X-ray absorption edge tomography
Electrochemistry Communications, 13 (8), 826–829 (2011)

K. Wippermann; R. Elze; C. Wannek; H. Echsler; D. Stolten
Influence of the ionomer type in direct methanol fuel cell (DMFC) anode catalyst layers on the properties of primary and secondary pores
Journal of Power Sources, 228, 57–67, (2013)

Stähler, M.; Friedrich, I.
Statistical investigations of basis weight and thickness distribution of continuously produced fuel cell electrodes
Journal of Power Sources, 242, 425–437, (2013)

Important patents

Patent applications:

Principal Inventor	PT	Description
Dr. M. Müller	1.2502	Method and device for producing membrane-electrode units for fuel cells
Prof. A.A. Kulikovsky	1.2544	Direct methanol fuel cell and process for operating the same

Patents granted:

Principal Inventor	PT	Description
J. Mergel	1.1886	Procedure for operating a fuel cell
J. Mergel	1.2062	Low-temperature fuel cell and process for operating the same
J. Mergel	1.2202	Low-temperature fuel cell and process for operating the same
Dr. M. Müller	1.2330	Fuel cell system and method for regulating a fuel cell system
Dr. M. Müller	1.2331	Fuel cell system and method for regulating a fuel cell system
Prof. A.A. Kulikovsky	1.2394	Method for recognizing and locating defects in a fuel cell within a fuel cell stack

3.5 Polymer Electrolyte Membrane Electrolysis

3.5.1 Objectives and fields of activity

Following a systematic analysis of the technological requirements and the scientific and technological expertise and resources at FZJ, it was decided to focus Jülich's activities on water electrolysis with polymer electrolyte membranes (PEM electrolysis). In order to ensure that PEM electrolysis technology can be realistically and sustainably implemented in industrial plants for the storage of renewable energies after 2020, further steps must be taken to solve outstanding technical issues in addition to scaling up the size of plants to the MW range in order to improve the inadequate stability and reduce the high costs of the technologies currently in use.

Work on the development of commercial electrolyzers with polymer electrolyte membranes (PEMs) is therefore pursued in cooperation with leading industrial enterprises in the field and concentrates mainly on reducing costs and increasing lifetime and power density. New membrane types are being developed for PEM electrolysis to replace the 175 – 200 µm thick extruded Nafion membranes currently used, as they do not possess sufficient mechanical or chemical stability for use in industrial systems under pressures of more than 50 bar. Another key target is to reduce and ideally completely replace metals from the platinum group – iridium, ruthenium and platinum – which are conventionally used for catalytic reactions with a loading of up to 6 mg/cm². The use of these platinum group metals therefore has to be reduced by at least 90 %, while the overload capability of the membrane electrode assemblies must be simultaneously increased to more than 4 W/cm² with a long-term stability of 40,000 hours. This will then allow PEM electrolysis to be commercially implemented on a GW scale for the storage of large quantities of energy from renewable electricity. Another work package focuses on developing new cost-effective materials and coating techniques for metallic separator plates and current collectors in order to reduce the costs associated with these components. At the moment, they account for 48 % of the stack costs (see chapter 5.2).

3.5.2 Important results

3.5.2.1 Catalyst-coated membrane (CCMs) development

Polymer electrolyte membrane electrolyzers for hydrogen production usually comprise titanium separator plates with flow fields which distribute the reactants through the porous current collectors and subsequently over the electrode surface (catalyst layer). The two porous catalyst layers (anode and cathode) are essentially fabricated by mixing the catalyst with an ionomer then coating this substrate over each side of the membrane electrolyte film (≈ 200 µm thick). A diagram of a catalyst-coated membrane (CCM) is shown in Fig. 46. The zero-gap concept, or Grubb cell [12], provided by this configuration, results in optimal mechanical stability of the CCM where the ohmic losses between the catalyst layer and membrane are attenuated. When the catalyst layers are coated directly onto the membrane,

[12] Grubb, W.T.: Ionic migration in ion-exchange membranes. Journal of Physical Chemistry, 63 (1959), 55–67

the gas bubbles are not released inside the interpolar area but at the rear side of the cell, preventing electrode delamination. The CCM configuration has also demonstrated better catalytic layer adherence, fewer dimensional changes when the membrane is dried, and lower levels of gas crossover. In this condition, catalyst particles in the subsurface region of the membrane promote the catalytic re-oxidation of cross-permeating hydrogen.

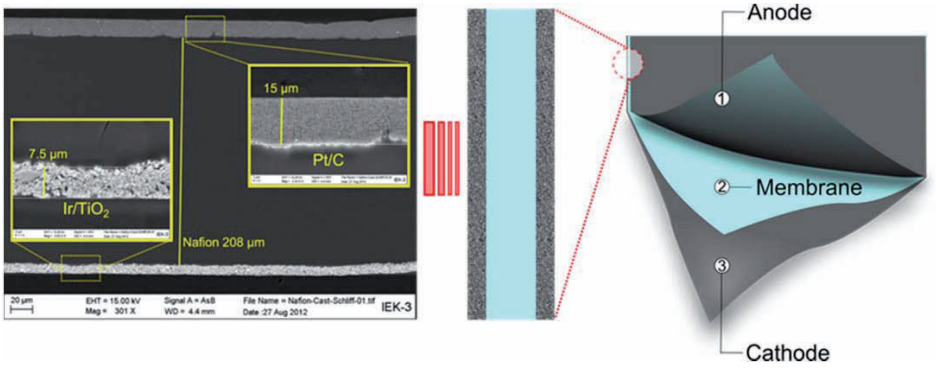

Fig. 46: Diagram of a catalyst-coated membrane for a PEM water electrolyzer. Scanning electron microscope (SEM) cross-sectional image of a commercial CCM

The methods used to fabricate CCMs play a fundamental role in the final performance, durability, and cost of the PEM electrolyzer. It is also important to evaluate suitable catalyst systems, ionomers, and membranes that will be incorporated in a CCM. In the next section, we will describe the results obtained for catalyst, ionomer and membrane screening, and the methods used to fabricate CCMs. We will also outline the first characterization results (physical and electrochemical) for the different components.

Catalyst screening

Catalysts for PEM water electrolysis were originally mainly fabricated using platinum black and iridium black materials, and for these early systems, high metal loadings were also used. On the cathode side, where the hydrogen evolution reaction (HER) takes place, platinum black was later substituted by platinum nanoparticles supported on carbon black materials due to successful results developing these catalysts for PEM fuel cells. According to the literature, loadings for the cathode side today range from 0.5 $mg \cdot cm^{-2}$ to 1 $mg \cdot cm^{-2}$ in commercial catalysts from different manufacturers (ETEK/BASF, Tanaka, and Johnson & Matthey). Due to extensive experience at IEK-3 working with catalysts manufactured by Johnson Matthey and using them for fuel cell development, the Pt/C catalyst from Johnson Matthey was chosen as a benchmark catalyst for different evaluations and comparisons. In addition, our collaboration with Solvicore GmbH also allowed catalysts from Umicore GmbH (also Pt/C) to be used as benchmark catalysts for the cathode. Cathode development for PEM electrolyzers concentrates on reducing platinum loading (< 0.2 mg cm^{-2}), improving catalyst utilization (homogeneity, particle size), and potentially substituting the noble platinum to create “platinum-free catalysts”.

On the anode side, where the oxygen evolution reaction (OER) takes place, Ir (IrO_2) is generally considered as the state-of-the-art for the OER. Ru (RuO_2) is more active than Ir, but problems related to instability (corrosion) limit its use. According to the literature, the

loadings for the anode catalyst layer are in the range of 2 mg cm^{-2} due to the low catalyst surface area and low utilization of these iridium catalyst systems. The main R&D aim today is to obtain anode systems with low metal loadings (< 0.6 mg cm^{-2}), improved performance and higher stability (> 40,000 hours). We used anode catalyst systems, such as iridium black from Alfa-Aesar and Ir/TiO_2 from cooperation partners, as benchmark catalysts.

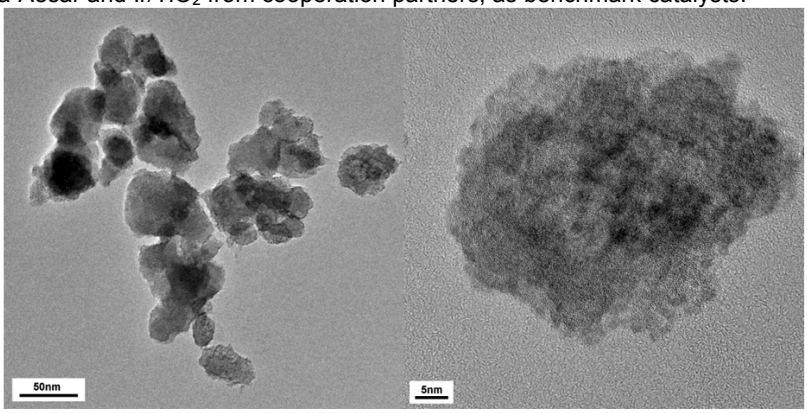

Fig. 47: Transmission electron microscopy (TEM) images for iridium black from Alfa-Aesar

The TEM analysis for the benchmark catalysts from Alfa-Aesar is presented in Fig. 47. The analysis suggests that these catalyst systems based on metal black structures present high agglomeration and consequently low utilization or a low electrochemical surface area for the OER. The iridium catalyst supported on TiO_2 particles yields a much better distribution of the nanoparticles, allowing a higher performance with a lower loading of the catalyst in a CCM configuration.

The most direct approach to electrochemically characterize these catalyst systems would be to produce catalyst-coated membranes (CCMs) and to measure their catalytic activity in a single-cell configuration. Unfortunately, it is generally very difficult to extract the intrinsic electrochemical activity of catalysts from CCM testing due to uncertainties related to undefined mass transport resistances, incomplete utilization of the electrocatalysts, and difficulties in water and gas management which are often related to the nature of the current collectors and design of the electrolyzer cell. One method of measuring the electrochemical performance of electrolyzers without interference from these phenomena is to use the rotating disk electrode (RDE) technique.

The general principle of fabricating an RDE loaded with electrocatalysts consists of supporting a defined amount of catalyst powder/binder mixture with an electrically conductive substrate (e.g. glassy carbon), resulting in the formation of a thin catalyst/binder layer on the rotating disk electrode (RDE) substrate (Fig. 48). For thick catalyst layers with a catalyst utilization of less than 100 % and mass transport limitations, this method can be used to demonstrate the relative differences between several catalyst systems before testing them in a CCM configuration.

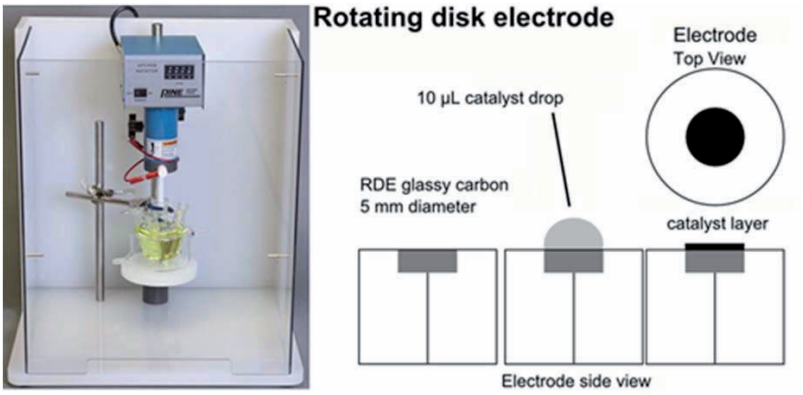

Fig. 48: Rotating disk electrode technique for the electrochemical characterization of electrocatalysts for PEM water electrolysis

Ionomer and membrane screening

In PEM water electrolysis, the commercial Nafion membrane from Dupont is usually used due to its chemical and thermal stability, mechanical strength, and high proton conductivity. Fig. 49 shows as an example the ion transport outcome for a Nafion 117 membrane. The results obtained at IEK-3 (black line - measured) agree with the results found in the literature (red and blue). However, the use of Nafion membranes also has disadvantages, including the high cost, and difficulties regarding its disposal due to the fluorine contained in the backbone structure. Membrane characteristics must also be improved in order to decrease the gas crossover and to improve the stability and durability over time, particularly at differential operational pressure (> 50 bar).

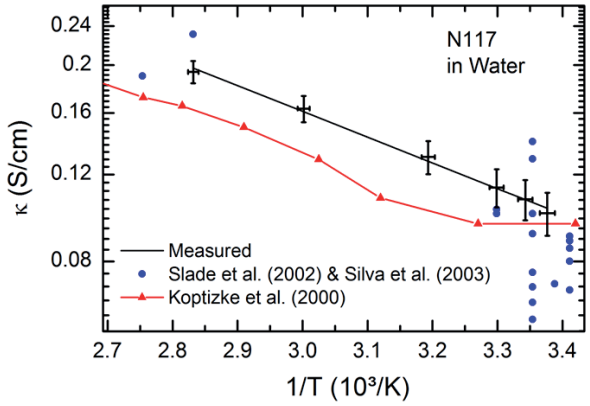

Fig. 49: Arrhenius plot of proton conductivity for Nafion 117 from Dupont

Our efforts concentrate on developing less expensive proton exchange membranes, and improving their ion exchange characteristics and durability for PEM electrolysis. Nafion membranes and their alternatives have been extensively studied in PEM fuel cells. However, it should be noted that the hydration state of the membrane differs between fuel cell operation and electrolysis operation. During PEM fuel cell operation, the membrane is

humidified by the humidified gases and equilibrated with water vapor, whereas during PEM electrolysis operation, the electrolyte membrane is exposed to a liquid phase of water and fully hydrated during water electrolysis.

Together with FuMA-Tech GmbH, we are evaluating perfluorosulfonic polymer membranes (PFS) and hydrocarbon (HC) membranes as potential alternatives to substitute and improve the characteristics of Nafion membranes. Nafion 117 will function as a benchmark membrane and it will be used for comparison with the developed membranes.

CCM fabrication

The performance obtained using CCMs for PEM water electrolysis is intrinsically affected by the number of available catalytic sites in the catalyst layer of a CCM. The performance is not only dependent on the number and surface area of the nanoparticles, but also on how accessible they are to the reactants. Hence, the method used to prepare the CCM will directly affect the performance and durability of the electrolyzer. The reason for this is that each method of preparing the catalyst substrate and the method used to coat the membrane will directly affect the mechanical stability and chemical composition of the catalytic layer and the disposition of the triple-phase structure.

Different methods can be used to prepare the CCMs, including hand brushing, spraying, screen printing, and blade coating. We have used the blade coating method on a PTFE fiberglass substrate, following by a transfer procedure to the membrane using a hot-pressing approach known as the decal method. In this method, the Nafion ionomer and catalyst particles are well mixed and well dispersed into a paste substrate. After transferring the substrate to the surface of the membrane, the quick evaporation of the solvents leads to the formation of a very porous network in the catalyst layer in which the catalyst is surrounded by a recast Nafion ionomer network.

Fig. 46 and Fig. 50 show SEM images of the microstructure of an iridium electrode on a CCM prepared by the decal method. The granular and coarse characteristics of the iridium electrode are clearly visible in comparison to conventional Pt/C electrodes. Further developments are necessary to obtain tailored iridium catalytic layers with an optimized porous network.

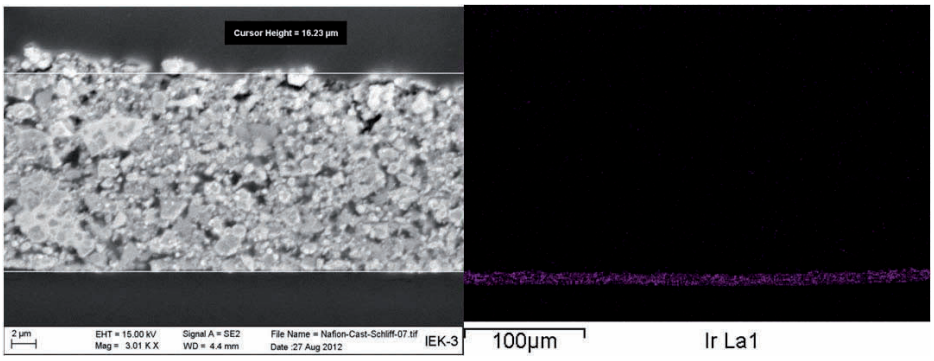

Fig. 50: Left: Scanning electron microscope (SEM) cross-sectional image of a CCM showing the anode electrode (iridium black); right: EDX elemental mapping of the anode electrode (iridium black)

The addition of polymer solutions with ionic transport properties (e.g. Nafion ionomer) to the catalytic layer has both positive and negative impacts on the electrode in PEM electrolysis. It promotes proton transport from the bulk of the catalyst layer (nanoscopic level) to the membrane, and acts as a binder providing a three-dimensional stable catalyst structure, lending mechanical stability and consequently durability to the electrode [13].However, it also decreases the electronic conductivity of the catalyst and makes the catalyst layer more hydrophilic, potentially reducing mass transport out of the catalyst layer. Therefore, the triple-phase-boundary and ionomer layer characteristics must be optimized. To date, only a very few studies [14, 15] have concentrated on this topic. In general, it can be concluded that the ionomer loading ranges from 20 % to 30 % over the dry catalyst weight. The method of ink and MEA preparation has a significant influence on the interfacial resistance [16].The optimal Nafion ionomer loading was found to be 25 wt% for the anode and 20 wt% for the cathode. Other studies are required in order to further optimize the triple-phase boundary [17].

Electrochemical characterization of the CCMs

Single-cell testing can be used to screen the developed components under a variety of operation conditions such as temperature, pressure, cell pressure (torque), flow of reactants, humidification, operating inputs, etc. The two main objectives of single-cell experiments are first to obtain performances that are comparable to the state of the art for PEM water electrolyzers, and second, to ensure that the performance is reasonably stable for long-term operation.

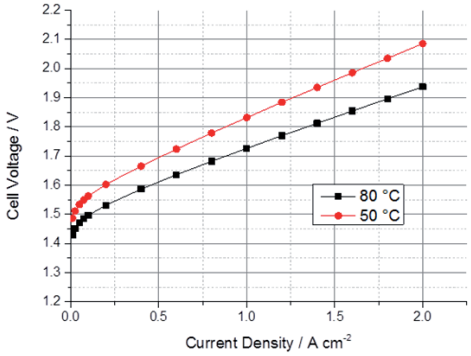

Fig. 51: Polarization curve for a CCM. Cathode: Pt; anode: Ir, Nafion membrane; cell area: 25 cm^2, at 80 and 50 °C

[13] Xu, W.; Scott, K.: The effects of ionomer content on PEM water electrolyseur membrane electrode assembly performance. Int. J. of Hydrogen Energy, 35 (2010), 12029 - 12037

[14] Goni-Urtiaga, A.; Presvytes, D.; Scott, K.: Solid acids as electrolyte materials for proton exchange membrane (PEM) electrolysis: Review. Int. J. of Hydrogen Energy, 37 (2012), 3358-3372

[15] Xu, J.; Miao, R.; Zhao, T.; Wu, J.; Wang, X.:. A novel catalyst layer with hydrogen-hydrophobix meshwork and pore structure for solid polymer electrlyte water electrolysis. Electrochem. Comm., 13 (2011), 437-439

[16] Zhang, Y.; Wang, C.; Wan, N.; Liu, Z.; Mao, Z.:. Study on a novel manufacturing process of membrane electrode assemblies for solid polymer electrolyte water electrolysis. Electrochem. Comm., 9 (2007), 667-670

[17] Carmo, M.; Roepke, T.; Roth, C.; dos Santos, A.M.; Poco, J.G.R.; Linardi, M.: A novel electrocatalyst support with proton cunduvtive properties for polymer electrolyte membrane fuel cell applications.: J. of Power Sources, 191 (2009), 330-337

Fig. 51 presents the performance of a single cell comprising a commercial SolviCore GreenerityTM E300 CCM, for which 1.3 A cm^{-2} was obtained at 1.8 V and 1.94 V at 2.0 A cm^{-2}. If this performance is compared with the state of the art presented in Fig. 52, it becomes clear that the result obtained here for the commercial CCM is within the range for PEM water electrolyzers given in many publications that have appeared since 2010. Further developments are likely to improve the different components and could lead to CCMs with better performance compared to the current state of the art.

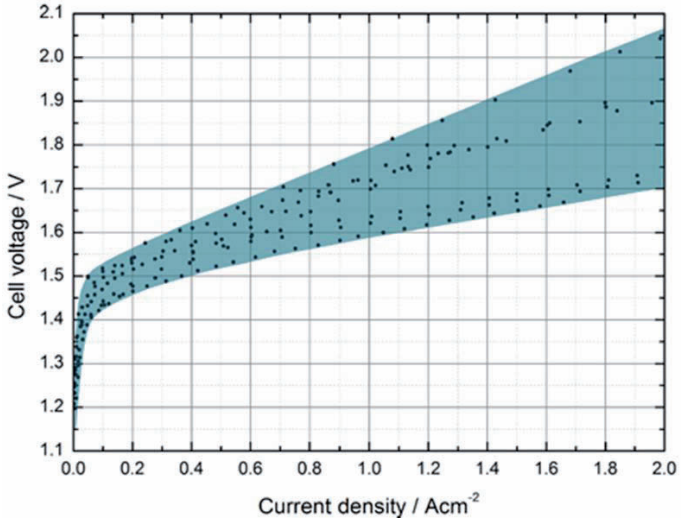

Fig. 52: Performance range of polarization performance curves published in 2010–2012 for a PEM electrolysis single cell operating with Ir anode, Pt cathode, and Nafion membrane at 80 °C

3.5.2.2 Separator plate development

Thermal balance analysis

The thermal analysis was performed using a model developed in-house derived from a combination of computational models found in the literature [18, 19, 20, 21, 22]. The Gibb's free energy approach was employed to accurately capture the effects of temperature, pressure and species concentration while modeling the open circuit voltage. This uses the

---

[18] Marangio, F.; Santarelli, M.; Cali, M.: Theoretical model and experimental analysis of a high pressure PEM water electrolyser for hydrogen production. Int. Journal of Hydrogen Energy, 34 (2009), 1143-1158

[19] P. Choi, N. H.: Thermodynamics and Proton Transport in Nafion. Journal of The Electrochemical Society, 152 (2005), 123-130

[20] Awasthi, A.; Scott, K.; Basu, S.: Dynamic modeling and simulation of a proton exchange membrane electrolyzer for hydrogen production. Int. Journal of Hydrogen Energy, 36 (2011), 14779-14786

[21] Nie, J.; Chen, Y.: Numerical modeling of three-dimensional two-phase gas–liquid flow in the flow field plate of a PEM electrolysis cell. Int. Journal of Hydrogen Energy, 35 (2010), 3183-3197

[22] Dale, N.V.; Mann, M.D.; Salehfar, H.: Semiempirical model based on thermodynamic principles for determining 6 kW proton exchange membrane electrolyzer stack characteristics. J. of Power Sources, 185 (2008), 1348-1353

enthalpy and entropy of the various species at the operating temperature and pressure in order to solve for the open circuit voltage [22]. The advantage of this approach compared to many others in the literature is its reliance on well-established data (enthalpy and entropy) to determine the open circuit voltage as opposed to the common empirical formulations that are accurate for only one specific electrolyzer configuration.

An electrical resistance model of great detail was selected due to the importance of resistivity (V=iR) at high current densities. This is especially important when modeling PEM electrolyzers due to their ability to operate in high overvoltage scenarios where the current density can reach over three times the nominal current density. The formulation for resistance was derived to capture many aspects of both the current collectors and the separator plates through a complex ohmic resistor network. This was designed to consider the channel support material, width and height, the current collector thickness, in-plane resistivity and through-plane resistivity, and the contact resistance between the current collector and the separator plate [18]. With this detailed model, many aspects can be evaluated with regard to Joule heating for the thermal analysis, as well as flow field and separator plate design for maximized flow and conductivity.

The transport of water and protons through the membrane is especially important when modeling PEM electrolyzers, as compared to the PEM fuel cell the operating pressure is higher and the membrane typically thicker. To accurately account for this transport phenomenon, the model developed by Choi et al. [19], which considers the Grothuss and bulk diffusion of protons along with the electro-osmotic drag of water molecules through the membrane, was employed.

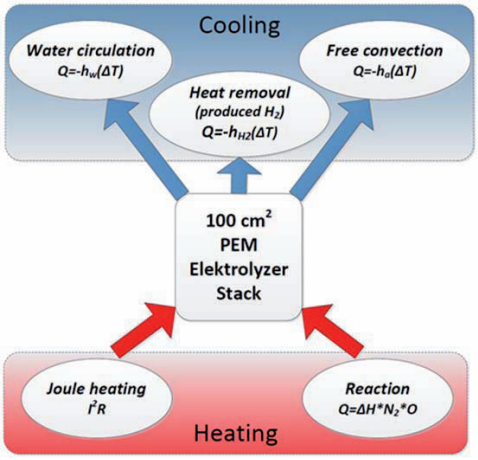

Fig. 53: Schematic of the thermal balance control volume used to determine heat exchanger requirements and whether or not additional heating and cooling is necessary to operate the electrolyzer

To test whether or not heating or cooling is necessary, a thermal balance was calculated for an operational range of 0 A cm^{-2} to 6 A cm^{-2}. The calculations follow the control volume analysis show in Fig. 53. The heat generation from cell operation was determined by the polarization curve and the current density in the operation range. Fig. 54 (left) shows a conservative polarization curve for the operation of a PEM electrolyzer. It simulates poor

performance, which requires a higher heat removal rate, creating a factor of safety for the least capable components of the system. A heat balance can be obtained by applying the polarization curve with the heat sinks and sources associated with a PEM electrolyzer.

For the thermal simulation, heat going into the system was considered positive and heat leaving the system was considered negative. The simulation was run with the supply water at a ΔT = -5 °C and a supply rate of λ = 150, which is well below the typical values currently used in industry (-10 °C < ΔT < 15 °C and 150 < λ < 300), to ascertain whether or not coolant circulation should be added to the system. Fig. 54 (right) shows the heat balance of the system when operating with the aforementioned parameters. When the thermal energy reaches or exceeds zero, this means the system requires additional external cooling and that the supply water at ΔT = -5 °C and λ = 150 is not sufficient to maintain the operating temperature. Either a higher flow rate of supply water or a larger temperature difference between the cell and incoming water is therefore needed.

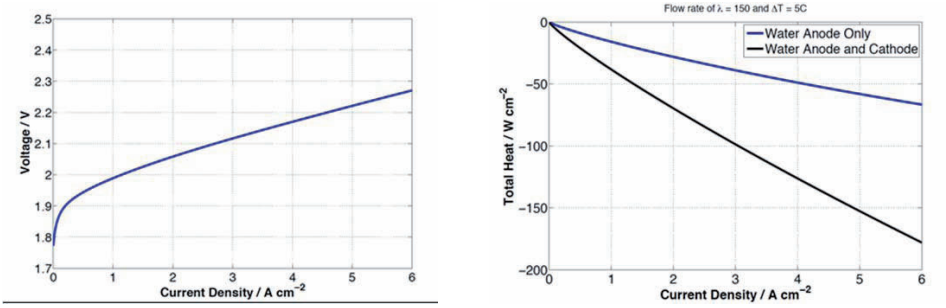

Fig. 54: Polarization curve simulated by a model developed in-house for the prediction of the thermal energy produced during cell operation (left). Thermal balance of a 10-cell electrolyzer demonstrating that the circulating water is capable of removing enough thermal energy to keep the cell from overheating at λ = 150 and ΔT = 5 °C (right)

Water circulation on both the anode and cathode sides of an electrolyzer would be helpful in dissipating any excess heat. Fig. 54 (right) compares thermal management with and without cathode water circulation and shows that neither setup requires a cooling loop. This is important due to the mass transport limitations that arise when circulating water on the cathode side. Without the need for water circulation on the cathode side, better performance and higher current densities can be achieved.

3.5.3 Staff members and fields of activity

Name	Tel. (+49 2461-61-) E-Mail address	Field of activity
J. Mergel	5996 j.mergel@fz-juelich.de	Head of Polymer Electrolyte Membrane Electrolysis
Dr. M. Carmo	5590 m.carmo@fz-juelich.de	Development of catalysts and membrane electrode assemblies for PEMs with optimized performance and long-term stability

Dr. D. Fritz	9384 d.fritz@fz-juelich.de	Modeling, development and optimization of current collectors, separator plates and stacks for PEM electrolysis
T. Höfner	9804 t.hoefner@fz-juelich.de	Development of membrane electrode assemblies for alkaline PEM electrolysis
M. Langemann	9759 m.langemann@fz-juelich.de	Development and evaluation of suitable substrates and coatings for metallic bipolar plates in PEM electrolyzers
P. Paciok	9801 p.paciok@fz-juelich.de	Reduction and substitution of platinum group metals in hydrogen electrodes for PEM electrolysis
C. Rakousky	9803 c.rakousky@fz-juelich.de	Development of cheap and sustainable catalyst materials for oxygen electrodes in PEM electrolysis
M. Schalenbach	9802 m.schalenbach@fz-juelich.de	Development and evaluation of membranes with higher conductivity and mechanical and chemical stability for PEM electrolysis

3.5.4 Important publications

Important publications

Carmo, M., Fritz, D.L., Mergel, J., Stolten D.
A comprehensive review on PEM water electrolysis
International Journal of Hydrogen Energy (2013, in press)

Mergel, J., Carmo, M., Fritz, D.L.
Status on Technologies for Hydrogen Production by Water Electrolysis
in Transition to Renewable Energy Systems (Stolten), Wiley-VCH Verlag GmbH & Co. KGaA (2013, in press)

3.6 Process and Systems Analysis

3.6.1 Objectives and fields of activity

The department performs process and systems analyses for planning and consulting. Data searches and system simulations are used to determine energy and mass balances, performance data, emissions and costs. These allow a quantitative comparison of energy systems. The priorities in the period under review were as follows:

- Energy strategy to meet the targets for reductions in greenhouse gas emissions set by the German federal government
- Design/cost of a hydrogen pipeline network to supply road traffic
- Fuel consumption of passenger cars with electric and conventional drive concepts
- Membrane-based CCS processes for coal power plants (post-/oxy-/pre-combustion) and module concepts for capturing oxygen
- Supporting the head of institute in organizing the second and third ICEPEs
- Screening analysis of the use of CO_2 for chemical synthesis

The first two topics and the last topic are dealt with in separate sections. The activities related to gas capture are currently being reduced to free up resources for other activities focusing on energy strategies, namely:

- Stationary hydrogen storage systems, regional storage requirements and network modeling
- Hydrogen infrastructure: operator concepts and detailed cost models
- Simulation of electrolyzers under dynamic load and their incorporation into the grid

3.6.2 Important results

3.6.2.1 Simulation-based fuel consumption analysis of passenger cars

With the aim of reducing fuel consumption and greenhouse gas (GHG) emissions, drives with an increasing utilization of electricity are being developed throughout the world for passenger cars. Fuel cell electric vehicles (FCVs) facilitate local zero-emission driving while generally maintaining the usual performance data. Battery electric vehicles (BEVs) also have zero emissions locally but for a considerably reduced range. They exhibit the lowest energy demand but require mains power. Internal combustion engine vehicles (ICVs) are continuously being optimized. In hybrid electric vehicles (HEVs), electric drive components optimize the mode of operation of the combustion engine and reduce consumption by recycling the braking energy. To assess drive systems, the provision of fuel and/or electricity must be analyzed (well-to-tank analysis, WTT) as must the energy utilization in the vehicle itself (tank-to-wheel analysis, TTW). The simulation-based tool described here is used for TTW analysis. The following types of passenger car are being assessed:

- passenger car with internal combustion engine, ICV
- parallel hybrid passenger car with internal combustion engine and battery, PAH
- electric passenger car with battery, BEV

- electric passenger car with fuel cells and battery, FCV

Vehicle parameters relevant to fuel consumption, such as resistance coefficients, vehicle mass and gear ratios, were kept uniform or determined using uniform procedures. For drives, in addition to the physical wheel-road model, parameters were also used to describe the drive motor. Batteries were represented on the basis of equivalent circuit diagrams. For fuel cells, current-voltage characteristics were taken into account. To determine the power requirements of the auxiliary consumers, masses and energy balances of the energy converters were taken into consideration. Particular attention was paid to the time-dependent description of electric power in the on-board power supply system and to the development of optimal operating strategies. The power requirements of the heating or cooling systems were determined using a specially developed model component as a function of the environmental conditions and vehicle speed (Fig. 55).

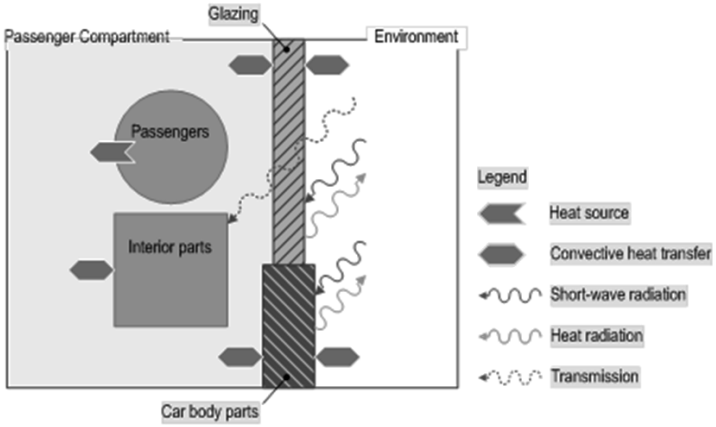

Fig. 55: Simplified model of the vehicle interior and designation of the heat flows considered. Source: IEK-3, adapted in accordance with

For a simulated C-segment passenger car, this model allows a maximal heating capacity of 4.3 kW and cooling capacity of 2.2 kW to be specified. These values apply for -15 °C in the case of heating and 36 °C in the case of cooling and a driving speed of 18 km h^{-1}. To minimize the fuel demand, optional operating points of converters were evaluated as part of the operating strategy in relation to the energy balance of the system as a whole. These optimally determined operating points were set as the desired values of the powertrain components. In hybrid systems, the operating strategy was supplemented by a storage strategy. The results of the analysis are expected in the first six months of 2013.

3.6.2.2 Post-combustion carbon capture (PCC) with polymer membranes

A comprehensive literature search was performed for CO_2-selective membranes. Rubbery block copolymers (e.g. Pebax® and Polyactive®) maintain their separation efficiency in the presence of steam. Their large-scale industrial production allows the mass fabrication of gas separation membranes today. The PVAm/PVA facilitated transport membrane is a very promising vitreous candidate because of its high CO_2/N_2 separation efficiency for wet feed flows. Despite efforts to improve the gas transport of these polymers, our calculations showed that CO_2 permeability is too low for PCC application. One characteristic of all

polymer membranes is that an increase in temperature enhances the CO_2 permeance but reduces the CO_2/N_2 permselectivity. A previous study on a binary feed gas (14 mol% CO_2 + 86 mol% N_2) was extended to include real wet flue gas. The Polyactive® membrane (Tab. 7) was used for this purpose. The operating parameters were equivalent to those of the NRW reference power plant (Tab. 8).

Temperature		**50 °C**	**30 °C**	**25 °C**
Permeance [Nm^3/m^2hbar]	CO_2	5	4.3	3
	H_2O	15	43.3	53
Permselectivity	CO_2/N_2	25	36	50
	O_2/N_2 Ar/N_2	2.8	2.8	2.8

Tab. 7: Properties of the Polyactive® membrane

Power gross / net	600 / 555 MW		
Net efficiency	45.9 %		
Steam parameters	285 bar; 600 / 620 °C		
Coal	Klein Kopje		
Flue gas pressure	1,05 bar		
Volume flow	1.6 million Nm^3/h		
Flue gas composition (mol%)	**Temperature**		
	50 °C	**30 °C**	**25 °C**
CO_2	13.5	14.7	14.9
N_2	70.1	76.4	77.2
O_2	3.7	4.0	4.0
H_2O	11.9	4.0	3.0
Ar	0.8	0.9	0.9

Tab. 8: Operating parameters and flue gas composition of the NRW reference power plant

As an example, results are shown for a vacuum-driven membrane cascade (Fig. 56). In order to set the temperature, the flue gas is cooled before the membrane process.

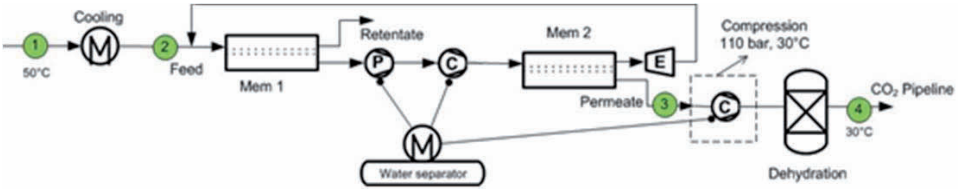

Fig. 56: Membrane cascade, permeate compression with 4/3 cooling steps before/after membrane 2

Due to the high permeability for steam, the temperature now has a great influence on energy consumption in contrast to binary gas (Fig. 57). For CO_2 separation efficiencies that are not too high, the membrane cascade only has energy-related advantages over MEA scrubbing at 25 °C and 30 °C. On the other hand, steam permeation has a sweeping effect, which increases the CO_2 separation efficiency for the given membrane area and the same vacuum compared to binary gas. For a separation efficiency of approx. 80 %, the required membrane area at 25 °C with 4.9 m^2/kW_{el} is 1.5 times higher than at 50 °C. An economic evaluation is planned to include module design and pressure losses.

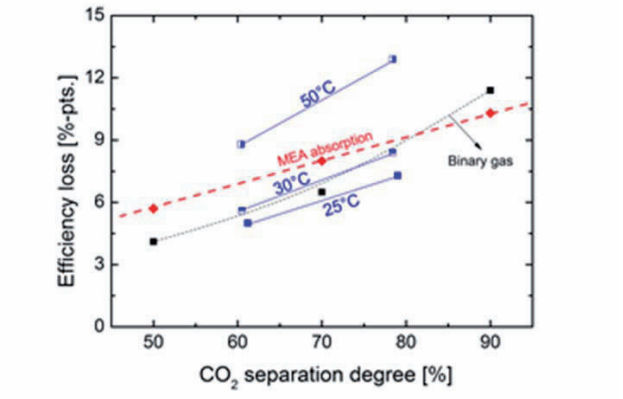

Fig. 57: Net efficiency losses. Polyactive® membrane cascade, real flue gas

3.6.2.3 Membrane-based oxyfuel process for carbon dioxide capture

Oxyfuel processes involve the removal of nitrogen from the combustion air in order to obtain a flue gas consisting almost exclusively of CO_2. Cryogenic air separation is state of the art. Its energy requirements depend on the degree of purity and range between 0.169 kWh_{el}/kg_{O2} and 0.245 kWh_{el}/kg_{O2}. In the membrane process investigated here, the driving force for oxygen transport was provided using a vacuum (Fig. 58).

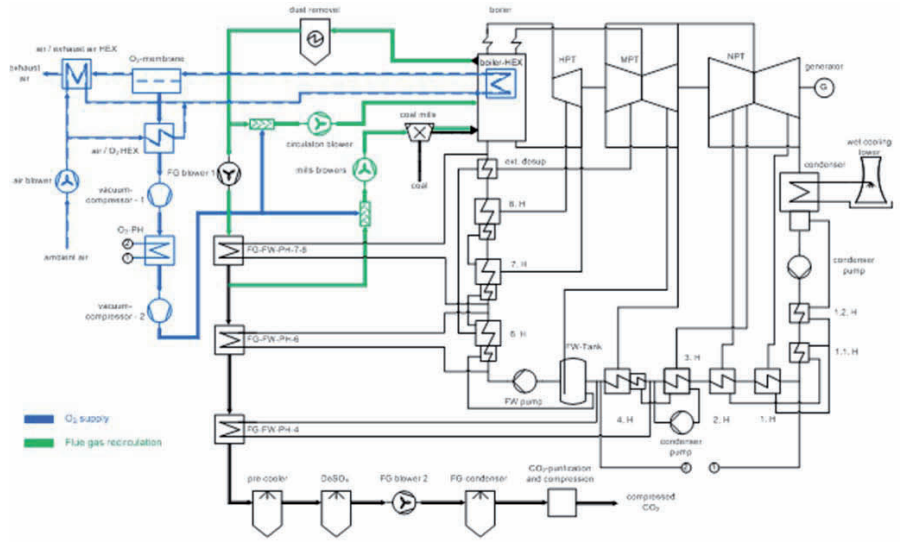

Fig. 58: Flowsheet of the simulated Oxy-Vac-Jül concept

Fresh air was warmed by means of heat recovery from the exhaust air and oxygen. The terminal temperature difference at the hot end was 43 K. The final heating of the fresh air using the flue gas occurs above the boiler. The analysis was based on the hard coal NRW reference power plant. The vacuum compressor efficiencies were 75 % isentropic and 95 % mechanical/electric. The waste heat use of the flue gas is limited by the acid dew point of 153 °C. The flue gas route from the pre-cooler is the same as that of the Vattenfall pilot plant.

The net efficiency exhibits a flat maximum at an oxygen separation efficiency of 60 % and is equal to 39.3 % here including CO_2 compression to 200 bar (Fig. 59). The efficiency losses here are 6.6 percentage points compared to the NRW reference power plant. For lower oxygen separation efficiencies, the main losses are caused by lost heat in the exhaust air flow and the capacity of the air blower, whereas at higher separation efficiencies, losses are predominantly caused by vacuum suction. The specific effort associated with supplying oxygen is therefore 0.12 kWh_{el}/kg_{O2}, which is clearly below that of cryogenic air separation. The increase in the oxygen partial pressure ratio from 1.1 to 1.3 requires a lower vacuum (76 mbar instead of 89 mbar). This causes the net efficiency of the process at the optimal point to decrease by 0.25 percentage points (Fig. 59). A change in the pressure drop on the air/exhaust air side from 2 % to 3 % of the inlet pressure reduces the net efficiency of the process at the optimal design point by 0.25 percentage points.

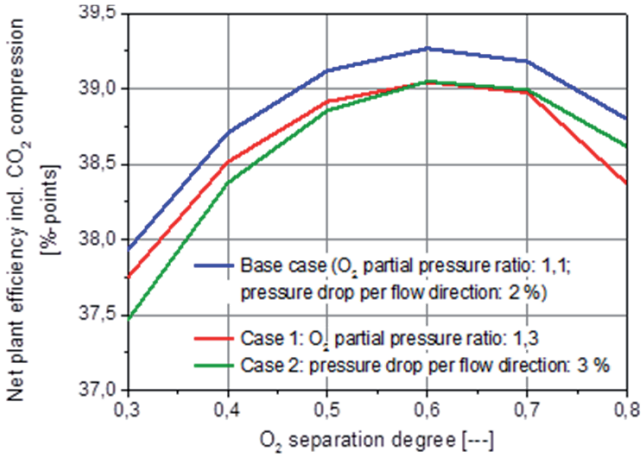

Fig. 59: Net efficiency in relation to oxygen separation efficiency

3.6.2.4 Pre-combustion carbon capture with water-gas shift membrane reactors

The integrated gasification combined cycle (IGCC) represents a highly efficient method of converting solid fuels into electricity. This process makes it possible by means of a water-gas shift reaction with added steam to convert the carbon monoxide produced in the gasification

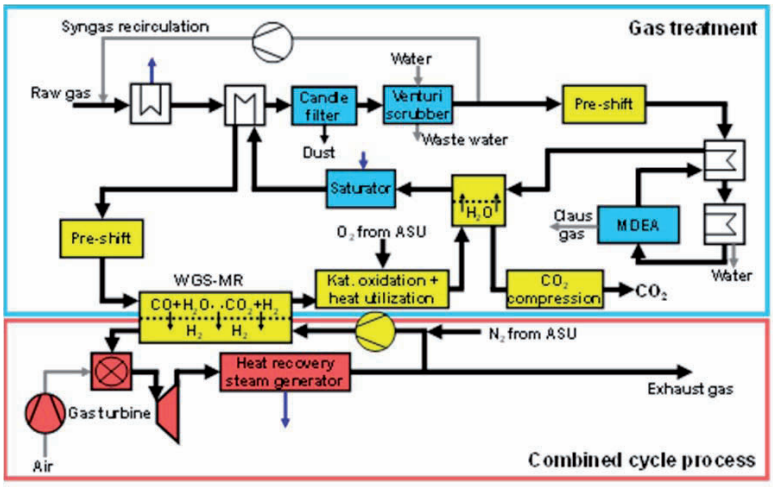

Fig. 60: IGCC process with WGS-MR and a membrane for steam recirculation

process into CO_2 and to remove it before combustion. Work focuses on designing and simulating process variants for efficient CO_2 capture. For comparison, a reference IGCC without CO_2 capture and one with Selexol scrubbing were simulated. The latter is a physical absorption process already used industrially for CO_2 capture. The calculations were performed using Aspen Plus and EbsilonProfessional and resulted in an overall efficiency of 48.0 % for the reference IGCC and 38.4 % for the Selexol IGCC with CO_2 compression to

120 bar, which is equal to a loss of 9.6 percentage points. To reduce this loss, a concept was developed on the basis of a water-gas shift membrane reactor combining the conversion of carbon monoxide to CO_2 with the separation of hydrogen using a H_2-selective membrane (Fig. 60).

The amount of steam can thus be reduced, while the CO conversion can be simultaneously increased. Sweeping the permeate side with inert gas at the same absolute pressure results in a H_2 partial pressure gradient without the necessity for hydrogen compression. The sweep gas used here is the exhaust gas of the combined cycle process, which evens out the temperature along the membrane by adsorbing the reaction heat, due to its large quantities. At a H_2O/CO ratio of 1.3, the overall efficiency losses are reduced to 4.7 percentage points.

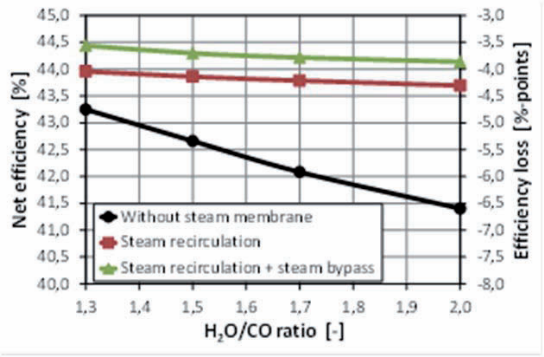

Fig. 61: Overall efficiency of the IGCC with WGS-MR for different variants

Further improvements could be made possible using membranes exclusively permeable to steam. An insert to recirculate the steam remaining in the retentate to pre-wet the syngas before water is added would lead to a further efficiency increase of 0.7 percentage points at the design point (Fig. 61). Furthermore, it would also reduce the impact of an increase in excess steam, which may be required to prevent soot formation. An insert to bypass the cold desulfurization would also appear to make sense: avoiding steam condensation leads to an improvement of 0.4 percentage points. This would reduce the overall efficiency losses to 3.6 percentage points, resulting in an overall efficiency of 44.4 %.

3.6.3 Staff members and fields of activity

Name	Tel. (+49 2461-61-) E-mail address	Field of activity
Prof. Dr. D. Stolten	3076 d.stolten@fz-juelich.de	Head of department (acting): energy strategy, hydrogen infrastructure, emissions
T. Grube	5398 th.grube@fz-juelich.de	Vehicle simulation, analysis of the provision of energy sources
B. Kumar	9743 b.kumar@fz-juelich.de	Alkaline electrolyzers for wind energy storage
S. Luhr	6689 s.luhr@fz-juelich.de	Polymer membrane modules for CO_2 capture

J. Nazarko	3742 j.nazarko@fz-juelich.de	Power plants, Oxyfuel, MEA scrubbing
A. Otto	4113 a.otto@fz-juelich.de	Oxygen transport membrane modules, CO_2 utilization
M. Robinius	3077 m.robinius@fz-juelich.de	Operator concepts and the costs of hydrogen infrastructure
S. Schiebahn	8731 s.schiebahn@fz-juelich.de	Pre-combustion capture, power-to-gas
Ms. V. Tietze	4113 v.tietze@fz-juelich.de	Stationary hydrogen storage systems and network modeling
Ms. L. Zhao	4064 l.zhao@fz-juelich.de	Gas separation processes with polymer membranes

3.6.4 Important publications, PhD thesis and patents

Important publications

Grube, Th.; Schindler, V.; Stolten, D.

Potential der Stromnutzung in Pkw-Antrieben zur Reduzierung des Kraftstoffbedarfs (*Potential of using electricity in passenger car drives to reduce fuel consumption*)

In proceedings: Innovative Fahrzeugantriebe 2012, Dresden, VDI Verlag GmbH Düsseldorf VDI-Berichte 2183, ISBN, 2012

Low, B. T.; Zhao, L.; Merkel, T.; Weber, M.; Stolten D.

A parametric study of the impact of membrane materials and process operating conditions on carbon capture from humidified flue gas

Journal of Membrane Science DOI: http://dx.doi.org/10.1016/j.memsci.2012.12.014

Baufumé, S.; Grüger, F.; Grube, T.; Krieg, D.; Linssen, J.; Weber, M.; Hake, J-F.; Stolten, D.

GIS-based scenario calculations for a nationwide German hydrogen pipeline infrastructure

Accepted for publication in International Journal of Hydrogen Energy

Nazarko, J.; Otto, A.; Herbergs, A.; Weber, M.; Stolten, D.

Auslegung einer membranbasierten Luftzerlegungsanlage für ein Oxyfuel-Kraftwerk *(Design of a membrane-based air separation unit for an Oxyfuel power plant*)

In Beckmann, Hurtado Kraftwerkstechnik 4, TK-Verlag, 2012, 978-3-935317-87-0

PhD

Krieg, D.:

Konzept und Kosten eines Pipelinesystems zur Versorgung des deutschen Straßenverkehrs mit Wasserstoff
(Concept and Cost of a Pipeline System to Supply Hydrogen to Fuel Cell Cars in Germany)

Schriften des Forschungszentrums, Reihe Energie & Umwelt, Band 144, ISBN: 978-3-89336-800-6

Important patents

Patent applications:

Principle Inventor	PT	Description
Dr. E. Riensche	1.2501	IGCC power plant with a water-gas shift membrane reactor (WGS-MR) and method for operating such an IGCC power plant with flushing gas
Dr. E. Riensche	1.2584	Method for operating two subprocesses with different steam requirements in an overall process
Dr. E. Riensche	1.2585	Method for operating a steam-requiring subprocess in an overall process

Patents granted:

Principle Inventor	PT	Description
Dr. E. Riensche	1.2366	Membrane power plant and technique for operating the same

3.7 Analysis

3.7.1 Objectives and fields of activity

In the Physicochemical Fuel Cell Laboratory, the basic structure-activity relationships of complex processes in electrochemical energy converters, such as fuel cells, are investigated with the aim of identifying ways of improving them. The physicochemical properties of cell components and model cells are explored. In situ and/or spatially resolved techniques are used to analyze structures and effects:

- Imaging and spatially resolved analysis techniques (SEM/EDX, CLSM, optical microscopy, MS for catalyst characterization)
- Spectroscopic methods (Raman, IR)
- Thermochemical and mechanical analysis techniques (TGA, DSC, elasticity/expansion measurements, BET, porosimetry, contact angle measurements)
- Electrochemical analysis techniques (EIS, CV, conductivity)

The methods are adapted as required and further developed. One aim is to verify and establish the mechanical and thermochemical perequisites for use in fuel cells. Another is to explain fundamental microscopic mechanisms, such as those responsible for the redox kinetics of electrodes or ion transport in the electrolyte membranes and how they depend on operating parameters.

3.7.2 Important results

3.7.2.1 Spectroscopic *ex situ* characterization of polybenzimidazole membranes doped with phosphoric acid

Polybenzimidazoles (PBIs) doped with phosphoric acid are among the most frequently used membrane materials for application in high-temperature polymer fuel cells (HT-PEFCs). The proton conductivity required for the cell to function is strongly dependent on temperature, the H_3PO_4 doping level and the water content, i.e. on the water vapor partial pressure in the gas chamber of the cell. Despite the fact that operating parameters, such as electrical load, fuel and air flow strongly influence the electrical output of the cell via the membrane's water content, little is known about the chemical equilibria in the ternary system PBI – H_3PO_4 – H_2O as a function of the composition. This includes the proton transfer processes between H_3PO_4, H_2O and the polymer, e.g. the dominating conduction mechanism for different H_3PO_4 doping levels and varying water content. Just as little is known about possible condensation equilibria of the phosphoric acid to long-chained poly acids, such as diphosphoric acid.

In cooperation with the Central Institute for Engineering, Electronics and Analytics (ZEA), Raman spectroscopic studies were performed to investigate the chemical interactions between H_3PO_4, H_2O and PBI as a function of the H_3PO_4 doping level. Raman spectroscopy was used to analyze cross-linked and non-cross-linked AB-PBI (Fig. 62, left). *Ex situ* studies in the wavenumber range 500 cm^{-1} – 2000 cm^{-1} provided information on the incorporation of H_3PO_4 and H_2O molecules between the polymer chains and the formation of H-bridges with the imidazole units of the chains. By referring to the data in the literature on analogous structures, the signal groups were successfully assigned to specific vibrational modes. For

doping levels with more than two H_3PO_4 molecules per imidazole unit, Raman signals appear that cannot be directly attributed to the polymer-bound H_3PO_4 molecules (Fig. 62, right).

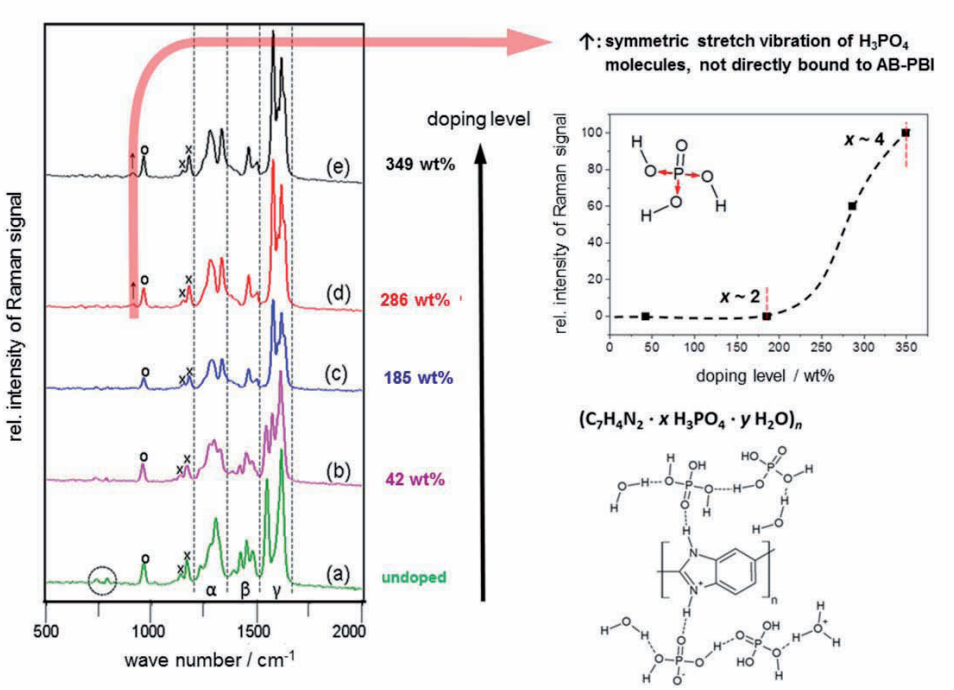

Fig. 62: **FT Raman spectra for (a) undoped AB-PBI and (b)–(e) AB-PBI doped with increasing levels of H_3PO_4 (left); increase in the intensity of the Raman signal of H_3PO_4 molecules not bound to AB-PBI (top right); (possible) structure of AB-PBI with H bridge network for a doping level of x = 4 (bottom right)**

Further information on the microscopic structure was obtained using nuclear magnetic resonance spectroscopy in cooperation with the Institute of Complex Systems (ICS-6) and the Central Institute for Engineering, Electronics and Analytics (ZEA). The first ^{1}H- und ^{13}C-NMR studies were performed with non-cross-linked *m*-PBI dissolved in dimethyl acetamide (Fig. 63, left). All proton groups and groups of C atoms and their mutual couplings were unambiguously identified. A temperature-dependent displacement and broadening of the resonance signal k was also observed for the proton at imidazole N (Fig. 63, right). This was caused by an increasing rate of tautomeric proton exchange between the two imidazole Ns. The strong broadening of the resonance signals of the C atoms b, i and j can be explained by the tautomerism in the imidazole ring.

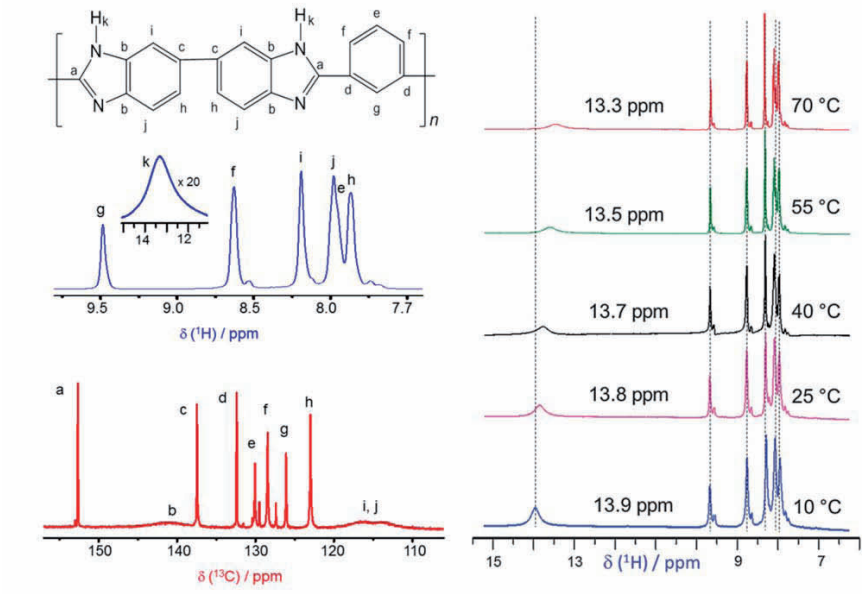

Fig. 63: Structure of the repeating unit of m-PBI (top left); 1H-NMR spectrum (middle left) and 13C-NMR spectrum (bottom left) of m-PBI dissolved in dimethyl acetamide at a temperature of 70 °C with the assignment of all resonance signals; temperature-dependent displacement of the resonance signal of the imidazole NH proton (right)

In addition to ^{1}H, ^{13}C and ^{31}P-NMR analyses of the polymer fully dissolved in phosphoric acid, solid-state NMR investigations examining the swollen polymer are also ongoing and/or being planned. Initial ^{31}P-NMR studies showed that direct interactions between the H_3PO_4 molecules first occur at high doping concentrations, i.e. when there are on average more than two H_3PO_4 molecules per imidazole unit. This verifies the results of the Raman studies with respect to the presence of phosphoric acids not directly bound to the polymer chains. The studies were performed in cooperation with ICS-6 at Forschungszentrum Jülich and the Department of Chemical Sciences at the University of Padua in Italy.

3.7.2.2 Electrical conductivity in the system H_2O – H_3PO_4 – PBI

In order to gain an in-depth understanding of the processes in a phosphoric acid based fuel cell, such as the HT-PEFC, the microscopic structure and properties of the ternary system H_2O – H_3PO_4 – PBI must be understood and the properties of the binary subsystem H_2O – H_3PO_4 must also be known. Detailed conductivity values for the operation temperature range of the HT-PEFC between 140 °C – 200 °C are therefore desirable in order to improve existing systems by means of modeling. Furthermore, when operating parameters such as electrical load, fuel and air flows change, it takes a relatively long time before a new state of equilibrium is observed. The reasons for this could be the exchange kinetics of water vapor with the doped membrane as well as with the unbound phosphoric acid in the electrodes. Diffusion processes and the formation kinetics of polycondensed phosphoric acids may also play a role. No satisfactory answers have been provided to date. In order to investigate the

subsystem H_2O – H_3PO_4, a conductivity cell made of quartz glass was therefore developed and fabricated in cooperation with the glassworks at the Central Technology Division (ZAT; see Fig. 64).

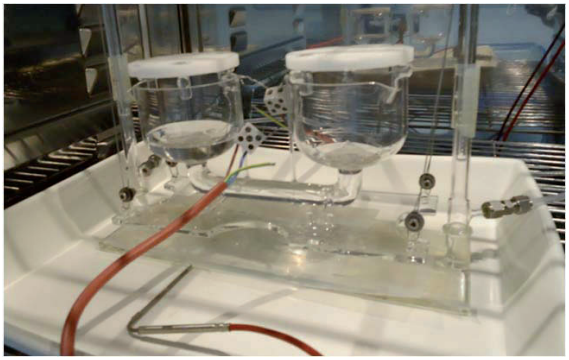

Fig. 64: 4-point cell for measuring the conductivity of phosphoric acid as a function of temperature and water vapor partial pressure

This cell allows four-point DC and AC conductivity measurements (impedance measurements) to be taken under the operating conditions of an HT-PEFC, i.e. up to more than 160 °C and variable water vapor partial pressure. The measurements are performed in a climate chamber in which humidity and temperature are kept constant. Measurements are possible with humidities up to a dew point slightly below 100 °C, which corresponds to the conditions in an atmospherically operated HT-PEFC. In order to achieve a uniform mix in the measurement cell when equilibrium is being established with the atmosphere, a pneumatic tilt mechanism was developed – again, in collaboration with the glassworks at ZAT. The extreme operating conditions in the climate chamber pose a problem. Following extensive tests and calibration, the first data are now available.

In the (well) stired conductivity cell, the measured conductivity shows an exponential convergence to a new equilibrium value, when chaniging the parameter temperature and water vapor partial pressure. As expected, the water uptake/release of the phosphoric acid solution exhibited first-order kinetics. Therefore, the equilibrium value of the conductivity can be determined very precisely by fitting a simple exponential approach. The reproducibility of the measurements was better than 1 %. Initial results show a strong dependence on composition for the rate of achieving equilibrium, i.e. for the water vapor exchange kinetics.

The water content was also determined using Karl Fischer titration so that electrical conductivity, water vapor partial pressure and acid concentration could be combined in the solution. The first measurements at 60 °C and 90 °C confirm the conductivity maximum at 50 wt.% – 58 wt.% H_3PO_4 and a water vapor partial pressure of 140 mbar – 440 mbar (Fig. 65). This corresponds to a molar ratio of 1:5 – 1:4 between H_3PO_4 and H_2O.

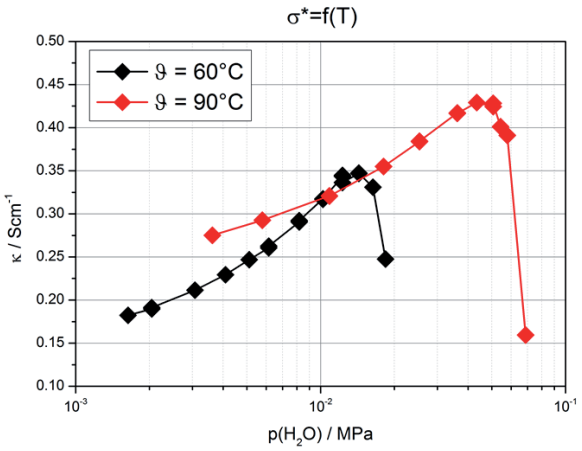

Fig. 65: **Conductivity of phosphoric acid as a function of temperature and water vapor partial pressure after equilibrium concentrations have been reached**

3.7.2.3 Spatially resolved measurements ity of the noble metal catalyst in the electrode layer. Particularly critical operating conditions in this respect are the state without current load (open cell voltage) and fuel depletion in a single cell of a stack. In order to investigate such processes, a locally resolved characterization of the activity of electrode catalyst layers is necessary.

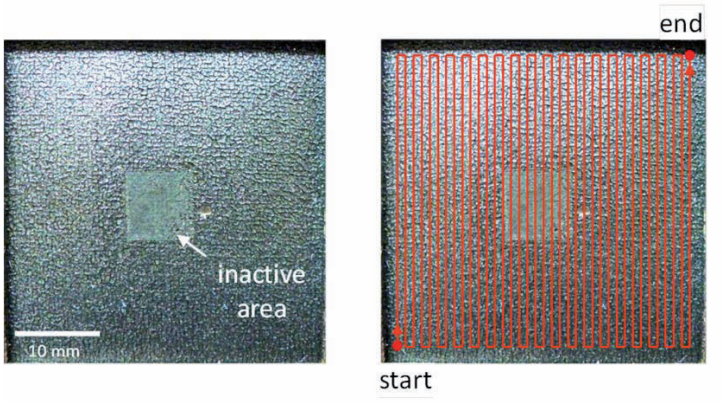

Fig. 66: **Cathode GDE, image of cathode layer; catalytically inactive area in the center (left); schematic showing the design of the meander scan with 37 x 37 = 1369 measurement points, increment of 1 mm and 45 s dwell time per measurement point (right)**

Spatially resolved mass spectrometry (SRMS) was used to automatically determine the spatial distribution of the heterogeneous catalytic activity of a cathode GDE in a DMFC comprising three layers, i.e. carbon fiber, microlayer (Vulcan carbon black + PTFE) and the catalyst layer (JM HiSPEC 13100 Pt/C catalyst + Nafion). In order to make the difference between catalytically active and inactive areas clear, an inactive area with no Pt catalyst

measuring around 1 cm² was also prepared in the center of the GDE cathode, as shown in Fig. 66. Hydrogen oxidation served as a heterogeneously catalyzed reaction. In contrast to methanol oxidation, it has the advantage that it can also be used for anode catalysts (see subsequent sections). An educt gas with the composition 99.0 % He / 0.5 % H_2 / 0.5% O_2 and a flow rate of 20 ml/min. was used. The surface temperature of the sample was 105 °C. The sample surface measuring approximately 4 x 4 cm² was subjected to a meander scan with a total of 37 x 37 = 1369 measurement points for a dwell time per measuring point of 45 s and a total measurement time of approx. 17 h (Fig. 66, right).

As shown in the image on the left and the 3-D image on the right in Fig. 67, comparing the active and inactive areas revealed differences in the concentration of hydrogen of up to 2000 ppm.

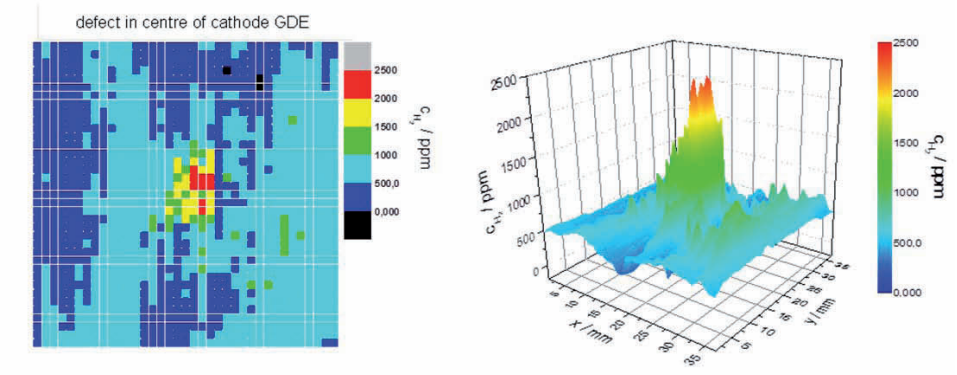

Fig. 67: Hydrogen concentration distribution as the result of the surface scan of a cathode GDE described in Fig. 66

Hydrogen oxidation was also used to investigate the local heterogeneous catalytic activity of PtRu in DMFC anode GDEs. The anode GDE comprises three layers, i.e. carbon fiber, microlayer (Vulcan carbon black + PTFE) and the catalyst layer (JM HiSPEC 12100 PtRu/C catalysat + Nafion). A circular hole with 9 mm Ø was punched out of the center of the GDE and a catalytically inactive section of a GDL (microlayer made of fleece) of the same size and shape was inserted into this hole (Fig. 68, left). Under the same operating conditions as described previously, a line scan was then performed from the inactive sample center to the left active sample edge with 17 equidistant spot measurements along the red line shown in Fig. 68 (left). The local hydrogen concentrations determined and the scan depth in the *z* direction are plotted in the image on the right in Fig. 68 as a function of *x*. At the transition from the inactive to the active cell area, the hydrogen concentration decreases significantly by approx. 70 %, corresponding to a difference of approximately 1000 ppm.

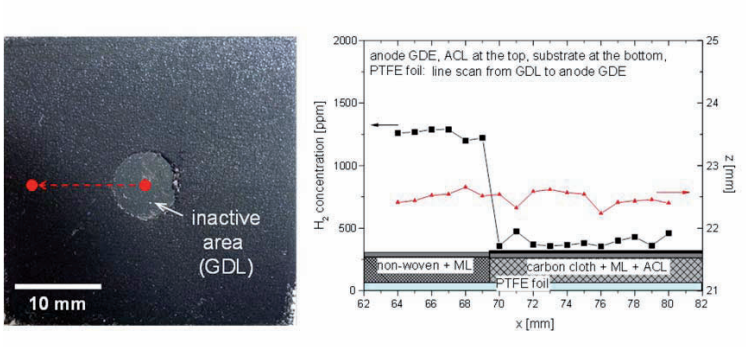

Fig. 68: **Line scan (dotted red line) on an anode GDE with 17 measurement points, increment of 1 mm and 3 min. dwell time (left); hydrogen concentration and vertical profile z (the larger the z value, the deeper the scan tip) along the line scan (right)**

3.7.3 Staff members and fields of activity

Name	Tel. (+49 2461-61-) E-mail address	Field of Activity
PD. Dr. C. Korte	9035 c.korte@fz-juelich.de	Head of the Physicochemical Fuel Cell Laboratory
T. Bergholz	1891 t.bergholz@fz-juelich.de	System evaluation: Li accumulators in different fields of application, aging processes
Ms. Dr. F. Conti	9568 f.conti@fz-juelich.de	Spectroscopic investigations: Raman, IR, NMR
Dr. H. Echsler	8710 h.echsler@fz-juelich.de	Imaging analysis techniques: SEM/EDX, CLSM
J. Keppner	1891 j.keppner@fz-juelich.de	Basic research on ion conduction and diffusion along phase boundaries in SOFC materials
Ms. K. Klafki	1895 k.klafki@fz-juelich.de	Conventional sample preparation
Ms. T. Mandt	1891 t.mandt@fz-juelich.de	Degradation in SOFCs, grain-boundary diffusion of Sr in CGO barrier layers
Dr. J. Wackerl	6228 j.wackerl@fz-juelich.de	Physical properties: DSC, TGA, mechanical properties, conductivity
K. Wedlich	9763 k.wedlich@fz-juelich.de	Electrical characterization of Li accumulators, aging processes
Dr. K. Wippermann	2572 k.wippermann@fz-juelich.de	Aging mechanisms in DMFCs, electrochemical investigations, spatially resolved measurements

3.7.4 Important publications and patents

Important publications

Wippermann, K.; Schröder, A.

Neutron radiography for the investigation of reaction patterns in direct methanol fuel cells

Chapter No. 8 in: Polymer electrolyte membrane and direct methanol fuel cell technology: In situ characterization techniques for low temperature fuel cells (Vol. 2), Edited by C Hartnig, Chemetall GmbH and C Roth, Technische Universität Darmstadt, Germany, Woodhead Publishing Series in Energy No. 31, Sawston 2012, pp. 2, ISBN 1-84569-774-X, ISBN-13: 978-1-84569-774-7

Korte, C.

Phosphoric acid, an electrolyte for fuel cells - Temperature and composition dependence of vapor pressure and proton conductivity

Chapter No. 12 in: Fuel Cells Science and Engineering – Materials, Systems, Processes and Technologies (Vol. 1), Edited by D. Stolten and B. Emonts, Forschungszentrum Jülich, Institut für Energie und Klimaforschung (IEK-3), Wiley-VCH, Weinheim 2012, pp.335-359, ISBN: 978-3-527-33012-6

Wackerl, J.

Analytics of Physical Properties of Low-Temperature Fuel Cells

Chapter No. 19 in: Fuel Cells Science and Engineering – Materials, Systems, Processes and Technologies (Vol. 1), Edited by D. Stolten and B. Emonts, Forschungszentrum Jülich, Institut für Energie und Klimaforschung (IEK-3), Wiley-VCH, Weinheim 2012, pp.521-536, ISBN: 978-3-527-33012-6

Conti, F.; Majerus, A.; Di Noto, V.; Korte, C.; Lehnert, W.; Stolten, D.

Raman study of the polybenzimidazole-phosphoric acid intercations in membranes for fuel cells

Phys. Chem. Chem. Phys. ***14*** *(2012) 10022–10026.*

Conti, F.; Willbold, S.; Mammi, S.; Korte, C.; Lehnert, W.; Stolten, D.

Carbon NMR investigation of the polybenzimidazole-dimethylacetamide interactions in membranes for fuel cells

New J. Chem., ***37*** *(2013) 152-156.*

Giffin, A. G.; Conti, F.; Lavina, S.; Majerus, A.; Pace, G.; Korte, C.; Lehnert, W.; Di Noto, V.

A vibrational spectroscopic and DFT study of poly(2,5-benzimidazole) (ABPBI)-phosphoric acid interactions in HT-PEFC membranes

Int. J. Hydrogen Energy, submitted.

Important patents

Patent applications:

Principal Inventor	PT	Description
Dr. J. Wackerl	1.2583	Device and method for qualitatively determining the operating state of a test object

3.8 Quality assurance

One of the quality assurance measures implemented in the area of MEA fabrication involved the construction of tools for the standardization of documentation on incoming goods. Other areas of work included methods of inspecting incoming goods and tools for the control of documents.

3.8.1 Objectives and fields of activity

For the fabrication of MEAs, many different materials and precursors, such as substrates, gas diffusion electrodes and catalysts, from various suppliers are used. Incoming goods must be documented properly in order to guarantee traceability of the MEA production as the materials in question are not fully developed and can differ from one production batch to the next in terms of their properties. These variations can have a considerable influence on the functionality of the MEAs produced.

As some of the goods purchased are products in the developmental stage, characterization methods are required to quantify the parameters relevant to production. Although the manufacturers of the goods supply product documentation, this is currently not sufficient for MEA product development.

Documentation tools that have already been developed and implemented, such as methods of calibrating measuring equipment, regularly generate documents which must be controlled in order to ensure that the relevant requirements within the framework of quality assurance are met, e.g. traceability.

3.8.2 Important results

Standardized incoming goods

Incoming goods, such as chemicals, substrates or gas diffusion layers, are first registered by entering them into the system using a form. They are assigned an incoming goods number, which ensures that they can be traced. A two-dimensional code is automatically generated, which produces text in a quadratic matrix (QR code). This system can store considerably more characters than a barcode. The goods are labeled with this code, thus ensuring that they can be unambiguously traced. Using an appropriate scanner, the information contained in the code can be decoded and read out as text, for example in laboratory logs. The aim is to extend the system to cover the entire electrode fabrication process.

Incoming goods inspections

Substrates delivered by commercial suppliers for MEA fabrication include data on physical properties, such as thickness and weight per unit area, but these data are not sufficient for the fabrication of homogeneous electrodes. For the production of electrodes, statistical data are required on these parameters in order to be able to evaluate the quality of the electrodes.

A characterization method was therefore implemented. The large substrates were first cut into small samples. From these samples, the physical parameters, such as weight per unit area and thickness, were then determined and the data sets were used to create contour and surface plots. These data sets were also used to calculate statistical parameters, which can

be used to evaluate the quality of the electrodes produced from the substrate in question. The results of such a characterization are outlined below.

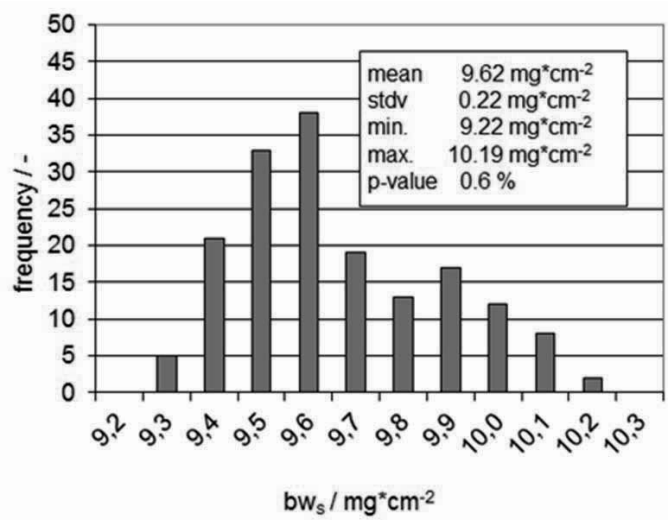

Fig. 69: Frequency distribution of the weight per unit area of an evaluated substrate

Fig. 69 shows the frequency distribution of the weight per unit area of an evaluated substrate. The specified p-value indicates whether the data could result from a normal distribution. A value of less than 5 % excludes this and indicates that undesired effects could arise in the material being tested. In the present case, periodic changes occurred in the weight per unit area of the substrate at intervals of 25 – 30 cm (see Fig. 70), which were found to cause large coating variations in the catalyst weight per unit area during electrode production (section 3.4.2.4).

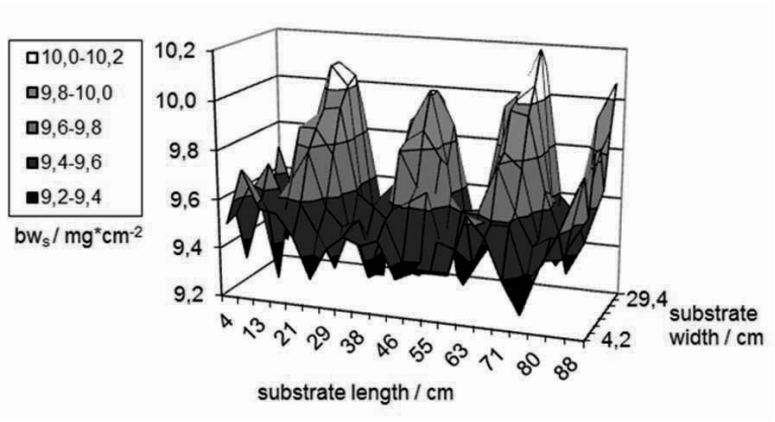

Fig. 70: Weight per unit area of a studied substrate as a function of substrate length and substrate width

Document control

The requirements for the control of documents laid down by Forschungszentrum Jülich were implemented: relevant scripts were written for automated registration, identification, control and approval of documents in line with the requirements of a quality management system. Experience to date has been positive but the personnel expenditure for updating such a system is very high.

3.8.3 Staff members and fields of activity

Name	Tel. (+49 2461-61-) E-mail address	Field of activity
Ms. D.Günther	2378 d.günther@fz-juelich.de	MEA Fabrication Techniques, quality management
Dr. M. Stähler	2775 m.staehler@fz-juelich.de	Head of MEA Fabrication Techniques

3.8.4 Important publications

Important publications

Stähler, M.; Friedrich, I.
Statistical investigations of basis weight and thickness distribution of continuously produced fuel cell electrodes
Journal of Power Sources, 242, 425–437, (2013)

4

Highlights

Selected Results

- Emission reduction using hydrogen from surplus wind power
- Improving the performance and long-term stability of direct methanol fuel cells in the kW class
- Investigation of degradation phenomena in SOFC stacks
- Investigating degradation procedures during autothermal reforming

4.1 Emission reduction using hydrogen from surplus wind power

Energy technology is undergoing a considerable transformation worldwide driven by climate change, supply security, industrial competitiveness and local emissions. Greenhouse emission reduction, in particular, has become an enormous challenge due to the accelerated phasing out of nuclear energy in the aftermath of Fukushima and the objections against CO_2 storage. Germany aims to cut greenhouse gas emissions compared to 1990 levels by 40 % by 2020, 55 % by 2030, 70 % by 2040 and 80 – 95% by 2050. The timeline requires that target enabling technologies leave the pure science level and be industrialized 20 years before each milestone. The institute has developed an energy supply concept for Germany that reduces CO_2 emissions by 55 % compared to 1990 levels. It is based on wind energy, electrolysis, and the use of hydrogen with fuel cells for road transportation. Residual load is covered by natural gas power plants. Work in this area includes a study on hydrogen transmission and distribution by pipelines [23, 24]. The full concept is described in [25].A brief summary follows here. References and further details are given in the published article. Current analysis activities concern underground and near-surface storage technology, regional storage requirements, location of electrolyzers, and economic aspects. Concept development is planned for further emission reduction. This work is carried out by the institute head and the systems analysis department.

4.1.1 Status of CO_2 emissions n

CO_2 emmision source		**Share of total emissions [%]**	
Energy sector (of which electricity)		37 (30)	
Transportation	Passenger cars	17	11
	Goods/other transport		6
Residential		11	
Industry (of which electricity)		19 (2)	
Trade & commerce		4	
Agriculture		8	
Other		4	
Total		100	

Tab. 9: CO_2 emission sources and their share of total emissions in 2009

In Germany, a total of 912 million tonnes of CO_2 equivalent were emitted in 2009. Tab. 9 shows the main contributors. Public electricity generation accounts for 30%. The energy sector as a whole is responsible for 37 %. 11 % of emissions originate in the residential sector and 23 % in industry, trade and commerce. 1 1% of CO_2 emissions are caused by

[23] Krieg, D.: Konzept und Kosten eines Pipelinesystems zur Versorgung des deutschen Straßenverkehrs mit Wasserstoff. Dissertation, FZJ, 2012

[24] Baufumé, S.; Grüger, F.; Grube, T.; Krieg, D.; Linssen, J.; Weber, M.; Hake, J-F.; Stolten, D.: GIS-based scenario calculations for a nationwide German hydrogen pipeline infrastructure. IJHE 38, S. 3813, 2013

[25] Stolten, D.; Emonts, B.; Grube, T.; Weber, M.: Hydrogen as an Enabler for Renewables. In: D. Stolten, V. Scherer (Hrsg.): Transition to Renewable Energy Systems. Wiley-VCH Heidelberg, im Druck, 2013

passenger cars and 6 % by heavy goods vehicles and rail, ship and air transportation. CO_2 emissions in Germany were already reduced by 27 % in 2009. However, in order to reduce emissions by 80 %, large sectors must become CO_2 neutral.

4.1.2 Power density as a key characteristic of renewable energies

Power density is a measure of the effort required to concentrate energy and convert it into electricity. The active area of the technical aggregate is taken as the reference point, for example the cell area in the case of photovoltaics. While hydropower has a power density in the range of a few kilowatts per square meter, wind power has a power density of approx. 150 W/m^2 and photovoltaics of around 15 W/m². The relationship between power density and economic potential is reflected by the capacities installed worldwide (Fig. 71). Hydropower in Germany is almost fully exploited, while wind power and photovoltaics still have huge potential for expansion. According to conservative estimates, the potential associated with onshore wind power is at least 189 GW. Wind power was chosen for the following scenario due to its higher power density. Other renewable primary energies retain their current status. These assumptions keep the scenario as simple as possible.

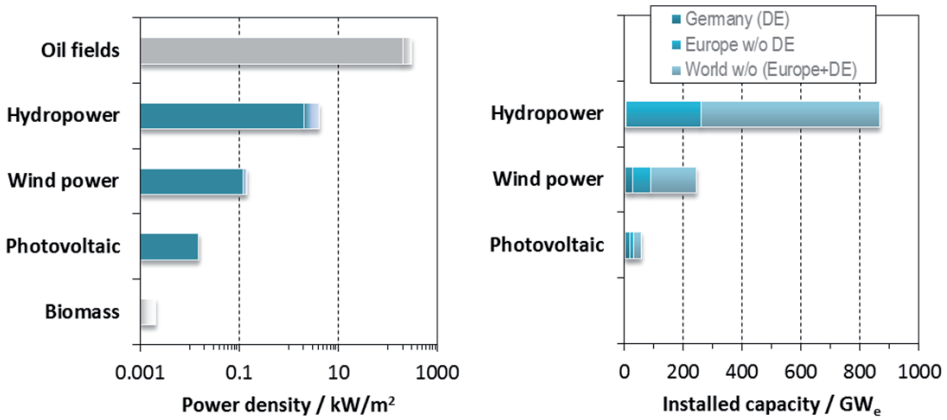

Fig. 71: Comparison of the power densities and installed capacities of renewable energies

Similar considerations hold for the selection of the preferred storage medium. Today, lithium-ion batteries have a storage density of around 5 MJ/l, when electrode materials only are considered, but in order to achieve a long life, they are only discharged to about 50 %. This results in considerably lower values of around 0.72 MJ/l or 0.36 MJ/kg for systems. Hydrogen at 700 bar has 3 MJ/l and 6 MJ/kg, both including the tank. The physical storage density in the liquid state is 8.46 MJ/l. We chose hydrogen as the storage medium for electric mobility because the storage density of hydrogen is four to six times greater than that of batteries. An overview of the storage densities is shown in Tab. 10. The excellent energy density of gasoline is not available for electric mobility.

There are two major basic options for hydrogen utilization: reconversion to electricity for the purpose of grid feed-in and its use as a fuel for transportation. The efficiency of reconversion – with or without prior feed-in into the natural gas grid – will correspond to that of the generation of electricity from natural gas. If hydrogen is transported in pure form in its own

	Physical storage density		Technical storage density	
	[MJ/l]	[MJ/kg]	[MJ/l]	[MJ/kg]
Gasoline	32	43	30	35*
Ethanol	21	27	19	22*
Hydrogen (700 bar)	5	120	3	6
Li-ion batteries	5	1.5	0.72	0.36

Tab. 10: Energy density of gasoline ant ethanol compared to hydrogen and batteries

infrastructure and used as a fuel in fuel cell vehicles, it reduces the energy consumed by a car (tank-to-wheel) by around 50 % compared to vehicles run on gasoline (Fig. 72). At the same time, the CO_2 emissions per unit of energy content (lower heating value) are 25% higher for the oil-based fuels than for natural gas, which means that the use of hydrogen for road transportation prevents 2.5 times more CO_2 emissions than its reconversion into electric power for the grid. Methanation is currently being discussed as an energy storage option, because it would allow the use of existing infrastructure for large quantities of hydrogen, but the cycle efficiency would decrease relatively by at least 20 %. The penalty would be even higher in cases where energy is needed to supply CO_2 (capture from flue gases or from air).

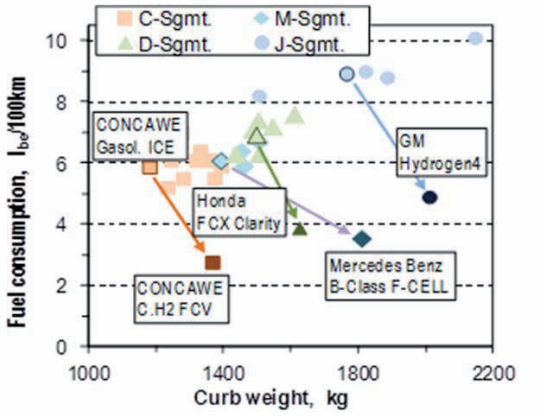

Fig. 72: Energy requiered by fuel cell vehicle prototypes and present-day gasoline cars

Fig. 72 compares current fuel consumptions for different vehicle segments: C represents medium cars, D large cars, M vans and multipurpose cars, and J sport utility cars. Dedicated fuel cell car designs (one tank only) will allow further reductions in weight and consumption.

4.1.3 Renewable scenario with a constant number of wind turbines

On the basis of the argumentation and data outlined, a scenario was designed with deliberately simple parameters. The following assumptions were made:

- The number of onshore wind turbines remains constant at the 2011 level, namely 22,500. The average capacity per turbine is increased from 1.23 MW to 7.5 MW and the capacity utilization from almost 1,400 to 2,000 full-load hours. The national mean for 3 MW turbines is already slightly higher than this last value.

- Offshore wind energy is expanded to 70 GW and full-load hours are assumed to be 4,000 h/a.
- Photovoltaic power is taken into account with an installed capacity of 24.8 GW as per the end of 2011.
- Electric power feed-in from onshore and offshore wind turbines and photovoltaic installations is considered as time-dependent values and is balanced with the time-dependent vertical grid load of the German electric transmission grid.
- The contribution of other renewable energies remains constant at the 2010 level.
- Variations in wind and solar energy are balanced as required by gas power plants. Other fossil energy carriers are no longer used. Residual load is covered by gas power plants; for accumulated demand times of more than 700 h/a, combined cycle technology is used. Partial load behavior is globally accounted for with an efficiency deduction of 15 % compared to the efficiency at nominal power.
- Excess electricity is used to produce hydrogen using electrolysis, pumped through hydrogen pipelines to filling stations and used in fuel cell vehicles. An efficiency of 70 % is assumed for electrolysis, and a minimum operation time of 1000 h/a is set as a condition. Extreme surpluses will not be used. Salt caverns provide seasonal storage.
- It is estimated that a vehicle will consume 1 kg hydrogen per 100 km. Mean mileage is taken as 11,400 km per year for each vehicle.
- In the residential heating sector, the amount of natural gas consumed is cut by half compared to 2010.

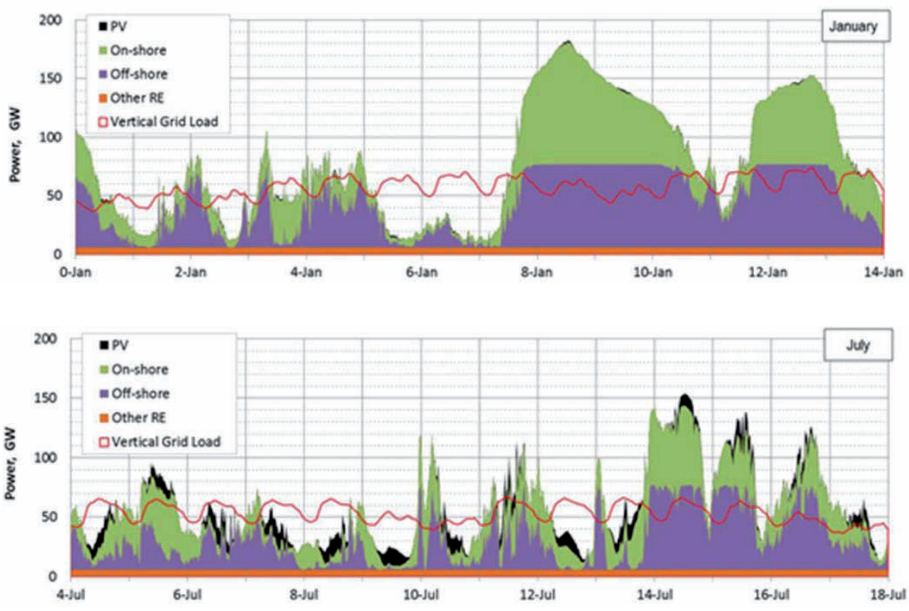

Fig. 73: Renewable power generation and grid load

Surplus power and residual load profiles are determined from the countrywide differences between feed-in and vertical grid load based on 2010 quarter-hour data. The total grid load is kept. Offshore wind power profiles were determined using wind measurement data and typical turbine characteristics. Fig. 73 shows the resulting profiles.

4.1.4 Results

The outlined energy system covers the grid load of 488 TWh and supplies the transportation sector with 5.4 million tonnes of hydrogen. 75 % of the grid load is supplied by wind and photovoltaics, 10 % by other renewables, and 15 % by natural gas. The natural gas volume used for electricity generation today is sufficient to fully cover the residual load. Substituting oil-based fuels in the transportation sector with the given quantities of hydrogen reduces the total CO_2 emissions of 2009 by almost 9 %. In the electricity sector, the total emissions are reduced by 27 % (Fig. 74). The emission targets for 2030 can be met with the proposed measures.

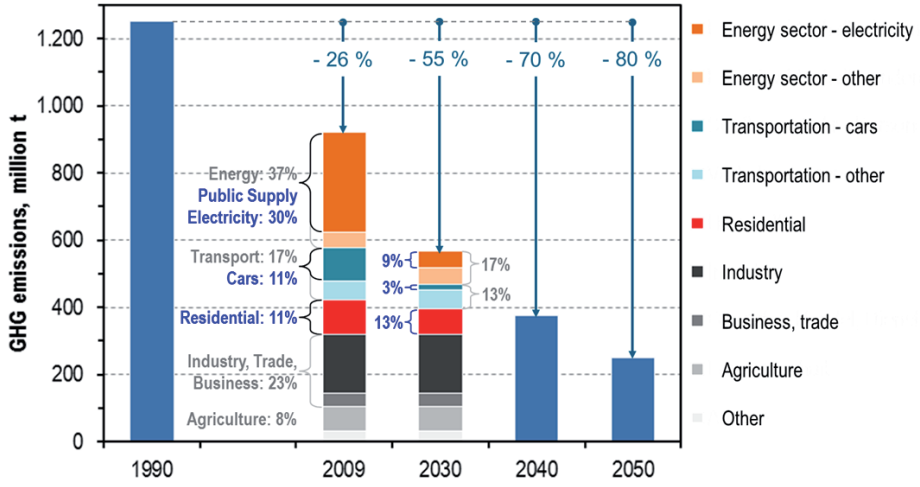

Fig. 74: Effect on national greenhouse gas emissions

4.1.4.1 Infrastructure and vehicle investments

In addition to the 22 GW of existing gas power plants, 42 GW of new capacity is needed. An installation of 84 GW of electrolysis is required under the condition of a minimum of 1000 equivalent full-load operating hours per year. Assuming a constant use of hydrogen over the year results in a storage capacity requirement of 800,000 t, i.e. a seventh of the annual production. A pipeline system for nationwide supply in Germany would necessitate some 12,000 km for a transmission grid connecting sources to centers in all districts, and 31,000 – 47,000 km for the distribution grid supplying a selection of 9,800 of today's 14,500 existing gas stations. Tab. 11 shows the investment volume required. The transmission pipelines and their compressors alone require about € 6 – 7 billion. The extra cost for fuel cell cars is calculated with a supplement typical for diesel hybrid vehicles today.

Components	Assumptions	Cost [€ billions]
Water electrolyzer	84 GW @ 500 €/kW	42
Pipeline system	43,000 – 59,000 km	19–25
Dome storage	Seasonal compensation 60-day reserve	5 5
Filling stations (9,800)	New stations: € 2 million/filling station Retrofitting: € 1 million/filling station	20
Peak electricity generation systems (GT, GuD)	Total of 42 GW (both systems)	24
Total cost of infrastructure		**110–121**
Fuel cell vehicles	28 million vehicles à € 5.000 €/vehicle	140
Total costs		**250–261**

Tab. 11: Components and costs for hydrogen supply

4.1.5 Economic assessment of hydrogen use options

In addition to or alternative to the use of hydrogen as an energy carrier for fuel cell vehicles, hydrogen could also be fed directly into the gas grid or methanized. If hydrogen was to be used in the transportation sector, fuel consumption would be halved and there would be a large difference between the direct cost of hydrogen (77 c/$l_{gasoline\ equivalent}$) and the allowable fuel cost (€ 1.40/$l_{gasoline\ equivalent}$). This would also allow taxes to be levied. For hydrogen feed into the natural gas grid, in contrast, there would be a markup of € 0.41 – € 0.50 per liter of gasoline equivalent (Tab. 12).

Assumptions	Calculation	Cost differential
Direct energy costs for hyrogen production with wind power		
Electricity costs: 6 c/kWh_{el}; Electrolysis efficiency: 70 %; *1 l gasoline = 9 kWh*	6 c/kWh_{el}/0.7 = 8.6 c/kWh_{H2} ≈ 77 c/$l_{Bgasoline}$	-
Revenue for fuel in the road transportation sector		
Production costs: 70 c/$l_{gasoline}$; *Efficiency improvement of a factor of two (fuel cells/comb. engine)*	70 c/$l_{gasoline}$ * 2 = € 1.40 /$l_{gasoline}$ *Surtax of ≈ 100 % possible*	63 c/$l_{gasoline}$
Revenue for direct feed-in into the natural gas grid		
Purchase price: 4 c/kWh	4 c/kWh * 9 kWh/$l_{gasolinen}$ = 36 c/$l_{gasoline}$ *In additional, taxes of 18 c/$l_{gasoline}$ must be levied*	-41 c/$l_{gasoline}$
Revenue for replacing natural gas with methanation		
Incentive: 4 c/kWh; Efficiency: 80 %	36 c/$l_{gasoline}$ * 0.80 = 27 c/$l_{gasoline}$	-50 c/$l_{gasoline}$

Tab. 12: Comparison of revenues for hydrogen in different areas of application

The price of natural gas is by far too low to make hydrogen feed-in attractive. In other words, hydrogen produced from “expensive” renewable energy should not be used to replace

“cheap” fossil fuels. Other options to save fossil fuels, such as improved insulations, are more attractive. Two other effects must also be considered: the economies of scale when a technology establishes itself on the market and the danger of the subsidy trap. When research and development efforts concentrate on a technology that is subsequently implemented on a large scale, learning effects and cost degression give rise to lower prices than in the case of a broad-based product portfolio. Subsidy traps emerge when a technology that appears promising continues to depend on subsidies long after the end of start-up financing in order to continue functioning. When subsidies end or are reduced, it becomes difficult to achieve a secure footing with competing technologies as the new situation is often too much for many providers. They have become used to the comfortable situation and are often incapable of implementing the necessary changes or unwilling to do so in order to survive. It can therefore be assumed that a provider will not voluntarily agree to do without subsidies and that the end of subsidies would automatically mean the end for many of these technologies. All parties involved are therefore caught in a trap. Comparing the potential uses of hydrogen clearly shows that it makes more sense economically to reduce oil imports and stop creating further subsidy traps (Tab. 13). It was assumed here that 5.4 million tonnes of hydrogen will be needed per year in 2050 to supply 40 million passenger cars with fuel.

Amount of hydrogen	Method	Assumptions	Economic impact
5.4 million tonnes/a	Direct feed-in into natural gas grid	Costs: 8.6 c/kWh; Avails: 4 c/kWh;	- € 8.27 billion
	Methanation & natural gas grid	Costs: 8.6 c/kWh/0.75 = 11.47 c/kWh; Avails: 4 c/kWh;	- € 13.4 billion
	Use in transportation sector	Costs: 8.6 c/kWh; Benefit: 40 million passenger cars; mileage of 12,000 km/a; 6 l/100 km; € 100/barrel	€ 2.5 billion

Tab. 13: Economic comparison of different possible uses of hydrogen

Direct feed-in requires annual subsidies of € 8.27 billion. Compared to current costs of € 14.1 billion per year, this is a substantial additional burden. A study of transmission pipeline operators concluded that a share of only 10% H_2 in the natural gas grid would demand modifications costing € 3.6 billion. It is assumed that the natural gas grid will no longer be able to accommodate hydrogen from as early as 2022 onwards due to material problems. The option of direct feed-in is therefore not a long-term solution.

Methanation does away with all material problems by converting hydrogen with CO_2 into CH_4. However, this process involves conversion losses. The thermodynamic efficiency is 83 % and the technical efficiency, depending on the size and complexity of the plant, is approx. 70 – 75 %. In the literature, an efficiency of approx. 51 – 65 % can be found for the energy chain for the production of methane from electricity. Peripheral components are not included in this.

Finally, hydrogen can be used as fuel in the transportation sector, and thus reduce oil imports. 97 % of the oil in Germany is imported. This impacts adversely on the balance of trade. In 2050, 40 million passenger cars will consume some 5.4 million tonnes of hydrogen

every year. If we assume that these vehicles are supplied with fossil fuels, travel 12,000 km in a year and consume 6 liters of fuel every 100 km, then imports worth € 18 billion per year would be necessary given an oil price of € 100 per barrel. These costs can be avoided. Against this, the costs for hydrogen production are € 15.5 billion. This represents savings of € 2.5 billion for the national economy. Furthermore, these measures would also reduce if not avoid geostrategic dependencies.

4.1.6 Summary

Comparing annual variations in grid load and electricity supply after a considerable expansion of wind power onshore and offshore shows:

- The demand for electricity can be covered when nuclear power, coal and mineral oil are no longer used without increasing natural gas imports.
- Connecting the electricity generation sector and the transportation sector via stored hydrogen has significant economic advantages.
- Only gas storage, preferentially in the form of hydrogen, will compensate for the strong seasonal fluctuations in renewable energy in Germany.

Hydrogen is the most suitable large-scale storage option, because

- other options such as pumped storage and batteries do not have sufficient potential capacities, and
- methanation is not feasible economically.
- Renewable energies then account for approximately 90% of electricity generation, where 34% of the electricity generated is excess energy for electrolysis.
- Excess wind power must be put to good economic use because of the large amounts involved.
- Excess electricity generation is enough, for example, to supply 28 million fuel cell vehicles with hydrogen. Based on typical consumption data from 2010, the use of hydrogen in the transportation sector will cut CO_2 emissions by 81 million tonnes, representing a 6.5 % decrease of total emissions in 1990.
- In the electricity sector, a reduction of 20 percentage points is achieved compared to 1990, and in the domestic heating sector 2.2 percentage points. Combined with the 26.5 percentage points already achieved in 2009, this results in a reduction of 55 %. The requirements for 2030 are therefore met.
- Investments are manageable. The expected costs for the complete hydrogen infrastructure, i.e. including pipelines, electrolyzers, storage systems and filling stations, are around € 100 billion. Around € 37 billion were spent maintaining, servicing and installing new pipelines in the natural gas grid between 1995 and 2010. Wind turbines were not considered as investments because future feed-in tariffs of 6 c/kWh were assumed here.

Further measures for reducing emissions by more than 55 % include:

- the use of biofuels in applications where fuel cells and batteries are unsuitable,
- energy saving measures,
- smart grids, heat pumps, etc.

4.2 Improving the performance and long-term stability of direct methanol fuel cells in the kW class

4.2.1 Motivation for direct methanol fuel cells of the kW class

Direct methanol fuel cells (DMFCs) convert methanol as a liquid fuel directly into electric current. This makes DMFCs attractive for different applications, particularly as replacements for batteries or accumulators as DMFC systems permit longer operating times thanks to the high energy density of methanol and refilling only takes a short time compared to long recharging times required by batteries. In the IEF-3 Report 2009, the first DMFC system V3.1 was presented for a forklift. Following this, IEK-3 at Forschungszentrum Jülich began a cooperation with industrial partners Ritter Elektronik GmbH, Jungheinrich AG, ebm-papst Landshut GmbH and AKG Verwaltungsgesellschaft and successfully replaced the battery tray of a forklift (Jungheinrich-ECE 220) with a further developed DMFC hybrid system of the kW class (DMFC system V3.3-1, cf. IEK-3 Report 2011). The weight of the system was reduced by a factor of two, the range increased by a factor of three and a lifetime of 3000 hours was demonstrated.

The DMFC combined with a lithium-ion battery formed the hybrid drive for electrically driven forklift used to transport goods in warehouses (cf. Fig. 75). The vehicles move along the rows of shelves and stop at set positions to either load or unload goods. The electric power of the drive motor is shown by the curves for start-up (peak power of up to approx. 7 kW), braking (energy recovery of up to more than 5 kW) and the time spent waiting for the pallets to be loaded.

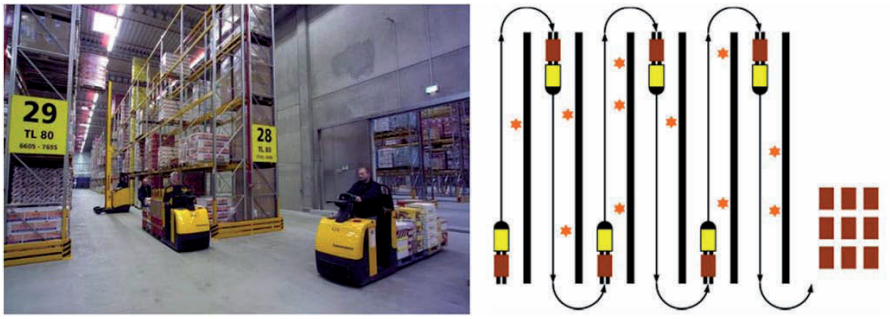

Fig. 75: Vehicles in operation

The vehicle is fueled by pure methanol to achieve a maximal vehicle range with the smallest possible space for the battery tray. An advantage of such energy systems is that there is no need for the relatively complicated and time-consuming recharging of conventional lead-acid batteries, nor are spare batteries required for multishift operation. A feasibility study and market analysis of the development verified that a system suitable for use in a forklift can be operated economically in a three-shift system.

A prerequisite for commercialization is uninterrupted use of the vehicle in three shifts and a DMFC stack lifetime of 10,000 operating hours. This development was achieved in several iteration cycles in which several prototypes of DMFC systems were constructed in order to validate R&D results and were subjected to dynamic investigations using real load profiles up

to end of life (EOL). All of the components used in the DMFC system were subsequently analyzed in order to learn more about the degradation mechanisms. The insights obtained were used to continuously extend the lifetime of the DMFC systems developed by IEK-3 to at present > 16,000 hours (DMFC system V3.3-2 as of December 2012; long-term testing still in progress). The essential technical and economic requirements for system commercialization have thus been fulfilled.

4.2.2 Improvements to the DMFC energy system V3.3-

The development and verification of the DMFC system V3.3-1 outlined in the IEK-3 Report 2011, which was subjected to long-term testing of 3000 hours with a realistic dynamic load profile, showed a stack degradation rate of 52 µV/h at 100 mA/cm^2. The degradation rate of short stacks measured in test stands with MEAs of the same design was lower by a factor of three.

The system was therefore analyzed after long-term testing to investigate the degradation mechanisms of the stack in a real system. One priority was the post-mortem analysis of the stack in order to identify reasons for aging. When the stack was taken apart, no abnormalities were initially detected. In the next step, the MEAs were subjected to a more detailed investigation. Several MEAs were removed at random and subjected to different investigations. One such investigation involved taking optical micrographs of microsections. These micrographs did not display any abnormalities compared to new unused MEAs.

SEM micrographs were taken in order to examine the composition of the individual layers. In combination with energy-dispersive X-ray spectroscopy, these images provide information on layer structure. Ruthenium was detected on the cathodic electrode. This was not the case for unused MEAs indicating that ruthenium migrated through the membrane from the anode to the cathode during operation. The transfer of ruthenium led to a decrease in performance. After 3000 h of testing, the average Pt/Ru ratio of three samples was around 40 on the cathode and around 2.6 on the anode. Furthermore, catalyst material also agglomerated on the cathode. This catalyst agglomeration can reduce the active surface and thus also cause a loss of performance of the cathodic electrode.

In addition to the micrographs, elemental analysis of individual MEA regions was also performed. Elemental analysis was also used to determine further elements in the MEA. The loading of the membrane with foreign ions is a parameter that is particularly interesting because the accumulation of cations in the membrane can reduce its protonic conductivity. In the membranes of the system tested, calcium, aluminum, potassium and iron deposits were found. The calcium contamination was ten times higher than that of the other substances.

It can be concluded that the migration of ruthenium and the introduction of ionic impurities can be considered the main reason for aging. While ruthenium migration can be reduced using new catalyst materials, optimized electrode structures and improved operating strategies, the introduction of foreign ions into the membrane is primarily due to the bipolar unit material and the sealing material of the condenser. These findings allowed several measures to be implemented in the DMFC system V 3.3-2 to improve long-term stability.

4.2.2.1 Stack modifications

In order to reduce the transfer of impurities from the stack components to the anode loop, the material (expanded graphite) for the flow distributors was subjected to a special heat treatment by the manufacturer. This reduced the measurable leaching compared to the untreated material. At the same time, a cleaning method was developed for expanded graphite to remove iron ions from the stack components.

For the DMFC V 3.3-2 project, another stack with small structural modifications was set up (MM-44). One difference, for example, was the thickness of the bipolar plates, which was increased by 0.2 mm as a certain type of material was no longer available. In addition, the stack was constructed with commercial MEAs acquired from Johnson Matthey, which had new catalyst materials with improved corrosion resistance of the PtRu catalysts [26].

A post-mortem analysis of the stack from the DMFC system V3.3-1 failed to explain why higher excesses of air are required during stack operation than for measurements on short stacks. When the DMFC system V3.3-2 was put into operation, the weakness was successfully identified. This weakness lay in the wick system used, which draws the liquid water out of the cathode channels and prevents these channels from becoming blocked. Forces of adhesion, however, mean that there is a danger of wet wicks clinging to each other, thus preventing air being supplied to the single cells. Integrating comb structures into the cathode exhaust of the stack prevents the wicks from clinging to each other (cf. IEK-3 Report 2011).

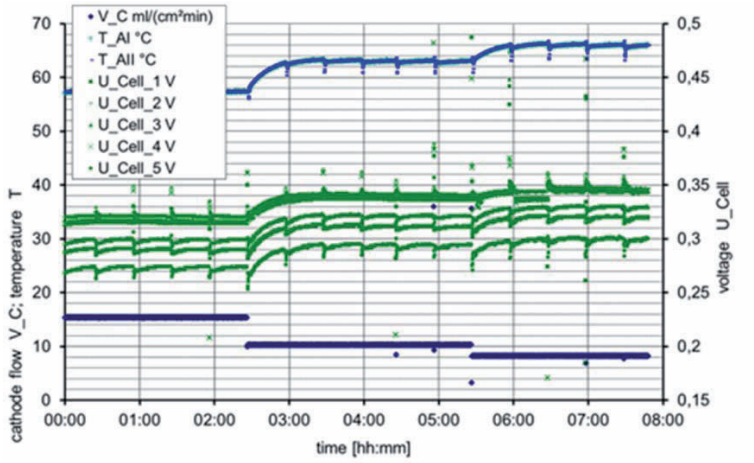

Fig. 76: Reference measurements for operation with low excesses of air

In order to verify that the problem really was caused by the behavior of the wicks, a short stack was re-constructed with the MEAs and bipolar plates that had already been tested in a 3000 h study. This time, the wicks were affixed with combs. This short stack was loaded in the test stand with a load of 0.14 A/cm² and the air volume was reduced from 15 ml/(cm²min) to 10 ml/(cm²min) and finally to 8 ml/(cm²min). All air volumes, even that of just 8 ml/(cm²min)

[26] Cabello-Moreno, N.; Crabb, E.; Fisher, J.; Russell, A.; Thompsett, D.: Improving the Stability of PtRu Catalysts for DMFC. ECS Meeting Abstracts, 902 (2009), pp. 983

allowed stable operation (cf. Fig. 76). Under these conditions, an operating temperature of 66 °C was achieved. This demonstrated that the MEAs used in the 3000 h test also function with lower excesses of air and that the increased volumes of air were due to the insufficient fixation of the wicks.

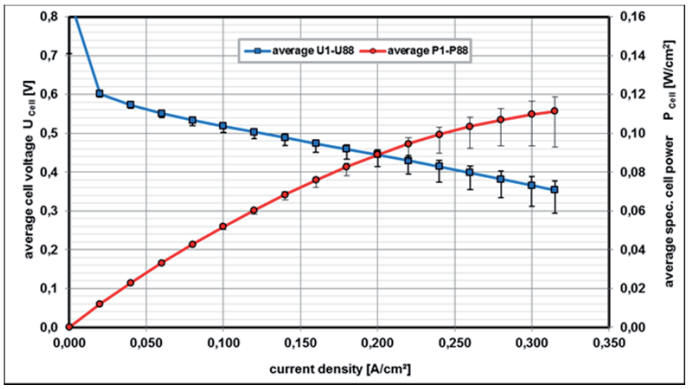

Specific operating conditions

Temperature:	**70 °C**
Methanol concentration:	**~ 1 mol/l**
Methanol permeation:	**~ 0.1 A/cm²**
Air feed:	**30 ml/(cm²*min)**

Fig. 77: Performance of MEAs in the stack (MM-44)

Fig. 77 shows a current-voltage characteristic as the mean cell voltage in a specific form of the stack set up for the DMFC system V3.3-2. Presenting the results in this way allows a comparison with values from other test cells. The current-voltage characteristic in blue is related to the left ordinate. The current-voltage characteristic in red is related to the right ordinate. The error bars indicate the highest and lowest cell voltage and the corresponding minimal and maximal specific power of the cells.

4.2.2.2 System operation and efficiency

Modifying the wick system facilitated stable operation for lower excesses of air. This gave rise to a considerable improvement in system operation as the stack in the system V 3.3-2 could be operated with less than 50 % of the cathode air volume of the predecessor stack. This had the following positive effects:

- The anode temperature (operating temperature) is increased.
- The methanol concentration can be reduced to minimize the permeation losses.
- The voltage-related efficiency and the fuel utilization rise leading to an increased system efficiency of 29 %.
- The internal energy consumption of the cathode blower is reduced.
- For water recovery from the cathode air, the reduced air volume in the cathode leads to an increased autarky temperature and thus a reduced cooling fan power. This automatically increases system efficiency.

This in turn means that the second DMFC system V 3.3 can be operated with efficiency-optimized operating parameters. Tab. 14 shows a comparison of the operating parameters and efficiencies at the beginning of life (BOL) of both systems.

Operating parameters	System DMFC V3.3-1	System DMFC V3.3-2
Cathode air volume [g/s]	11	5
Methanol volume flow [l/h]	0.9	0.6
Methanol concentration [mol/l]	0.8	0.45
Anode temperature [°C]	55	61
Stack efficiency (BOL) [%]	27	29
System efficiency (BOL) [%]	23	28

Tab. 14: Comparison of operating parameters and efficiencies of both systems

The measures described increased the system efficiency by 5 percentage points to 29 %. Fig. 78 shows the proportions consumed by the individual consumers and the impacts of reducing the cathode air on the system operation of DMFC V 3.3-2 compared to the predecessor system. The mean electric power consumption of the peripheral components in the system operation of DMFC V 3.3-1 was 186 W. Reducing the cathode air volume in the DMFC system V 3.3-2 had a direct impact on the power consumption of the cathode blower and the condenser fans and was around 40 W. The cooling fans, however, remained the largest individual consumers in the system. Optimizing cathode air supply and water recovery thus helps to increase the efficiency of the system.

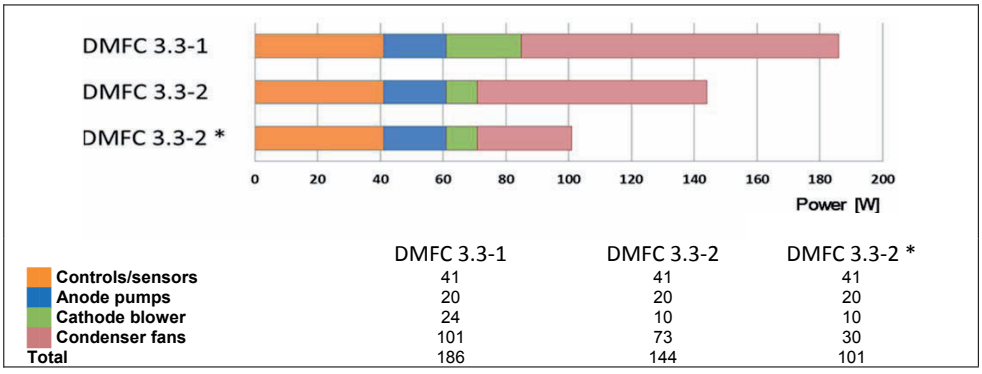

	DMFC 3.3-1	DMFC 3.3-2	DMFC 3.3-2 *
Controls/sensors	41	41	41
Anode pumps	20	20	20
Cathode blower	24	10	10
Condenser fans	101	73	30
Total	186	144	101

Fig. 78: Comparison of the peripheral power

During long-term operation of the DMFC system V3.3-2, the cooling fans were equipped with a temperature controller (DMFC 3.3-2*) in order to increase the system efficiency even further. The cooling fan temperature controller minimizes their electric power consumption and reduces the peripheral power by approx. 40 W, which is equivalent to an improvement in the overall peripheral efficiency of 6 %.

Optimizing the cooling fan drive led to a reduction in peripheral consumption of approx. 100 W in total. By saving peripheral power, the stack can be operated at the same driving cycle power on average at higher cell voltages. This in turn increases the voltage efficiency.

In addition to work on system operation and efficiency, the fabrication method used for the condenser was converted from adhesive bonding to welding. This prevents contaminations from the sealants and adhesives leaching into the condensate and also contributes to the long-term stability of the system.

4.2.2.3 Long-term stability and availability

In July 2010, long-term tests began on the DMFC system V 3.3-2. The long-term test with a realistic and highly dynamic load profile of a forklift is still in progress (as of 31 December 2012). To date, 16,907 operating hours have been achieved. Fig. 79 shows stack degradation (determined from data filtered by current densities) for different current densities. The degradation rate of the stack is about 10 µV h-1 at 0.1 A cm-². The modifications implemented in the DMFC system V 3.3-2 therefore successfully reduced the degradation rate by more than a factor of five from 52 µV/h in the first system to 10 µV/h in the current system.

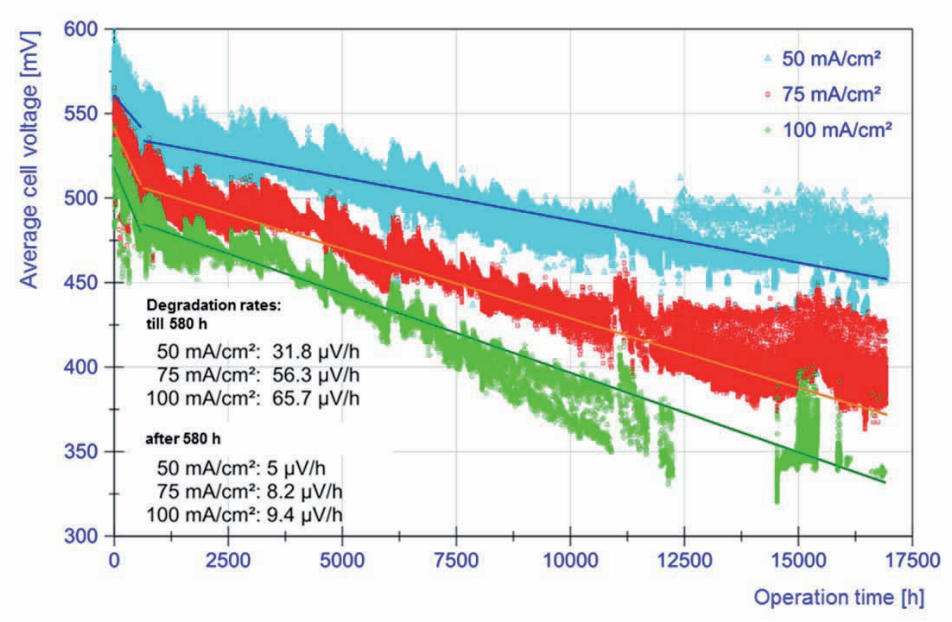

Fig. 79: Stack degradation for the DMFC system V3.3-2 shown as voltage loss at a constant current density (filtering of mass data; as of 31 Dec. 2012)

The availability of the second system was simultaneously increased by 15 % (cf. Tab. 15). If the number of error messages are plotted against time, it becomes clear that the error density was greater at the beginning. This can be explained by communication problems between the system components in particular. In June 2011, in April 2012 and in November/December 2012, parameters also had to be adapted as a result of stack degradation. The temperature-dependent control of stack voltage had to be set in relation to the rate of current change in order to ensure that the necessary average power was available. During the search for parameters, cell voltage disturbances were frequent at these particular times. In future, degradation-related parameters could be used to counteract this.

	DMFC V3.3-2	DMFC V3.3-1
Start long-term test	5 July 2010; 09:47	25 Oct. 2009; 23:08
Time of evaluation (V3.3-2) End of long-term test (V3.3-1)	1 Jan. 2013; 11:12	8 Mar. 2010; 14:57
Calendar hours recorded	21,865 h	3208 h
Planned downtimes	1988 h	17 h
Hours of operation	16,931 h	2225 h
Number of error messages	525	272
Availability	85 %	70 %

Tab. 15: Comparison of the availability of DMFC systems V3.3

Fig. 80 shows the errors that led to the DMFC system V3.3-2 being shut down. The main cause of system outages was cell voltage disturbances (28 %). However, at least one third of these outages were unnecessary shutdowns caused by contacting problems. As cell voltages are measured as differences between two cells, a contacting problem between the stack and the cell voltage monitoring (CVM) gives rise to a cell voltage being recorded as too low in one cell and too high in the neighboring cell. If we consider the mean value, it matches the rest of the cells. The second major reason is parameter modification, which was made necessary by stack degradation but was not always successfully implemented.

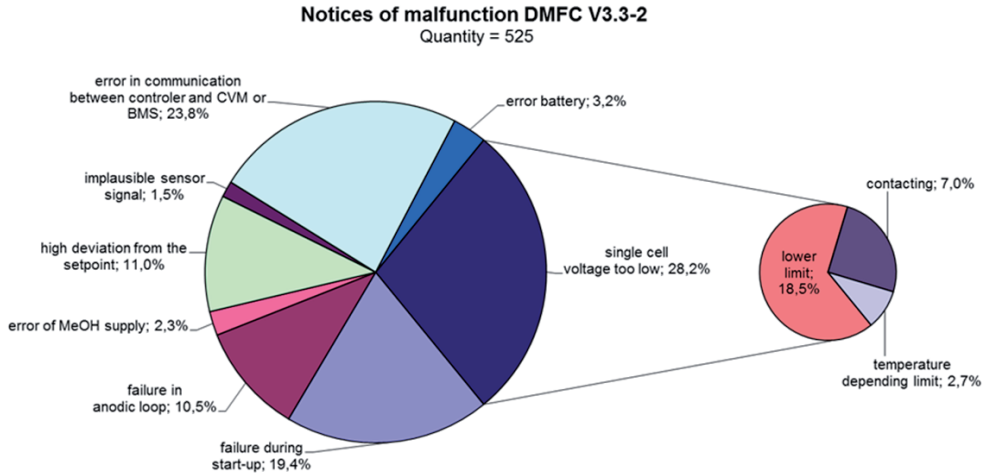

Fig. 80: Disturbance statistics DMFC system V3.3-2 (as of 1 Jan. 2013)

With almost 24 %, communication malfunctions between the control system, battery management system (BMS) and cell voltage monitoring are the second most important factor. These components communicate within a CAN-BUS. Using software updates for system control (including clock cycle changes and reduction of the data to be recorded to extreme values) considerable improvements were achieved. However, some outages have yet to be explained and may have been caused by unknown or incorrectly interpreted coding by the software manufacturer for the BMS and CVM.

A further 20 % of errors occurred during start-up. Most of these were due to the fact that the stack was not heated quickly enough to operating temperature during start-up or that the filling level criteria in the anode loop were violated. These points can be slightly improved by altering the parameters and only account for a small proportion of the lack of availability.

Overall, it can be concluded that system control troubleshooting is logical and cost-effective. It has allowed some 16,900 operating hours to be achieved to date (as of December 2012).

4.3 Investigation of degradation phenomena in SOFC stacks

Long-term stability is still one of the main requirements for fuel cells, especially in stationary applications, where at least 40,000 hours of operation are required combined with an allowed power loss of less than 10 %. Within the framework of the European project Real-SOFC (2004-2008), a first systematic study of the degradation behavior of SOFC stacks with planar anode-supported cells was initiated [27].Three series of SOFC stacks, each with two or four ASCs, were operated for durations of 3000 to 10,000 hours under varying fuel and electrical load conditions [28]. This study revealed that depending on the material combinations and operating conditions, selected processes leading to unwanted progressive degradation behavior can occur rather soon, i.e. after 1500 – 2000 hours of operation, or they can be postponed beyond the maximum operating time of 10,000 hours reached in the study. Based on this experience, it is necessary to perform real long-term testing beyond 10,000 hours to find out whether physical or chemical effects can occur and cause sudden death of a component or whether different processes occur over time causing various degradation rates. With the help of intensive post-test analyses and basic investigations on the reaction mechanism between the materials detailed, an understanding of the mechanism is being sought.

4.3.1 Short-sack tests

Stack ID	Temp. [°C]	Cathode	Fuel	Protective coating*	Duration [h]	Voltage Degradation [%/1000h]
F1002-95	700	LSCF	H_2 (20% H_2O) u_F = 40%	Mn-oxide by WPS	17,660	1.4
F1002-97	700	LSCF	H_2 (20% H_2O) u_F = 40%	Mn-oxide by WPS	> 47,000	1.0
F1002-132	800	LSCF	H_2 (20% H_2O) u_F = 40%	Mn-oxide by WPS	15,144	2.2
F1004-08	800	LSM	H_2 (20% H_2O) u_F = 40%	MnCoFe-spinel by APS	19,036	0.5
F1004-21	700	LSCF	H_2 (20% H_2O) u_F = 40%	MnCoFe-spinel by APS	> 17,000	0.1

* WPS: wet powder spraying; APS: atmospheric plasma spraying

Tab. 16: Durability tests – stacks, parameters and results

[27] Steinberger-Wilckens, R.; Bucheli, O.; de Haart, L.G.J.; Hagen, A.; Kiviaho, J.; Larsen, J.G.;.Pyke, S.; Rietveld, G.; Sfeir, J.; Tietz, F.; Zahid, M.: Real-SOFC – A Joint European Effort to Improve SOFC Durability. ECS Transactions, 25 (2009), 43-56

[28] de Haart, L.G.J.; Mougin, J.; Posdziech, O.; Kiviaho, J.; Menzler, N.H.: Stack Degradation in Dependence of Operation Parameters; the Real-SOFC Sensitivity Analysis. Fuel Cells – from Fundamentals to Systems, 9 (2009), 794-804

The durability tests were mainly conducted on two- and four-cell short stacks of the Jülich F design for planar-type cells, which has been in use since 2002. Anode substrate cells measuring 10 cm x 10 cm with an effective electrode area of 80 cm² were used in all stacks.

Cells either had a double-layer LSM/YSZ composite cathode or a single-layer LSCF cathode. In the latter case, a CGO diffusion barrier was applied between the YSZ electrolyte and the LSCF cathode layer.

Tab. 16 lists a number of short stacks which were operated for at least 10,000 hours over the last five years. All durability tests were conducted at a constant current density of 0.5 A cm^{-2} and the cell voltages were monitored as a function of time.

Fig. 81 shows the average cell voltages during operation as a function of time and the starting date for the five short stacks listed in Tab. 16. Note the scale of the graph, which extends over more than five years. The stack F1002 97 with a wet powder sprayed (WPS) protective layer and LSCF cathodes was put into operation in August 2008, and achieved about 47,000 hours of operation, showing a mean degradation of 8 mV/1000 h, which corresponds to a power loss of 1 %/1000 h. This operating time represents a world record for planar SOFC stacks and has thus proven that the targeted 40,000 hours of operation are feasible. It impressively showed that even in the case of long operating times, progressive degradation caused by unexpected material interactions does not necessarily occur.

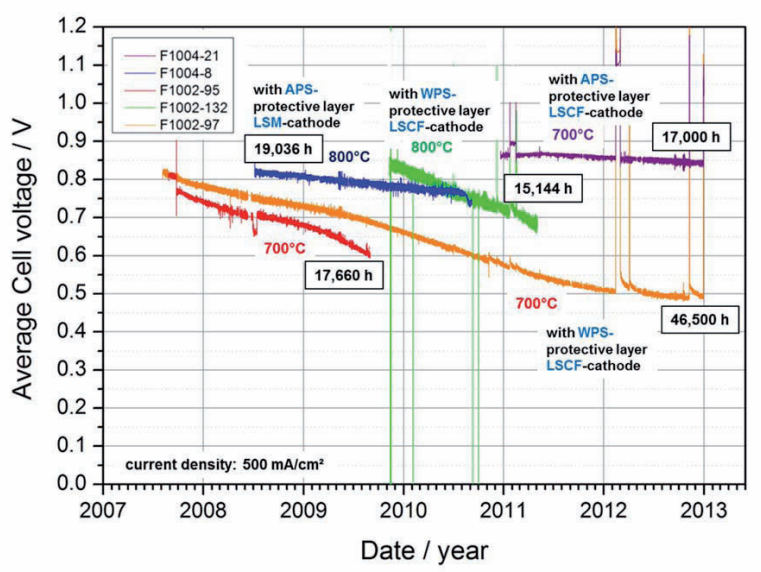

Fig. 81: Average cell voltages as a function of date for short stacks

The short stack (F1004-21) with an atmospheric plasma sprayed (APS) protective layer and LSCF cathodes achieved about 17,000 hours of operation with a degradation of less than 1 mV/1000 h, which corresponds to a power loss of about 0.1%/1000 h (see Fig. 82). This means that the envisaged degradation rate of 0.25%/1000 h could clearly be underrun. The effects of operating temperature and cathode material were investigated in further long-term tests of between 15,000 and 20,000 hours. The post-test analysis revealed that after 15,000 operating hours at 800 °C using LSM cathodes, the electrolyte is mechanically damaged by

manganese diffusion from the cathode into the electrolyte grain boundaries. This probably caused a decrease in ionic conductivity and a mechanical weakening and eventually led to the separation of the grain boundaries and crack growth. The growth of these cracks eventually resulted in the fracture of one cell, the burning of fuel gas and sudden failure of the stack [29].The post-test characterization methods used here are described in [30]

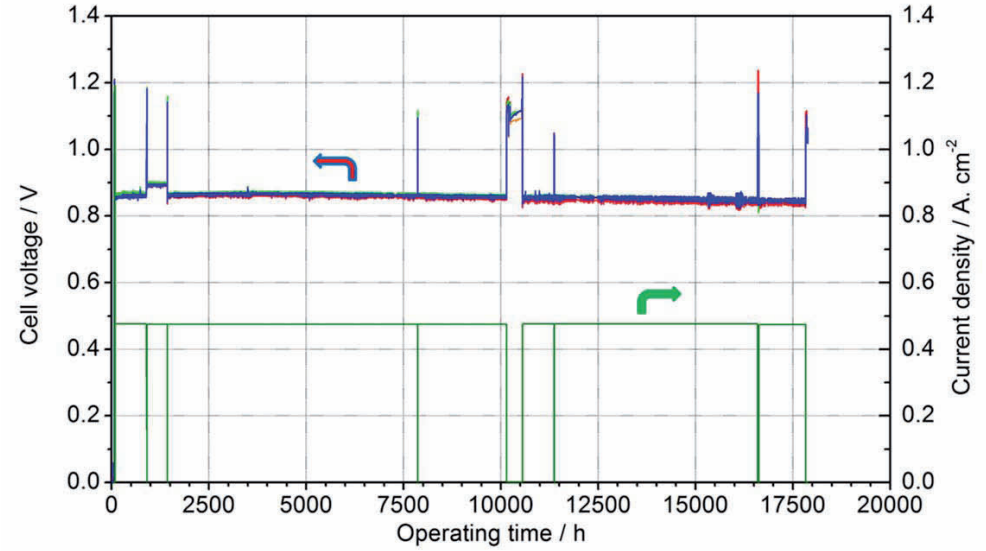

Fig. 82: F1004-21: long-term test at 0.5 A/cm² and 700 °C with hydrogen; APS protective layer on cathode side

Tab. 16 gives the resulting relative degradation rates per 1000 hours for all stacks studied as a voltage drop at the end of life in relation to the initial cell voltage.

4.3.2 Investigation of material interactions

4.3.2.1 Objectives and fields of activity

Ionic transport in oxide ceramics is a prerequisite for the functioning of solid oxide fuel cells (SOFCs) and oxygen sensors (lambda probes). In addition to the desired transport of oxide ions, the diffusive transport of cations also causes (high-temperature) degradation phenomena. Ion conduction and diffusion along the inner and outer interfaces, such as grain boundaries, phase boundaries and surfaces, is usually much faster than in a bulk phase.

With the increasing miniaturization of functional units and the application of thin films, the proportion of interfaces and areas near interfaces increases in relation to the total volume. This also increases the impact of interfacial transport on the general properties of the

[29] Malzbender, J.; Batfalsky, P.; Vaßen, R.; Shemet, V.; Tietz, F.: Component interactions after long-term operation of an SOFC stack with LSM cathode. Journal of Power Sources 201 (2011), 196-203

[30] Menzler, N.H.; Batfalsky, P.: Post-Test Characterization of Solid Oxide Fuel-Cell Stacks. WILEY-VCH, FC Science & Engineering: Materials, Processes, Systems and Technology, edited by D. Stolten and B. Emonts, ISBN 978-3-527-33012-6 (2012), 469-4

system. The stability of microstructures/nanostructures is therefore limited by interfacial transport (and surface energy) and determines the lifetime of the functional unit as a whole. The following issues related to SOFCs are therefore being investigated:

- Diffusion of oxide components in the cathode material through diffusion barrier layers, influence of the grain structure of the barrier layer on long-term degradation behavior
- Fundamental investigations on oxide transport in YSZ multilayers, influence of interface structures and local mechanical strain fields

4.3.2.2 Important results

SrO diffusion in CGO barrier layers

In order to minimize cell resistance in an anode-supported SOFC, a thin layer of cubic (yttrium oxide) stabilized zirconium oxide, $Zr_{0,85}Y_{0,15}O_2$ (YSZ), is applied as the oxide-ion-conducting electrolyte. To use lanthanum-strontium-cobalt-iron oxide $La_{1-x}Sr_xCo_{1-y}Fe_yO_{3-\delta}$ (LSCF) as a cathode material, a diffusion barrier layer of oxide-ion-conducting $Ce_{0,8}Gd_{0,2}O_2$ (CGO) is applied between the electrolyte and cathode in order to minimize the diffusive transport of SrO (and La_2O_3) to the YSZ electrolyte layer. The SrO reacts with YSZ and forms a $SrZrO_3$ layer, which conducts oxide ions very poorly and increases the total resistance of the cell thus reducing the available electric power [31].There is very little literature on the diffusion coefficients D_{Sr2+}(bulk) of Sr^{2+} in the bulk phase or on the grain boundary diffusion coefficient D_{Sr2+}(gb) [31, 32, 33, 34]. However, the available data indicate that grain boundary diffusion is at least two orders of magnitude faster than bulk transport (Fig. 81).

As part of a study (DegraSOFC-S) financed by the technology transfer fund, the mean diffusion coefficient D_{Sr2+} of Sr^{2+} in CGO thin films will be investigated as a function of the grain boundary density and structure. CGO thin films were therefore applied with a thickness of approx. 500 nm to 1 µm to different YSZ substrates with different grain boundary densities using various fabrication techniques and fabrication parameters. The morphology of the samples was determined by means of scanning electron microscopy (SEM) and the crystalline structure and texture by means of X-ray diffraction (XRD) and pole figure measurements. The XRD and pole figure measurements were performed in cooperation with IEK-2. Initial investigations showed a broad variation of the layer texture depending on the sample fabrication and the substrate (see Fig. 83).

[31] Knibbe, R.: Hauch, A.; Hjelm, J.; Ebbesen, S.D.; Mogenssen, M.: Durability of Solid Oxide Cells. Green, 1 (2011), 141

[32] Sakai, N.; Kishimoto, H.; Yamaji, K.; Horita, T.; Brito, M.E.; Yokokawa, H.: Interface Stability of Perovskite Cathodes and Rare-Earth Doped Ceria Interlayer in SOFCs. Journal of the Electrochemical Society, 154 (2007), B1331

[33] Sakai, N.; Kishimoto, H.; Yamaji, K.; Horita, T.; Brito, M.E.; Yokohawa, H.: Degradation Behaviour at Interface of LSCF Cathodes and Rare Earth Doped Ceria. ECS Transactions, 7 (2007), 389

[34] Sakai, N.; Yamaji, K.; Horita, T.; Yokokawa, H.; Kawakami, A.; Matuoka, S.; Watanabe, N.; Ueno, A.; Extended Abstract of the 13th Symposium of SOFC Society of Japan. (2004) 58-63

YSZ substrate	CGO layer	Texture	
(100) YSZ single crystal	Magnetron sputtering (IEK-1)	(100) CGO || (100) YSZ [010] CGO || [010] YSZ, only one orientation, only minimal misalignment ($\phi \approx$ +/- 5°)	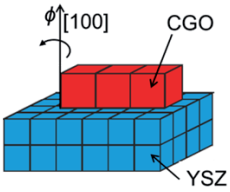
Screen-printed YSZ layer with no preferred orientation (SOFC substrate)	Magnetron sputtering (IEK-1)	(100) CGO || (100) YSZ, , fiber texture, no preferred azimuthal orientation	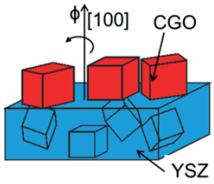
Screen-printed YSZ layer with no preferred orientation (SOFC substrate)	Electron beam evaporation (IEK-1)	No clear preferred orientation	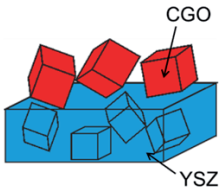

Fig. 83: Variation of CGO layer texture using different coating techniques

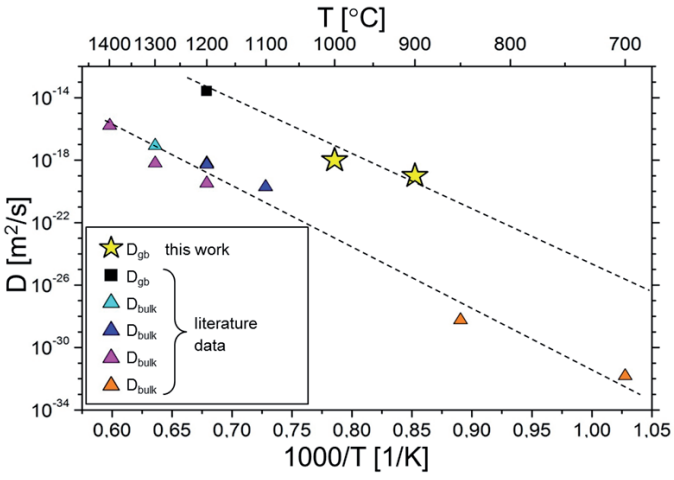

Fig. 84: Diffusion coefficient $D_{Sr^{2+}}$ of Sr^{2+} in CGO (bulk) and along the grain boundaries (gb) as a function of the reciprocal temperature; first results b of ToF-SIMS analyses (asterisk) compared to literature data from [31 - 34]

As a source for the diffusion experiment, a SrO layer was deposited on the CGO thin-film sample by means of molecular beam epitaxy (JCNS-2/PGI-4). The diffusion experiments were conducted by exposing the samples to air in the temperature range 600 – 1000 °C. The resulting Sr concentration profiles in the CGO layers were analyzed by means of ToF-SIMS at the Central Institute for Engineering, Electronics and Analytics (ZEA). According to first estimates for the diffusion coefficients of Sr^{2+} along grain boundaries, D_{Sr2+}(gb) was in the range of 10^{-19} m^2/s (900 °C) and 10^{-20} m^2/s (1000 °C), see Fig. 84.

These values for the grain boundary diffusion D_{Sr2+}(gb) and the dependence of the mean diffusion coefficients D_{Sr2+} on the grain boundary density and structure of the barrier layer can be used to estimate the influence of these processes on the long-term degradation of an SOFC, i.e. for lifetimes longer than 40,000 h. A maximal grain boundary density, which does not have a limiting effect on the lifetime of the SOFC, can be derived from specifications for conducting the coating processes. In principle, unsuitable coating techniques leading to grain boundary densities that are too high can thus be excluded.

O^{2-}transport in YSZ multilayers

Inner and outer interfaces of solid ion conductors generally show a significantly different ionic conductivity and diffusivity than the bulk phase. Currently, there are no general model concepts for interfacial transport that account for all aspects observed to date. At a solid-solid phase boundary, there must be a transition between two lattice structures with different crystal plane spacings and lattice symmetries. In addition to spatial charge effects and segregation effects, misfit dislocations, structurally disordered transition zones and elastic strains also occur in interface regions. This work aims to investigate the basic relationships between interface microstructure and the changed interface conductivity.

	YSZ/Gd_2O_3	**YSZ/Dy_2O_3**	**YSZ/Y_2O_3**	**YSZ/Er_2O_3**	**YSZ/Lu_2O_3**	**YSZ/Sc_2O_3**
Misfit %	5.08	3.70	3.09	2.43	1.02	–4.28

Tab. 17: Misfit percentage for model systems with different structural materials

To systematically investigate these phenomena, pulsed laser deposition (PLD) was used to fabricate multilayers from the oxide-ion conductor YSZ and an insulating rare earth sesquioxide R_2O_3 with bixbyite structure (R = rare earth metal). As a substrate, (0001) Al_2O_3 single crystals were used. The bixbyite structure was crystallographically derived from the fluorite structure of YSZ. By varying the rare earth metal, interfaces can be prepared as model systems with different misfits but comparable structures (see Tab. 17). On the model systems, the (ionic) conductivity σ_{O2-} and the $^{18}O^{2-}$ tracer diffusion D^*_{O2-} were measured parallel to the layers. Interfacial transport can be determined from the change in total conductivity with variation of the thickness of the YSZ layers.

Within a DFG project (Ko1859/3-1), more extensive studies are planned as is the further elaboration of the theoretical description. Studies have already been performed on YSZ/Y_2O_3, YSZ/Sc_2O_3 and YSZ/Lu_2O_3 multilayer systems in previous work [35],[36],[37].

During the course of the project to date, YSZ/Y_2O_3 multilayers have been fabricated once again as a reference in cooperation with PGI-9. YSZ/Gd_2O_3 multilayers were prepared for the first time. The thickness of the layers was varied systematically between 1 µm and 10 nm and the oxide-ion conductivity was determined using impedance spectroscopy in the temperature range 350 – 700 °C. Measurements of the $^{18}O^{2-}$ tracer diffusion coefficients are being planned in cooperation with PGI-7 and ZEA (ToF-SIMS analysis).

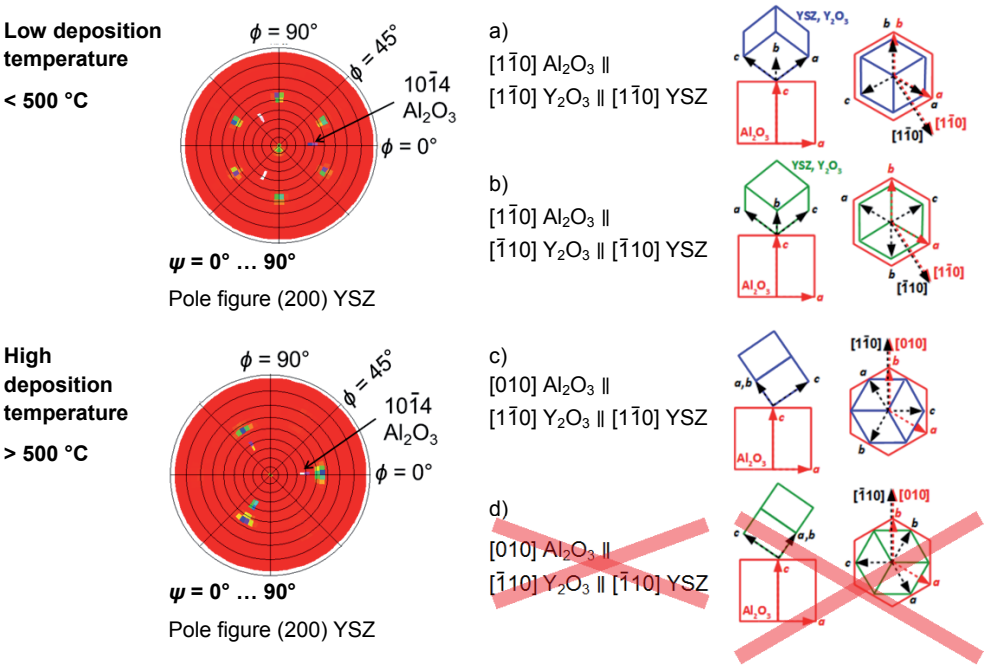

Tab. 18: Orientation variants of YSZ/Y_2O_3 for low and high deposition temperatures

The morphology, crystalline structure and texture of the multilayers are characterized by means of SEM, XRD and pole figure measurements. The XRD and pole figure measurements were performed in cooperation with IEK-2. In the case of the newly fabricated

[35] Korte, C.; Peters, A.; Janek, J.; Hesse, D.; Zakharov,N.: Ionic conductivity and activation energy for oxygen ion transport in superlattices - The semicoherent multilayer system YSZ (ZrO_2 + 9.5 mol% Y_2O_3)/Y_2O_3. Phys. Chem. Chem. Phys., 10 (2008), 4623

[36] Schichtel, N.; Korte, C.; Hesse, D.; Janek, J.: Elastic strain at interfaces and its influence on ionic conductivity in nanoscaled solid electrolyte thin films-theoretical considerations and experimental studies. Phys. Chem. Chem. Phys., 11 (2009), 3043-3048

[37] Korte, C.; Schichtel, N.; Hesse, D.; Janek, J.: Influence of interface structure on mass transport in phase boundaries between different ionic materials Experimental studies and formal considerations. Monatsh. Chem. – Ch 140 (2009), 1069-1080

YSZ/Gd_2O_3 multilayers, only one (main) orientation was found, as is the case for YSZ/Y_2O_3 and YSZ/Sc_2O_3:

(0001) Al_2O_3 || (111) SE_2O_3 || (111) YSZ

The c axis from Al_2O_3 and the [111] direction in YSZ and SE_2O_3, each with trigonal symmetry, are parallel to each other. For the same orientation of the axes perpendicular to the substrate, however, azimuthally rotated variants occur. In the case of YSZ/Y_2O_3, the formation of the possible orientation variants is now being investigated in more detail. Three different variants exist depending on the deposition temperature (see Tab. 18):

At low deposition temperatures, a mixture is created of the orientation variants a) and b) at an angle of 180° to each other. At higher deposition temperatures, orientation variant c) is formed almost exclusively. The conceivable variant d) at an angle of 180° to c) does not occur on an appreciable scale.

TEM/SAED and HRTEM studies were conducted in cooperation with the Max Planck Institute of Microstructure Physics in Halle. The results confirm the orientation relationships between the layers found by means of XRD and pole figures. In all multilayers fabricated to date, mean crystallite sizes of 30 – 100 nm were found. HRTEM micrographs show phase boundaries between columnar crystallites that are almost dislocation-free (coherent). These observations indicate that mechanical stresses caused by misfits only occur in a limited zone and that they may relax with increasing distance from the interface.

Mechanical stresses that occur in YSZ/Y_2O_3 multilayers were also investigated in detail for the first time as a function of the thickness of the YSZ layers by means of radiographic techniques. The detailed analysis of reflection planes of the (111) YSZ and (222) Y_2O_3 crystal planes parallel to the layer plane (0°) and almost perpendicular to it (70.5°) confirmed the relaxation of the mechanical stresses in the crystallite bulk and localization in a zone near the interface (Fig. 85, top). For large layer thicknesses, the reflection planes are determined by the slightly strained volume fraction and are approximately equivalent to the literature values. For small layer thicknesses, the volume fraction decreases so that the reflection planes are increasingly determined by the strained zones near the interface. The crystal plane spacing in YSZ perpendicular to the interface increases continuously while that in Y_2O_3 decreases until, in accordance with the coherent interface structure, they approach a common value. Conversely, lateral contraction causes the crystal plane spacing parallel to the interface to increase in YSZ and decrease in Y_2O_3.

In previous work on multilayers, the oxide ion interfacial conductivity and diffusion were shown to increase with dilative strain (YSZ/Y_2O_3) of YSZ and decrease with compressive strain (YSZ/Sc_2O_3) compared to the bulk phase (Fig. 85, bottom). For the YSZ/Y_2O_3 multilayer, the increase in the proportion of mechanically (dilatively) strained interface region correlates with an increase in the ionic transport.

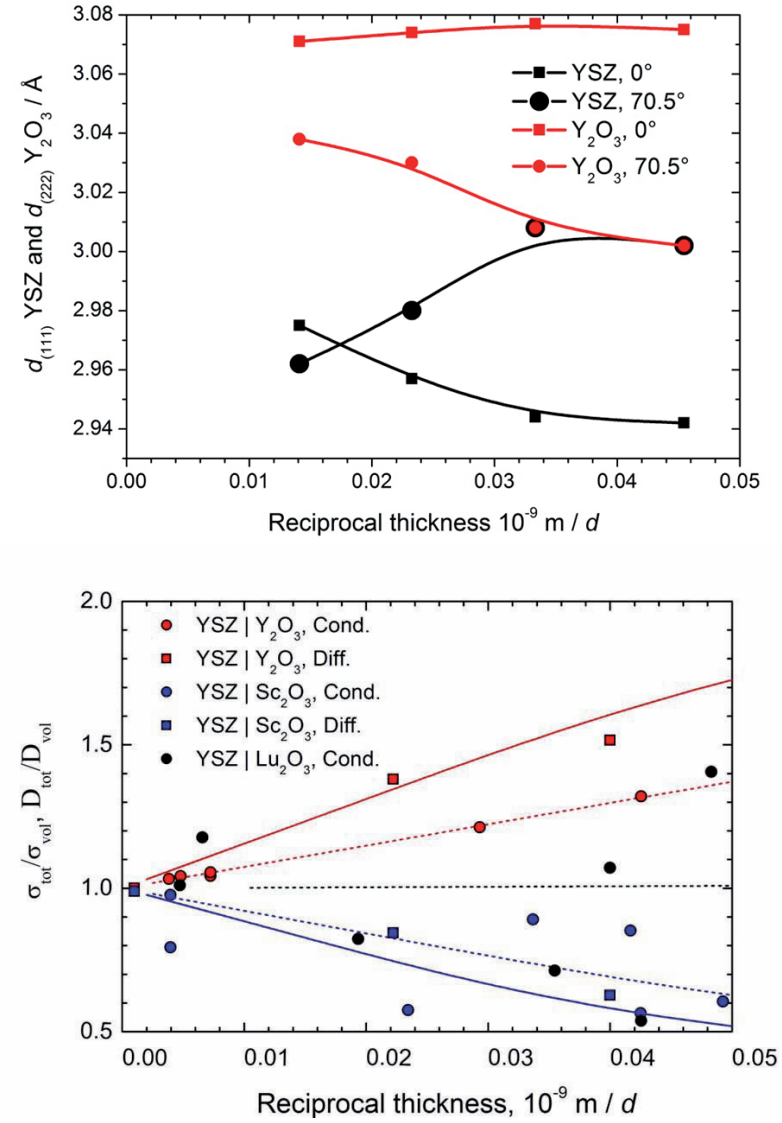

Fig. 85: **(Mean) lattice constant in a YSZ/Y_2O_3 multilayer sample parallel to the substrate plane (0°) and approximately perpendicular (70.5°) to it as a function of single layer thickness *d* (top). Mean ionic conductivity and diffusion coefficient (normalized with respect to the volume values) as a function of single layer thickness *d* for YSZ/Y_2O_3, YSZ/Lu_2O_3 and YSZ/Sc_2O_3 multilayers (bottom). Literature data from previous studies [35 - 37]**

Based on the observations, an analytical model was refined to describe the relationship between mechanical strain fields in solid-solid interfaces and their effect on ionic conductivity σ_{tot} (and diffusion) parallel to the interface. The basis was provided by shearing, which causes strain fields to relax exponentially beginning from the phase boundary between two crystallites. The prerequisites for relaxation by means of shearing are comparatively small

crystallite cross-sections in the layer planes. The latter is already known from HRTEM analyses (30 – 100 nm). The maximal strain ε_0 depends on the lattice mismatch between the phases. For simplification, properties are assumed (description only with one Young's modulus *Y* and Poisson's ratio *v*). The mechanical strain ε_0 resulted in an isostatic pressure, which depending on the activation volume $\Delta V^{\#}_{m}$ influenced the ionic transport processes (pressure dependence of Arrhenius law):

$$\frac{\sigma_{tot}(d*)}{\sigma_{vol}} = \frac{1}{d*}\int_0^{d^*} exp\left(\alpha\varepsilon_0 \frac{coshz'}{coshd^*}\right) dz' mit\ d^* = \frac{d}{2\delta_0}, \delta_0 = \frac{1}{4}\sqrt{\frac{2}{3}\frac{1-v}{1+v}}\ /und\ \alpha = \frac{2}{3}\frac{\Delta V_m^{\#}}{RT}\frac{Y}{1-v}$$

The extent of the increase in the mean oxide-ion conductivity σ_{tot} (and diffusivity) of the multilayer and its functional progress as a function of layer thickness *d* for YSZ/Y_2O_3, YSZ/Sc_2O_3 and YSZ/Lu_2O_3 can be described well using the derived relation. Here, σ_{vol} is the ionic conductivity of the unstrained bulk phase. The only parameters included are the mechanical constants *Y*, *v* and the activation volume $\Delta V^{\#}_{m}$ of YSZ as well as the mean crystallite cross-section *l*. The values for the crystallite cross-sections *l* determined by curve fitting agree with the HRTEM analyses (30 – 50 nm). For an ion transport mechanism via vacancies such as in YSZ, the activation volume is always positive, i.e. in the transition state, the lattice is locally expanded by the (oxide) ion taking up the vacancy. In accordance with the model, we can therefore generally say that the ionic conductivity along the interface must be increased for a dilative interfacial strain and decreased for a compressive strain.

4.4 Investigating degradation procedures during autothermal reforming

The strategic approach of work in the fuel processing and systems group at IEK-3 is governed by the aim of developing an HT-PEFC system based on the autothermal reforming of middle distillates such as diesel and kerosene. The envisaged power class is 5 – 10 kW_{el}. This range is particularly interesting for the use of HT-PEFC systems as auxiliary power units (APUs) to supply on-board power in the aviation and heavy goods vehicle sectors. The decisive criterion for the maturity of a new technology is its long-term stability under conditions typical of the planned application. In order to collect initial data on this, the autothermal reformer ATR 9.2 – one of the central components of a fuel cell system – was subjected to a long-term experiment under laboratory conditions, which was still ongoing at the time of writing this report. The experiment aims to demonstrate a long-term stability of 10,000 hours. The structure of the ATR 9.2, with respect to its materials, tube wall thicknesses, welding consumables, etc., is designed to operate for this time.

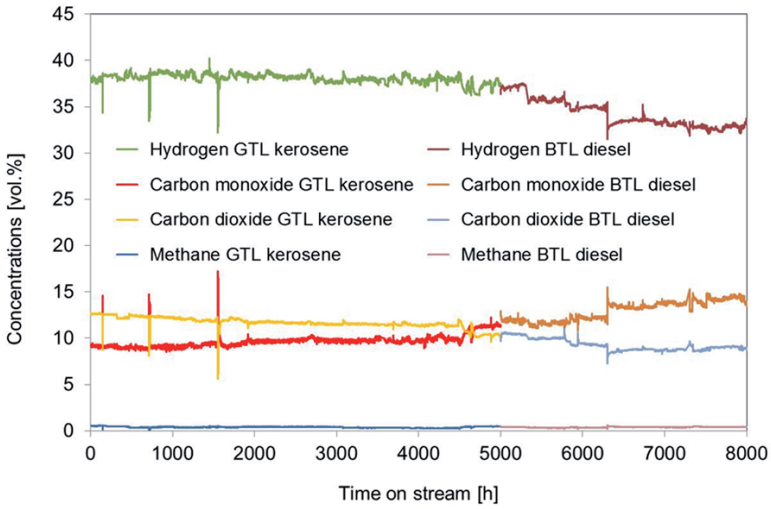

Fig. 86: Concentrations of hydrogen, carbon monoxide, carbon dioxide and methane during a long-term experiment with the ATR 9.2 for an O_2/C molar ratio of 0.47 and a H_2O/C molar ratio of 1.9 using GTL kerosene and BTL diesel

Fig. 86 shows the concentrations of H_2, CO, CO_2 and CH_4 when GTL kerosene and BTL diesel are used as fuel over the course of the first 7800 hours of this long-term experiment. GTL kerosene was used for the first 5000 hours of the test and BTL diesel for the next 2800 hours of operation. Tab. 19 lists the most important physical and chemical properties of the two fuels used.

According to the first two equations in Tab. 20 for endothermic steam reforming and exothermic partial oxidation, H_2 and CO are the desired products of autothermal reforming, while CH_4 and CO_2 occur during the water-gas shift reaction and the methanation reaction. Fig. 86 shows that the concentrations of H_2, CO, CO_2 and CH_4 remained constant during the first 4500 hours of the test. The H_2 concentration was in the range of 38.0 vol.% – 38.6 vol.%, that of CO was approx. 9.2 vol.%–10.0 vol.%, and the concentration of CO_2 varied between

Fuel	Supplier	Distillation temperature (90 %) °C	Mass fraction aromatics Ma.-%	Summation forumula
GTL kerosene	Shell MDS Malaysia	185	< 0.1	$C_{10}H_{22}$
NExBTL diesel	NESTE Oil Finnland	295	< 0.1	$C_{17}H_{34}$

Tab. 19: Physical and chemical properties of the two fuels used in the long-term experiment with ATR 9.2

12.5 vol.% and 11.5 vol.%. CH_4 had a concentration of approx. 0.3 vol.%. During the last 500 hours of operation with GTL kerosene, a slight deactivation of the catalyst was observed in relation to its activity for the water-gas shift reaction. The concentrations of H_2 and CO_2 sank slightly, while that of CO increased simultaneously.

$C_nH_m + n\,H_2O$	⟷	$n\,CO + (m/2 + n)\,H_2$	endothermic
$C_nH_m + n/2\,O_2$	⟷	$n\,CO + m\,H_2$	exothermic
$CO + H_2O$	⟷	$CO_2 + H_2$	exothermic
$CO + 3\,H_2$	⟷	$CH_4 + H_2O$	exothermic

Tab. 20: Reaction equations for the reaction system of autothermal reforming

When the fuel supply was switched to BTL diesel, the concentrations of all components in the product gas of the autothermal reforming changed continuously to a small extent over the next 1300 hours of operation. The concentration of H_2 dropped to the range of 34.7 vol.% to 36.0 vol.%, while the value for CO was in the range of 11.0 vol.% to 12.4 vol.%. The CO_2 concentration in the reformate varied between 9.5 vol.% and 10.5 vol.%, while that of CH_4 remained almost constant compared to the experiment with GTL kerosene and exhibited values of approx. 0.3 vol.%. For stoichiometric reasons (cf. Tab. 19 and Tab. 20) the concentration of H_2 in the reformate must be lower when BTL diesel is used. This is clear when the summation formula of BTL diesel ($C_{17}H_{34}$) and GTL kerosene ($C_{10}H_{22}$) are compared, taking into account the first two reaction equations in Tab. 20.

After a total of 6300 hours of testing, problems were encountered with the water supply to the ATR 9.2, and the test stand was shut down because the pressure in the water supply lines was below the minimal value. It is not clear whether the water used at this time was still of a sufficiently good quality. For autothermal reforming, de-ionized water must be used as a reactant, because chloride or sulfate ions, for example, could adsorb on the active centers of the catalyst and thus deactivate the catalyst. A regeneration of the centers is only possible to a limited extent. In addition, when the test stand was re-started, strong temperature peaks were observed in the catalyst of the ATR 9.2. These were caused by the combustion of carbon-containing deposits that had formed during operation (or during shut-down) of the ATR 9.2 before this point in time on the catalyst. Experimentally, this incident caused the concentrations of H_2 to decrease over the next 1500 hours of operation to values between

32.5 vol.% and 33.5 vol.%, while the CO concentration increased to values between 13.5 vol.% and 14.5 vol.%. The concentration of CO_2 varied between 8.5 vol.% and 9.1 vol.%, while that of CH_4 remained almost constant once again at 0.4 vol.%.

The conversion of hydrocarbons contained in GTL kerosene and BTL diesel is defined as complete when no molecules other than H_2, CO, CO_2 or CH_4 (cf. Tab. 20) are found in the gas phase or in the condensed water. The analysis of the gas phase focusing on formed hydrocarbons with two to seven carbon atoms (C2 to C7 hydrocarbons), such as ethane, ethene, propene, butene or benzene, was negative for the test phase using GTL kerosene. For this reason, it is not included in Fig. 86. From the point in time when BTL diesel was used as a fuel, undesirable by-products, such as ethene, ethane, propene, propane, butene, pentene, and hexene, were detected in the gas phase. In addition to the test stand and operating problems described above, small amounts of benzene were also found among the by-products.

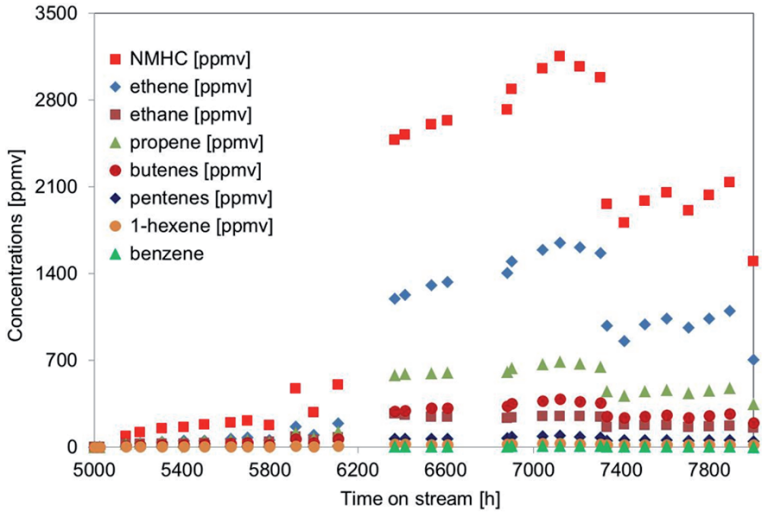

Fig. 87: Concentrations of by-products in the gas phase during the long-term experiment with the ATR 9.2 for an O_2/C molar ratio of 0.47 and a H_2O/C molar ratio of 1.9 using BTL diesel

Fig. 87 shows the concentrations of the individual components listed as well as the value for non-methane hydrocarbons (NMHC). The NMHC value is the sum of the concentrations of all of the individual components detected among the by-products. It is clear from Fig. 87 that the NMHC value continuously increased during the first 1300 hours of testing using BTL diesel and that it reached a maximal value of 500 ppmv. The concentration of ethene during this time was always highest compared to the concentrations of the other by-products and increased to a maximum of 200 ppmv. Propene had the second-highest concentration with a maximal value of 125 ppmv. This increase can be explained by a slight deactivation of the catalyst in the ATR 9.2. As a result of the above-mentioned test stand and operating problems after 6300 hours, significantly higher values were detected for all by-products and the NMHC value in the period between 6300 and 7300 hours of testing. The NMHC value during this time was max. 2270 ppmv with ethene concentrations of 1,1150 ppmv and propene concentrations of 490 ppmv. The catalyst of the ATR 9.2 was clearly damaged and

deactivated by the test stand and operating problems after 6300 hours. Active centers on the catalyst may have been irreversibly blocked by inorganic, ionic deposits from the reaction water. The strong temperature peaks observed when the system was re-started may have led to sintering of the active catalyst particles, which would have decreased their number. Furthermore, it is conceivable that carbon-containing deposits were still present on the catalyst during this test phase, which blocked the active catalyst centers for the reactants of the reforming process in a similar manner to ionic deposits. A post-mortem analysis of the catalyst after the completion of the long-term experiment can provide information on the individual deactivation processes that occurred. An alternative to catalyst regeneration that can be tested during experimental operation involves leaving the catalyst in air flow for a longer period of time at an elevated temperature of 150 °C in order to remove possible carbon-containing deposits from the catalyst surface. This increases the catalyst surface available to the reaction again. Maintenance work on the laboratory infrastructure, which was necessary after 7300 hours of operation, allowed this regeneration mode to be set for a period of approx. seven days. When the system was re-started after regeneration, the temperature in the catalyst did not increase uncontrollably. This observation indicates that any carbon-containing deposits that had been present beforehand were indeed combusted during the regeneration phase. Fig. 87 supports this conclusion that regeneration was at least partially successful. The NMHC value was reduced for the test period of 7300 to 7800 hours from more than 2000 ppmv to the range of 1300 ppmv to 1450 ppmv. The ethene concentration was still between 600 ppmv and 720 ppmv, that of propene between 300 ppmv and 330 ppmv. However, the concentration level of the undesirable by-products was still found to be significantly higher than at the beginning of the test phase with BTL diesel despite successful combustion of the carbon-containing deposits. A possible deactivation of the catalyst by inorganic ionic deposits or sintering processes is largely irreversible. The NMHC value is not expected to decrease significantly during the subsequent course of the long-term experiment. If the concentrations of the undesirable by-products continue to increase, switching to the regeneration mode again may have to be considered. In general, it can be concluded from this experiment that it makes sense to interrupt the process of autothermal reforming at defined intervals, even in future applications in airplanes or heavy goods vehicles (e.g. every 200 hours of operation for 24 hours) to regenerate the catalyst and thus ensure a consistently high quality of the reformate, which in turn prevents damage to the subsequent components in fuel cell systems (water-gas shift reactor, reactor for preferential oxidation, fuel cell).

From the literature, ethene is known as a mechanistic precursor for the formation of carbon-containing deposits. In their publication, Yoon et al. [38] describe different methods of suppressing the formation of such carbon-containing deposits induced by ethene. They successfully varied the O_2/C molar ratio and used what is known as an ultrasonic diesel injector to reduce the amount of ethene formed. Karatzas et al. [39, 40, 41, 42] published a

---

[38] Yoon, S.; Kang, I.; Bae, J.:Suppression of ethylene-induced carbon deposition in diesel autothermal reforming. Int. J. of Hydrogen Energy, 34 (2009), 1844

[39] Karatzas, X.; Dawody, J.; Grant, A.; Svensson, E.E., Pettersson, L.J.: Zone-coated Rh-based monolith catalyst for autothermal reforming of diesel. Appl. Catal. B: Environmental 101 (2011), 226-238

[40] Karatzas, X.; Jansson, K.; Dawody, J.; Lanza, R.; Pettersson, L.J.: Microemulsion and incipient wetness prepared Rh-based catalyst for diesel reforming. Catal. Today 175 (2011), 515-523

series of papers on the autothermal reforming of diesel fuel. In [41] the authors investigated different RhPt catalysts on various substrates (CeO_2, ZrO_2, Al_2O_3, TiO_2, SiO_2, La_2O_3, MgO, Y_2O_3) for the autothermal reforming of low-sulfur diesel fuel. Their experiments revealed a minimal ethene concentration of approx. 1000 ppmv at 98 % conversion of the diesel fuel for the best catalyst system RhPt/CeO_2-ZrO_2.

In order to comprehensively evaluate the reforming process, an analysis of the condensed unconverted water downstream of the reformer must also be performed in addition to the evaluation of the gas phase. Polar by-products o

f the reaction are predominantly released here. Fig. 88 shows the concentrations of non-purgeable organic carbon (NPOC) for the whole of the test period to date for GTL kerosene and BTL diesel, as well as the total organic carbon (TOC) found in the condensed water for the experiment with BTL diesel. The NPOC value increased slightly during the first 5000 hours of testing from 10 ppmv to 25 ppmv. This can be explained by a very slight deactivation of the catalyst during the first 5000 hours of operation. After the fuel supply was changed to BTL diesel, the NPOC and TOC values increased significantly.

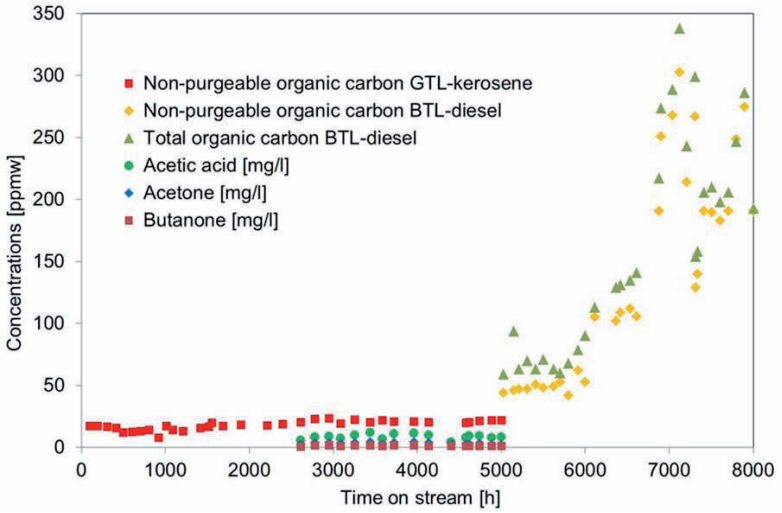

Fig. 88: Dissolved amounts of total organic carbon (TOC) and non-purgeable organic carbon (NPOC) in condensed unconverted water during the long-term experiment with the ATR 9.2 at an O_2/C molar ratio of 0.47 and a H_2O/C molar ratio of 1.9 for the use of GTL kerosene and BTL diesel

As shown in Fig. 88, operation with BTL diesel also leads to the three phases found in Fig. 87, which deactivate the catalyst to different degrees. In the first 1300 hours (5000 – 6300 hours overall), the NPOC and TOC values were between approx. 50 ppmv and

[41] Karatzas, X.; Jansson, K.; González, A.; Dawody, J.; Pettersson, L.J.: Autothermal reforming of low-sulfur diesel over bimetallic RhPt supported Al_2O_3, Ce-O_2-ZrO_2, SiO_2, TiO_2. Appl. Catal. B: Environmental 106 (2011), 476-487

[42] Karatzas, X.; Creaser, D.; Grant, A.; Dawody, J.; Pettersson, L.J.: Hydrogen generation from n-tetradecane, low-sulfur and Fischer-Tropsch diesel over Rh supported on alumina doped with ceria/lanthana. Catal. Today 164 (2011), 190-197

100 ppmv, and the TOC value was always slightly higher than the NPOC value. The analysis procedure used to determine the NPOC value did not allow slightly volatile organic components in the water to be measured at the same time. The TOC value includes the concentrations of these substances. In the second phase between 6300 and 7300 hours of testing after the above-mentioned test stand and operating problems, a small and then very strong increase was detected in the NPOC and TOC values. Their maximal values were between 300 ppmw and 350 ppmw. After the described regeneration phase, the two values decreased very strongly to the range of approx. 150 ppmv and stabilized at values of approx. 200 ppmv. Fig. 88 also shows that the NPOC value was composed mainly of the concentrations of acetic acid, acetone and butanone for the period of 2500 – 5000 hours of testing.

These results agree very well with those from Fig. 87 and the data from Tab. 19. Both figures clearly show that it is considerably more difficult to perform autothermal reforming with BTL diesel than with GTL kerosene. BTL diesel exhibits higher boiling temperatures and a larger molar mass. As a result, its individual components require a higher enthalpy flow in the evaporation chamber of the reformer in order to be fully transferred to the gas phase. In the case of BTL diesel, there is a larger risk that droplets of liquid could hit the catalyst, pyrolyze there and block the active centers on the catalyst. In addition, under these conditions it is conceivable that zones with non-homogeneous mixing of the reactants (oxygen, steam, evaporated fuel) will form more frequently in the mixing chamber of the reformer than when GTL kerosene is used.

Tab. 21 ists the hydrocarbon conversions determined at different points in time during the long-term experiment. They account for the above-mentioned by-products in the gas phase and in the condensed water. At 7042 hours, an oily phase comprising non-converted hydrocarbons on the condensed water was also gravimetrically determined. Such a phase did not occur at the other three times.

Fuel	Time t H	Conversion X %
GTL kerosene	5000	99.99
NExBTL diesel	5966	99.67
NExBTL diesel	7042	96.72
NExBTL diesel	7706	98.49

Tab. 21: Conversion of GTL kerosene and BTL diesel at different points in time during the long-term experiment

The different phases of the long-term experiment are also reflected in this table. During the first 5000 hours of testing, when GTL kerosene was used, hydrocarbons were almost fully converted with a conversion of approx. 100 %. In the first phase when BTL diesel was used before the above-mentioned test stand and operating problems, a very high conversion of

approx. 99.67 % was also achieved. Only after the above-described deactivation of the catalyst after 6300 hours of testing did the conversion drop considerably to approx. 96.72 %. The by-products in the gas phase shown in Fig. 87 were the main cause of this, accounting for around 2 percentage points of the decrease. Around 1 percentage point of the conversion decrease can be attributed to the oily phase on the condensed water. The fact that the above-described simple regeneration after 7300 hours of operation at an elevated temperature in air flow was successful is clear from Tab. 21. The conversion was increased by almost 2 percentage points and after 7706 hours of operation was back up to 98.49 %. It can be assumed that the regeneration made those active centers on the catalyst available again which had previously been covered with carbon-containing deposits.

After the first 7800 hours of operation of the ATR 9.2, it can be concluded that this reformer generation can be operated with high fuel conversions for GTL kerosene and BTL diesel of almost 100 % over periods of time that would be sufficiently long for technical application in an APU on board an airplane or in a heavy goods vehicle.

5

Outlook

Outlook for New R&D Projects

- Biofuels for use in fuel cells
- Development objective large-scale PEM electrolysis system
- Utilization of CO_2 from flue gases for chemical processes

5.1 Biofuels for use in fuel cells

5.1.1 Initial situation and objectives

In the transport sector, around 95 % of the fuels used are fossil-based. Biocomponents account for 7 % and 10 % in the fuels diesel and gasoline, respectively, the latter in the form of ethanol. With an annual consumption in Germany of 19.6 million tonnes of gasoline and almost 33 million tonnes of diesel in 2011, these large quantities will mean considerable changes in the supply chain when the share of sustainably generated fuels is increased.

Process and systems analysis aims to evaluate the different routes from the primary energy carrier to fuel in terms of energy, ecology and economics. Such analyses must also account for the fact that when waste materials from wood processing, for example, are used to produce fuel, considerable quantities can no longer be used in the existing recycling process. The food production industry, in particular, is faced with competition in terms of direct use (bioethanol or flour from wheat) and in terms of the use of agricultural land (cultivation of rape for biodiesel production or the cultivation of cereals for the food industry). To evaluate this, criteria such as ILUC (indirect land use change) have been defined and are used for the assessments. This is usually done in the form of life cycle assessments (LCAs), which evaluate the entire life cycle of a product in terms of energy and materials. This form of analysis cannot always be found in the literature for all of the fuels discussed here. Life cycle assessments are not performed at IEK-3, but the results of such evaluations are taken into account in defining strategies. Furthermore, the fact that the conversion of waste materials into energy is most efficient in many cases in the form of combined heat and power must also be taken into account. If a technologically advanced fuel technology cannot be implemented even in the long term, then this is definitely the best option. On the other hand, increasing the proportion of sustainable energy in the transport sector is not feasible simply by considering the best possible efficiency.

The transport sector is responsible for 17 % of CO_2 emissions in Germany and almost 25 % in the EU (EU-27). In order to considerably reduce CO_2 emissions, the amount of CO_2 released by fuels must be considerably reduced – from extraction and production to combustion in vehicles.

Fig. 89 shows some different routes of producing fuel using fossil oils, biomass, coal, natural gas and wind power. The primary energy carriers biomass and wind power are available on a sustainable basis. Wind power can be used directly to cover electricity demand or it can be stored indirectly in the form of hydrogen produced via water electrolysis. The energy concept foresees the use of hydrogen as a fuel for fuel cell powertrains in the transport sector. By means of several process chains, biomass can be used to produce fuels such as ethanol, biodiesel, methanol, DME and biogas. The process chains of hydrotreating, oil extraction and fermentation, gasification and synthesis will be discussed in the following sections.

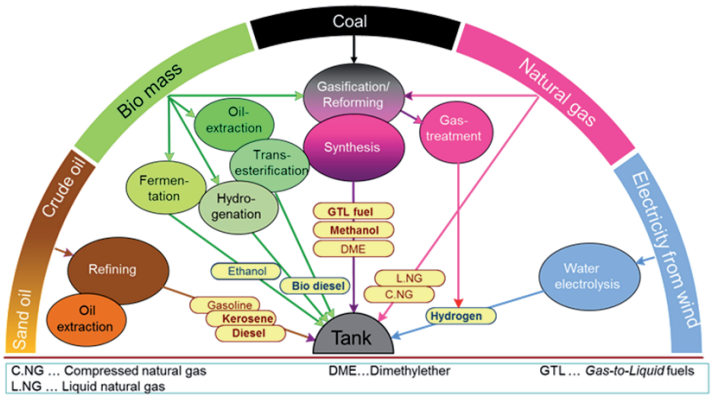

Fig. 89: Different routes of producing fuel using fossil oils, biomass, coal, natural gas and wind power

Two applications for the use of biofuels are interesting in terms of the strategic orientation of the institute. The first is the direct methanol fuel cell (DMFC), which can be used for light traction in forklift and involves a potential changeover to biomethanol. The second is that of on-board power supply in airplanes, ships and heavy-duty vehicles, which should utilize the fuel already used on board for the powertrain. In the long term, these will be biodiesel and biokerosene. The amount of fuel consumed in Germany in 2011 in the form of diesel for heavy goods vehicles was 20 million tonnes and in the form of kerosene 14 million tonnes, which still remains quite high.

5.1.2 Priorities at IEK-3

Taking the fuel cell systems being investigated experimentally at IEK-3 as a basis, the process chains that lead from various types of biomass to biodiesel, biokerosene and biomethanol are evaluated. Biofuels are classified according to generation:

- First-generation biofuels make use of the fruit of a plant, i.e. corn and cereal grains for ethanol production and plant oil from rape flowers.
- Second-generation biofuels are based on using the whole plant by gasifying wood or straw or fermenting the entire plant using special bacterial strains, including cellulose and hemicellulose.

In the literature, there is no uniform definition of third-generation biofuels, despite the fact that this is a recurrent term. Fig. 90 illustrates the division of biofuels into first and second generation. First-generation biofuels are found as additives on the fuel market and compete with food production. Processes for producing second-generation biofuels still require intensive development work on an industrial scale.

At IEK-3, second-generation fuels have been prioritized in relation to future use. In order to gain initial information, use is also made of fossil-based fuels and those of the first generation produced in processes that are also suitable for the second generation. This includes the use of GTL fuels from natural gas, for example, or the hydrotreating of palm oil (hydrotreated vegetable oil, HVO).

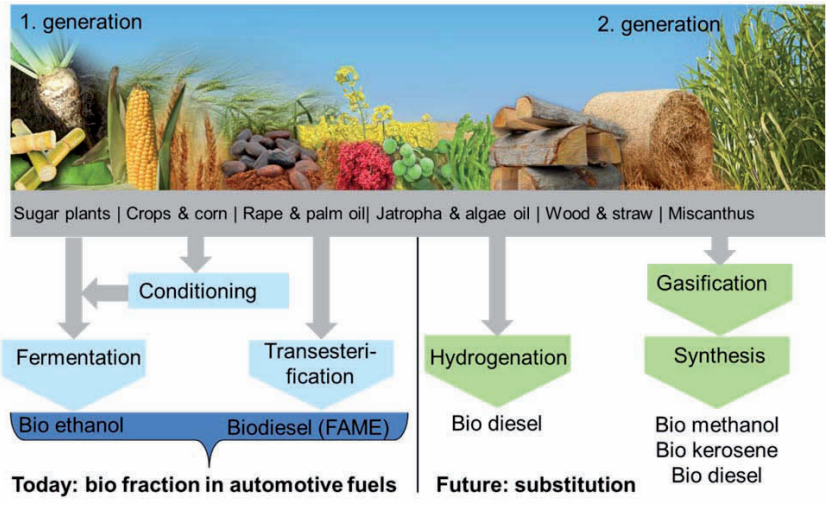

Fig. 90: Classification of first- and second-generation biofuels and their use today and in the future

5.1.3 Methodology

5.1.3.1 Well-to-tank analysis

A well-to-tank analysis evaluates energy consumption and greenhouse gas emissions over the entire fuel path, i.e. from the starting fuel to the tank or the gas pump. Usually, different scenarios are defined. This applies to crude oil processing in the refinery, different supply concepts for natural gas, the mix for electricity generation, and the very individual fuel pathways for the use of renewable energies. In the past, the European association for the conservation of clean air and water in Europe (CONCAWE) has gained recognition for its reports on well-to-tank data, which are freely available online. These data are therefore used when possible.

Analysis of new fuel chains

In relation to the production of diesel fuels from sandy shale, sand oils and algae oil, the CONCAWE database does not contain any information on the energy required to produce these fuels or the specific CO_2 emissions associated with supplying them. Ideally, literature searches should provide a wide range of data for a new chain. For sand oil and algae oil, only limited data are currently available. As new manufacturing processes are often only designed for use on an industrial scale or are not provided in an energy-optimized process, optimized processes can be derived relatively quickly, as shown in the table. In relation to the extraction of algae oils, for example, the dry product can be combusted and the resulting heat can be used for the drying process. Electricity is therefore no longer needed to power electrical heating elements. Furthermore, the balance limits must be adhered to. Data on the transport and distribution of the product can be taken from CONCAWE data. As Willson did not evaluate the hydrogen required for oil hydrotreating, this must be derived from

CONCAWE data, taking into account the chemical composition of the oil. Algae oils contain oleic acids with triple unsaturated bonds, while palm oil only has a much lower number of double bonds. Using the process implemented commercially by NesteOil, each diesel molecule formed requires an average of 12.5 moles of hydrogen. Converting this gives rise to a requirement for algae oil of 21 moles of hydrogen per mole of diesel, and thus to energy requirements that are almost 70 % higher than the NesteOil hydrotreating route.

Process steps sand oil	Energy required MJ/ MJ_{Fuel}	Specific CO_2 emissions g_{CO2}/ MJ_{Fuel}	Process steps algae oil	Energy required MJ/ MJ_{Fuel}	Specific CO_2 emissions g_{CO2}/ MJ_{Fuel}
Exploration	0.14 – 0.35	6.3 – 16.1	Algae cultivation	0.86 – 1.1	5.3 – 42.0
Transportation	0.01	0.9	Provision of H_2	0.25	11.3
Refinery	0.08	8.6			
Distribution	0.02	1.0	Distribution	0.02	1.0
Total	0.25 – 0.46	16.8 – 26.6	Total	1.13 – 1.37	17.9 – 54.5

Tab. 22 Evaluation of energy required and specific CO_2 emissions for the production of diesel and kerosene from sand oil and algae oil

Tab. 22 shows the evaluation of the required energy and specific CO_2 emissions for the production of diesel and kerosene from sand oil and algae oil. Ranges are given for the energy required and specific CO_2 emissions of both chains. For the exploitation of oil sand, different processes are possible and measures for reducing CO_2 could potentially decrease the specific emissions. The process of extracting algae oil generally necessitates the use of the energy of the dry mass to dry the algae with no external electricity supply. It should be noted that the combustion of diesel produced from oil sand gives rise to specific emissions of 72.9 g CO_2/ MJ_{Fuel}, which is not allowed for in the case of renewable energy carriers. However, the data in Tab. 22 clearly indicate that both fuels have similar values in terms of specific CO_2 emissions by the time they reach the tank. The efficiency of fuel production in extracting the “crude oil” is much lower for algae oil than for sand oils. While the oil extraction from oil sands has already been implemented industrially, algae oil exploitation on a large industrial scale is still in its infancy.

Process engineering analysis

In special cases, the production process must be analyzed in detail with commercial simulation programs, such as PRO-II (SimSci) or Aspen plus (Aspen Technology Inc.). This is the case, for example, when the necessary technical data on energy consumption and process sequence are not available or are insufficient for a detailed evaluation. Fig. 91 shows a simplified process flow diagram for a specific process using wood as raw material. A product flow of 203.7 kg/h can be produced from a tonne of wood per hour with the emphasis on diesel and kerosene (approx. 154 kg/h). The electricity balance gives a consumption of max. 446 kW_e, which can be reduced using by-products such as steam and by coupling to an existing air separation unit. Therefore, the energy required to produce fuel from 1 t/h wood at 4.15 kWh/kg plus 446 kW_e electricity minus the energy remaining in the product is equal to

0.92 MJ/ MJ_{Fuel}. This value is approximately equal to that of CONCAWE with 1.08 MJ/ MJ_{Fuel} but contains a higher level of detail.

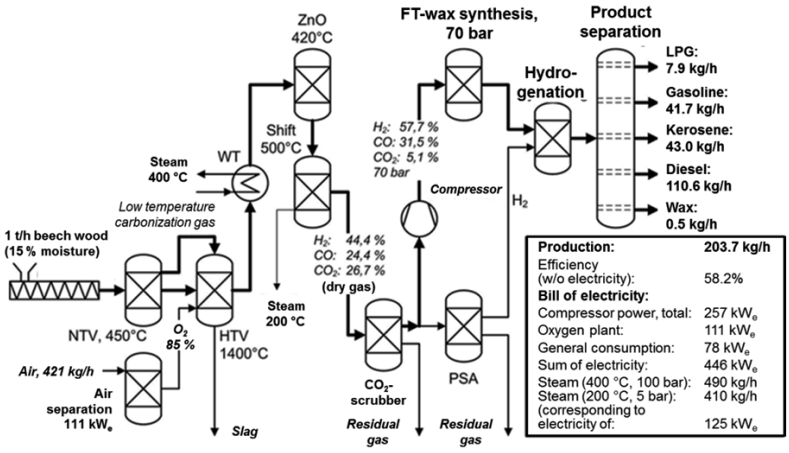

Fig. 91: Simplified process flow diagram with data on gas composition and output for a specific process using wood as raw material

5.1.3.2 Life cycle assessment

A life cycle assessment (LCA) incorporates different criteria for evaluation. These include indicators for climate change, resource depletion, fresh water consumption, over-fertilization in fresh water, in soil and in the sea, soil acidification, photochemical ozone formation, particles, land use, fresh water pollution, and toxins for humans. Presenting the results demands a high transparency in terms of the assumptions made and the data underlying the studies. Although such analyses are not performed at IEK-3, the results of such analyses are critically examined and incorporated into the development of strategies.

5.1.4 Results

5.1.4.1 Well-tank anlaysis

First-generation fuels are already available on the market. Fig. 92 shows the net greenhouse gas emissions in CO_2 equivalent per MJ_{Fuel} and the energy required to produce different types of fuels. The CONCAWE study considers the esterification of plant oils, e.g. from soy beans, sunflower seeds, rapeseed and palm oil, as well as the hydrotreating of such oils as hydrotreated vegetable oils (HVOs). As a reference for first-generation diesel fuels, the value pairs are given for diesel and kerosene. In the case of fossil fuels, the CO_2 released when they are used is included for full combustion processes. For fuels produced on a sustainable basis, the CO_2 arising during combustion originates in the atmosphere and is released back into it. From the energy required to produce fuel, an efficiency of between 43 % and 60 % was calculated, depending on the raw material and process. The specific CO_2 emissions are in the range 15 – 50 g_{CO_2} / MJ_{Fuel} and thus on average half that of the fossil reference chain (graph on the right in Fig. 92). Soy beans as a raw material are energetically very inefficient

and only slightly reduce specific emissions. The graph on the left in Fig. 92 shows the corresponding data for middle distillates produced using the Fischer-Tropsch process. The basis for xTL is coal (x = C), natural gas (x = G) or biomass (x = B). Biomass is defined as woody waste, farmed wood, straw or black liquor, and for other fuel chains waste, materials and manure as well. The gasification of natural gas and coal with the subsequent synthesis of middle distillates has no advantages compared to fossil energy carriers when specific CO_2 emissions are taken into account, even when CO_2 capture is incorporated. Furthermore, the efficiency of GTL fuel production is only 61 % compared to 88 % for fossil diesel. Second-generation biofuels from wood and straw have much lower specific CO_2 emissions with values below 10 g_{CO_2} / MJ_{Fuel}. However, this clear advantage over first-generation biofuels is counteracted by the fact that industrial-scale development is still at a very early stage of maturity and the investment costs required are high. The efficiency of fuel production is 46 – 52 %.

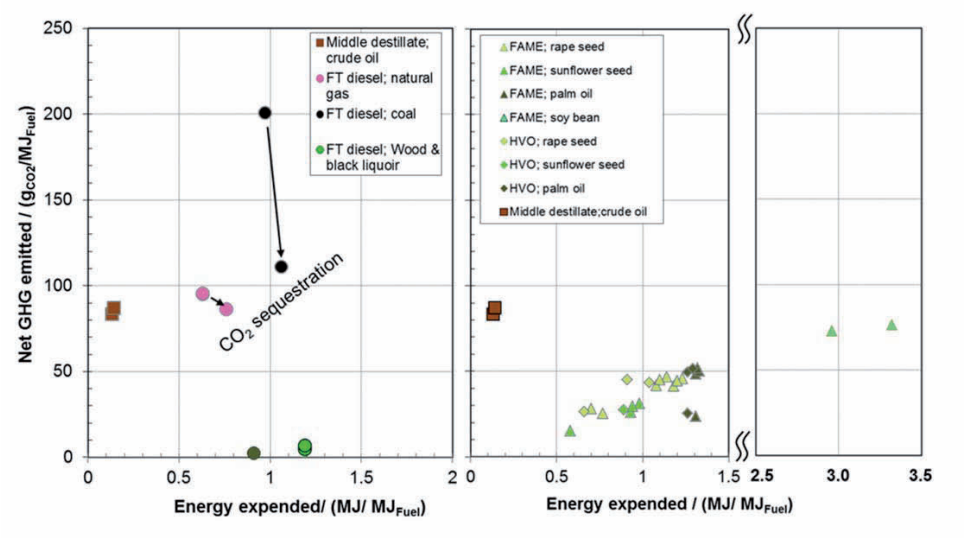

Fig. 92: Net greenhouse gas emissions in CO_2 equivalent per MJ_{Fuel} and energy required to produce different types of fuels. Abbreviations: FT: Fischer-Tropsch; FAME: *fatty acid methyl ester*; HVO: *hydrotreated vegetable oil*; GHG: *greenhouse gas*. Left graph: Fischer-Tropsch processes; right graph: esterification and hydrotreating process for different fuels of the first generation. Data taken from CONCAWE

Fig. 93 shows the net greenhouse gas emissions and the energy required to produce different types of fuels with a focus on different fuel cell applications. For light traction, the environmental importance should be evaluated in relation to the local environment with respect to limited emissions and the manageability of the energy carrier. Commercial batteries that are charged using electricity produced from the EU mix produce approx. 130 g_{CO_2} / MJ_{el}. As the long-term aim is to use only sustainable energy carriers, the basis of the production of gaseous hydrogen and methanol must be changed to biomass or wind power via electrolysis. Wind power is used as the ideal case in the diagram. For this application, the manageability and ultimately the economic efficiency of the energy carrier are decisive. In aeronautic applications, GTL fuel and HVO kerosene are already in use for

flight operation. In ongoing demonstration projects, liquid hydrogen (LH_2) is used to show the functionality of fuel cells in flight operation. BTL kerosene is interesting in the long term.

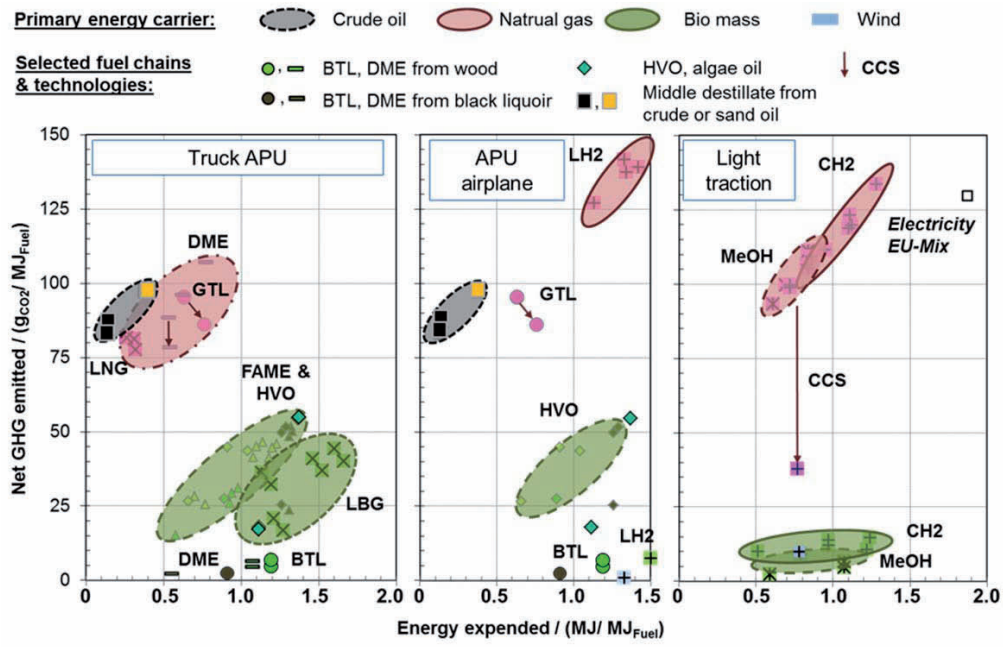

Fig. 93: **Net greenhouse gas emissions in CO_2 equivalent per MJ_{Fuel} and energy required to produce different types of fuels with a focus on fuel cell applications. Abbreviations: GHG: *greenhouse gas;* GTL: *gas-to-liquid*; BTL: *bio-to-liquid*; FAME: *fatty acid methyl ester*; HVO: *hydrotreated vegetable oil*; DME: dimethyl ether; MeOH: methanol; *CH_2*: compressed hydrogen; LH_2: liquid hydrogen; LNG: liquid natural gas; LBG: liquefied biogas; CCS: carbon capture and sequestration**

As shown in Fig. 93, the use of liquid hydrogen produced from natural gas leads to a 50 % increase in specific CO_2 emissions. As a result, liquid hydrogen must be produced from wind energy via electrolysis or from wood gasification. The efficiency of hydrogen production is slightly lower at 40 – 42 % than that of producing BTL kerosene from wood (46 %); however, this is compensated by higher fuel cell efficiencies in hydrogen operation. The ACARE targets for 2020 are as follows: reduce the fuel consumption of airplanes by 50 % before 2020, produce 50 % less carbon dioxide (CO_2) and 80 % less nitrogen oxide (NOx), and halve the perceived noise level. Simply changing to HVO kerosene leads to a 50 % reduction in specific CO_2 emissions. To make the HVO process using algae oil competitive compared to the Fischer-Tropsch process in terms of CO_2, combustion of the algae dry mass must be used to dry the algae.

In addition to Fame and HVO oils, Fischer-Tropsch diesel fuels, liquefied natural gas or DME can also be used to replace diesel fuels. All of these fuels can be produced theoretically from biomass. DME exhibits – particularly when black liquor is used – the best values in terms of energy required and specific CO_2 emissions. For the use of biogases, a combination of

compressed biogas (CBG), which is subsequently fed into the natural gas network, and a liquefaction of the natural gas (LNG) is chosen. This process chain leads to considerably worse characteristics. It is improbable that low-maintenance engines in heavy goods vehicles can be operated with pure biodiesel (Fame) or highly blended mixtures. Hydrotreated vegetable oils are similar to fossil diesel in terms of their production processes, but they can be stored better and do not give rise to unwanted secondary reactions like FAME in diesel.

In conclusion, the analyses showed that lower CO_2 emissions based on renewable primary energy carriers lead to a higher energy expenditure during fuel production of approx. 0.9 – 1.5 MJ/ MJ_{Fuel} compared to 0.1 MJ/ MJ_{Fuel} for fossil energy carriers. Technologies for the use of second-generation biomass are not yet technically mature, which means that specific routes cannot be unequivocally prioritized. In terms of energy and ecology, the use of waste materials, such as waste wood, black liquor, manure or household waste, is advantageous. It should be noted, however, that the technologies pose a particular challenge as the raw materials could be contaminated with toxic substances and the usable quantities are limited.

Furthermore, it should be noted that the production of diesel fuel from sand oils is already industrially mature, and compared to conventional oils, only exhibits a decrease in efficiency of around 7.5 % (absolute) to 72.5 % and to an increase in specific CO_2 emissions of around 12 %. A business-as-usual (BAU) scenario with a long-term changeover to sand oils and heavy crude oils is economically and technically feasible, but it would not reduce CO_2 emissions.

5.1.4.2 Life cycle assessment

Life cycle assessments (LCAs) of the different biofuels evaluate a range of environmental impacts that occur when the plants are cultivated. Two studies are used here for this: EMPA (2012) and ifeu (2006). For illustration purposes, numerical results are shown relative to the biofuel FAME (first generation) from rape oil (see Fig. 94). For comparison, data on diesel from crude oil and sand oil are included in the EMPA study. The results for oil sands show that the more complex production process has negative impacts compared to conventional oils on greenhouse gas emissions, nutrient release, particle formation and the transformation of large areas of land. The impact of residues from oil exploration and production, which are certainly significant, could not be taken into account due to a lack of data. Water consumption was particularly pronounced with a factor of 200 compared to the use of rape.

The cultivation of jatropha on barren, partially erosive land that was not previously used for agricultural purposes contributes to land recovery. To produce sufficient oil yields, however, adequate irrigation and fertilization is essential. The impacts of palm oil extraction are similar in certain respects such as water consumption, photochemical ozone formation and ozone depletion. The impacts on soil over-fertilization and acidification are the same as for FAME, but smaller than for jatropha. The evaluation criteria of resource consumption and greenhouse gas emissions are generally negative.

The ifeu study shows that the use of cereal (triticale) and wood has advantages over the use of FAME in terms of energy required, greenhouse gas emissions (here versus climate change), acidification, over-fertilization and ozone depletion. The use of waste materials is particularly advantageous, although the resources are limited – as also shown in our own analysis on the use of wood. According to the EMPA study, wood and energy grasses are

preferable. As EMPA prefers gasification into methane and gaseous use, the corresponding chains are not shown in Fig. 94.

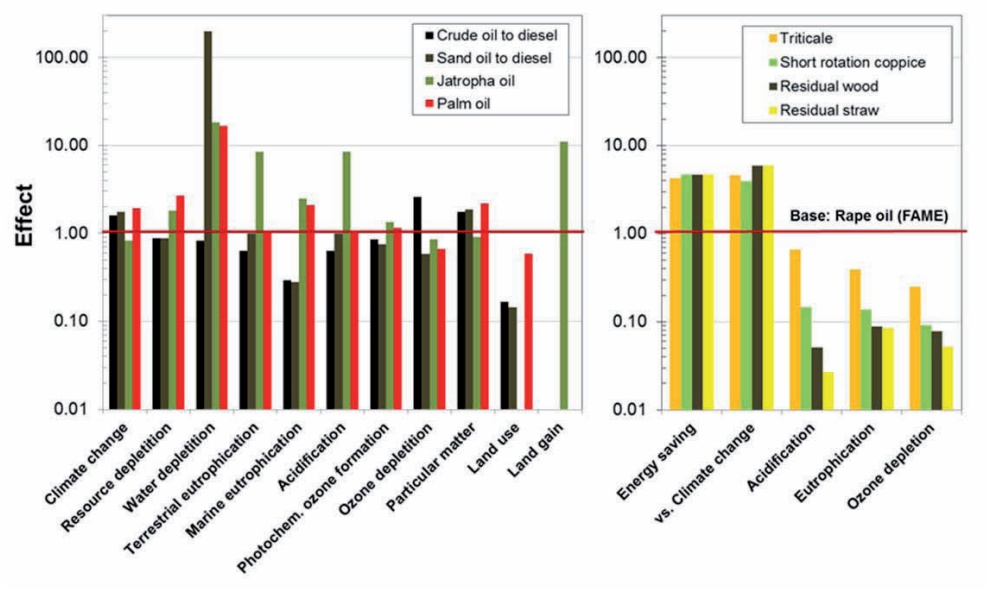

Fig. 94: Normalized representation of two studies evaluating biofuels by means of life cycle assessments, each using FAME from rape oil as the reference substance (effect = 1). Left graph: EMPA study (2012); right graph: ifeu study (2006). Triticale is a hybrid of wheat and rye

5.1.4.3 Focus on biodiesel

Over the last few years, the focus within biofuels has shifted to algae as a producer of vegetable oils, hydrogen and ethanol. Fig. 95 shows the yields of different biofuels in liters per hectare. BTL was converted into FAME in relation to the higher energy density. Accordingly, the yield per unit area is higher than that of rape oil by a factor of 400 – 500. For palm oil, this value was approx. 6000 liters per ha and for BTL (FAME eq.) approx. 2000 – 3000 liters per ha. In addition to the yields per unit area, production costs for different fuel chains are also of interest. For BTL, the costs range from 60 ct/l to 1.5 €/l. A comparative study calculated fuel costs for algae products of between 2.1 €/l to 2.6 €/l. The costs of producing FAME range from 0.35 – 0.75 ct/l, whereby the volumetric energy content is 10 % lower than that of commercial diesel. Furthermore, it should be noted that the cost of extracting crude oil from sand oils varies depending on the process used between 0.15 ct/l and 0.3 ct/l. These costs must be added to the production costs of a fossil fuel of 40 – 50 ct/l, minus the amount for conventional crude oil extraction. From an economic point of view, retaining fossil sources is very attractive, but from an ecological perspective, it is extremely negative. First-generation fuels, such as FAME from rape oil, have justifiable additional costs, but they are also associated with disadvantages in that they compete directly with food. A unilateral preference for algae oils over BTL is therefore not justifiable in terms of potential cost.

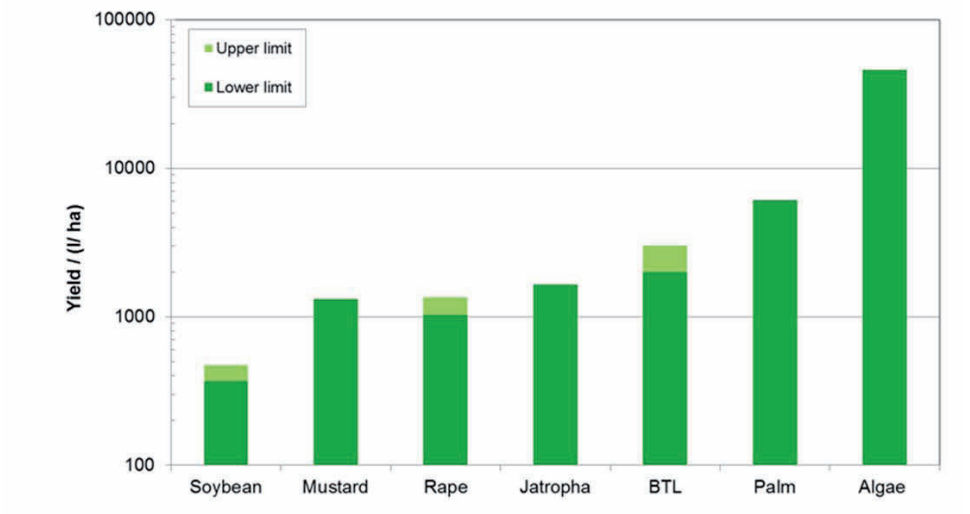

Fig. 95: Yields of different biofuels in l/ha. BTL was converted into FAME in relation to the higher energy density

5.1.4.4 Focus on methanol

For the production of biomethanol, chemical technologies, such as the synthesis gasification of wood and straw with subsequent methanol synthesis, are preferable to biological processes, for example, wood fermentation using bacteria. A possible production pathway is straw gasification, which is being developed at KIT in Karlsruhe and which produces a sludge-like suspension comprising an oily liquid and a solid residue. This can be gasified in a special Lurgi gasifier and then fed into methanol synthesis after suitable gas conditioning.

The gasification of glycerin from biodiesel production and subsequent methanol synthesis improves the ecobalance of biodiesel (FAME) production via esterification. All of the methanol used for this can be taken from glycerin gasification. Using this biomethanol in another way involves replacing it with methanol from fossil natural gas for the esterification stage.

In addition, methanol can be produced using renewably generated hydrogen and CO_2. This process is described, for example, in Olah et al. 2006 “Beyond Oil and Gas: The Methanol Economy” p. 239. A company in Iceland produces methanol by means of this process, whereby the CO_2 used is a by-product of the geothermal provision of electrical energy.

Another priority involves investigations on the applicability of methanol produced in this manner. It should be noted that methanol from renewable sources does not always meet the purity requirements of conventionally produced methanol. Comprehensive analyses are being conducted to evaluate the composition of biomethanol. Its general suitability for use is also being tested in cells and stacks, and results will provide additional information on long-term stability when biomethanol is used.

5.2 Development objective large-scale PEM electrolysis system

Energy technology is currently undergoing a considerable transformation worldwide. The generally accepted factors driving this transition are climate change, supply security, industrial competitiveness and local emissions. With its 2010 energy concept, the German federal government has set course for an environmentally friendly, reliable and affordable energy supply, in which renewable energies will account for the biggest share in the energy mix of the future – a move that will lead to a rapid rise in the share of intermittent wind and solar energy in the power supply system. The storage of large quantities of energy will then become indispensable. Chemical storage such as in the form of hydrogen, which can be produced from renewably generated electricity using electrolysis, is a promising alternative. As shown in Fig. 96 potential markets for hydrogen produced from renewably generated electricity using electrolysis comprise transport, reconversion into electric power for the grid, methanation, and direct feed-in into the natural gas grid, as well as use in industrial processes.

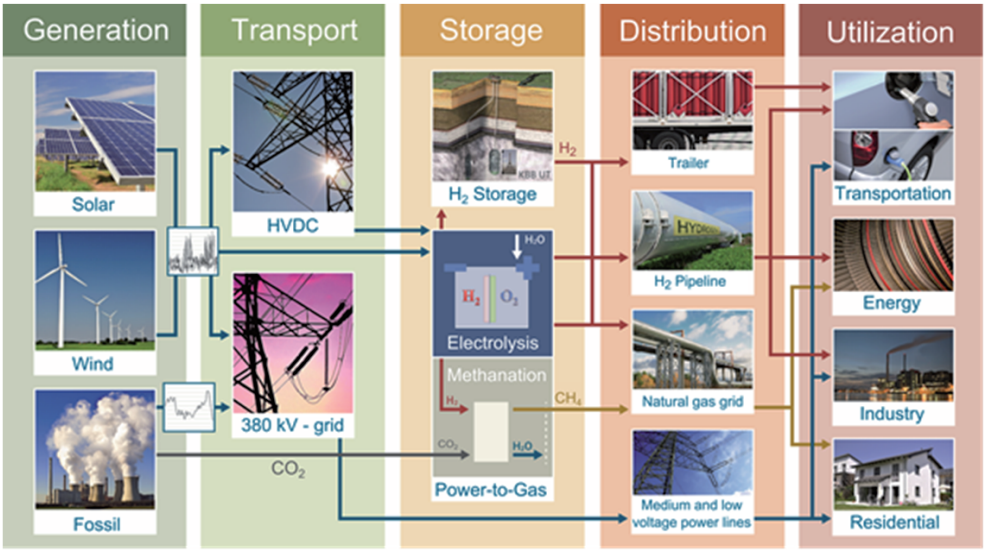

Fig. 96: Hydrogen as a storage medium for renewable energies

The production of hydrogen and oxygen from water using water electrolysis is a technological process that has been well established throughout the world for 100 years and more. However, electrolysis is currently used to produce only 4 % of hydrogen worldwide. One of the main reasons for this is the higher cost of producing electrolytic hydrogen compared to producing hydrogen from fossil primary energy sources, such as natural gas (77 %) and coal (18 %) [43].

The decomposition of water by electrolysis involves two partial reactions separated by an ion-conducting electrolyte. The three relevant processes of water electrolysis are

[43] Wöhrle, D.: Wasserstoff als Energieträger – Eine Replik. Nachrichten aus Chemie, Technik und Laboratorium, 39 (1991), pp. 1256-1266

distinguished by the electrolyte used, and are shown in Fig. 97 together with their partial reactions for the hydrogen evolution reaction (HER) and the oxygen evolution reaction (OER), the typical temperature ranges, and the ions for the related charge transport:

- alkaline electrolysis with a liquid alkaline electrolyte,
- acidic PEM electrolysis with a proton-conducting polymeric solid electrolyte, and
- high-temperature electrolysis with a solid-oxide electrolyte.

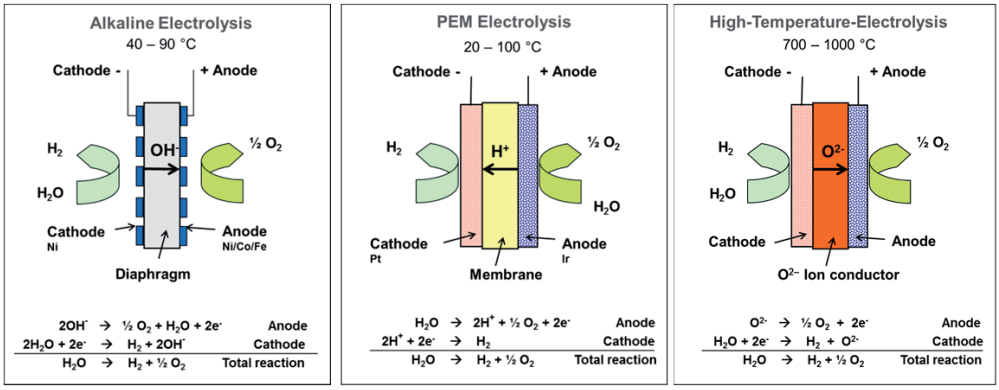

Fig. 97: Operating principles of the different types of water electrolysis

Water is usually added on the cathode side of alkaline electrolysis and on the anode side for PEM electrolysis. In the case of high-temperature electrolysis, the required steam is supplied at the cathode.

At the moment, commercial electrolyzers are only available for alkaline electrolysis and PEM electrolysis. In the case of alkaline electrolysis, they have been produced commercially for several decades in a variety of power classes up to approx. 750 Nm³/h, whereas product development in PEM electrolysis only began twenty years ago and there are few commercial products (< 65 Nm³/h) on the market. High-temperature electrolysis is not currently being pursued by industry, which means that no commercial products are yet available.

Both of the commercially available electrolysis technologies have advantages and disadvantages leading to the challenges associated with each technology (s. Tab. 23):

- For example, alkaline water electrolysis does not require a catalyst made of platinum group metals, whereas PEM electrolysis does. However, this also means that current densities are five times lower for alkaline water electrolysis.
- The use of polymer membranes makes the gas qualities and partial load toleration of PEM electrolyzers more suitable than alkaline electrolyzers for intermittent operation with strongly fluctuating outputs.

Alkaline water electrolysis	PEM-electrolysis
Advantages - well-established technology - no noble metal catalysts - high long-term stability - relatively low costs - modules up to 760 Nm³/h (3.4 MW) **Challenges** - increase current densities - expand the partial load range - system size and complexity (footprint) - reduction of gas purification efforts - total material required (stacks currently on a scale of several tonnes)	**Advantages** - higher power density - higher efficiency - simple system configuration - good partial load toleration - ability to accommodate extreme overloads (depending on system size) - extremely rapid system response for grid stabilization - compact stack design permits high-pressure operation **Challenges** - increase long-term stability - scale-up of stack and peripherals to the MW range - cost reduction by reducing or replacing noble metal catalysts and cost-intensive components (current collectors/separator plates)

Tab. 23: Comparison of alkaline and PEM water electrolysis

Fig. 98 compares the typical current-voltage characteristics for alkaline and PEM electrolysis and shows typical operating ranges. The demands made on the electrolyzers vary depending

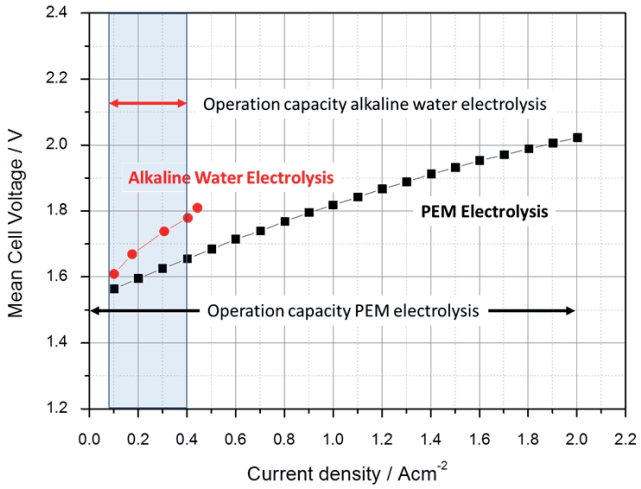

Fig. 98: Typical current-voltage characteristics and operating ranges for alkaline and PEM electrolysis [takem from 44]

[44] Mergel, J., Carmo, M., Fritz, D.L.: Status on Technologies for Hydrogen Production by Water Electrolysis. in Transition to Renewable Energy Systems (Stolten), Wiley-VCH Verlag GmbH & Co. KGaA (2013, in press)

on the integration of wind-hydrogen systems in the grid. Intermittent energy from renewables is a key process engineering challenge for each of the electrolysis technologies. A specific problem is the partial load behaviour, in particular in alkaline electrolyzers due to increasing gas impurities. For instance, the lower partial load range of alkaline electrolyzers is only 20 – 40 % of nominal load because contaminating gases, in particular H_2 in O_2, quickly reach a critical concentration of 2 %, for example, which requires the system to be switched off for safety reasons. As can be seen in Fig. 98, this problem does not occur for PEM electrolysis as the use of polymer membranes facilitates a larger partial load range (5 – 100 %) than for alkaline electrolysis, which is a significant advantage for coupling to renewable energies.

In contrast to alkaline electrolysis, PEM electrolysis can accommodate extreme overloads when the cells have sufficient capacity, which is particularly advantageous for using an electrolyzer as an operating reserve to stabilize the grid fed by highly intermittent renewables. Although a certain amount of efficiency is lost in the overload regime (Fig. 99), the investment costs decrease per kW of installed capacity. In a study on optimizing the technology and reducing the costs of electrolyzers performed in cooperation with a consulting company established in this field, the impact of factors such as electricity costs, operating costs, control, and investment costs on hydrogen production costs was investigated for different electrolysis technologies. Depending on different scenarios, an installed electrolysis capacity of 64 – 84 GW was forecast for Germany in 2030.

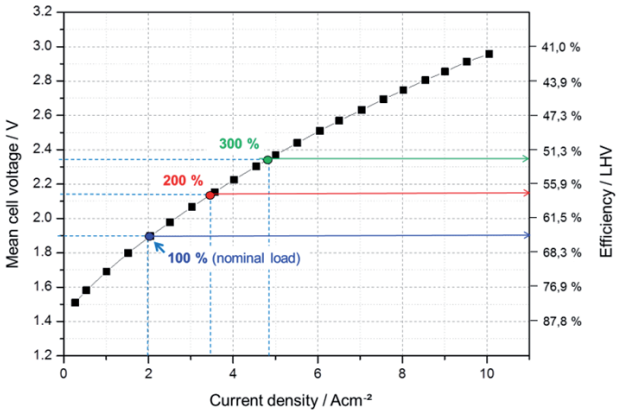

Fig. 99: Current-voltage characteristics and efficiency of optimized PEM electrolysis with the option of operating at overload [44]

Fig. 100 shows the investment costs in €/kW for different electrolyzers in the MW range for 2015, and the predicted costs in 2030 for the two technologies, where PEM electrolysis can be operated with 2.5 or 3 times the overload. The investment costs include on-site installation and containers. The investment costs for alkaline electrolysis in 2030 are similar to those for PEM electrolysis but PEM electrolysis can be operated with three times the overload. In other words, the costs per kW of installed capacity drop by a factor of three – or for an assumed electrolysis capacity of 84 GW in 2030, only 28 MW nominal power of PEM electrolysis must be installed (Fig. 100, right). With respect to the costs, however, this

requires the catalyst loading to be reduced by a factor of ten while maintaining the same efficiency for PEM electrolysis.

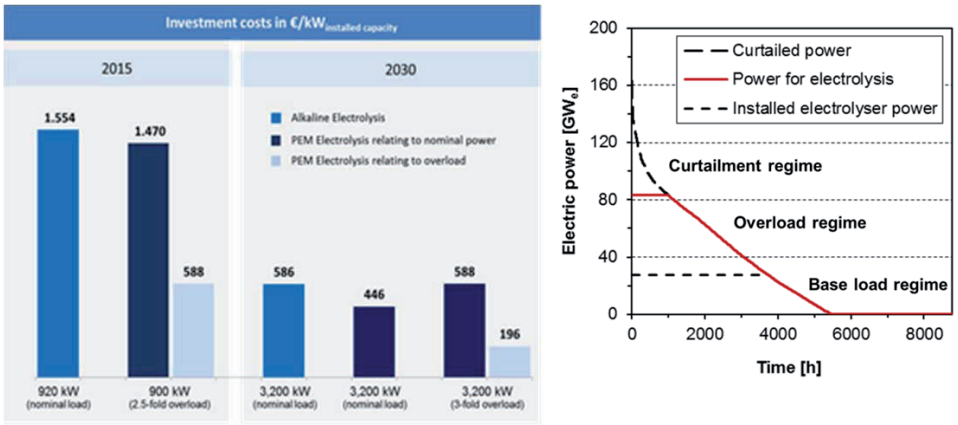

Fig. 100: Investment costs for electrolyzers and installed electrolysis capacity

In today's commercial PEM electrolyzers, the anode comprises around 6 mg/cm² iridium, and the cathode contains around 1 – 2 mg/cm² platinum as a catalyst. Catalyst development activities for PEM electrolysis therefore concentrate on reducing or completely replacing noble metals in the membrane electrode assemblies while retaining comparable performance. If water electrolysis technology, and indeed PEM electrolysis, are to be widely and sustainably used on the mass market for the storage of renewable energies after 2020, further steps must be taken to solve outstanding technical issues, such as improving low power densities and the inadequate stability, as well as reducing the high costs associated with the technologies currently in use. In the short and medium term, alkaline water electrolysis as a technology that is already quite mature today should be able to cover the increasing demand for electrolytic hydrogen, although there is still a need for development and optimization in terms of expanding the partial load range and the ability to deal with overload. In the long term, PEM electrolysis may play a greater role, as its advantages over alkaline electrolysis will make it interesting for larger applications with systems > 1 MW. However, the electrode and cell areas will first have to be scaled up to more than 1000 cm².

Development work on large-scale PEM electrolysis systems therefore concentrates on cutting costs, increasing long-term stability in highly dynamic operation, and expanding system size to the MW range. These activities are supported by two collaborative projects on PEM electrolysis within a joint energy storage systems funding initiative involving BMWi, BMBF and BMU.

5.2.1 EKOLYSER project

The EKOLYSER project (new cost-effective and sustainable materials for PEM electrolysis for the production of hydrogen from renewable energies) is one of the flagship projects aiming to couple wind and hydrogen and is coordinated by IEK-3. In cooperation with the Max Planck Institute for Chemical Energy Conversion and the industrial partners FuMA-Tech, SolviCore and Gräbener Maschinentechnik, cost-effective and sustainable materials are being developed for PEM electrolysis for the production of hydrogen from renewable energies with the aim of launching PEM electrolysis technology on the mass market after 2020.

The collaborative project, which is being funded by BMWi, is divided into three subareas, all of which involve specific scientific and technological challenges:

- lowering of costs by decreasing catalyst loading and/or replacing noble metal catalysts
- membranes with a higher conductivity and mechanical and chemical stability
- use of cost-effective and corrosion-resistant bipolar plates and current collectors

The project aims to develop membranes, MEAs and a short stack with the potential to reduce the costs of future PEM electrolyzers by using cost-effective materials while maintaining comparable performance characteristics and long-term stability. By the end of the project, near-market products are expected to be available, which will then be used to demonstrate the technical and economic potential of PEM electrolysis for use on the energy storage mass markets.

5.2.2 MAPEL project

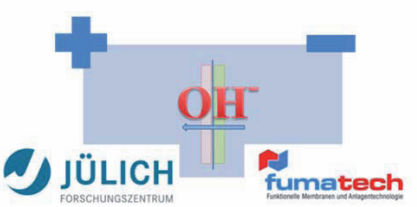

Various activities have already been announced and/or initiated by different companies aiming towards the application of electrolysis technology to store electricity from renewable sources. Systems for the different electrolysis techniques are implemented based on material and catalyst technologies that are available available. Another approach involves targeted research and development efforts, which aim to improve alkaline electrolysis and PEM electrolysis for flexible hydrogen production with rapid and frequent load changes for application in the area of renewable energy generation.

The BMBF-funded MAPEL project (membrane electrode assemblies for alkaline PEM electrolysis for the production of hydrogen from renewable energies) aims to combine the advantages of alkaline and PEM electrolysis using anion exchange membranes.

In close cooperation with FuMA-Tech GmbH, who boast extensive experience in membrane fabrication and membrane process engineering with a particular focus on anion exchange membranes, novel efficient membrane electrode assemblies (MEAs) are being developed for

alkaline PEM electrolysis. The main challenges here are improving the chemical stability of existing membranes at higher temperatures, increasing the conductivity, and integrating the ionomer into the catalyst layers so that the alkali ions will no longer be needed in the electrolysis cycle. Another approach aims to develop membranes that are stable in alkaline solutions, which will then be used to improve their partial load toleration in conventional alkaline electrolysis and to increase the current densities.

5.3 Utilization of CO_2 from flue gases for chemical processes

German anthropogenic CO_2 emissions in 2011 totaled approximately 804 million tonnes. According to the Kyoto Protocol (1997), Germany is obliged to reduce its greenhouse gas emissions by 40 % compared to levels in 1990. The German federal government has set targets for cutting emissions by as much as at least 80 % by 2050. These targets can be achieved by avoiding emissions using more efficient technologies and modernizing buildings as well as by expanding renewable energies, such as wind power, solar energy and hydropower [45]. However, to safeguard the energy supply, fossil power plant processes cannot be completely eliminated everywhere in the medium term. In addition, non-energy industrial processes also emit CO_2. Carbon capture technologies are therefore being researched and developed. However, the underground storage of the resulting carbon dioxide is a topic of controversy in Germany, and is currently legally limited to 4 million tonnes per annum [46]. A general disadvantage of storage is that it requires large amounts of energy, as the CO_2 must be compressed to a pressure of at least 80 bar and then transported to the reservoirs.

As an alternative to storage, CO_2 can be used as a C1 building block in the chemical industry. The fact that it can be utilized makes the waste product more valuable and the energy expenditure and costs associated with storage become irrelevant. Today, approx. 132 million tonnes of CO_2 per annum, which is equal to 16.4 % of German emissions, are used as a raw material to produce urea, methanol, salicylic acid, inorganic and organic carbonates and polycarbonates (Tab. 24).

Substance	Produced using CO_2 million t/annum	CO_2 mass fraction %	CO_2 bound in products million t/annum	Year
UREA	146	0.73	107	2008 [47]
Methanol	6	0.44	2.6	2007 [48]
Salicylic acid	0.17	0.32	0.05	2011 [49]
Inorganic carbonates	45	0.49	22,5	2008 [47]
Organic carbonates	0.1	≈ 0.49	≈ 0.05	2009 [47]
Polycarbonates	< 0.01	≈ 0.43	≈ < 0.004	2011 [47]
Total			**≈ 132**	

Tab. 24: Utilization of CO_2 as a raw material today

Carbon dioxide is an unreactive compound with a standard formation enthalpy of $\Delta H°_{(298K)}$ = -393.51 kJ mol^{-1}. The molecule has no dipole moment due to its linear geometry, but polar C = O bonds mean that the carbon atom is an electrophilic center and the oxygen

---

[45] Energy Concept for an Environmentally Sound, Reliable and Affordable Energy Supply, 28. September 2010, http://www.bmwi.de (Dezember 18, 2012)

[46] Carbon dioxide storage act (Kohlendioxid-Speicherungsgesetz – KSpG), 17 August 2012

[47] Kember, M.R., A. Buchard, and C.K. Williams: Catalysts for CO_2/epoxide copolymerisation. Chem. Commun., 47 (2011), p. 41-163

[48] Aresta, M.; Dibenedetto, A.: Utilisation of CO_2 as chemical feedstock: opportunities and challenges. Dalton Trans., 28 (2007), p. 2975-2992

[49] Carus, M.: An overview on conventional and innovative use of carbon dioxide and economical aspects for new options for CO_2 utilization. in CO_2 as chemical feedstock - a challenge for sustainable chemistry 2012. Haus der Technik, Essen

atoms are nucleophilic centers. It is therefore possible to convert the CO_2 molecule using catalysts (usually transition metal complexes) with reactive reaction partners. A reaction involving a catalyst reduces the activation energy and increases selectivity and yield. The conversion of carbon dioxide into more valuable products can be performed chemically, electrochemically, biochemically or photochemically (Fig. 101). Depending on the nature of the conversion process, the energy required is supplied thermally, electrically, chemically or by light. In addition to the preparation of material products, the conversion of CO_2, for example into methane, can also be used as an energy storage solution for renewable energies (power-to-gas). Future work at the institute will initially focus on the chemical conversion of CO_2 into valuable material products.

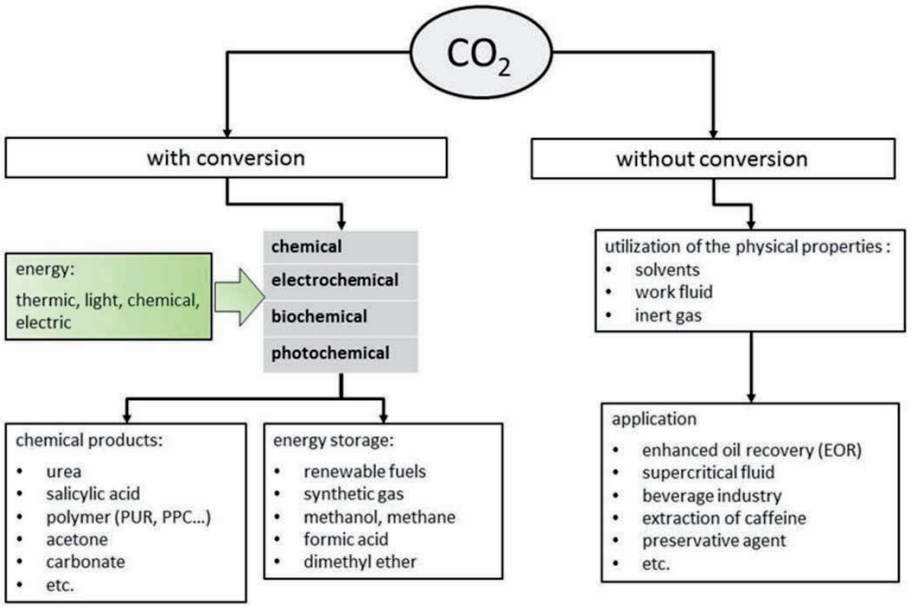

Fig. 101: Possible CO_2 utilization routes: conversion or direct use

5.3.1 Conversion of CO_2 into more valuable products

The literature lists numerous reactions in which CO_2 is used as the educt. These include reactions where carbon dioxide is hydrogenated directly with hydrogen and products such as methanol, formic acid or methane result. These reactions are exothermic. However, providing hydrogen is connected with an enormous energy expenditure. Reactions with what are known as H-active molecules are also described. These include compounds with α-acid hydrogen atoms (e.g. acetone), compounds with hydrogen atoms directly at triple carbon bonds and aromatic substances with hydrogen atoms in an ortho or para position to form functional groups. Furthermore, CO_2 can react with different hydrocarbons (e.g. alkanes, alkenes, alkines, etc.), strained cyclic hydrocarbons (cyclopropanes), heterocycles (epoxides) and with sulfurous compounds such as ammonia or amines (Tab. 25).

Reaction partner	Product classes	Examples
H_2	Acids, esters, ketones, aldehydes, higher saturated and unsaturated hydrocarbons	Formic acid, methane, methanol, formaldehyde, dimethyl ether, oxalic acid, etc.
H-active inorganic compounds	Carboxylic acids	p- and o-hydroxybenzoic acids, phenylpropiolic acid, acrylic acid, etc.
Alkanes	Aldehydes, ketones, carboxylic acids	Acetaldehyde, acetic acid, acetone, etc.
Alkenes	Acids, esters, alcohols, epoxides	Propanol, ethylene oxide, acrylic acid, etc.
Alkines	Pyrones, lactones	3,4,5,6-tetraethyl-2H-pyran-2-one, etc.
Allenes	Lactones, esters	3,4,5,6-tetramethyl-2H-pyran-2-one
Dienes	Lactones, acids, esters	Hex-3-ene dicarbonic acid
Epoxides	Cyclic carbonates	Ethylene carbonate, propylene carbonate
Cyclopropanes	Lactones	4,5,5-trimethylfuran-2(5H)-one
Ammonia and amines	Urea/urea derivatives, carbamates, amino acids, carbamide acids, cyclic carbamates, alkanolamines	Urea, 1,3 dicyclohexylurea, 2-aminopropanoic acids

Tab. 25: Reaction partners and the resulting product classes as well as examples [50,51,52,53,54]

Some of the reactions with CO_2 lead to products that re-release the previously bound carbon dioxide after they have served their purpose. Some of these primary products can be converted in secondary reactions to substances with longer CO_2 fixation times. Urea and formaldehyde can react to form urea-formaldehyde resins (UF resins) [52], which can be used for example as adhesives in the manufacturing of wood products. The fabrication of certain polymers is made possible by a reaction between CO_2 and epoxides. CO_2 reacts with ethylene oxide or propylene oxide when cobalt- or chromium-selenium complexes are used as the catalyst under alternating copolymerization to form polyethylene carbonates (PECs) or polypropylene carbonates (PPCs). These polymers are used as pore-forming agents in the ceramics industry as well as bioregenerative plastics. When double metal cyanide catalysts (DMC catalysts) are used, polyether polycarbonate polyols are created in which both carbonate units and ether units are formed. This polyol is the starting material for polyurethane foams, which are used for example as insulating material and cushioning material (Fig. 102).

---

[50] Aresta, M.: Carbon Dioxide as Chemical Feedstock, M. Aresta, Editor 2010, WILEY-VCH: Weinheim

[51] Inoue, S.; Yamazaki, N.: Organic and Bio-organic Chemistry of Carbon Dioxide1982, Japan: KODANSHA SCIENTIFIC BOOKS

[52] Kuckshinrichs, W., et al.: Weltweite Innovationen bei der Entwicklung von CCS-Technologien und Möglichkeiten der Nutzung und des Recyclings von CO_2. Schriften des Forschungszentrums Jülich Reihe Energie & Umwelt, 2010,Band 60

[53] Peters, M.; Köhler, B.; Kuckshinrichs, W.: Chemical Technologies for Expoiting and Recycling Carbon Dioxide into Value Chain. ChemSusChem, 4 (2011), p. 1216-1240

[54] Xiadoing, X.; Moulijn, J.A.: Mitigation of CO_2 vy Chemical Conversion: Plausible Chemical Reactions and Promising Products. Energy & Fuels, 10 (1996), 305-325

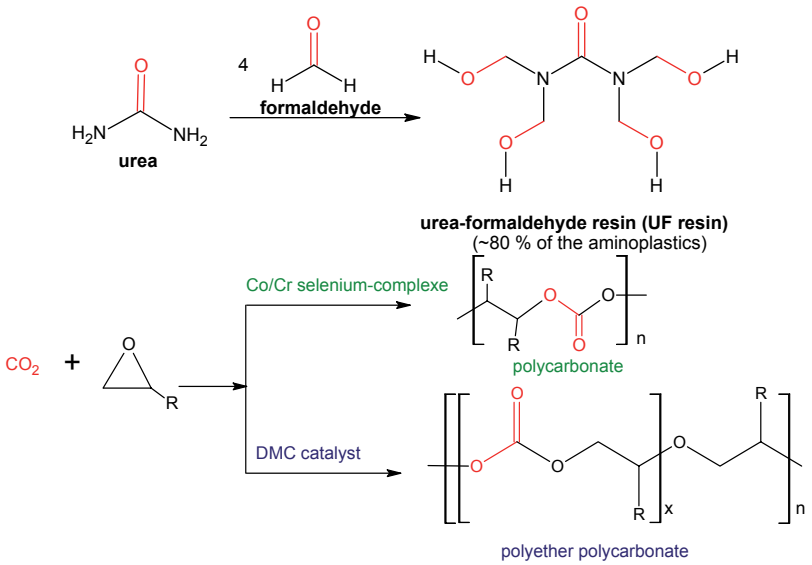

Fig. 102: Chemical structural formula of exemplary reaction products

5.3.2 Appraisal of possible reactions

A PhD thesis currently in progress aims to identify reactions and processes that could put CO_2 to good use as an alternative to storage. Products with a high value and high market volume are particularly interesting. The processes should be economically and energetically competitive compared to conventional methods and they should lead to the avoidance of CO_2. The potential integration of processes into CO_2 emission sources should also be considered and assessed. Secondary advantages are also of particular interest, for example those that could arise out of the use of CO_2 as a raw material, such as the avoidance of reactants, intermediate products and by-products which are toxic and harmful to the environment. This can considerably improve the economic efficiency of a process as costs for disposal and processing are avoided. One example is the fabrication of dimethyl carbonate (DMC), which is an important starting material for polymers. Since 1970, DMC has been manufactured using a reaction between phosgene and methanol. The main disadvantage of this reaction is the toxicity of phosgene and the associated restrictions on transporting and storing it. In addition, chlorinated waste is produced by the reaction. A phosgene-free synthesis of dimethyl carbonate is possible using methanol and urea, whereby both educts are accessible via CO_2. Alternatively, the direct conversion of CO_2 with methanol leads to DMC.

5.3.3 Methods

Using energy and CO_2 balances, conventional processes can be compared and evaluated in relation to CO_2 routes. If required, process simulation can be used to support the evaluation. The institute's long-standing experience in the areas of power plant and process simulation is indispensable for this work.

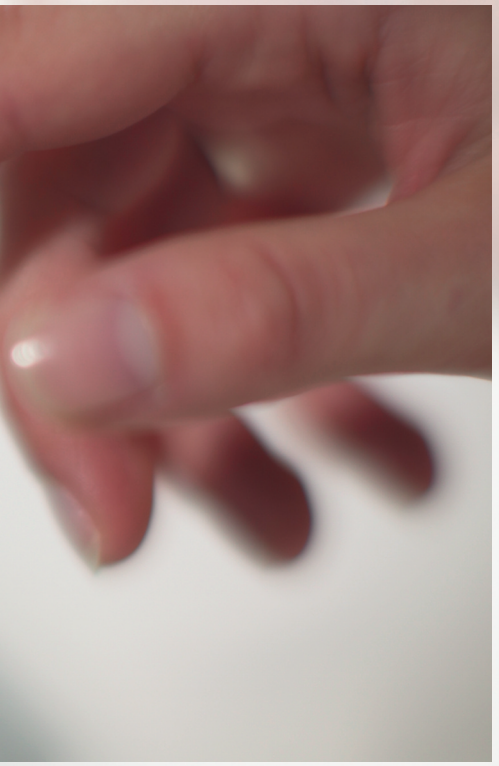

6

Data

Data, Facts and Figures

- The Institute of Energy and Climate Research – Electrochemical Process Engineering (IEK-3)
- Overview of department expertise
- Publications, technology transfer and resources
- Committee work
- Contributions to trade fairs and exhibitions
- How to reach us
- List of abbreviations

6.1 The Institute of Energy and Climate Research – Electrochemical Process Engineering (IEK-3)

In response to the new orientation in research, energy and climate policy as part of the transformation of the energy sector, the Institute of Energy and Climate Research (IEK-3), which had previously focused on fuel cells, expanded its R&D priorities to include hydrogen technologies and batteries. The element linking these three fields of R&D is electrochemical process engineering as a proven core competency of IEK-3. As a consequence of this thematic expansion, IEK-3 was renamed “Electrochemical Process Engineering” in the middle of 2012. The R&D topics were adjusted accordingly, leading to the implementation of five R&D priorities. The ceramic high-temperature fuel cell (SOFC), the direct methanol fuel cell (DMFC), the high-temperature polymer electrolyte fuel (HT-PEFC), the reforming and desulfurization of liquid energy carriers to provide fuel cells with hydrogen, and polymer electrolyte membrane electrolysis (PEM-EL) are now part of IEK-3’s R&D portfolio, as shown in Fig. 103 in combination with the respective areas of expertise.

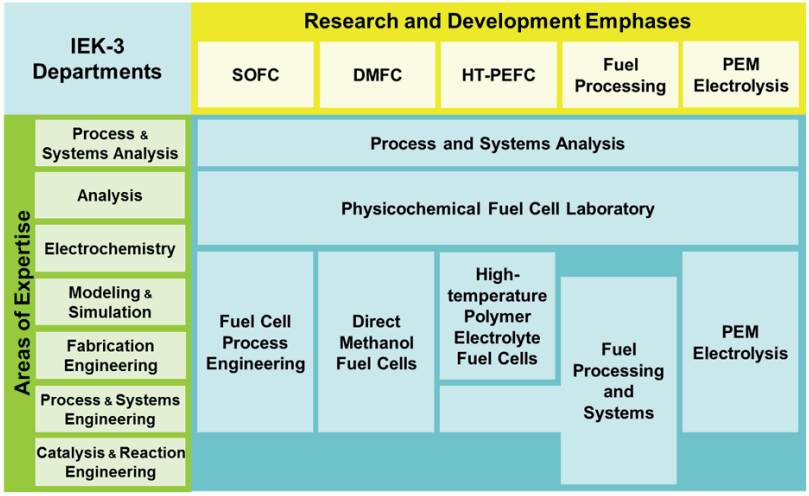

Fig. 103: Departments, areas of expertise and R&D priorities

Concentrating on five different technologies and simultaneously focusing on concrete fields of application makes it possible to address these R&D priorities with teams of supercritical size, beginning with the basic phenomena and extending to process engineering for the whole system. In these endeavors, synergies are unlocked between the specialized disciplines and all stages of research are implemented ranging from theory up to the pilot-plant stage. The applicability of stationary, portable and mobile applications up to and including complete systems with fuel cells, along with their cost aspects, are evaluated by process and systems analysis. They are also compared to competing systems from a technical, energetic and economic perspective. A new area is the evaluation of pioneering energy supply concepts with respect to their potential for reducing CO_2 and their investment costs. Furthermore, application-oriented R&D activities are accompanied by basic research aiming to clarify structure-activity relationships using selected advanced analysis methods.

IEK-3 aims to conduct research that is socially, ecologically and economically relevant and thus generate ground-breaking results on an international level. This quality of work is achieved by closely coordinating basic research with technical development work. International cooperations with partners from research and industry are particularly important in this respect. The institute focuses on transforming research results into innovative products, procedures and processes. Collaboration with universities, universities of applied sciences, training departments and training centers is designed to promote opportunities for further education and training.

Institute of Energy and Climate Research
IEK-3: Electrochemical Process Engineering
Forschungszentrum Jülich GmbH
52425 Jülich
Germany

With around 160 employees, Jülich has the largest institutional fuel cell research team in Europe. Of these, around half work on the SOFC, and approx. one-third of these are involved in IEK-3 activities. Another three institutes also work in the field of SOFCs: IEK-1 is responsible for manufacturing materials, IEK-2 tests the materials and conducts steel research, and IEK-9 focuses on the electrochemical principles. The Central Institute of Engineering and Technology (ZEA-1) is responsible for stack construction. The other 95 or so of the 110 employees at IEK-3 work on advancing low-temperature fuel cells and PEM electrolysis. A coordinator is responsible for the fields of work at IEK-3, and is also available to answer questions on generic topics investigated at the institute.

Head of Institute

Prof. Dr.-Ing. Detlef Stolten
Tel.: +49 2461 61-3076
Email: d.stolten@fz-juelich.de

Deputy head of institute and scientific coordinator

Dr.-Ing. Bernd Emonts
Tel.:+49 2461 61-3525
Email: b.emonts@fz-juelich.de

6.2 Overview of department expertise

Direct Methanol Fuel Cells

High-Temperature Polymer Electrolyte Fuel Cells

Fields of work, range of services

Work on direct methanol fuel cells ranges from membrane electrode assemblies to stacks within the department, and extends to systems in close cooperation with process engineering. New materials for membranes and catalysts are characterized, facilitating the development and fabrication of innovative membrane electrode assemblies. The structure-activity relationship of the electrode layers is a priority. Stack modeling and design together with new analytical techniques in stack technology, as well as automated fabrication methods on a pilot-plant scale, guarantee the bridging function between science and technology.

Work on the HT-PEFC ranges from the electrode to the stack and is conducted in cooperation with partners. New electrode structures and preparation methods are developed, MEAs are fabricated and electrochemically characterized. Moreover, intensive studies are conducted on structure-activity relationships in the electrode layers. This work is accompanied by modeling in order to obtain an in-depth understanding of the processes. In addition, simulation activities are pursued on a cell and stack level. This supports the development of air-cooled and liquid-cooled stacks with high volume-specific and weight-related power densities.

Facilities, processes, methods

Equipment

- Test stands for electrochemical investigations of DMFCs, PEFCs and stacks
- Apparatus for magnetotomographic investigations of current density distribution in single cells and stacks
- Apparatus for characterizing membranes for PEFCs and DMFCs
- Desk coater for the continuous fabrication of MEA components
- Robot facilities for the automated fabrication of cell components (stamping and pressing) and stacks (assembling)

Equipment

- Test stands for the electrochemical characterization of MEAs
- Test stands for electrochemical studies on stacks up to 5 kW_{el}
- Equipment for the fabrication of gas diffusion electrodes

Models

- Simulation models to describe mass, charge and heat transport processes in cells and stacks

---

Contacts

Dr.-Ing. Martin Müller
Tel.: +49 2461 61-1859
Email: mar.mueller@fz-juelich.de

PD Dr. rer. nat. Werner Lehnert
Tel.: +49 2461 61-3915
Email: w.lehnert@fz-juelich.de

Polymer Electrolyte Membrane Electrolysis

Fuel Processing Systems

Fields of work, range of services

Advanced PEM electrolyzers facilitate the economic production of H_2 from surplus electricity from renewable sources. With support from project partners in research and industry, development work concentrates on reducing and even completely replacing the platinum group metals required for catalytic reactions in membrane electrode assemblies (MEAs) while retaining comparable performance. New types of membranes should lend planned large-scale systems sufficient stability. Further topics include the identification of cost-effective materials and the development of fabrication techniques for metallic bipolar plates.

Hydrogen for fuel cells produced from commercially available fuels will make it possible to introduce fuel cell technology in a short space of time. The institute specializes in reforming middle distillates – diesel, kerosene and fuel oil. Work is carried out on the entire system, including desulfurization and CO purification. The focus is on reactors in the 3 – 50 kW power class, which are integrated into high-temperature PEFC or SOFC systems. Complex, realistic models, which are used to design and construct reactors, are reinforced by the use of glass models in which similarity theory is used to visualize flows.

Facilities, processes, methods

Equipment

- Test stands for the electrochemical characterization of electrocatalysts
- Test stands for the electrochemical characterization of CCMs
- Apparatus for characterizing membranes, current collectors and metallic bipolar plates
- Test stand for electrochemical studies up to 30 kW_{el}

Models

- Simulation models to describe mass, charge and heat transport processes in cells and stacks

Equipment and models

- Test stands for the investigation of reactors for reforming, water-gas shift reaction, preferential oxidation and desulfurization
- Test stands for screening and investigating catalysts with regard to activity and selectivity
- Analytical devices to determine concentrations (GC, GC/MS, NDIR) of reaction gases
- Apparatus for fractional distillation of fuels
- CFD simulation programs for visualizing educt mixing and reactor design

Contacts

Dipl.-Ing. Jürgen Mergel
Tel.: +49 2461 61-5996
Email: j.mergel@fz-juelich.de

Prof. Dr.-Ing. Ralf Peters
Tel. +49261 61-4260
Email: ra.peters@fz-juelich.de

Fuel Cell Process Engineering **Physicochemical Fuel Cell Laboratory**

Fields of work, range of services

Designing and building efficient fuel cell systems requires detailed knowledge of the cell and the complete system. The intensive interactions between cells and the system as a whole represent a development challenge, which is fully explored here. Three DMFC test facilities (2 kW) and two SOFC test facilities (1 kW, 20 kW) have been constructed in close collaboration with Cell and Stack Engineering. Work focuses on developing new system concepts, testing and evaluating these concepts, developing components in cooperation with industry, and testing and developing control and regulating concepts.

As technical development becomes more and more advanced, scientific work is becoming increasingly important in terms of understanding future energy systems. This is the reason why this department focuses on determining material and structural properties as well as their efficiency when implemented in the core components of energy technologies. Imaging, physical and spatially resolved analysis techniques are used to determine chemical and structural changes, mechanical and thermodynamic suitability, and fluid dynamic and electrochemical performance.

Facilities, processes, methods

Equipment and models

Test stands for

- high-temperature heat exchangers up to 850 °C and 200 m^3 air/h
- reformers and afterburners for SOFC stacks with a power of 5 kW
- air compressors up to 100 m^3/h and exhaust-gas-heated steam generators for SOFC systems
- process engineering investigations of DMFC stacks and system components
- CFD models to determine flow distribution in stacks
- simulation models for the design of fuel cell systems

Equipment and methods

- Imaging analysis techniques:
  field emission scanning electron microscope (FE-SEM) with EDX analysis, optical microscopes and confocal laser scanning microscope
- Spatially resolved analysis techniques:
  segmented cell technology (SCT), magnetic resonance and mass spectroscopy (SRMS)
- Physical analysis techniques:
  thermogravimetrical analysis (TG and TGA), dynamic differential calorimetry (DSC), climate cabinet, tensile testing machine with climate chamber, standard porosimeter, particle size measuring unit

Contacts

Prof. Ludger Blum
Tel.: +49 2461 61-6709
e-mail: l.blum@fz-juelich.de

PD Dr. Carsten Korte
Tel.:+49 2461 61-9035
e-mail: c.korte@fz-juelich.de

Process and Systems Analysis

Fields of work, range of services

Die Auswahl sinnvoller zukünftiger Energiesysteme und die Steuerung ihrer Entwicklung erfordern einen systemischen Ansatz, der hier für Brennstoffzellen betrieben wird. Basis der Untersuchungen sind Energiekettenbetrachtungen, Benchmarks zu anderen Anwendung- und Herstelltechnologien und wirtschaftliche Vergleiche. Durch die breite experimentelle Basis und das weiterreichende Modelling im Institut können in gesamte Systeme modellmäßig aufgebaut und mit konkurrierenden Techniken realitätsnah verglichen und Entwicklungspotenziale, wie auch Defizite aufgezeigt werden. Studien für die Industrie werden auch mit Informationsschutz durchgeführt.

Facilities, processes, methods

Methods

- Design engineering for fuel processing and energy systems with fuel cells
- Integrated evaluation methods (life cycle analyses) for energy systems

Ansprechpartner

Dr.-Ing. Michael Weber
Tel.: +49 2461 61-8626
Email: m.weber@fz-juelich.de

6.3 Publications, technology transfer and resources

The results of scientific and technical work carried out at IEK-3 are published in relevant journals and presented to interested specialist audiences at national and international conferences. Important journals in which three or more peer-reviewed papers from IEK-3 were published during the period under review were the Journal of Power Sources (2011: 9; 2012: 1), the Journal of Hydrogen Energy (2011: 5, 2012: 4), the Journal of the Electrochemical Society (2011: 2, 2012: 3), Electrochimica Acta (2009: 2, 2010: 2), and Electrochemistry Communications (2011: 2, 2012: 1). The most important conferences in which IEK-3 participated in 2011 were the International Conference on Energy Process Engineering in Frankfurt am Main with 3 contributions, the 12th International Symposium Solid Oxide Fuel Cells (SOFC-XII) in Montreal, Canada, with 3 contributions, and the 219th ECS Meeting in Montreal, Canada, with 2 contributions. In 2012, IEK-3 participated in the 10th European SOFC Forum in Lucerne, Switzerland, with 3 contributions, and in the 8th VDI conference on innovative vehicle drives in Dresden with 2 contributions. The various departments within IEK-3 also contributed to numerous other specialist conferences with papers and presentations both within Germany and abroad. In addition, five PhD theses were completed during the period under review (2011–2012) focusing on HT-PEFCs (2), DMFCs (1), SOFCs (1) and fuel processing (1). One undergraduate dissertation was also completed on the introduction of a H_2 infrastructure in Germany.

Year		2011	2012
Publications	Peer-reviewed journals[1)]	23	23
	Books and Journals	8	12
	Paper in a book	12	27
	Theses and dissertations	2	4
Technology transfer	Ongoing projects with third-party funding	43	48
	HGF initiatives and portfolios	4	4
	Patent applications	4	6
	Patents granted	1	7
Resources[2)]	Personnel (PoF[3)]/third-party funding)	105 (71/26)	106 (66/27)
Explanatory notes	[1)]According to ISI-citation index [2)]Data in PY/a [3)]PoF: Program-oriented funding		

Tab. 26: IEK-3 core data for 2011 and 2012

To ensure successful technology transfer, IEK-3 was involved in numerous R&D projects (2011: 43; 2012: 48) which received funding from the European Commission, the Federal Ministries of Economics (BMWi) and Education and Research (BMBF), the Ministry of Economics of the State of North Rhine-Westphalia, and projects financed by industry. IEK-3 was also responsible for managing and coordinating some of these projects. Additional funding from the Helmholtz Association was used during the two-year period under review to set up and substantially support a total of four basic research and system-oriented R&D projects on batteries, electrolyzers and membranes. The numerous patent applications (2011: 4; 2012: 6) and patents granted during the period under review (2011: 1; 2012: 7) represent another step towards smooth technology transfer.

IEK-3 has around 110 employees, who are partially financed by program-oriented funding (POF) from the Helmholtz Association of National Research Centres (HGF) and partially by third-party funds. Some of the personnel at IEK-3 are employed on a part-time basis. The effective personnel capacity was 105 PY/a in 2011 and 106 PY/a in 2012.

6.4 Committee work

IEK-3's national and international reputation as leading experts in fuel cells and hydrogen technology is reflected in the fact that several IEK-3 scientists are members of and collaborate with national and international committees. One example of international recognition is the role played by Prof. Stolten as Chairman of the 2nd International Conference on Energy Process Engineering 2011 (2nd ICEPE 2011) and the coordination of ICEPE, facilitated by the active involvement of numerous scientists at IEK-3. Furthermore, Prof. Stolten, Dr. Samsun and Dr. Müller hold important positions on the committees responsible for fuel cells within the International Energy Agency (IEA). On a national level, Prof. Stolten is a member of the National Organization for Hydrogen and Fuel Cell Technology (NOW) where he represents the part played by HGF in the German research area. The committee work performed by IEK-3 employees on the various levels is set out in detail below.

IEA Advanced Fuel Cells Implementing Agreement
since 2000, Prof. Dr.-Ing. D. Stolten
Vice-Chairman of the Executive Research on Polymer Electrolyte Fuel Cells

since 2004, Dipl.-Ing. J. Mergel
Member of Annex 22 Collaborative Research on Polymer Electrolyte Fuel Cells

since 2009, Dr.-Ing. R.C.Samsun
Member of the Executive Committee

since 2009, Dr.-Ing. M. Müller
Operating Agent for Annex 27

since 2011, Prof. Dr.-Ing. D. Stolten
Chairman of the Executive Committee

GVC Energy Process Engineering Expert Committee/VDI Society for Process Engineering and Chemical Engineering
since 2003, Prof. Dr.-Ing. D. Stolten
Member of the Energy Process Engineering Expert Committee

since 2006, Prof. Dr.-Ing. D. Stolten
Vice-Chairman of the Energy Process Engineering Expert Committee

since 2008, Prof. Dr.-Ing. D. Stolten
Chairman of the Energy Process Engineering Expert Committee

Masterflex AG Supervisory Board
2004 - 2011, Prof. Dr.-Ing. D. Stolten
Vice-Chairman of the Supervisory Board

Fuel Cell Qualification Initiative
since 2005, Dr.-Ing. B. Emonts
Member of the Executive Committee

BREZEL Expert Committee of the Association of German Engineers
since 2005, Prof. L. Blum
Member of the Expert Committee

Global Roundtable on Climate Change, Columbia University, New York
since 2006, Prof. Dr.-Ing. D. Stolten
Member

DKE "Portable Fuel Cell Systems" Standardization Working Group
since 2006, Dipl.-Ing. J. Mergel
Member of the Working Group

WILEY-VCH "Fuel Cells" Journal
since 2006, Prof. Dr.-Ing. D. Stolten
Member of the Advisory Board

National Organization for Hydrogen and Fuel Cell Technology
since 2007, Prof. Dr.-Ing. D. Stolten
Member of the Advisory Board and HGF representative for research

Fuel Cells and Hydrogen Network NRW
2007–2011, Dr.-Ing. H. Janßen and Dipl.-Ing. N. Kimiaie
Members of the Complete System and Stack Design and Assembly Working Groups

N.ERGHY in EU FCH Undertaking
since 2008, Prof. Dr.-Ing. D. Stolten
Representative of full member Forschungszentrum Jülich

since 2008, Prof. Dr.-Ing. R. Peters
Member of the Working Group for AA Transport and Refuelling Infrastructure

Research Alliance for Renewable Energies (FVEE)
since 2009, Dr.-Ing. B. Emonts
Representative of Forschungszentrum Jülich for Fuel Cells

Ruhr h2 Network
since 2009, Dr.-Ing. B. Emonts
Member

since 2012, Dr.-Ing. B. Emonts
Deputy Chairman

IEA Experts' Group on Science for Energy (EGSE)
since 2009, Prof. Dr.-Ing. D. Stolten
Co-Chairman

Working Group of Electrochemical Research Facilities (AGEF)
since 2010, Dipl.-Ing. J. Mergel
Member of the Board of Directors

2nd International Conference on Energy Process Engineering 2011: Efficient Carbon Capture for Coal Power Plants, Frankfurt am Main
since 2010, Prof. Dr.-Ing. D. Stolten
Conference Chairman as Chairman of the Energy Process Engineering Groups of Dechema/VDI, Head of the Organizing Committee

since 2010, Dr.-Ing. M. Weber
Member of the Organizing Committee

Fuel Cells and Hydrogen Network NRW
since 2012, Dr.-Ing. B. Emonts and Dipl.-Ing., Dipl. Wirtschaftsing. T. Grube
Chairmen of the hydrogen platform and the working group for H_2 systems

3rd International Conference on Energy Process Engineering 2013: Transition to Renewable Energy Systems, Frankfurt am Main
since 2012, Prof. Dr.-Ing. D. Stolten
Chairman of the Organizing Committee

since 2012, Dr.-Ing. B. Emonts
Member of the Organizing Committee

6.5 Contributions to trade fairs and exhibitions

IEK-3 has set itself the objective of showcasing its capacity for innovation by demonstrating new technologies and pioneering developments made possible by the institute's R&D priorities. The most important annual presentation forum for the highlights of the year is the technology trade fair in Hannover. In 2011, IEK-3 showcased the latest technology developments on three R&D topics. The most compact modules for fuel processing and a new HT-PEFC stack illustrated the current state of development in on-board power supply for the heavy transport sector. The current state of the art in SOFC development was demonstrated by a 5 kW stack, which was constructed according to the latest principles, thus avoiding excessive thermal stress, which could cause leaks. The DMFC exhibits revealed what design measures were implemented in current system development in order to achieve a minimum of 5000 hours in long-term testing. Minister Remmel (shown in Fig. 104, right) visited Jülich's stand as a representative of the Climate Protection Ministry of North Rhine-Westphalia, and was given an overview of R&D by Prof. Stolten.

Fig. 104: Hannover Messe 2011: Jülich's stand (left) and Minister Remmel visiting the stand (right)

Over the course of the year, IEK-3 took part in two other trade fairs and exhibitions. Details of these fairs and exhibitions are listed below.

2011

Hannover Messe 2011 4. - 8.04.2011, Hannover *Fuel cell research and technology development*
CeMat 2011 2. - 6.05.2011, Hannover *Forklift with DMFC supply module*
H2 Expo 2011 8. - 9.06.2011, Hamburg *On-board power supply for the aviation sector*

A year later, at the Hannover Messe 2012, IEK-3 showcased contributions to R&D in the areas of DMFC, HT-PEFC, SOFC, and fuel processing (see Fig. 105, left). The exhibition

focused on the latest successes in extended long-term tests on a DMFC system with two different SOFC stacks and a kerosene reformer.

Fig. 105: IEK-3 traide fair booths: Hannover Messe 2012 (left) and 18th WHEC 2012 (right)

IEK-3 also had an exhibition area in the German pavilion at the 19th World Hydrogen Energy Conference 2012 in Toronto, where the institute's scientists explained the opportunities for collaboration on topics of relevance to all technologies, such as modeling and simulation, analysis, manufacturing technology and process analysis (see Fig. 105, left). An overview of the events in which IEK-3 participated in 2012 and the topics concerned is given below.

2012

Hannover Messe
23. - 27.04.2012, Hannover
Fuel cell research and technology development

19th WHEC 2012
3. – 7.06.2012, Toronto, Kanada
Expertise for fuel cell and electrolysis research

9th European SOFC Forum
26. - 29.06.2012, Lucerne, Switzerland
SOFC research and technological development

f-cell 2012
8. – 10.10.2012, Stuttgart
Fuel-cell based energy systems for electromobility in the kW class

6.6 How to reach us

6.6.1 By car

Coming from Cologne on the A 4 motorway (Cologne – Aachen) leave the motorway at the Düren exit, then turn right towards Jülich (B 56). After about 10 km, turn off to the right onto the L 253, and follow the signs for “Forschungszentrum”.

Coming from Aachen on the A 44 motorway (Aachen – Düsseldorf) take the “Jülich-West” exit. At the first roundabout turn left towards Jülich, and at the second roundabout turn right towards Düren (B 56). After about 5 km, turn left onto the L 253 and follow the signs for “Forschungszentrum”.

Coming from Düsseldorf Airport, take the A 52 motorway (towards Düsseldorf/Mönchengladbach) followed by the A 57 (towards Cologne (Köln)) to Neuss-West. Then take the A 46 (towards Jüchen/Grevenbroich), before turning onto the A 44 (towards Aachen). Continue as described in “Coming from Düsseldorf”.

Coming from Düsseldorf on the A 44 motorway (Düsseldorf – Aachen) you have two choices:

1. (Shorter route but more traffic) turn right at the Jülich-Ost exit onto the B 55n, which you should follow for approx. 500 m before turning right towards Jülich. After 200 m, before the radio masts, turn left and continue until you reach the “Merscher Höhe” roundabout. Turn left here, drive past the Solar Campus belonging to the University of Applied Sciences and continue straight along Brunnenstrasse. Cross the Römerstrasse junction, continue straight ahead onto Wiesenstrasse, and then after the roundabout and the caravan dealers, turn left towards “Forschungszentrum” (signposted).

2. (Longer but quicker route) drive until you reach the “Jülich-West” exit. At the first roundabout turn left towards Jülich, and at the second roundabout turn right towards Düren (B 56). After about 5 km, turn left onto the L 253 and follow the signs for “Forschungszentrum”.

Fig. 106: Map of Meuse Rhine Euroregion

Sat-nav systems: In your navigation system, enter your destination as “Wilhelm-Johnen-Strasse”. From there, it is only a few hundred meters to the main entrance – simply follow the signs. Forschungszentrum Jülich itself is not part of the network of public roads and is therefore not recognized by navigation systems.

6.6.2 By plane

Cologne Bonn Airport: From the railway station at the airport, either take the S13 to Cologne main train station (Köln Hauptbahnhof) and then continue with the regional express to Düren, or go to Köln-Ehrenfeld by regional express and then take the S12 to Düren. Continue from Düren as described in “By train”.

By train from **Düsseldorf Airport**: From the railway station at the airport, travel to Cologne main train (Köln Hauptbahnhof) station and then continue on to Düren. Some trains go directly to Düren whereas other connections involve a change at Cologne main train station. Continue from Düren as described in “By train”.

6.6.3 By train

Take the train from Aachen or Cologne to Düren’s main train station (Hauptbahnhof). Then take the local train to Jülich (“Rurtalbahn”) and get out at the “Forschungszentrum” stop. From here, you need to keep right and walk towards the main road before turning right towards Forschungszentrum Jülich. The main entrance to Forschungszentrum Jülich is about 20 minutes by foot.

Fig. 107: Location of Forschungszentrum Jülich

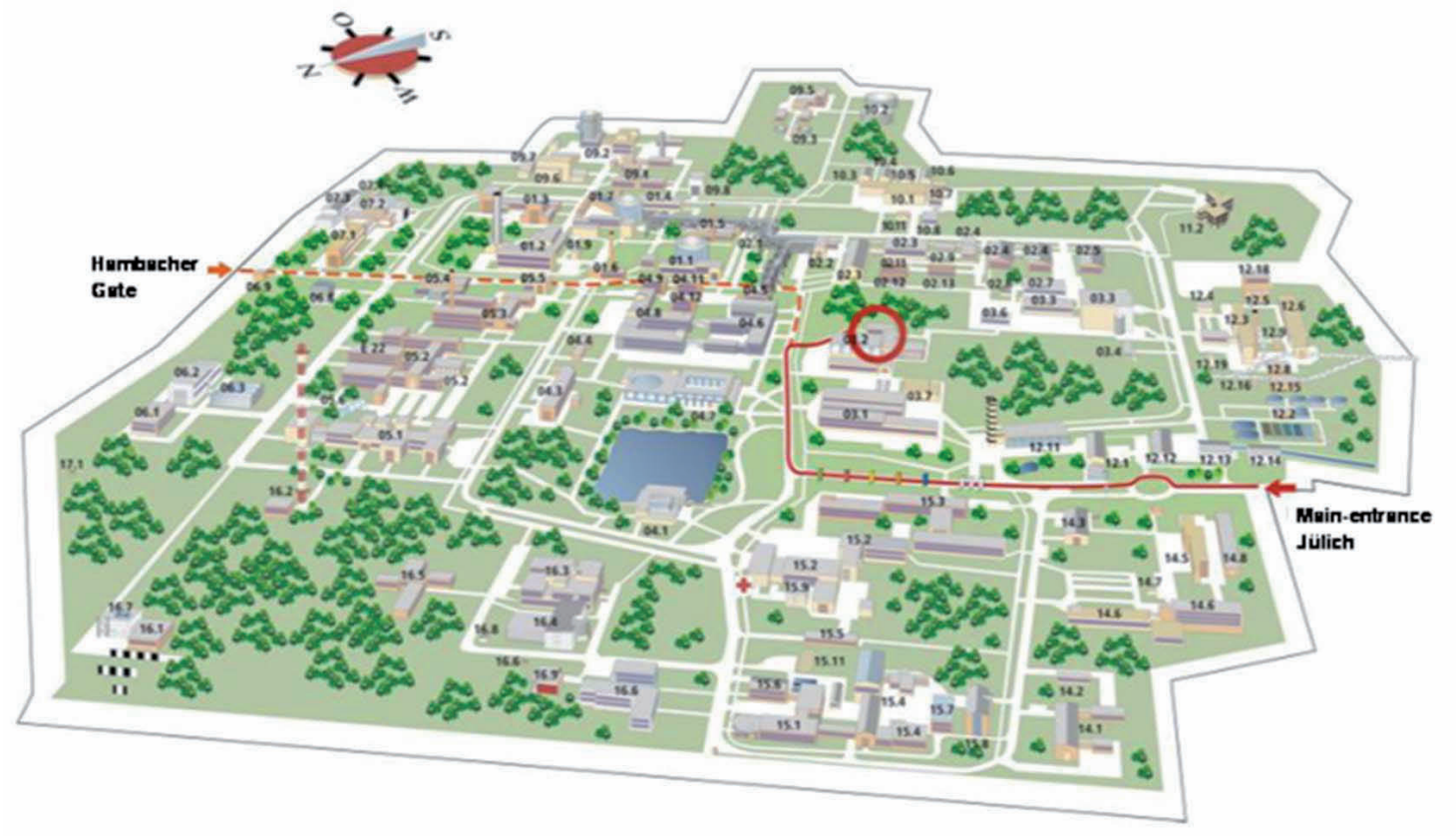

Fig. 108: Location of the Institute of Energy and Climate Research (IEK-3: Fuel Cells), Helmholtz-Ring H8, building no. 03.2

6.7 List of abbreviations

ABPBI	poly-2,5-benzimidazole
AC	Alternating Current
ACARE	Advisory Council for Aeronautics Research in Europe
ADELHEID	NRW Project „Out of the laboratory into the air“ (ger.: Aus dem Labor heraus in die Lüfte)
AGEF	Group of Electrochemical Research Facilities (ger: Arbeitsgemeinschaft Elektrochemischer Forschungseinrichtungen e.V.)
APS	atmospheric plasma sprayed
APU	auxiliary power unit
ATR	autothermal reforming
BAU	business-as-usual
BET	analytical method for the size determination for surfaces (Brunauer-Emmett-Teller)
BEV	battery electric vehicle
BMBF	German Federal Ministry of Education and Research (ger.: Bundesministerium für Bildung und Forschung)
BmWi	Federal Ministry of Economics (ger.: Bundesministerium für Wirtschaft)
BMS	battery management system
BMU	German Federal Ministry for the Environment, Nature Conservation and Nuclear Safety (ger.: Bundesministerium für Umwelt, Naturschutz und Reaktorsicherheit)
BOL	beginning of life
BREZEL	Expert Committee Fuel Cells of the Association of German Engineers
BTL	bio-to-liquid
CAB	catalytic burners
CAN-BUS	Controller Area Network
CCM	catalyst coated membrane
CCS	carbon dioxide capture and storage
CFD	computational fluid dynamics
CGO	cerium gadolinium oxid: $Ce_{0.8}Gd_{0.2}O_{2-\delta}$
CLSM	confocal laser scanning microscope
CO	carbon monixide
CONCAWE	conservation of clean air and water in Europe
CSM	computational structural mechanics
CV	cyclovoltametry
CVD	chemical vapour deposition
CVM	cell voltage monitoring
DC	direct current
Decal	transfers structure
DECHEMA e.V.	German Society for Chemical Technique and Biotechnology (ger.: Gesellschaft für Chemische Technik und Biotechnologie e.V.)
DFG	German Research Association (ger.: Deutsche Forschungsgemeinschaft)
DKE	Commission for Electrical, Electronic & Information Technologies (ger.: Deutsche Kommission Elektrotechnik Elektronik Informationstechnik)
DME	dimethylether

DMC	dimethylcarbonate
DMFC	direct methanol fuel cell
DSC	differential scanning caloriemeter
EBSD	electron backscatter diffraction
EDX	energy-dispersive X-ray spectroscopy
EGSE	Experts Group on Science for Energy
EIS	electrochemical impedance spectroscopy
EKOLYSER	BMWi-Project „New low-cost and sustainable materials for PEM-Electrolysis for hydrogen production from renewable energy”
EMPA	Swiss Research Institute for Materials Science and Technology
EL	extra light heating oil
EOL	end of life
ETEK/BASF	Manufacturer for components of PEM Fuel Cells
EU	European Union
FAME	fat acid methyl ester
FCH	fuel cell and hydrogen
FCV	fuel cell electric vehicle
FEM	finite element modelling
FuMa-Tech	Functional Membranes and Plant Technology (ger.: funktionelle Membranen und Anlagentechnologie)
FVEE	Research Alliance for Renewable Energies (ger.: ForschungsVerbund Erneuerbare Energien)
FZJ	Research Centre Juelich (ger.: Forschungszentrum Jülich GmbH)
GC/MS	gas chromatography with mass spectroscopy
GDE	gas diffusion electrodes
GDL	gas diffusion layer
GHG	greenhouse gas
GTL	gas-to-liquid
GuD	gas and steam process (ger.: Gas- und Dampfprozess)
GVC	Society for Process Engineering and Chemical Engineering (ger.: Gesellschaft Verfahrenstechnik und Chemieingenieurwesen)
HC	heating cartridge
HDS	hydro desulfurization
HER	hydrogen evolution reaction
HEV	hybrid electric vehicle
HGF	Hemholtz Association of National Research Centres (ger.: Helmholtz-Gemeinschaft Deutscher Forschungszentren)
HPB	high-temperature polymer electrolyte fuel cells (ger.: Hochtemperatur-Poymerelektrolyt-Brennstoffzellen)
HRTEM	high-resolution transmission electron microscopy
HT-PEFC	high-temperature polymer electrolyte fuel cell
HTS	high-temperature section
HVO	hydrotreated vegetable oils
ICEPE	International Conference on Energy Process Engineering
ICS-6	Institute of Complex Systems
ICV	internal combustion engine vehicle
IEA	International Energy Agency
Ifeu	Institute for Energy and Environmental Research (ger.: Institut für Energie- und Umwelttechnik GmbH)

IGCC	integrated gasification combined cycle
IQ-BZ	Fuel Cell Qualification Initiative (ger.: Initiative Qualifizierung Brennstoffzelle)
IEK-1	Institut for Energy and Climate Research – Material Synthesis and Processing (ger.: Institut für Energie- und Klimaforschung - Werkstoffsynthese und Herstellungsverfahren)
IEK-2	Institute for Energy and Climate Research – Microstructure and Properties of Matierals (ger.: Institut für Energie- und Klimaforschung - Werkstoffstruktur und –eigenschaften)
IEK-3	Institute for Energy and Climate Research – Electrochemical Process Engineering (ger.: Institut für Energie- und Klimaforschung - Elektrochemische Verfahrenstechnik)
IEK-9	Institute for Energy and Climate Research – Fundamental Elechtrochemistry (ger.: Institut für Energie- und Klimaforschung - Grundlagen der Elektrochemie)
JCNS-2	Jüllich Centre for Neutron Science – Scattering Methods (ger.: Jülicher Zentrum für Neutronenforschung – Streumethoden)
JUROPA	Jülich Research on Petaflop Architectures
KIT	Karlsruhe Institute of Technology
LBG	liquid biogas
LCA	life-cycle-assessment
LSCF	lanthanum-strontium-ferrite cobaltite cathodes
LED	light-emitting diode
LNG	liquiefied natural gas
LSM	lanthanum strontium maganese oxide: $La_{0.65}Sr_{0.3}MnO_3$
LTS	low-temperature shift stage
LuFo IV	BMWi project within the aviation research programm IV
MAPEL	BMBF project „Membran electrode assemblies for alkaline PEM electrolysis for hydrogen production from renewable energies“
MATLAB	programming language for technical calculations
MBE	molecular beam epitaxy
MCFC	molton carbonate fuel cell
MEA	membrane electrode assembly
MeOH	methanol: CH_3OH
MGO	marine gas oil
NDIR	nondispersive infrared adsorption analyser
N.ERGHY	New European Research Grouping on Fuel Cells and Hydrogen
NESTE Oil	Finnish rafination and distribution company
NExBTL	palm oil based fuel
NMHC	non-methane hydrocarbons
NMR	nuclear magnetic resonance spectroscoy
NPOC	non-purgeable organic carbon
NRW	North Rhine Westphalia (ger.: Nordrhein-Westfalen)
OCV	open cell voltage
OER	oxygen evolution reaction
OpenFOAM	open source field operation and manipulation
Oxyfuel	Combustion process with high flame temperature
PAFC	phosphoric acid fuel cells
PAH	parallel hybrid passenger car with internal combustion engine and battery

PBI	polybenzimadzole
PCC	post combustion carbon capture
PEC	polyethylencarbonate
PEFC	polymer electrolyte fuel cell
PEM	polymer electrolyte membrane
PEM-EL	polymer electrolyte membrane electrolysis
PEMFC	polymer electrolyte membrane fuel cell
PFSs	perfluorosulfonic polymer membranes
PGI-4	Peter Grünberg Institute – Scattering Methods
PGI-7	Peter Grünberg Institute - Electronic Materials
PLD	pulsed laser ablation/deposition
P-NMR	phosphor-31 nuclear magnetic resonance spectroscopy
POF	program-oriented funding
PRO-II	process analysis software
ProcessNet	Initiative of DECHEMA and VDI-GVC
ProMiNat	student academy
PTFE	polytetraflueroethylene
PVA	polyvinyl alcohol
PVAm	polyvinylamine
QR	quick resonance
RAG	company name (ger.: Ruhrkohle Aktiengesellschaft)
RAIRS	reflection-adsorption infrared spectroscopy
RDE	rotating disk electrode
Real-SOFC	EU project „Realising Reliable, Durable Energy Efficient and Cost Effective SOFC Systems“
R&D	research and development
RWTH	RWTH Aachen University (ger.: Rheinisch-Westfälische Technische Hochschule Aachen)
SAED	selected area electron diffraction
SCT	segmented cell technology
SEM	scanning electron microscopy
SNIFTIRS	subtractively normalized interfacial fourier transform infrared spectroscopy
Shell MDS	shell middle distillate synthesis
SimSci	Simulation software for process design
SOFC	solid oxide fuel cell
SRMS	magnetic imaging and mass spectroscopy
TEM	transmission electron microscopy
TG	thermogravimetrical analysis
TGA	thermogravimetry analyzer
TOC	total concentration of total organic carbon
ToF-SIMS	time-of-flight secondary ion mass spectroscopy
TTW	tank-to-wheel
UPS	power supply
USV	uninterruptable power supply
VDI	Publishing company (ger.: Verein Deutscher Ingenieure e.V.)
WBZU	Fuel Cell Education and Training Centre, Ulm (ger.: Weiterbildungszentrum Brennstoffzelle Ulm e.V.)
WGS	water-gas shift reactor

WGS-MR	water-gas shift membrane reactor
WHEC	World Hydrogen Energy Conference
WILEY-VCH	Publishing company (ger.: WILEY-Verlag Chemie)
WPS	wet powder sprayed
WTT	well-to-tank
XRD	x-ray diffraction
YSZ	yttria-stabilized zirconia
ZEA-1	Central Institute for Engineering, Electronics and Analytics – Engineering and Technology (ger.: Zentralinstitut für Engineering, Elektronik und Analytik)
ZEA-3	Central Institute for Engineering, Electronics and Analytics - Analytics (ger.: Zentralinstitut für Engineering, Elektronik und Analytik)

Band / Volume 171
Pulvermetallurgische Herstellung von porösem Titan und von NiTi-Legierungen für biomedizinische Anwendungen
M. Bram (2013), X, 238 pp
ISBN: 978-3-89336-866-2

Band / Volume 172
IEK-3 Report 2013. Langlebige Elektrochemische Verfahrenstechnik
(2013), ca. 185 pp
ISBN: 978-3-89336-868-6

Band / Volume 173
Combined Steady State and High Cycle Transient Heat Load Simulation with the Electron Beam Facility JUDITH 2
Th. Loewenhoff (2013), XVI, 108 pp
ISBN: 978-3-89336-869-3

Band / Volume 174
High-Quality Thorium TRISO Fuel Performance in HTGRs
K. Verfondern, H. Nabielek, M.J. Kania, H.-J. Allelein (2013), viii, 109 pp
ISBN: 978-3-89336-873-0

Band / Volume 175
Characterization of effective hydraulic properties of unsaturated porous media using spectral induced polarization (SIP)
K. Breede (2013), xiv, 72 pp
ISBN: 978-3-89336-875-4

Band / Volume 176
Zur Mikrostruktur siliziumbasierter Dünnschichten für die Photovoltaik
F. Köhler (2013), i, 100 pp
ISBN: 978-3-89336-876-1

Band / Volume 177
Grundlagen für die Transformation von Energiesystemen
Texte und Ergebnisse der Cadenabbia-Tagung 2012 der Konrad-Adenauer-Stiftung und des Forschungszentrum Jülich GmbH
L. Gruber, J.-F. Hake (Eds.) (2013), VI, 114 pp
ISBN: 978-3-89336-877-8

Band / Volume 178
Thermo - mechanical investigations and predictions for oxygen transport membrane materials
G. Pećanac (2013), 143 pp
ISBN: 978-3-89336-878-5

Band / Volume 179
Thermomechanische Charakterisierung neu entwickelter Feuerfestwerkstoffe
E. Skiera (2013), III, 133 pp
ISBN: 978-3-89336-885-3

Band / Volume 180
Entwicklung und Herstellung von metallgestützten Festelektrolyt-Brennstoffzellen mit Hilfe des Hohlkathoden-Gasflusssputterns
M. Haydn (2013), XVI, 174 pp
ISBN: 978-3-89336-886-0

Band / Volume 181
Characterization and stability investigation of water dispersible colloids (WDCs) in natural soils
C. Jiang (2013), X, 102 pp
ISBN: 978-3-89336-887-7

Band / Volume 182
Monazite-type Ceramics for Conditioning of Minor Actinides: Structural Characterization and Properties
C. Babelot (2013), x, 127 pp
ISBN: 978-3-89336-889-1

Band / Volume 183
High-rate growth of hydrogenated amorphous and microcrystalline silicon for thin-film silicon solar cells using dynamic very-high frequency plasma-enhanced chemical vapor deposition
T. Zimmermann (2013), x, 126 pp
ISBN: 978-3-89336-892-1

Band / Volume 184
IEK-3 Report 2013. Durable Electrochemical Process Engineering
(2013), ca. 180 pp
ISBN: 978-3-89336-893-8

Weitere ***Schriften des Verlags im Forschungszentrum Jülich*** unter
http://wwwzb1.fz-juelich.de/verlagextern1/index.asp

Institute of Energy and Climate Research - Electrochemical Process Engineering (IEK-3)

IEK-3 is one of nine subinstitutes within the Institute of Energy and Climate Research (IEK) at Forschungszentrum Jülich GmbH. IEK-3 aims to conduct research that is socially, ecologically and economically relevant and thus generate ground-breaking results on an international level. This quality of work is achieved through basic research, which is closely coordinated with technical development work in relevant scientific and technical fields of expertise. International cooperations with partners from research and industry are particularly important in this respect.

By implementing research results in innovative products, procedures and processes in cooperation with industry, IEK-3 hopes to help bridge the gap between science and technology. Collaboration with universities, universities of applied science, training departments and training centers is designed to promote opportunities for further education and training.

With a staff of approximately 110, IEK-3 concentrates on the basic topics of electrochemistry and process engineering for fuel cells and electrolyzers. In an integrated approach, the five key areas of work in the institute – solid oxide fuel cells, fuel processing systems, high-temperature polymer electrolyte fuel cells, direct methanol fuel cells, and polymer electrolyte membrane electrolysis – are accompanied by systems analysis and theoretical investigations, basic modeling and simulations, and by experimental and theoretical systems evaluations. The information generated in these areas is used to design and verify functional systems. In addition, particular attention is given to the development, configuration and application of special measuring techniques for the structural analysis of membrane electrode assemblies, for flow simulation and visualization, and for the characterization of stacks.

The 20 kW test stand pictured here is a compact SOFC system that can be used to supply heat and power. It comprises four 5 kW modules, which contain all of the hot system components (> 500 °C). In this first development stage with simple process engineering, the system can achieve a net electrical efficiency of between 41 % and 48 %.

The fuel processing module pictured here comprises an autothermal reformer, a two-stage water-gas shift reactor, a catalytic burner, a heat exchanger and two electric heating cartridges. The system has a volume of 85 liters and can supply HT-PEFC stacks with fuel gas. The latter then generate an electric power of up to 10 kW.

The energy supply module pictured here can be used as an alternative to large batteries for light traction. The hybrid system with direct methanol fuel cells is supported by a small battery and achieves a continuous output of around 1 kW. It is operated with pure methanol and achieves an efficiency of 29 % when operated under high dynamic loading. The system has been in continuous operation for more than 10,000 hours.

Energie & Umwelt / Energy & Environment
Band / Volume 184
ISBN 978-3-89336-893-8

JÜLICH
FORSCHUNGSZENTRUM